School of Surveying and Land Information

Satellite Derived Vegetation Indices for Monitoring Seasonal Vegetation Conditions in Western Australia

Michael L Roderick

This thesis is presented as part of the
requirements for the award of the
Degree of Doctor of Philosophy
of
Curtin University of Technology

August 1994

ABSTRACT

The monitoring of continental and global scale net primary production remains a major focus of satellite-based remote sensing. Potential benefits which follow are diverse and include contributions to, and improved scientific understanding of, ecological systems, rangeland management, famine warning, agricultural commodity trading, and the study of global climate change.

A NOAA-AVHRR data set containing monthly observations of green vegetation cover over a ten year period was acquired and analysed, to extract information on seasonal conditions. The data were supplied as a vegetation index, commonly known as the Normalised Difference Vegetation Index (NDVI), with a spatial resolution of approximately five km. The data set was acquired from three different satellites, and calibration problems were known to exist. A new technique was developed to estimate, and subsequently remove, the calibration bias present in the data.

Monthly rainfall measurements were used as surrogate ground truth to validate the NDVI data. For regions of native vegetation, linear models relating NDVI to previous rainfall were derived, using transfer function techniques in common use in systems engineering. The models demonstrate that, in mid-latitude regions, the NDVI is a linear function of rainfall recorded over the preceding seven or eight months.

Annual summaries of the image data were developed to highlight the amount and timing of plant growth. Three fundamental questions were posed as an aid to the development of the summary technique: where, when and how much? These summaries highlight the extraordinary spatial and temporal variations in plant growth, and hence rainfall, over much of Western Australia each year.

Standard analysis techniques used in time series analysis, such as classical decomposition, were successfully applied to the analysis of NDVI time series. These techniques highlighted structural differences in the image data, due to land use, climatic factors and vegetation type.

Overall, the results of the research undertaken in this study, using NOAA-AVHRR data in Western Australia, demonstrate that vegetation indices acquired from satellite platforms can be used to monitor continental scale seasonal conditions in an effective manner. As a consequence of these results, further research using this type of data is proposed in rangeland management and climate change modelling.

ACKNOWLEDGMENTS

Throughout this research project, many people have given of their time to assist the study. To those who are not mentioned, I apologise.

Jeremy Wallace from the CSIRO in Perth has provided expert statistical advice, over the telephone, on several occasions. Dr Doug Arbrecht and Alec Holm, of the Western Australian Department of Agriculture, were always able to provide the advice or data requested, no matter how obscure the request. Also from that organisation, Dr Shane Cridland has provided many hours of his time in discussions on possible approaches to adopt, and the ramifications of some of the research findings.

My supervisors, Professor Graham Lodwick and Dr Richard Smith, have both provided continual guidance and support. In particular, Professor Lodwick has enabled me to get on with it, and for that I thank him warmly. Dr Richard Smith has provided extensive support throughout the work, and without that contribution, the thesis would not have eventuated.

Most of all, I thank my wife, Jane, and daughter, Katherine, who supported the study in so many unsung but essential ways.

DEDICATION

To Peter, who loved both the Australian landscape, and scholarly pursuits, but never saw the beginning of this work.

TABLE OF CONTENTS

Table of Contents (continued)

Table of Contents (continued)

Table of Contents (continued)

Table of Contents (continued)

Table of Contents (continued)

LIST OF FIGURES

List of Figures (continued)

List of Figures (continued)

List of Figures (continued)

LIST OF TABLES

LIST OF ACRONYMS

API	Annual production index
ARMA	Autoregressive moving average
AVHRR	Advanced Very High Resolution Radiometer
BRDF	Bidirectional reflectance distribution function
CSIRO	Commonwealth Scientific and Industrial Research Organisation
FFT	Fast fourier transform
GAC	Global area coverage
GCP	Ground control point
GIS	Geographic Information System
HRPT	High resolution picture transmission
IGBP	International Geosphere Biosphere Program
IPAR	Intercepted photosynthetically active radiation
LAC	Local area coverage
LAI	Leaf Area Index
LST	Local Solar Time
MSS	Multispectral scanner
MVC	Maximum value composite
NASA	National Aeronautical and Space Administration
NDVI	Normalised Difference Vegetation Index
NOAA	National Oceanographic and Atmospheric Administration
NPP	Net primary production
PAR	Photosynthetically active radiation
PCA	Principal components analysis
PDF	Probability Density Function
PVI	Perpendicular vegetation index
SAVI	Soil adjusted vegetation index
TIR	Thermal region of electromagnetic spectrum
TSAVI	Transformed soil adjusted vegetation index
VIS	Visible region of electromagnetic spectrum
WST	Western Standard Time

Chapter 1

INTRODUCTION

1.1 Background

Vegetation is the primary trophic level of production and is essential for all higher order consumers including humans (Odum, 1963). In addition to its direct role as a food source, vegetation functions as a primary link in the carbon, hydrologic and other biogeochemical cycles through photosynthesis, transpiration and nutrient uptake. Maintenance of these functions is of prime concern in a number of areas including food production and climate change. In addition to these broader global issues, variability in primary production, through either natural or human induced changes, has major impacts on Australia's rural communities and trade balance.

Modern agricultural industries in Australia are intensive production systems typified by high inputs of fertiliser, energy, labour and capital. They are highly mechanised and efficient. In Australia, these activities are concentrated in the more reliable and higher rainfall areas of the southeast, southwest and eastern coastal regions of the continent. In contrast, the extensive pastoral industries of the arid and semi-arid zone are typified by low inputs and the harvesting of natural vegetation by livestock (Waring, 1969).

While Australia is typically characterised as an arid land, the Australian climate is unique for rainfall variability rather than aridity

(Russell, 1981). In the arid and semi-arid regions of Australia, rainfall variability has been proposed as a key feature of the ecology of the region (Stafford Smith and Morton, 1990; Nix, 1982). Management under these conditions has always been a significant problem for agricultural and pastoral land users (Campbell, 1966). Pastoral activities in the arid and semi-arid lands are thus sensitive to the variable rainfall, and subsequent variability in pasture production (Stafford Smith and Foran, 1992).

Plant growth is mainly a function of the level of sunlight, soil water and nutrients (Fitzpatrick and Nix, 1970). In Australian pastoral areas, solar energy is rarely limiting (Nix, 1982). Availability of soil water remains the major factor limiting production in most areas, in all but the best rainfall events. Rainfall is the major source of recharge to the soil water (Fitzpatrick and Nix, 1970). With the exceptional variability of rainfall already noted, net primary production can vary by orders of magnitude between years (Foran et al., 1982).

To monitor seasonal conditions over large scales, satellite remote sensing of plant growth remains the only measurement tool available that can cope with the spatial and temporal variability inherent in these systems (Graetz, 1987). This has been recognised since the launch of the first earth resources satellite, Landsat, in 1972 (Davis et al., 1991). The monitoring of net primary production remains a major objective of many earth scientists and ecologists,

studying a variety of problems including climate change, agricultural production, regional food deficits and land degradation.

Tucker (1983, 1985b), from the National Aeronautical and Space Administration (NASA), first demonstrated the feasibility of using data from polar orbiting meteorological satellites to monitor green vegetation over continental sized regions. These satellites provide daily coverage of the globe. By processing daily data from these meteorological satellites, he was able to generate cloud free images of the land surface at approximately weekly intervals. This interval was comparable to the temporal scale required for successful monitoring of plant growth. While the size of each pixel (~1-5 km) was large, this helped focus attention on more extensive regions.

Numerous applications have since been reported in the literature describing the use of meteorological satellite data for a variety of purposes, including continental land cover classifications (Norwine and Greegor, 1983; Justice et al., 1985; Lloyd, 1990), famine early warning systems (Henricksen and Durkin, 1986; Hutchinson, 1991), agricultural crop monitoring (Philipson and Teng, 1988; Quarmby et al., 1993) and modelling global primary productivity (Box et al., 1989; Prince, 1991b).

1.2 Monitoring Terminology

One of the problems in monitoring is the widely variable

context in which the term is used in various professions and disciplines (Holm, 1986; Bennett, 1979). The context in which "monitoring" is used in this thesis is described below.

It is proposed here that the process commonly known as monitoring is actually composed of four separate tasks as follows:

(a) Measurement,

(b) Monitoring,

(c) Interpretation,

(d) Management or control.

Measurement relates to the quantitative description of a phenomenon. Monitoring is the repeated measurement of that phenomenon through time, for the purpose of detecting changes in the phenomenon being measured. Interpretation involves the description and prescription of possible causes for variations observed in the monitoring data. Management or control is the intervention in the operation of a system to bring about some change in the level of the phenomenon being monitored.

1.3 Vegetation Monitoring

Maintenance of the productive capacity of vegetation communities, whether in agricultural or natural systems, remains a primary focus of the ecologically sustainable development (ESD) debate in Australia and other countries. As the ESD debate

develops, monitoring and subsequent interpretation of the state of various natural resources, including vegetation cover, will represent an essential scientific contribution to the broader community debate. Information collected from earth resource and meteorological satellites will be essential to understand the changes occurring in the large and sparsely populated arid and semi-arid regions of Australia. These regions are commonly referred to as the rangelands (Graetz, 1987).

Changes in vegetation cover occur at a number of temporal scales. These range from responses to rainfall over several days, to long term changes in the composition of perennial plants over hundreds of years (Graetz, 1987). In undertaking studies assessing change in vegetation resources over time, there is often a need to attribute the change to some specific factor or factors to allow management intervention. This requires a clear model of vegetation change against which the monitoring data can be assessed.

In extensive rangeland environments, 'Clementsian' succession has traditionally been assumed as the appropriate model to use when assessing vegetation change (Smith, 1988). This model essentially assumes that climax vegetation communities evolve at a particular site. These communities are both 'natural' and stable through time.

In arid and semi-arid rangelands, this view has recently been

challenged (Noy-Meir, 1973; Westoby, 1980; Noy-Meir and Walker, 1986; Westoby et al., 1989) as too simplistic. Westoby (1980) argues for a new model based on modern dynamic system concepts, where change is not as predictable as previously thought. The existing state of the vegetation may be persistent, and change between states is often unidirectional. This latter model is still the subject of controversy in ecological circles (Stafford Smith, 1992). In addition to the clear link between seasonal conditions and vegetation production, seasonal influences may also influence the longer term dynamics of vegetation communities. For example, out-of-season rainfall after a peculiar sequence of events could offer a window of opportunity for a particular species.

Regardless of the model chosen to describe change in vegetation, current and previous seasonal conditions need to be considered. The quality of a particular season has a dominant control on the net primary production in the landscape (Foran et al., 1982). Given this background it is clear that successful vegetation monitoring systems must have a number of attributes including:

(a) Appropriateness for the phenomena being studied,

(b) Objectivity and repeatability,

(c) Be defensible scientifically,

(d) Sample in the correct space time location (Graetz, 1987),

(e) Have a reporting capability.

Recent vegetation monitoring studies using satellite data have

been undertaken in a number of areas, including estimation of net primary production (Tucker, 1985b; Box et al., 1989; Prince, 1991a), land degradation (Graetz et al., 1988a; Pickup, 1989; Pickup et al., 1993; Millington, 1992) and drought (Hellden, 1984; Tucker and Choudbury, 1987; Gutman, 1990; Peters et al., 1991). These studies have a variety of aims ranging from purely scientific purposes to operational monitoring programs.

1.4 Seasonal Monitoring Techniques

The concept of a season refers to a period of time in the annual cycle in which climatic conditions promote plant growth. Typically, in the arid and semi-arid regions of Australia, this relates to the dominant period of effective rainfall. In the arid zone, this rainfall may fall at any time throughout the year. As such, in this zone, season commonly refers to the prevailing rainfall conditions at the time.

Current seasonal monitoring strategies use rainfall measured at a number of discrete sites. To simulate the effectiveness of that rainfall, water balance models which account for varying evaporation are often used (Slatyer, 1957; Fitzpatrick et al., 1967; McAlpine, 1970; Ritchie, 1972; McCown, 1973; Smith and Johns, 1975; Rickert and McKeon, 1982). These models typically use measured or estimated rainfall and long term average climatic statistics for evaporation, temperature and solar radiation (Fitzpatrick and Nix,

1970). No distinction is made between various plant species and their individual phenologies (Mott, 1973), or variations in soil type and regional hydrology (McAlpine, 1970; McCown, 1973). While more sophisticated models of plant growth do exist in agricultural applications (Hammer et al., 1987), they are generally very specific to a particular species and management regime (Smith et al., 1985). Spatial coverage of these models is achieved by interpolating the discrete rainfall data (Brook et al., 1992).

Remotely sensed measurements of radiation interactions with the earth's surface offer an alternative technique for monitoring plant growth. Remote sensing in the visible and near infrared parts of the spectrum has been shown to be related to plant growth (Kumar and Monteith, 1982). Sensing these measurements remotely avoids the extensive data requirements needed for modelling studies, to derive plant growth estimates (Brook et al., 1992). The spatial coverage of the satellite imagery also avoids the need for interpolation of measurements. The Advanced Very High Resolution Radiometer (AVHRR) carried on board the National Oceanographic and Atmospheric Administration (NOAA) meteorological satellites is one such satellite borne instrument which has been used extensively for this purpose.

1.5 NOAA Satellites

The NOAA satellites were originally designed to provide cloud

cover information several times per day in an operational environment for meteorological applications (Kidwell, 1991). Provided the land surface is cloud-free, the observations in the red and near infrared parts of the spectrum may be used for estimating plant growth.

The satellites are owned by the United States government and operated by NOAA. No charge is levied for data access, in contrast to other satellite systems such as Landsat and SPOT. However, the user is required to purchase and maintain a data receiving system. The policy on data access has promoted the use of the data in various research programs throughout the world.

The NOAA satellites have been operated continuously since 1979, and extensive archives exist within various organisations throughout the world (e.g. WASTAC, 1991). The existence of these archives has promoted an interest in the use of the data for monitoring plant growth over continental sized regions.

1.6 Study Area

This study concentrates on the analysis and interpretation of satellite data for monitoring seasonal vegetation conditions in Western Australia. However, the techniques developed are expected to be broadly applicable to other arid and semi-arid areas throughout the world.

Western Australia is the largest of the Australian states and occupies approximately 2.5 million sq km which represents some one-third of the total mainland area. The State population of 1.6 million is highly centralised, with some 1.1 million living in the capital city, Perth.

Biogeographical regions within the State vary from semi-arid tropical savanna in the north of the State, with summer dominant rainfall, to a major agricultural region in the southwest corner of the State (see Figures 3.1 and 3.2). Land use within the agricultural region is dominated by cereal and sheep production. This latter area experiences a mediterranean climate with cool wet winters and hot dry summers (Beard, 1990). Significant areas of arid lands exist which do not receive adequate rainfall for permanent agriculture to exist. They are used for either extensive rangelands (cattle and/or sheep grazing) or are unoccupied. While the soils are generally poor, the environment is still predominantly water limited. The agricultural and pastoral industries are the major land users by area within the State.

Existing mapping is generally good by world standards (Graetz, 1987). The vegetation of the entire State has been mapped and published at 1:1000000 using standard structural classification systems (Beard and Webb, 1974). Various land system surveys (Christian and Stewart, 1968) have also been undertaken by the CSIRO and Western Australian Department of Agriculture in the

extensive rangelands (Mabbutt et al., 1963; Payne et al., 1987), although this coverage is not complete.

General climatic data is available from the Bureau of Meteorology. Approximately 1500 stations record rainfall although not all of these are at daily intervals. The majority of these stations are in the settled areas in the southwest of the State (approximately 1300), with a very sparse network in the arid pastoral areas.

1.7 Aims of the Study

This study seeks to investigate the use of NOAA-AVHRR data for describing broad scale variations in vegetation growth across Western Australia. The satellite data available to support the study comprise a ten year sequence of monthly images of green vegetation cover from July 1981 to March 1991 inclusive.

Hypothesis: *That imagery from the NOAA-AVHRR satellite can be used to effectively monitor spatial and temporal variations in seasonal vegetation conditions across Western Australia.*

A number of specific topics are investigated including:

(a) The calibration of multi-temporal observations from the AVHRR instrument,

(b) The relationship between the satellite data and point based

rainfall estimates,

(c) The vegetation response to rainfall in various biogeographic regions,

(d) The extraction and subsequent display of ecologically relevant information from the time series satellite imagery.

Chapter 2

NOAA DATA FOR VEGETATION MONITORING: A REVIEW

2.1 Physical Principles of Remote Sensing

Remote sensing is the science concerned with acquiring information about an object without physically interfering with that object. Any remote sensing system requires a source of energy, a target and a sensor for recording the interactions of electromagnetic radiation with that object. On striking an object, energy may be either reflected, absorbed or transmitted. Typically the reflected energy is measured using a specially designed sensor system. Measurement of the amount of energy reflected allows some inferences to be made about the nature of target.

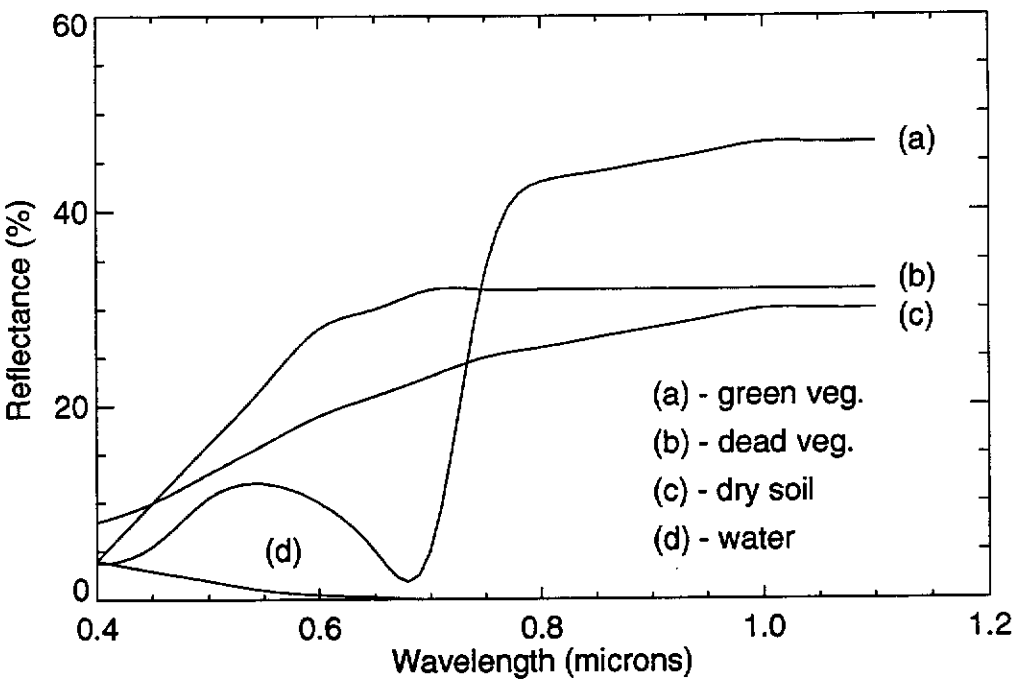

Figure 2.1 Spectral reflectance of typical targets

The typical reflectance characteristics of four major earth surface targets are shown in Figure 2.1. The differentiation between living and dead plant material is clear in both the red and near infrared parts of the spectrum. Absorption of red light by chlorophyll pigments causes a lower reflectance for healthy living plant tissue in that part of the spectrum. Due to the presence of water in the layered structure of leaf tissue, healthy green plant tissue reflects more near infrared light than dead or stressed plant tissue (Curran, 1985). Surface water has a typically low reflectance in all wavelengths, and the reflectance is inversely related to wavelength. Soil reflectance shows a clear linear relationship with wavelength (Curran, 1985). Reflectance measurements can be used to differentiate between various earth surface targets, and in some cases infer differences in vegetation condition from the spectral measurements (Tucker, 1979; Tucker et al., 1980; Tucker et al., 1981).

The measurements shown in Figure 2.1 are derived from laboratory and field based studies. For remote sensing from satellite platforms, the intervening atmosphere modifies the signal recorded by the satellite as depicted in Figure 2.2. Referring to Figure 2.2, the total radiance recorded at the satellite, L, is given by:

$$L = P + D + I \tag{2.1}$$

The direct radiance component D is often described as "top of canopy

radiance", and the total radiance received at the sensor L is often called "top of atmosphere radiance". Field based measurements which are unaffected by the atmosphere, are equivalent to D.

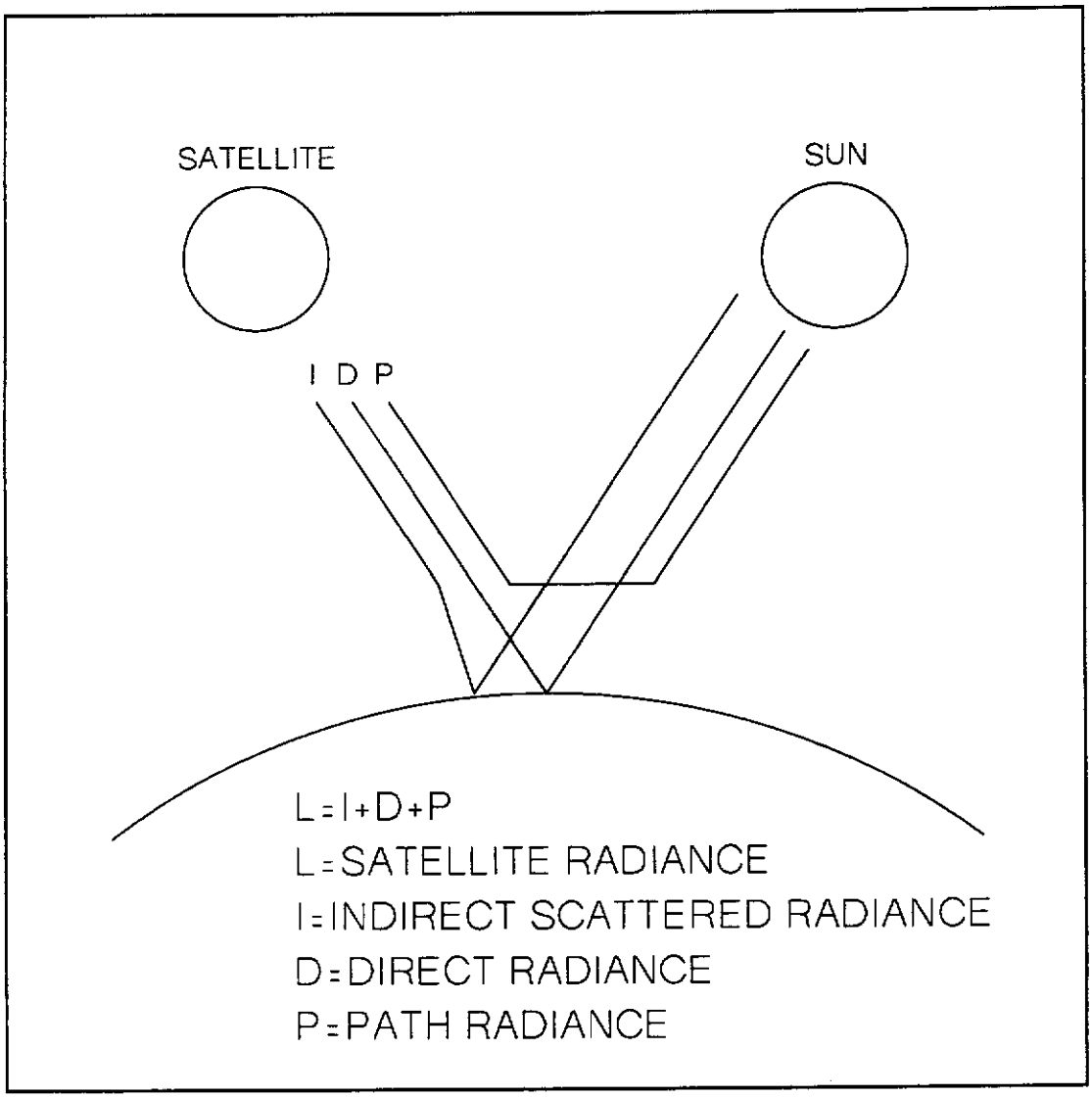

Figure 2.2 Atmospheric component in remote sensing (Kaufman, 1989)

2.2 NOAA Based Monitoring - A Conceptual Basis

Clouds frequently cover 50 percent or more of the earth's surface on any given day (Tarpley et al., 1984). These clouds

obscure the earth surface, and prevent observation of the vegetation in the visible (VIS) and near infrared (NIR). For Landsat studies, the 16 or 18 day repeat cycle is not generally sufficient to ensure cloud free observations for operational monitoring. In arid and semi-arid environments such as Western Australia, cloud cover will generally be present during plant growth periods. In some parts of the world, cloud cover can remove all hope of an operational vegetation monitoring program in the VIS and NIR regions of the spectrum (Justice et al., 1985; Legg, 1991).

The daily coverage of the NOAA satellite can be used to overcome most of the cloud problems. By taking multiple images over a period, the cloud free observations over that period can all be combined into one (cloud free) image. The resulting image is known as a 'composite' and the technique is known as compositing (Holben, 1986). The spectral observations in a composite image can thus come from any individual image during the composite period. The length of period over which the composite is taken depends on both the application, and persistence of cloud cover. Typical periods are a week (Tarpley et al., 1984), fortnight (Cridland et al., 1994) and month (Tucker et al., 1991).

Vegetation indices, computed from the spectral measurements, have been used almost exclusively to represent the condition of vegetation at the earth's surface. These essentially seek to collapse a multivariate set of spectral observations into a single index. Many

different types of vegetation index have been used (see Section 2.4.5 for a full discussion). For NOAA based remote sensing, the most common of these is the Normalised Difference Vegetation Index (NDVI) (Rouse et al., 1974). This index is calculated as (N-R)/(N+R) where N is the near infrared and R the red reflectance. The index varies from -1 to 1. Typical values of the NDVI are clouds (-0.2), water bodies (-0.1), bare soil (0 - 0.1) and vegetated targets (> 0.2).

2.3 NOAA Satellite Details

2.3.1 Characteristics

The essential characteristics of the NOAA satellite and AVHRR instrument are shown in Table 2.1.

Spatial Resolution	1.1 km at NADIR ~8 km at 55 degree view angle
Temporal Resolution	9 day repeat cycle for orbit giving 2 images per day (one in day, one at night) Sun synchronous orbit at 830 km altitude
Spectral Resolution	Name — Bandwidth (microns)[1] Band 1: 0.6-0.7 (RED) Band 2: 0.7-1.1 (NIR) Band 3: 3.5-3.9 (MIR)[2] Band 4: 10.5-11.5 (TIR)[3] Band 5: 11.5-12.5 (TIR)[4]
Radiometric Resolution	10 bit quantisation
Calibration Details	Bands 3,4,5: on board calibration Bands 1,2: deep space counts only
Archive Commenced	1979 (NOAA)

[1] Approx. only. The precise boundaries vary on each instrument.
[2] Mid infrared
[3] Thermal infrared
[4] On even numbered satellites (6, 8, 10) band 4 is repeated as band 5

Table 2.1 NOAA AVHRR essential characteristics

2.3.2 Missions

The NOAA satellites are polar orbiting and two major orbital programs are used. Even numbered satellites (6, 8, 10 and 12) ascend over the equator in the early evening at approximately 1930 hours local solar time (LST). The odd numbered satellites (7, 9 and 11) have a different phase, ascending over the equator in the early afternoon at approximately 1400 hours LST. The nominal equatorial overpass times for each mission are shown in Table 2.2.

Satellite	LST (hrs) of Ascending Node	LST (hrs) of Descending Node
TIROS-N	1500	0300
NOAA-6	1930	0730
NOAA-7	1430	0230
NOAA-8	1930	0730
NOAA-9	1420	0220
NOAA-10	1930	0730
NOAA-11	1340	0140
NOAA-12	1930	0730

Table 2.2 Nominal equatorial crossing times of NOAA satellites in local solar time (Kidwell, 1991, pp. 1-7)

By operating an even and odd numbered satellite at the one time, meteorologists can get estimates of cloud cover twice per day. For vegetation studies, the early afternoon overpass from the odd numbered series has been used almost exclusively. On even numbered satellites, the sun is typically very low at the time of overpass and there is insufficient light for reflectance measurements.

Satellite	Launch Date	Data Range Held by NOAA
TIROS-N	10/10/1978	19/10/1978 - 30/01/1980
NOAA-6	27/06/1979	27/06/1979 - 05/03/1983, 03/07/1984 - 16/11/1986
NOAA-7	23/06/1981	19/08/1981 - 07/06/1986
NOAA-8	28/03/1983	20/06/1983 - 12/06/1984, 01/07/1985 - 31/10/1985
NOAA-9	12/12/1984	25/02/1985 - 07/11/1988[1]
NOAA-10	17/09/1986	17/11/1986 - Present
NOAA-11	24/09/1988	08/11/1988 - Present
NOAA-12	14/05/1991	14/05/1991 - Present

[1] NOAA-9 has recently been reactivated following the failure of NOAA-13.

Table 2.3 Key mission dates for the NOAA satellite missions (Kidwell, 1991)

The launch dates of each satellite, and dates from which the data were archived by NOAA, are shown in Table 2.3. The small gap between launch and operational recording of the data (by NOAA) is used for testing of the satellite systems.

Two modes of data acquisition are available for AVHRR data on each of the NOAA satellites. During orbit the data are broadcast continuously (called high resolution picture transmission (HRPT) direct readout) and can be recorded by independent ground stations, such as that operated by the Western Australian Satellite Technology and Applications Consortium (WASTAC, 1991). In addition, each NOAA satellite has on board recorders which can be programmed from earth control stations for data acquisition. When the satellite comes within view of a NOAA receiving station, the recorded data can

be transmitted to earth and subsequently archived. This on board recording facility can only hold ten minutes of full resolution data (Kidwell, 1991). Thus global coverage of full resolution (one km) data is currently not possible. To achieve global coverage using the on board storage facility, NOAA subsample the HRPT data to (approximately) five km pixels. This data format is called global area coverage (GAC). Using this scheme, data from the NOAA satellites have been used to construct global maps of surface reflectance, and other biophysical parameters (Rossow et al., 1989).

The so called GAC data are generated by averaging the first four pixels out of every five along a scan line of image data, and retaining these averages from every third scan line. The spatial resolution at nadir is thus 1.1 x 4 km (Malingreau and Belward, 1992; Belward, 1992). The averaged pixel is then assumed to represent a 4 x 4 km area on the ground. While this scheme has been criticised as being unrepresentative (Justice et al., 1989), it does reduce the data handling (processing and storage) required on board the satellite. This reduction in handling has enabled the creation of global data sets for vegetation monitoring (Tarpley et al., 1984; Hutchinson, 1991; Robel, 1991; Tucker et al., 1991; Eidenshink, 1992; Bullock, 1992).

It has been found that throughout the life of the odd numbered NOAA satellites, the time of equatorial crossing gets progressively later each year (Gutman, 1992; Ohring et al., 1992; Brest and

Rossow, 1992). This problem is due to the original orbital geometry chosen (Ohring et al., 1992). Thus an annual trend will exist in the sun-sensor viewing geometry. Brest and Rossow (1992) found this trend to exist in the raw satellite observations, and developed analytical procedures to remove the trend on various surface cover types. The actual equatorial crossing times for the afternoon satellites are shown in Figure 2.3.

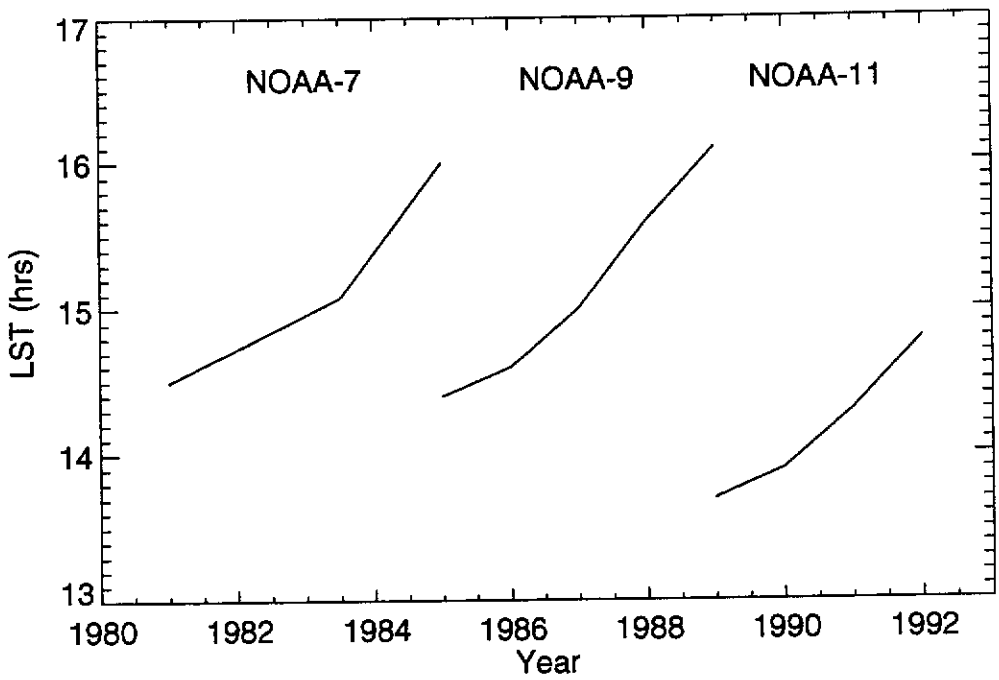

Figure 2.3 Equatorial crossing times in local solar time (LST) for afternoon satellites (Gutman, 1992; Brest and Rossow, 1992)

2.4 Data Processing

Processing the data received from earth resource satellites into useful products has occupied much of the research effort in remote sensing to date. Even coarse resolution sensors such as the AVHRR generate gigabytes of raw data every week. The extraction of useful information from this data stream is a complex process involving many individual steps, and is essentially a serial process. Data from the AVHRR sensor is available at no cost to any person or organisation that has a capacity to collect the data. The acquisition of the raw data is only the beginning, and in some respects the easiest part of the process of information extraction. These steps are outlined below, and discussed in the following sections:

(a) Acquire raw data,

(b) Recover radiance from digital counts,

(c) Atmospheric correction,

(d) Convert radiance to reflectance,

(e) Image rectification,

(f) Extract vegetation information.

2.4.1 Data Calibration

An essential component of any monitoring program is instrument calibration. In satellite remote sensing, calibration involves the conversion of the observed digital counts to a physical quantity, namely spectral radiance. Traditionally, this physical aspect was ignored, as most applications used images in a

qualitative manner (see Jensen, 1986). The need for calibration has been sparked by an increasing interest in the use of long term data sets for monitoring biophysical phenomena (Price, 1987a).

The importance of calibration for the comparison of vegetation indices over time, and between different sensors, was first demonstrated by Price (1987b). The conversion of digital counts to radiance, and then reflectance, is essential for long term studies of earth surface changes using vegetation indices.

The AVHRR instruments carried on each successive NOAA mission were constructed in batches, and subsequently stored in a vault until launch (Che and Price, 1992). Prior to being placed in storage, the instruments were calibrated against a standard to derive a linear relationship (i.e. gain and offset) between digital counts and spectral radiance (NOAA, 1987; Kidwell, 1991). This calibration was adopted by NOAA and is known as the 'pre-flight' calibration. Once in space, there is no on-board facility to determine the gain of the solar channels (one and two). The offset for these channels is routinely determined by observations of deep space.

Various AVHRR data sets were developed for application studies which adopted the pre-flight calibration results. This assumes that both the gain and offset of the instrument were stable over time. However, in the late 1980's several studies demonstrated that the actual calibration values were not stable over time and

differed from the published pre-flight values (Frouin and Gatier, 1987; Slater et al., 1987; Holben et al., 1990; Brest and Rossow, 1992; Mitchell et al., 1992; Teillet and Holben, 1992; Che and Price, 1992; Kaufman and Holben, 1993). It is proposed that the launch trauma, and subsequent degassing of the instrument (when in space), both contribute to the calibration differences reported (Che and Price, 1992). In addition to these difficulties, the calibration coefficients for NOAA-11 were changed by NOAA after a re-examination of the original instrument data and calibration methodology (Abel, 1990).

With the lack of on board calibration facilities for measuring the instrument gain, and the obvious importance to multi-temporal studies, many other studies were undertaken to determine suitable calibration coefficients. Many different techniques of post flight calibration for the AVHRR have been proposed including:

(a) Measure radiance on an invariant target using a simultaneous aircraft or satellite overpass (Smith et al., 1988),

(b) Use of invariant targets, such as desert, ocean and clouds, and removal of the atmospheric component by radiative transfer modelling (Fraser and Kaufman, 1986; Frouin and Gatier, 1987; Holben et al., 1990; Mitchell et al., 1992; Kaufman and Holben, 1993),

(c) Assume the total reflected energy over very large areas is stable on a seasonal (i.e. annual) basis, and statistically estimate a relative calibration (Brest and Rossow, 1992). By subsequently

linking to an absolute calibration at a particular time, this relative result may then be anchored.

One approach similar to (c) that has recently been used in multi-temporal studies using Landsat data (Pickup et al., 1993) is to statistically adjust the limits of the data space to occupy a similar position in a cross plot of the individual bands. This assumes that there are no truly invariant targets, but that the fundamental scene elements (bare soil, trees, etc.) remain constant. This approach is particularly suited to long term studies, where the aim is to extract information on vegetation and soil in a landscape. It will generally not be suitable for studies requiring absolute measures of reflectance such as surface energy balance studies (Rossow et al., 1989; Smith et al., 1992).

Unfortunately, the results of several post-flight calibration studies using different methods vary substantially. In a review by Che and Price (1992), the results of several calibration studies were compiled and compared. Significant differences were noted, between both the techniques used and results from individual studies. They eventually took a pragmatic approach, and calculated an average calibration (NOAA 7, 9 and 11) for use by application scientists. This 'average' calibration shows a loss of instrument sensitivity of approximately five percent per year for channel 1, and seven percent per year for channel 2 (excluding channel 2 on NOAA-11 which showed four percent per year). However, in all cases, the post-flight

calibration values recommended for use at launch time were significantly different from the pre-flight values recommended by NOAA (Kidwell, 1991).

The International Global Biosphere Program (Townshend, 1992), which is constructing a 'pathfinder' (one km resolution) data set for global monitoring purposes, has recommended the method and results of Holben et al. (1990) and Kaufman and Holben (1993) be used. While these particular studies were used by Che and Price (1992) in their derivation of an average calibration, the average figures quoted by them are at odds with this recommendation.

For real time data users, such as those involved in operational monitoring programs (Cridland et al., 1994; Philipson et al., 1988; Quarmby et al., 1993; Hutchinson, 1991), this lack of calibration creates a dilemma. Many of these organisations will not have the resources or expertise to design their own calibration programs. For these users, the only current option is to adopt a particular study, and then assume the trends so far observed, will continue into the future. While NOAA have an active research program in this area (Teillet and Holben, 1992), they have made no specific recommendations on methodology or results. Users should be aware that NOAA also issue a disclaimer (Kidwell, 1991) that they will not be responsible for any errors caused by incorrect satellite calibration. For application scientists it is simply a case of 'caveat emptor'.

Many operational and scientific programs receive vegetation index data as a product (Tarpley et al., 1984; Bullock, 1992; Eidenshink, 1992), rather than the original bands. The calculation of these indices using pre-flight calibration data will be in error (Price, 1987b; Goward et al., 1991). A number of studies have recommended corrections to be applied to correct the data for these errors (Holben et al., 1990; Che and Price, 1992; Kaufman and Holben, 1993; Los, 1993). This is a complex area and a detailed discussion is given in Chapter 5 of this thesis.

Without on board calibration of the AVHRR instruments, the post-flight calibration procedure is unlikely to improve. Che and Price (1992) have prepared error budgets for post-flight calibration of the AVHRR sensors and believe that absolute calibration is possible to within 10 percent of the true value. However, they also found that the AVHRR is relatively stable over time. From these estimates, it is clear that users will have problems in achieving a reliably calibrated data set using data acquired from several satellites. However, within a series of measurements from the one satellite, the calibration problem is considerably diminished. The relative calibration methods (Brest and Rossow, 1992) can be used for one particular satellite.

2.4.2 Atmospheric Corrections

Traditionally, the removal of atmospheric influences on

remotely sensed data has not generally been undertaken (Jensen, 1986). This is often acceptable in studies using single date imagery, which use visual interpretation or simple digital analysis of imagery such as classification. However, long term studies require a more rigorous approach. It is essential to remove or minimise variations in the signal received which are not the object of study (Gutman, 1989; Gutman, 1991; Goward et al., 1991). The atmosphere itself is dynamic, with conditions varying over several spatial and temporal scales (Graetz, 1987). These varying conditions complicate the interpretation of multi-temporal satellite signals. It is often not possible to be sure if the change noted is due to a real change on the land surface, or just an artefact of data processing, atmospheric influences or variations in the viewing geometry (see Ohring et al., 1992).

Two distinct aspects of atmospheric corrections can be identified (Paltridge and Mitchell, 1990):

(a) Reflection (i.e. scattering) and absorption of radiation by various atmospheric constituents,

(b) Bidirectional reflectance distribution function (BRDF) of the target.

Radiation is both absorbed and reflected (called scattered in this context) by atmospheric constituents such as molecules, aerosols and water vapour. These interactions are dependent on the viewing geometry (BRDF) for each observation. The BRDF has often

been dealt with as an atmospheric correction (see Paltridge and Mitchell, 1990). However, bidirectional reflectance is an intrinsic physical characteristic of remote sensing. As such it is described separately in Section 2.4.3.

The technique of maximum value compositing (MVC) described by Holben (1986) has been widely used to minimise the effect of both variation in the atmosphere and variable viewing geometry. The selection of the maximum NDVI over a particular composite period, tended to favour near nadir observations which were least atmospherically affected (Holben and Fraser, 1984; Holben, 1986; Lee and Kaufman, 1986). Because of the nature of the NDVI, this also tended to select cloud free image data. It is noted that this technique was really a pragmatic solution to a difficult problem, and in that context has been successful. The MVC technique has been found to reduce atmospheric and BRDF effects more effectively when used over longer composite periods such as one month (Holben, 1986; Gutman, 1991).

Problems have, however, been noted with this technique. If all possible satellite overpasses are used, most of the data are collected with viewing angles greater than 30 degrees (Gutman, 1987, 1991). Statistically, this will tend to bias the maximum NDVI value to an off-nadir view, particularly in periods of heavy cloud cover. Variation in the aerosol optical depth (Holben et al., 1991; Soufflet et al., 1991) has been shown to cause errors in NDVI of ± 0.02 units. This is

small in comparison with the likely effect of calibration errors (Che and Price, 1992). Absorption of near infrared radiance by atmospheric water vapour has also been shown to effect the NDVI by similar amounts (Justice et al., 1991). Soufflet et al. (1991) have looked at a whole range of atmospheric effects and found atmospheric corrections to account for errors of up to ± 0.08 NDVI units. In a similar study, Tanre et al. (1992) found errors due to atmospheric factors could depress the NDVI by up to 0.1 units, which is in close agreement. Goward et al. (1991) quote figures of 30 percent lower NDVI values if no atmospheric corrections are made. It is noted that all these results pertain to data collected from individual overpasses and that improvements are made when using the MVC technique described above.

The atmospheric correction schemes proposed typically require climatic data for use in radiative transfer models. Two approaches are possible to provide these data:

(a) Average climatic data such as the US standard atmosphere,

(b) Measurement using ground based instruments, or other satellite instruments.

The approach using average climatic data has been implemented in an operational scheme by Paltridge and Mitchell (1990), and subsequently refined (Mitchell and O'Brien, 1992). An obvious disadvantage with average climatic data is the inability to cope with extreme events. For example, aerosols from the Mt.

Pinatubu volcanic explosion in June 1991 have been detected in NOAA imagery (Lynch and Marsden, 1992). The effect over India was sufficient to disrupt an operational drought monitoring program (Jeyaseelan and Thirruvengadachari, 1993).

Perhaps the best solution is to redesign the satellite sensors to deliver 'atmospherically resistant' vegetation indices. One such approach has been advocated by Kaufman and Tanre (1992). They propose the addition of a channel in the blue portion of the spectrum. Radiance measurements from this new channel, can be used to correct for atmospheric effects on the red channel. While this approach offers the best method for future space missions, it does not offer a solution at the moment.

2.4.3 Bidirectional Reflectance Modelling

The variation of reflected radiation received at a sensor as a function of viewing geometry is termed the bidirectional reflectance distribution function (BRDF). For a so-called lambertian target, reflectance is assumed independent of viewing geometry. Unfortunately, vegetation, soil, water and other targets are not lambertian, but exhibit a strong dependence on the illumination and viewing geometry (Kimes, 1983; Rao et al., 1979; Kriebel, 1978).

The wide viewing angle (± 55 degrees) used by the AVHRR instrument provides daily observations of the earth's surface. This

also creates variable viewing geometry on sequential observations (Gutman, 1991). The variation in viewing geometry is a natural consequence of seasonal change in the solar position, and the orbital geometry of the NOAA satellites. As such the effect of the BRDF of the target needs to be considered in any monitoring program. A vegetation monitoring program should aim to detect changes in surface conditions, rather than changes in viewing geometry (Huete et al., 1992).

The BRDF of natural targets has been extensively studied (in the solar spectrum) and found to relate primarily to the interaction between canopy structure, surface cover, soil background and atmospheric conditions (Rao et al., 1979; Deering and Eck, 1987; Deering et al., 1990; Baret et al., 1992; Huete et al., 1992). In agricultural applications, the arrangement and orientation of planting also has a major effect on the BRDF (Lord et al., 1988; Ranson et al., 1985)

Vegetation indices are one means of minimising the variations caused by bidirectional reflectance for vegetation monitoring purposes (Jensen, 1986). In studies using ground based measurements, the NDVI has been found to minimise BRDF effects (Kirchner et al., 1982; Kimes et al., 1985). The reduction of the BRDF effect using NDVI has been found to depend on the optical properties of the target. Kimes et al. (1985) found a general decrease in variation across a wide range of cover types in Northern Africa.

However, there were some notable exceptions. Residual variation in NDVI caused by the BRDF was most severe in a water limited wheat crop (± 0.05 NDVI units).

Lee and Kaufman (1986) have assessed the effect on the NDVI due to atmospheric and BRDF effects using a computer model. The model uses radiative transfer theory, and assumed atmospheric profiles, to estimate the upwelling radiance as a function of viewing geometry. While they found significant effects on the upwelling radiance (consistent with results reported in Section 2.4.2), the effect on the NDVI was relatively minor (± 0.04 NDVI units). This was attributed to the BRDF effect being approximately equal in both the red and near infrared regions. They noted that the NDVI performed best under clear atmospheric conditions at a high sun angle and that directional reflectance in the atmosphere had a greater effect on the NDVI. This result confirms other similar results derived using computer modelling (Holben and Fraser, 1984; Holben, 1986).

Gallo and Eidenshink (1988) studied the viewing angle effects on NDVI using simultaneous data from the NOAA-9 and 10 satellites. The combination of data from a morning and afternoon overpass allowed the effects of view geometry to be studied. They found substantial effects in the individual bands (one and two), but that the NDVI substantially reduced these effects across scan lines for each data set. A slight decline in NDVI was reported as the satellite viewing angle increased. The NDVI computed from NOAA-9

observations was found to be approximately 40 percent higher than that from NOAA-10. This difference was not explained, although a linear regression was proposed to correct the NOAA-10 data to that observed by NOAA-9 (R^2 = 0.92).

These results were generally confirmed in field experiments undertaken to measure the red and near infrared BRDF (in the AVHRR bands) under a variety of atmospheric conditions ranging from clear to hazy (Deering and Eck, 1987). Deering and Eck found higher NDVI values on clear days than hazy days (~ 0.07 NDVI units). The variation of NDVI with view angle was in the order of ± 0.05 NDVI units. However, a soya bean crop was found to have higher NDVI values on hazy days which was attributed to the architecture of the canopy.

Recent studies have looked at using these directional reflectance effects to recover specific biophysical variables (Kimes et al., 1991; Kimes and Holben, 1992; Li and Strahler, 1986; Jupp et al., 1986; Jupp and Woodcock, 1992). In these cases, specific mathematical models of the vegetation canopy are formulated and, using measured reflectance, estimates are made of canopy attributes such as height and crown cover, using standard model inversion techniques.

2.4.4 Image Rectification

Accurate image rectification is essential for any vegetation monitoring program using remotely sensed data. This allows both the comparison of observations in a temporal context, and the use of ancillary data in a geographic information system (GIS) (Cihlar et al., 1989; Loveland et al., 1991; Roderick and Smith, 1992; Brook et al., 1992). To achieve this, the image data are first referenced in a geocentric coordinate system, and then resampled to a standard map projection system.

The large scan angle used on the NOAA satellites (± 55 degrees) creates geometric distortions of a greater magnitude than other earth resource satellite systems such as Landsat. Due to this large scan angle, the location of NOAA images requires the formulation of a rigorous mathematical model to describe the sensor geometry. This contrasts with the common usage of empirical polynomial based mapping procedures used with Landsat and SPOT imagery (Jensen, 1986).

The orbital elements required for image rectification may be estimated using ground control points (GCP's) or derived from existing satellite tracking information (Emery et al., 1989). The use of several GCP's can result in accuracies of less than 1 pixel (Emery and Ikeda, 1984) given an appropriate orbital model (Legeckis and Pritchard, 1976). From a practical viewpoint, the selection of

numerous GCP's is possible over (cloud free) land surfaces. Over the oceans, no easily identifiable features are available.

An alternative method is to use predictions of the orbital elements, derived from tracking station measurements, such as the TBUS bulletin service available from NOAA (Marsouin and Brunel, 1991). Using this TBUS ephemeris data, Marsouin and Brunel were able to achieve accuracies of ± 3 km in position. To achieve this they incorporated clock error corrections (and predictions). Errors in the on-board satellite clock have been noted in other studies (Brush, 1988; Kone, 1992). Since the satellite travels in an approximately north-south direction, the clock errors generate locational error primarily in latitude (i.e. the along-track direction).

Marsouin and Brunel (1991) analysed the spatial structure of navigation errors in AVHRR imagery and attributed the along track error to clock bias. Errors in the across track direction were attributed to misalignment of the sensor on board the spacecraft. Due to the systematic nature of the error, it is possible to achieve accuracies of ± 1 km by selecting one or two additional GCP's, and applying a bulk shift (Emery et al., 1989). The additional GCP's may be selected by operator intervention or using automated image matching techniques.

The consequences of navigation error have received little attention in the literature, which has concentrated on atmospheric

corrections. Holben (1986) noted the interaction between the MVC process and locational error. Given locational error, areas of high NDVI, which are adjacent to areas of low NDVI, will tend to artificially expand when using MVC. Since MVC selects the maximum value, the high values will be smeared over the local neighbourhood. A classic example of this is water/land boundaries, such as a coastline. Land, typically has a higher NDVI than water. The use of the MVC technique, and presence of locational error, will select NDVI values for land over true water pixels.

The effect of navigation error on the results of monitoring using remotely sensed images was further explored by Townshend et al. (1992). They artificially 'moved' images to synthesise navigation errors ranging from 0.2 to 10 pixels. The effect of the navigation error was assessed by subtracting the original and synthesised image and computing spatial statistics of this difference image. Various statistics, such as the semi-variance (Jupp et al., 1988), were calculated and compared for the various shifts. A relationship was found between the spatial structure of the image and the semi-variance calculated for each artificial shift. Where spatial frequency was high, such as regions with small agricultural fields, accurate registration was critical to derive the correct difference. For four of the areas studied (seven areas studied in total), they found a locational error of only one pixel (a typical value quoted in the literature) created between 50 to 100 percent error in the actual difference value. In these areas, to reduce the error to ± 10 percent

of the true value required locational accuracies of less than 0.2 pixel. In the other areas studied, this level of accuracy could be achieved with locational errors of between 0.5 to 1 pixel.

In essence, their results suggest that monitoring changes over edge features will generally be impossible. Over edges, small changes in spatial position generate large changes in the signal received, as the proportion of cover types varies on either side of the edge. A good place to generally check this result is over the coastline, where a ready made, and constant edge exists. This effect is explored further in Chapter 6.

2.4.5 Vegetation Indices

Vegetation indices have been used extensively as a technique to extract vegetation information from remotely sensed multispectral measurements. All of the indices essentially seek to collapse a multivariate data set of observations to a single index that is related to some biophysical parameter of the target, such as leaf area index (LAI), biomass or height.

The main reasons for using vegetation indices are:

(a) Reduce variation in observations due to viewing geometry,

(b) Extract vegetation information from an observation of a mixed soil-vegetation scene.

Aspects of (a) have been discussed in Sections 2.4.2 and 2.4.3. This

section focuses on the application of vegetation indices to reason (b).

Two distinct vegetation canopy types can be recognised in terrestrial ecosystems, closed (LAI > 1) and sparse (LAI < 1) (Graetz, 1990). In sparse canopies, since leaf area index (LAI) is less than one, this implies sunlight reaches and reflects off the background soil and is recorded by the sensor. To further complicate matters, some plant canopies, such as crops and grasses, change from a sparse to closed architecture during a growth period. The major spectral components of a vegetated scene include vegetation (leaf and woody material), soil and shadow. For vegetation monitoring purposes, it is necessary to extract the vegetation information, independent of any variations in soil reflectance or shadow.

Two classes of vegetation indices can be identified in the literature:

(a) Linear combinations of original bands, such as the greenness index (Kauth and Thomas, 1976), perpendicular vegetation index (PVI) (Richardson and Wiegand, 1977), geometric based indices (Pech et al., 1986) and PD45 (Pickup et al., 1993),

(b) Non-linear ratio-based indices, such as the simple ratio (Pearson and Miller, 1972), NDVI (Rouse et al., 1974), soil adjusted vegetation index (SAVI) (Huete, 1988), transformed soil adjusted vegetation index (TSAVI) (Baret et al., 1989), and other as yet unnamed indices (Price, 1993).

These indices have been shown to be related to a number of biophysical variables, including photosynthetically active biomass (Tucker, 1979; Wiegand and Richardson, 1984), the rate of photosynthesis (Sellers, 1985; Tucker and Sellers, 1986), and LAI (Holben et al., 1980; Asrar et al., 1984; Hatfield et al., 1985; Wiegand and Richardson, 1990; Wiegand et al., 1992). As well as the atmospheric and bidirectional reflectance effects previously noted, the colour of the soil background has been found to effect these indices (Huete et al., 1984; Huete and Tucker, 1991; Huete and Jackson, 1987; Baret et al., 1989; Baret and Guyot, 1991; Huete, 1988; Jasinski, 1990; Williamson, 1989).

Kauth and Thomas (1976) developed a linear combination of four original MSS (multispectral scanner) bands to rotate the data space into a new data space capable of physical interpretation. The four new bands could be physically interpreted as a soil line (or plane), green vegetation, yellow vegetation (i.e. senescence) and a channel of noise (which they called the 'non-such index'). The transformation became known as the tasselled cap. The first two new axes typically contained 95 percent of the image variance, and the fit for bare soil spectra along the soil line was excellent (some 98 percent of the variance).

A cross plot of the near infrared and red reflectance of a typical 'natural' scene contains a clearly identifiable structure, which is described as the tasselled cap or cover triangle (Kauth and Thomas,

1976; Graetz and Gentle, 1982). This structure has been confirmed and used in numerous previous studies (Kauth and Thomas, 1976; Richardson and Wiegand, 1977; Graetz and Gentle, 1982; Huete et al., 1984; Elvidge and Lyon, 1985; Huete et al., 1985; Huete, 1987; Foran, 1987; Huete, 1988; Williamson, 1989; Jasinski, 1990; Major et al., 1990; Pickup et al., 1993), and forms the basis of remote sensing of vegetation in these wavelengths. A simplified plot of the N-R space is shown in Figure 2.4.

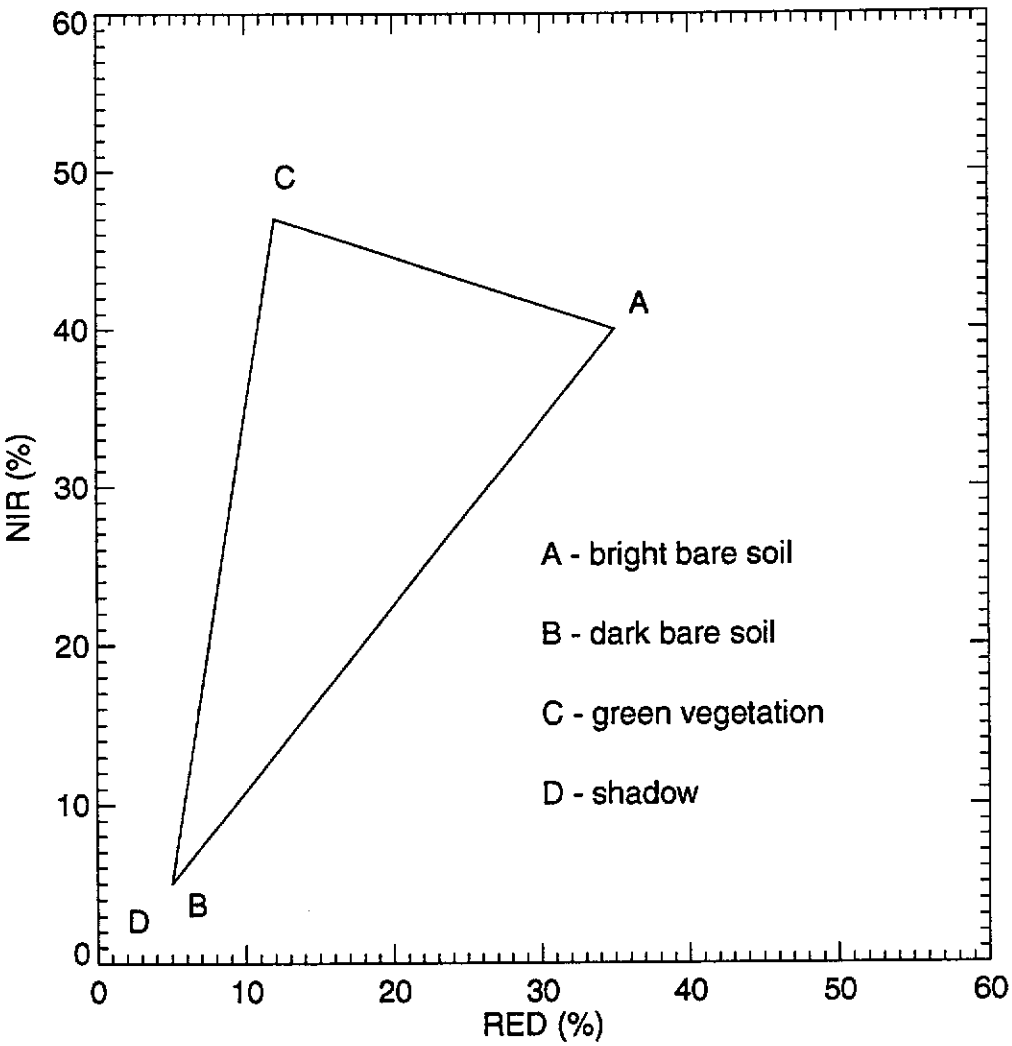

Figure 2.4 Typical plot of NIR and RED reflectances

Many of the initial studies were empirically based and used vegetation indices for convenience (Price, 1993; Huemmrich and Goward, 1992) rather than physical principles. Principally through the work of Huete, a more rigorous background has been developed to the use of vegetation indices. Huete (1987) developed a simple canopy reflectance model that included a variable soil background and first order interactions between the vegetation and soil. The model was verified using an experimental data set involving a cotton canopy over variable soil backgrounds. Using these results Huete proposed a new index, the soil adjusted vegetation index (SAVI), which approximates the radiation interactions between the canopy and the underlying soil (Huete, 1988).

The nature of vegetation indices has been commonly demonstrated using contour maps of the index in the NIR - R space. Figure 2.5 is a contour map of the NDVI. The isolines shown in Figure 2.5 indicate that the NDVI is based on a soil line along the line NIR = R. Most soil lines do roughly follow this behaviour (Baret et al., 1989; Graetz and Gentle, 1982; Pickup et al., 1993). The widespread success in the global application of the NDVI is attributed to this phenomena. In many studies the soil line has actually been found to be a soil 'cloud' (Huete et al., 1984; Williamson, 1989), and hence residual variation in the vegetation index due to soil colour can be expected. In addition, atmospheric influences can also modify the position of the soil line in each image (Pickup et al., 1993).

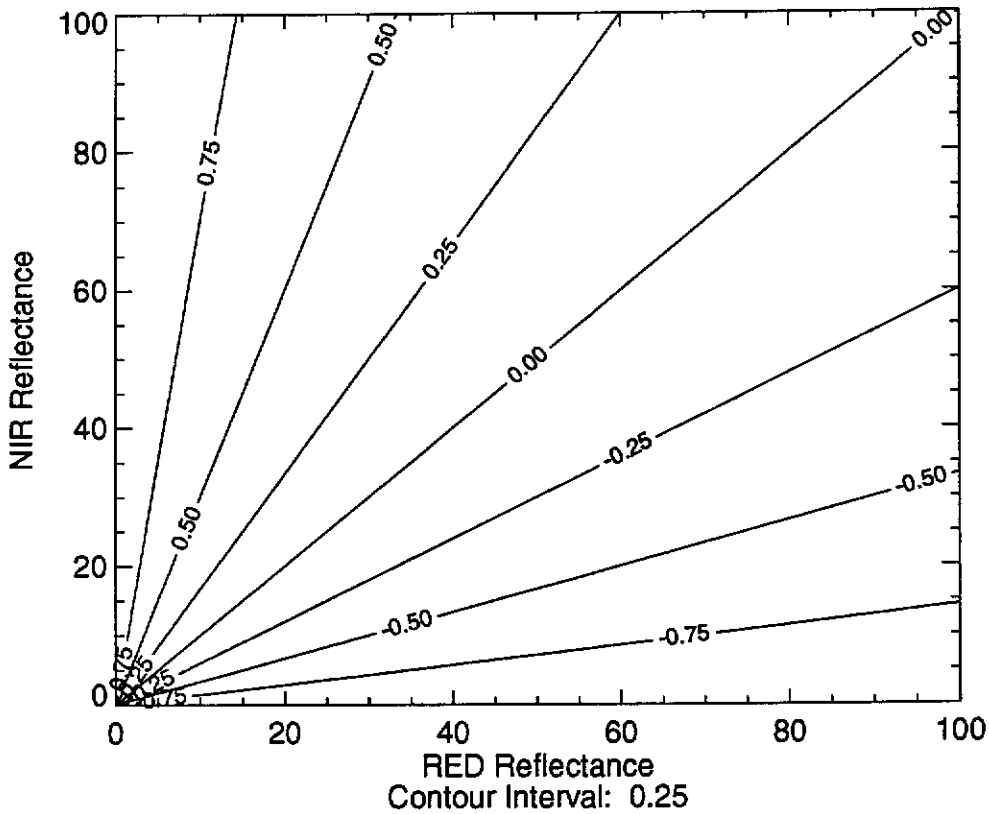

Figure 2.5 Contours of the NDVI function

Indices, such as the PVI (Richardson and Wiegand, 1977), the geometric based indices of Pech et al. (1986) and PD45 (Pickup et al., 1993) require the analyst to identify a soil line. This has a further advantage in that the effect of variable atmospheric influences is minimised (Pickup et al., 1993). In contrast, the simple ratio (N/R), NDVI, SAVI and TSAVI all assume an invariant soil line (see contour diagrams in Baret and Guyot, 1991). While certainly easier to compute, they are not ideal for vegetation monitoring. A variable soil

background can cause changes in the index, and confuse the interpretation of imagery (Huete and Tucker, 1991; Huete, 1984; Holben, 1986). Clearly these results are due to the actual soil line (or cloud) not agreeing with that proposed by the vegetation index used.

Price (1992, 1993) has used the previous concepts to propose techniques for recovery of biophysical variables (LAI and fractional green vegetation cover) from near infrared and red reflectance. This involves specification of a (simple) canopy model, and mathematical inversion techniques. The user is required to identify a soil line in the data. Sensitivity studies of the relation between biophysical canopy parameters and vegetation indices indicate the importance of the vegetation canopy architecture (Huemmrich and Goward, 1992; Begue, 1993). This accords with the results of Price, and suggests the need for prior knowledge of the vegetation canopy geometry to select an appropriate canopy model for use with remotely sensed data sets. Price (1993) argues that the prior knowledge is a pre-requisite to the successful use of remote sensing to characterise earth surface processes.

2.4.6 Temporal Composites

Compositing techniques such as the MVC aim to create a cloud free image of the scene or study area. The fundamental parameters to be decided are the length of time over which to

composite, and the technique to be used. The length of time is clearly a function of the application in question, the typical amount of cloud cover experienced, and the orbital geometry of the sensor.

For example, for monitoring of herbaceous vegetation production in an arid environment, two weeks (or a month) might be an appropriate observation interval. Next, the analyst must check how much residual cloud cover will typically contaminate the images over this period. A trade-off situation exists between temporal frequency and removal of cloud. In some areas of the globe, such as the tropics, a year might be required to construct a completely cloud free image (Justice et al., 1985). The compositing period chosen should also consider the time period over which the orbital geometry repeats. For NOAA satellites, a nine day repeat period exists in viewing geometry (Goward et al., 1991), and nine, 18, or some other multiple would be preferred on technical grounds. A 10 day composite period was recommended by the International Geosphere Biosphere Program (IGBP) (Townshend, 1992) based on orbital geometry considerations.

The dominant technique used to composite images has been MVC (Holben, 1986). By selecting the maximum NDVI observed over the composite period, this has been shown to remove both cloud cover and minimise atmospheric effects in the signal (see Section 2.4.2). However, other techniques have also been proposed. Gutman (1987, 1989) analysed the variations in NDVI as a function

of viewing geometry over a nine day cycle on the Great Plains (USA), and found a bias caused by bidirectional viewing geometry. Gutman (1989) subsequently proposed that the composited value should be 80 percent of the maximum value as it gave a better representation of mean growing conditions.

2.5 Net Primary Production Studies

Annual estimates of net primary production (NPP) at continental and regional scales have significant benefits for such diverse interests as drought monitoring (Henricksen, 1986; Gutman, 1990; Peters et al., 1991), crop and herbage production (Tucker et al., 1985b; Henricksen and Durkin, 1986; Prince, 1991a), food security (Hutchinson, 1991) and understanding links between global climate change and vegetation production (Tucker et al., 1986; Box et al., 1989). A clear understanding of what is meant by NPP is necessary before looking at applications.

NPP is defined as the difference between gross primary production (GPP) and respiration (RES) as shown in Equation 2.2.

$$NPP = GPP - RES \tag{2.2}$$

GPP is the amount of assimilate produced by photosynthesis, while RES represents the energy used for maintenance of various plant functions (Odum, 1963; Box et al., 1989). The above ground standing biomass is the integral of above ground NPP less vegetation

losses over time. This integral can be expressed as a difference equation of the form (adapted from Box et al., 1989):

$$B_t = B_{t-1} + NPP_t - LF_t - H_t \qquad (2.3)$$

where

B_t = *standing biomass at time t*

B_{t-1} = *standing biomass at time t–1*

NPP_t = *NPP at time t*

LF_t = *litter fall (or senescence) at time t*

H_t = *harvesting by herbivores at time t*

Typical values of NPP range from 0.5 grams per sq m per day for desert environments to 10 grams per sq m per day for highly productive agricultural ecosystems and tropical rainforests (Odum, 1963; Walter, 1984). The nature of the relationship shown in Equation 2.3 will vary depending on the form and life strategy of the vegetation. For annual crops and many grasslands, the initial biomass over any season is virtually zero. While for forest environments, B may be far greater than the increments accrued through time.

Two basic approaches have been used for the estimation of NPP. The first relies on empirical observations relating transpiration to productivity in various plant species (Briggs and Santz, 1913). These techniques have been applied in crop modelling applications at both local (Doorenbos and Kassam, 1979; van Keulen, 1975) and

larger scales (Pittock and Nix, 1986; Box et al., 1989). Satellite data have been used to estimate evaporation from terrestrial ecosystems, and these estimates can be used in empirical relationships to directly estimate NPP. Estimates of B are normally derived using a model such as that shown in Equation 2.3 (see McKeon et al. (1982) for an example in use in Australian rangelands).

The second approach is based on theoretical considerations. NPP can be related to the amount of solar radiation absorbed by the plant canopy (Monteith, 1972; Warren Wilson, 1981; Charles-Edwards et al., 1986) and subsequently converted to dry matter. This relationship is expressed as (Charles-Edwards et al., 1986):

$$NPP = (e \times IPAR) - v \qquad (2.4)$$

where

e = *conversion efficiency (solar energy to dry matter)*

$IPAR$ = *intercepted PAR*

PAR = *photosynthetically active radiation*

v = *loss of plant matter (any cause)*

Various techniques have been used to calculate a value of e from experimental results. The use of different experimental techniques makes it virtually impossible to compare values of e without careful scrutiny of the experimental technique used (Prince, 1991b; Charles-Edwards et al., 1986).

IPAR can be expressed as:

$$IPAR = f_{IPAR} * PAR \quad (2.5)$$

where

f_{IPAR} = *fraction of PAR intercepted by canopy*

(*range* 0 - 1)

The NDVI has been shown to relate (linearly) to the proportion of PAR (f_{IPAR}) which is absorbed by the canopy in modelling studies (Kumar and Monteith, 1982; Asrar et al., 1984; Sellers, 1985; Asrar et al., 1992; Huemmrich and Goward, 1992) and from experimental evidence (Kumar and Monteith, 1982; Hatfield et al., 1985; Gallo et al., 1985). Over large scales, PAR is primarily a function of season, latitude and atmospheric conditions (Monteith, 1972) and can be estimated from simple formulations (Charles-Edwards et al., 1986, pp. 192-200). When considered at local scales, available PAR may be substantially modified by topography and the arrangement of plants in a sward or crop, which both affect the occurrence and position of shadows.

Assuming that NDVI may be substituted for f_{IPAR}, Prince (1991b) proposed that the instantaneous NPP at time t may be estimated by the relation:

$$NPP_t = e_t \times (NDVI_t \times PAR_t) \quad (2.6)$$

Total seasonal production is estimated by integrating Equation 2.6, over the growing season as follows:

$$B = e * \int (NDVI * PAR) \quad dt \tag{2.7}$$

Both Equations 2.6 and 2.7 explicitly ignore leaf fall and herbivory. The effects of this should be minimal as the NDVI is a measured quantity which will respond to changes in standing biomass and the subsequent effect on f_{IPAR} caused by these factors. The modelling framework developed ignores plant phenology. Phenology can be considered using empirical evidence such as crop calendars (Gupta, 1993). By using crop calendars in an agricultural application, the start and end times for integration can be defined to explicitly include phenology and cultural practices. In natural environments various species respond differently depending on the time of the year and other species specific factors. In Western Australia, Mott (1973) has observed this phenomena.

The integration technique described above was first investigated by Tucker et al. (1981). The NDVI was computed from field based measures of R and N, taken throughout the growing season. Total above ground biomass was also sampled throughout the growing season. Some 79 percent of the variance in total above ground accumulated dry matter was explained by the NDVI integral. The study concluded that it was feasible to emulate the results using

the NOAA-AVHRR satellite on a regional and global scale.

Subsequent studies in Northern Africa (Tucker et al., 1983, 1985b) using observations from NOAA-AVHRR confirmed the speculation. Field measurements of herbaceous biomass were taken at approximately 60 ground sampling sites (this varied each year) throughout the growing season for the years 1980-1983. The integrated NDVI was computed between mid July and early October (start and end of the growing season in the study area). The resulting integral was regressed on total standing dry biomass at the end of the season, with observations pooled for the years 1981-1983. The resulting linear regression explained 69 percent of the variance in standing biomass.

The linear relationship was then used to predict total dry biomass across the study area for each year. Typical annual rainfall for the study area varied from 79 to 465 mm during the study. The authors noted a lack of sensitivity in the integrated NDVI - biomass relationship for areas of low biomass (biomass < 250 kg/ha). To overcome this they regressed maximum NDVI throughout the season on the above ground biomass for these regions (R^2 = 0.64). They concluded that the technique was viable for monitoring seasonal production in areas with a rainfall range of 250 - 500 mm and a woody vegetation cover of less than 10 percent.

Implicit in the assumption of integrating NDVI in the above study are two factors:

(a) That e (efficiency), remains constant throughout the life history of a plant,

(b) PAR is a constant.

While it is known from experimental evidence that various environmental factors affect e (see review in Prince, 1991b), it is likely that when considered over a growth season e remains relatively constant within a species (Kumar and Monteith, 1982; Prince, 1991b). The second assumption is clearly incorrect (Monteith, 1972; Steven et al., 1983; Choudbury, 1987). Prince (1991b) argues that variation in PAR is minor in comparison to the variation in f_{IPAR} (Monteith, 1977) and is thus not a major source of error at a gross level.

Prince (1991a) summarised previous NPP studies in Northern Africa which used NOAA data. Nine extensive field data sets were used covering the 1984-1988 period. A regression between annually integrated NDVI and end of season biomass reported an R^2 of 0.80. Diallo et al. (1991) working in Western Africa (Senegal) explicitly considered biomass accumulated on trees and shrubs in addition to herbaceous material. The regression relationship (to integrated NDVI) was improved by some 16 percent when biomass production on trees was included in the regression.

Foran and Pearce (1990) applied the integration technique at a regional scale in Central Australia for use in pastoral management. Due to a lack of a reliable growing season in this region, they had no defined starting and ending dates. They weighted summer growth as twice the value of winter growth. This was based on personal knowledge that preferred pastoral grasses will only germinate following summer rainfall. In addition, they interfaced the NDVI images with a raster based GIS for reporting purposes. Individual reports on green vegetation were prepared for each property. One interesting feature is the relationship between green vegetation cover and NDVI (Foran and Pearce, 1990, Figure 1, p. 201). While a regression was proposed to model the data, these data could have also been modelled using a binary classification. The field sampling sites either received or missed rainfall.

Danaher et al. (1992) used multi-temporal NDVI (44 monthly images) to estimate standing tree cover over the entire state of Queensland (Australia) for subsequent use in pasture simulation models. They noted that the NDVI time series in areas of high tree cover had lower variance than sites with low tree cover. They then classified tree cover using the mean and CV (coefficient of variation) and other higher moments (such as skewness and kurtosis) of the NDVI time series. Using field data, a log linear model, relating mean NDVI to basal area was established (R^2 = 0.62). A conceptual model (Danaher et al., 1992, Figure 6, p. 133) was proposed that described major vegetation communities in the mean-CV data space. Typically,

annual dominated communities (crops, grasslands) had a medium mean NDVI and high CV. In contrast, areas with a high perennial component (woodlands, rainforest) had a higher mean and lower CV.

Various other studies have been conducted which largely confirm the relationships discussed above. Seasonally integrated NDVI have been correlated with several parameters, including rainfall (Hielkema et al., 1986; Foran and Pearce, 1990; Davenport and Nicholson, 1993; Dregne and Tucker, 1988), estimates of soil water (Henricksen and Durkin, 1986; Cihlar et al., 1991), actual evapotranspiration (Seguin et al., 1989; Kerr et al., 1989; Smith and Choudbury, 1990), literature estimates of NPP (Box et al., 1989; Goward et al., 1985) and land surface temperature (Achard and Blasco, 1990; Toure et al., 1991; Smith and Choudbury, 1991).

2.6 Phenological Studies

Phenology involves the study of periodic phenomena in plants (Abercrombie et al., 1980). Such phenomena can include the time of, and mechanisms responsible for, events such as germination, growth, flowering and death. The high temporal frequency of NOAA AVHRR data provides opportunities to study plant phenology over large scales previously not available. Previous Australian studies (Mott, 1973; Pook, 1984; Friedel et al., 1993) using direct observation of natural plant life cycles have been limited, largely due to the logistical difficulty of running long term experiments. Over

larger scales, growth periods have been estimated using readily available climatic data (Fitzpatrick et al., 1967; Fitzpatrick and Nix, 1970; McAlpine, 1970; McCown, 1981; Smith and Johns, 1975; Smith and Stephens, 1976). The extreme variability of rainfall over the Australian continent, and sparsity of the rainfall recording network, makes it difficult to use climatic data for monitoring the spatial variation in vegetation growth.

A key element of phenological studies is to study the dynamic functioning of vegetation. Vegetation functions as an integral component of both the global carbon and hydrologic cycles, through primary production (carbon fixation) and evapotranspiration (surface energy balance) (Chahine, 1992; Tucker et al., 1986). Existing vegetation mapping in Australia and other parts of the world has largely been based on vegetation community structure and floristic composition (Carnahan, 1981; Beard and Webb, 1974). Key elements of the vegetation function can be inferred from structural information (Specht, 1981; Graetz, 1990). However, the map based information is static, while vegetation is itself dynamic. Improved knowledge of vegetation dynamics is a key element of global change studies (Graetz et al., 1992) and can be used to improve our understanding of both natural and agricultural ecosystems.

Initially, studies of vegetation process dynamics using NOAA AVHRR NDVI data were qualitative in nature. Time traces were extracted from multi-temporal image data and displayed for various

biomes, across a number of continents (Justice et al., 1985; Townshend and Justice, 1986; Justice et al., 1986). These time traces clearly differentiated between major vegetation types based on the timing of seasonal growth as well as NPP. Justice et al. (1985) noted the difficultly in ground truthing such frequent and large scale information.

In a study of the phenology of various African land cover types Justice et al. (1986) noted the variability in time traces within a single vegetation type. They attributed this to variability in the timing and amount of rainfall. That study sounds a clear warning for analysts using traditional image classification routines to define land cover types from multi-temporal NDVI data. Traditional image classifications typically attach equal weight to each observation in the time series. In the above case, the known homogeneous land cover would have been classified into several cover classes simply because of differences in the timing and amount of rainfall.

This strong relationship between NDVI and rainfall has been noted in numerous studies in arid and semi arid areas (Henricksen and Durkin, 1986; Dregne and Tucker, 1988; Foran and Pearce, 1990; Azzali, 1991; Maselli et al., 1992; Davenport and Nicholson, 1993; Bonifaco et al., 1993). In temperate climatic regions, NDVI time series from the NOAA satellite have been related to changes in actual evapotranspiration (AET) (Cihlar et al., 1991). Using ground based reflectance measurements to compute the NDVI, Peterson

(1992) could distinguish between growth on soils of varying nutritional status. This result suggests the observed NDVI is better able to integrate other site factors affecting plant growth than are simple climatic indices.

A lag between rainfall (or soil water) and NDVI time series observations has been noted by a number of researchers (Henricksen and Durkin, 1986; Davenport and Nicholson, 1993; Kennedy, 1989). Using lag correlation analysis, Henricksen and Durkin (1986) analysed the lag between NDVI time series and a moisture index. The moisture index used in that study is based on the ratio between soil moisture and potential evapotranspiration and had previously been used to estimate NPP. They found NDVI to be a very strong indicator of the start of the growing season (R^2 range from 0.99 to 0.49, with typical values of 0.80). In their study area, an NDVI greater then 0.1 was used to indicate the start of growth, and an NDVI of less than 0.22 indicated the cessation of that growth. The lag noted in the NDVI-rainfall relationship relates to the time for vegetation to respond to soil water inputs.

The interpretation of NDVI time series measurements is dependant on the vegetation cover type. Townshend and Justice (1986) found similar NDVI values had different meanings in different cover types, and recommended that a stratification of the image data was required for correct interpretation. This compositional effect has also been found in Western Australia (Cridland et al., 1994). Kogan

(1990) proposed a new index, the VCI (vegetation composition index) to overcome the problems of differing vegetation types. In essence, the VCI rescales the current value of NDVI into the historical range for that particular site, and expresses the result as a percentage. This index potentially avoids the need to stratify an area before analysis.

The time series NDVI measurements have often been found to be noisy due to residual cloud, atmospheric and BRDF effects. A number of researchers have used smoothing techniques to improve the NDVI time series (Townshend and Justice, 1986; Malingreau, 1986; Viovy et al., 1992). Van Dijk et al. (1987) proposed retaining all NDVI measurements (rather than compositing them) and then applying smoothing operations on these noisy series. Various techniques were evaluated, but the selection of a specific technique was dependant on the nature of the application for which the data are to be used. Rather than adopt specific mathematical treatments, Lo Seen Chong et al. (1993) designed an algorithm to recognise cloud and atmospherically affected NDVI measurements from composited time series. This avoided using these measurements in the smoothing process and subsequently corrupting the 'good' data in the series.

Ehrlich et al. (1994) identified a need to develop better quantitative tools for extracting information from multi-temporal imagery. One technique along these lines was developed by Lloyd

(1989a, 1989b, 1990). He proposed a classification scheme which used the timing of specific events in addition to the magnitude of the NDVI to describe the time series. This scheme has been designed as a global phenological classification scheme. Some typical variables derived from the NDVI time series are (Lloyd, 1990):

(a) Time of maximum photosynthetic activity,

(b) Length of growing season,

(c) Annual mean photosynthesis.

These variables were computed using appropriate definitions on a pixel by pixel basis for each image in the time series, and then simplified to three or four appropriate classes in each category. By combining all possible combinations of classes in each category, 21 'super-classes' were defined. One distinct advantage of this technique is the derived classes are easily interpreted, as they were defined by the analyst. This technique was used to prepare global maps of vegetation phenology (Lloyd, 1990).

Principal components analysis (PCA) has long been used in remote sensing to deal with multi-temporal image data for change detection purposes (Lodwick, 1978). Tucker et al. (1985a) used PCA to classify continental land cover over Africa. In a more recent study, Eastman and Fulk (1993) used standardised PCA (Jensen, 1986) to classify a 36 month time series of NDVI data over Africa. The resulting component images were analysed and various mechanisms were proposed for the patterns evident in the images. However, in contrast to the work of Lloyd, a major limitation of PCA is the need

for the analyst to interpret and explain the classes. The work of Lloyd results in classes that are capable of interpretation using the original definition of the classes.

An alternative and new technique for summarising the time series image data has been developed by Menenti et al. (1991) to classify agro-ecological zones. In this technique, a time series of (equally spaced) observations is created for each pixel in the multi temporal image data set. A FFT (fast fourier transform) is then used to transform the series to the frequency domain (Hamming, 1989). From the frequency domain, a phase and power spectrum can be computed for each of the individual harmonic frequencies. The power at each harmonic indicates how much of the variance of the total signal occurs at that frequency. The phase indicates when it occurs.

In NDVI time series there is a clear seasonal signal, relating to a period of 12 months, which will clearly show out in the power spectrum. Menenti et al. (1991) settled on periods at 12, 6 and 3 months as being indicative of differences in growth conditions for ecological purposes. At the corresponding frequencies, the power and phase were extracted, and various colour (three band) images synthesised. Maximum likelihood classification of the power and phase images (at the above frequencies) produced classes that were clearly different from the existing mapping. On this basis, they concluded that the FFT based technique could give a better

representation of agro-ecological zones than existing climatic indices. During the study, no attempt was made to look at the actual climatic conditions for that year, and compare those data with the map based classification. Since the map based classification used 'average' climatic values, it is possible that the weather experienced in the region (Zambia and Somalia) at the time of this study was different from the 'mean' climatic variables used to prepare the map.

2.7 Summary

A number of significant issues have been identified based on previous work. These are set out below, and were used as a guide for the development of this research.

The NDVI is only one of a number of vegetation indices which have been used for the extraction of vegetation information from spectral observations in the red and near infrared regions of the spectrum. Most of these indices have been based on a soil line either explicitly (e.g. PVI of Richardson and Wiegand, 1977) or implicitly (NDVI, SAVI).

Many of the soil lines have actually been found to be soil clouds. Thus, even in indices which use an explicit soil line, there will be variation in that index due to residual variations in soil colour not modelled by a soil line. Additional sources of variation in vegetation indices are the interaction between the soil background

colour and the vegetation canopy.

The NDVI values reported by different studies should theoretically be comparable. Unfortunately, this is not the case. Variations exist depending on whether the NDVI was computed with digital counts, radiances or reflectances. Thus, when using the results from other studies, care needs to be taken to ascertain how the NDVI was computed in that study. This situation is compounded by the numerous methods used to rescale the NDVI for representation in integer based image processing systems.

The NDVI is computed from measurements of red (R) and near infrared (N) reflectance. Numerous studies have quoted the effect on the NDVI due to errors in N and R caused by atmospheric contamination of the signals. In contrast, it has been shown that quantisation of the signal can also cause large errors in the NDVI. Quantisation is a fundamental process underpinning all digital systems, and sets a finite limit on the precision with which samples can be represented. It would be a waste of time to be making corrections to N, R and the NDVI which were significantly smaller than the finite limit of precision for these data. This requires the development of a formal statistical framework.

Conversion of the digital counts recorded by the AVHRR instrument to radiance is a linear calibration problem requiring a gain and offset. These values were originally determined at the time

of construction of each instrument, resulting in a pre-flight calibration. A number of studies have established that the pre-flight calibration parameters have changed following launch on all NOAA satellites. Two distinct changes have been recognised:

(a) Large change in calibration following launch,

(b) Slow drift in calibration over time.

The changes in calibration for the individual channels will affect the NDVI if those changes are not identical. It is anticipated that this calibration problem will need to be addressed in this study.

The maximum value compositing (MVC) technique has been used extensively to remove cloud from time series images. This technique selects the maximum NDVI from a number of images and writes that value to the output composite image. An interaction between the MVC technique and locational accuracy of the imagery has also been noted. In particular, along land/water boundaries, MVC ensures the NDVI from the land is always accepted as the final output NDVI. Thus, small locational errors are compounded along these boundaries, and features with a high NDVI will tend to 'spread' across the image.

Integrals of the NDVI time series have been used to estimate NPP over continental sized regions. The validity of this approach is based on a linear relationship between NDVI and f_{IPAR}. Many studies have used integrals of the NDVI to provide estimates of NPP. In many cases, rainfall data has been used as a surrogate for ground

truth of these seasonal production estimates due to the logistical difficulties of acquiring actual biomass data.

The bounding dates for integration of the NDVI have mostly been fixed by using a crop calendar or cultural knowledge. In the arid and semi-arid rangelands of Australia, rainfall is highly variable through space and time. There are no generally fixed times for seasonal events. This is anticipated to pose a problem for the estimation of NPP in the Western Australian rangelands.

The development of new techniques for processing time series imagery has not proceeded with the same pace as the measurement techniques. In particular, the acquisition frequency of NOAA-AVHRR imagery challenges traditional approaches developed for the analysis of high resolution earth resource satellites such as Landsat and Spot. One of the most effective techniques is the inspection of time series plots extracted for a single or group of pixels. However, it is not possible to inspect all possible time series in an image based data set. New analysis techniques will be required, to take advantage of the highly frequent multi-temporal data sets now becoming available.

Chapter 3

STUDY AREA AND RESEARCH DATA

3.1 Introduction

The satellite time series data coverage used for this study was limited to Western Australia, and the surrounding ocean areas. This section introduces both the satellite data, and other supporting data sets which have been used as an aid to interpretation of the satellite data.

The use of ancillary data is essential in any remote sensing study (Jensen, 1986). The minimal supporting data requirements, identified in this study for broad scale interpretation of NDVI data (from NOAA AVHRR), include a land use map, climatic data and existing vegetation mapping. An overview of the data sets and their potential use in the study is presented in the following sections.

In addition to these data sets, commonly used names for several regional areas within Western Australia have been identified. These regional areas are referred to extensively in later chapters and have been included to assist readers not familiar with the geography of Western Australia.

3.2 NOAA-AVHRR Satellite Data

A long term sequence of 117 monthly NDVI (GAC) satellite images was acquired from Dr C J Tucker (NASA Goddard Space Flight Centre) by Dr R D Graetz (CSIRO-Canberra) and Dr R G C Smith (CSIRO-Perth) to support the study. Details of this data set are shown in Table 3.1.

Temporal resolution	Monthly
Image Dates	July 1981 to March 1991 inclusive
Total No. of Images	117
Data Type	GAC
Processing Technique	Maximum value composite (MVC)
Atmospheric Corrections	None
No. images used in monthly composite	~ 30 (one per day)
Data Format	NDVI
Original Source	NASA Goddard Space Flight Centre
Calibration data	NOAA pre-flight
Map Grid	Geographic
Map Grid Resolution	3 minutes (square)
Coordinate of upper left hand corner	111° 58' 30" E, 12° 58' 30" S
Coordinate of bottom right hand corner	130° 01' 30" E, 36° 01' 30" S

Table 3.1 NOAA NDVI time series image data set

The data are a subset of a global GAC (NDVI) data set created by NASA. An overview of the processing techniques used in the creation of this data set is given Tucker et al. (1991). The global and Australian NDVI images shown in Graetz et al. (1992, pp. 22-25) are also from the same original data set.

The NDVI data were originally supplied in a two byte integer format where 0 to 1023 mapped into an NDVI range of -1 to 1. The data were subsequently reprocessed to a single byte range, where 0 to 200 mapped into an NDVI of -1 to 1. This decision was based on the results of a study described in Chapter 4 of this thesis.

3.3 Land Use

A knowledge of land use is essential to differentiate between vegetation that is managed in a predominantly agricultural environment and the native vegetation elsewhere. The agricultural species are typically annuals, and their growth is highly regulated by management. Existing vegetation mapping is not adequate in this context as the available maps indicate the climax vegetation communities that existed prior to agricultural development (Beard and Webb, 1974) rather than the actual vegetation existing now.

The broad scale land use in Western Australia is shown in Figure 3.1. While areas of land are set aside for nature conservation purposes, they are typically small, and have been ignored to preserve the broad scale focus of the map. The region covers approximately 2.5 million sq km, and represents approximately one third of the Australian land mass.

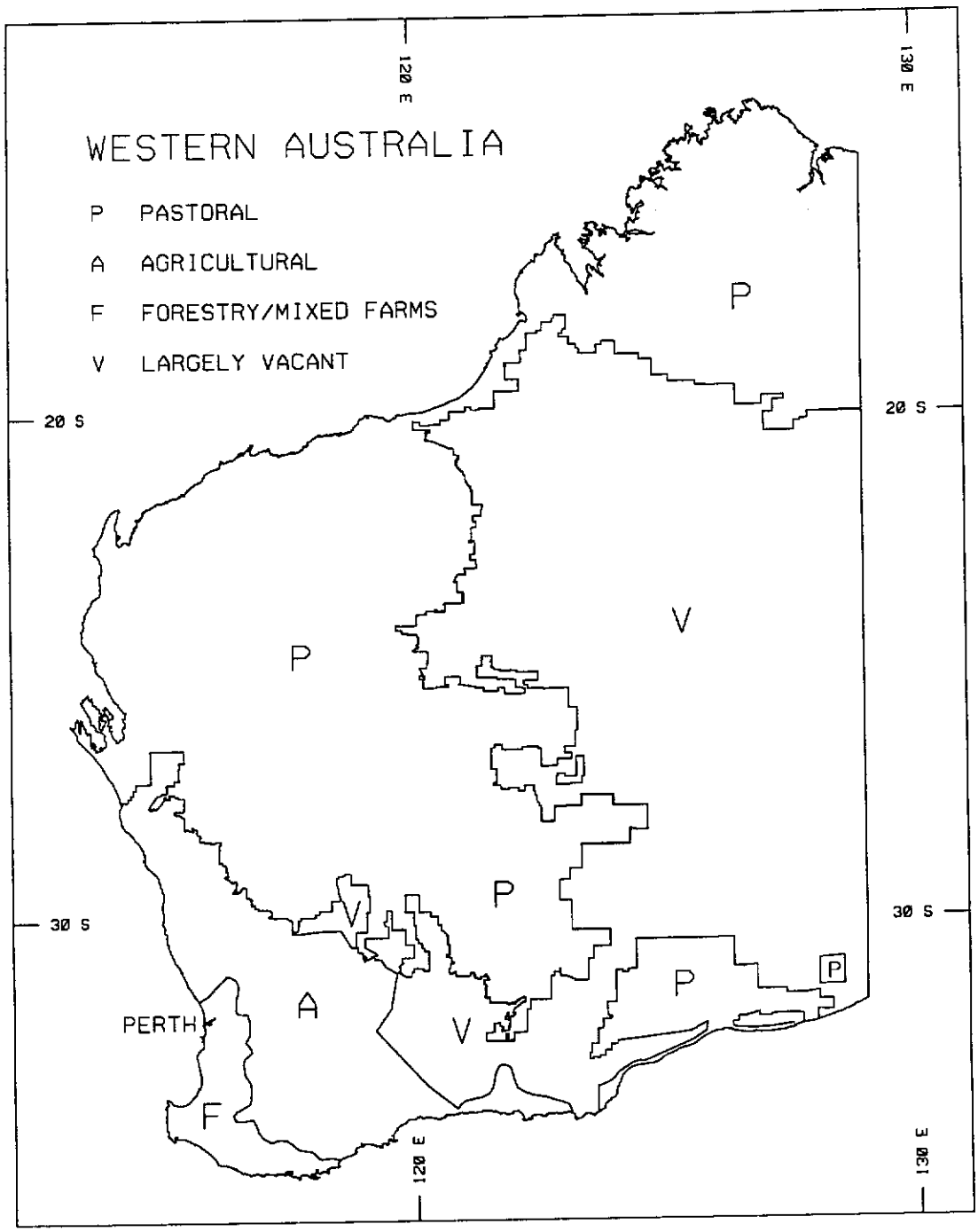

Figure 3.1 Broad scale land use in Western Australia

The area indicated on Figure 3.1 as agricultural use is primarily used for wheat-sheep farms and is known as the 'wheatbelt'. The outer (northern and eastern) margins of the wheatbelt are defined by a fence known as the 'rabbit proof fence'. This fence is located approximately at the 250 mm rainfall isohyet, which was historically deemed the outer limit for arable agriculture in Western Australia. In terms of broad scale satellite monitoring, this fence provides an excellent contrast between the reflected radiance from croplands and native vegetation and has been used in comparative studies (Smith et al., 1992).

In the pastoral areas, sheep are grazed (for wool) in the southern half, with cattle dominating in the northern half. Pastoral properties are very large (typically greater than 250000 ha) with variable stocking rates depending on landscape productivity. All pastures are composed of native species. There are approximately 500 individual pastoral properties in Western Australia.

In contrast, forestry (and mixed farming in places) is restricted to the high rainfall lands adjacent to the coastal strip in the extreme southwest corner of the State. The balance of land within the State is largely vacant of permanent land use. Clearly, pastoral and agricultural activities comprise the major existing land use.

3.4 Climate

Three climatic data sets were used to support the study, including an existing map of bioclimatic regions, monthly rainfall data and statistical data describing a number of key climatic variables important for plant growth.

The bioclimatic regions provide a broad perspective to the analysis. Monthly rainfall data have been used as a surrogate of plant growth for ground truth purposes, and to develop an improved understanding of the vegetation response to rainfall. The climatic statistics describe the overall environment for plant growth over a typical (average) year, and include estimates of evaporation, temperature and solar radiation.

3.4.1 Bioclimatic Regions

Within Western Australia, bioclimatic regions have been proposed by Beard (1990) based on the mean number of dry months each year and their time of occurrence. His regions are shown in Figure 3.2. The strong relationship between climate and land use is obvious from inspection of Figures 3.1 and 3.2. Agriculture is restricted to the region of mediterranean climatic conditions in the south west. Virtually all extensive pastoral land use occurs in climates which have eight or more dry months per year. The eastern limit of the pastoral lands is approximately defined by the start of spinifex country (see Figure 3.6).

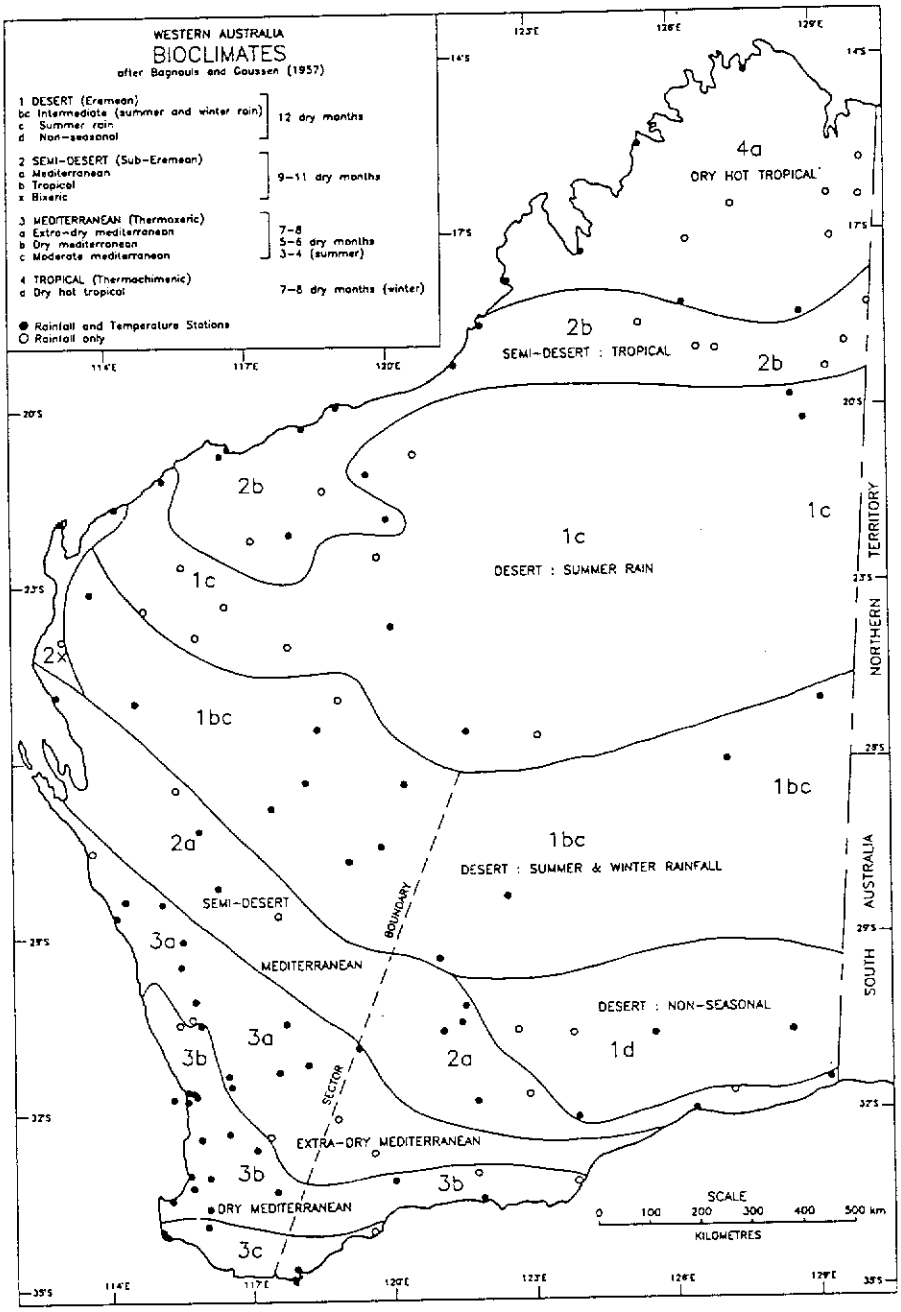

Figure 3.2 Bioclimatic regions (from Beard, 1990)

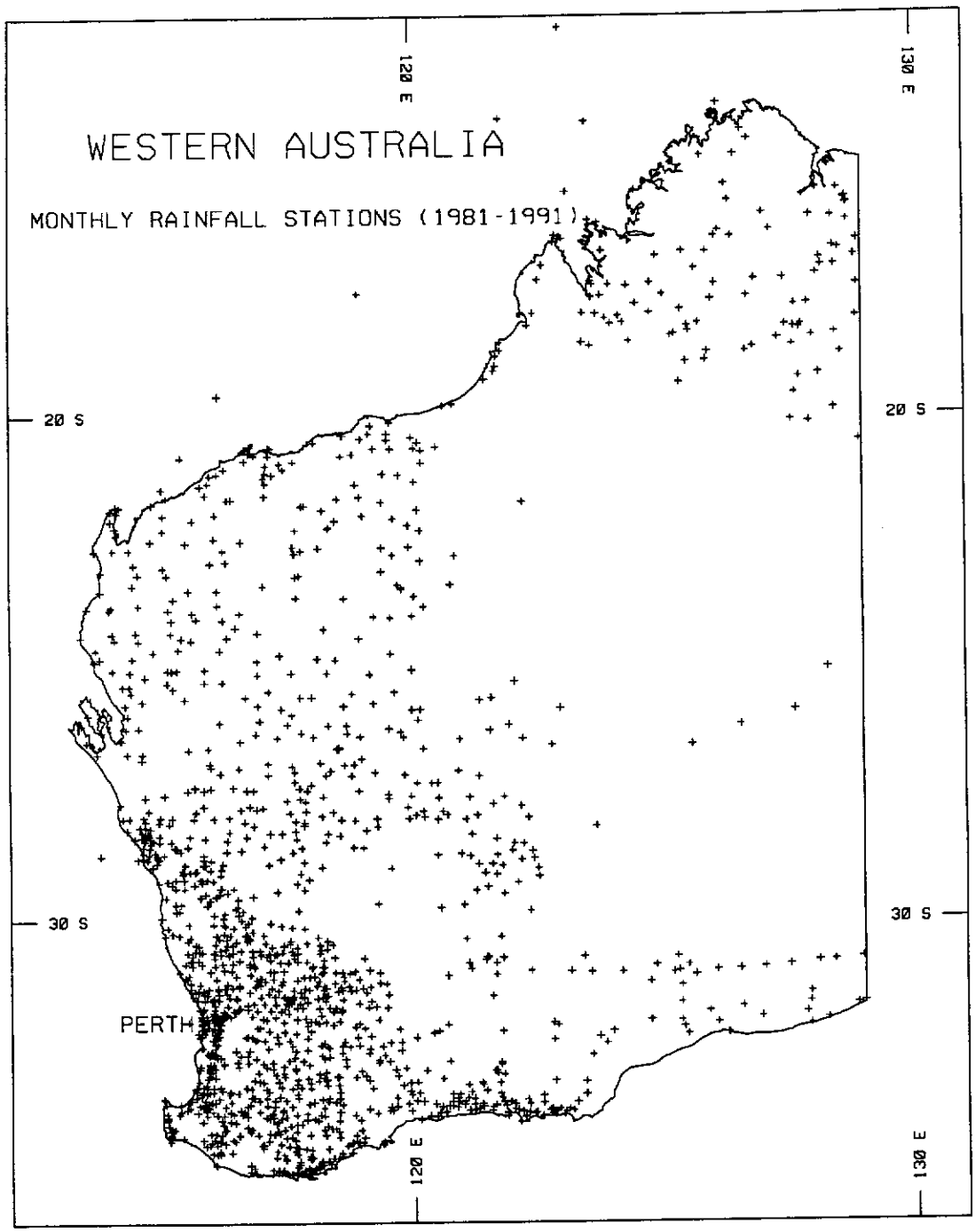

Figure 3.3 Monthly rainfall stations

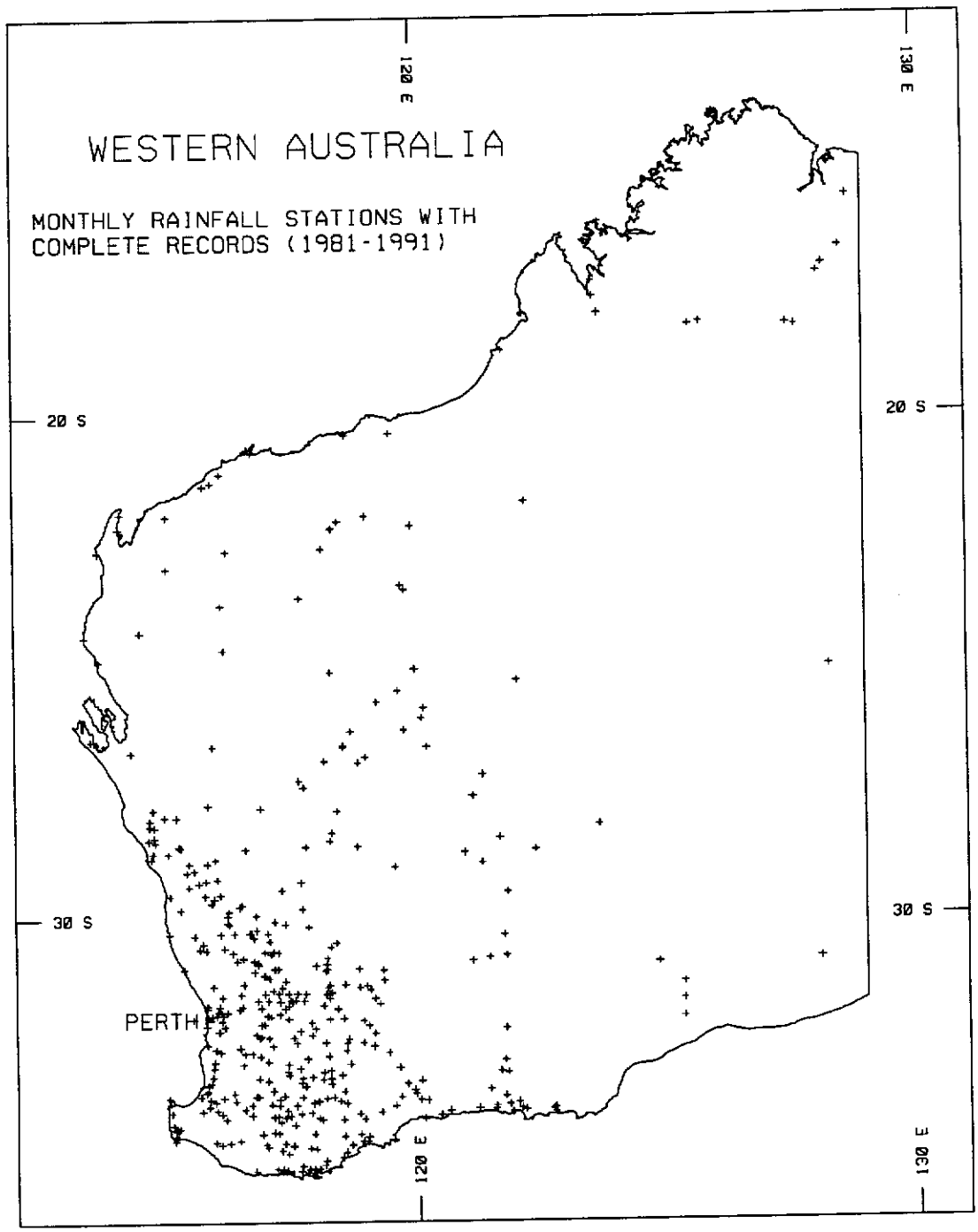

Figure 3.4 Monthly rainfall stations with no more than one missing monthly record (over the period 1981-1991)

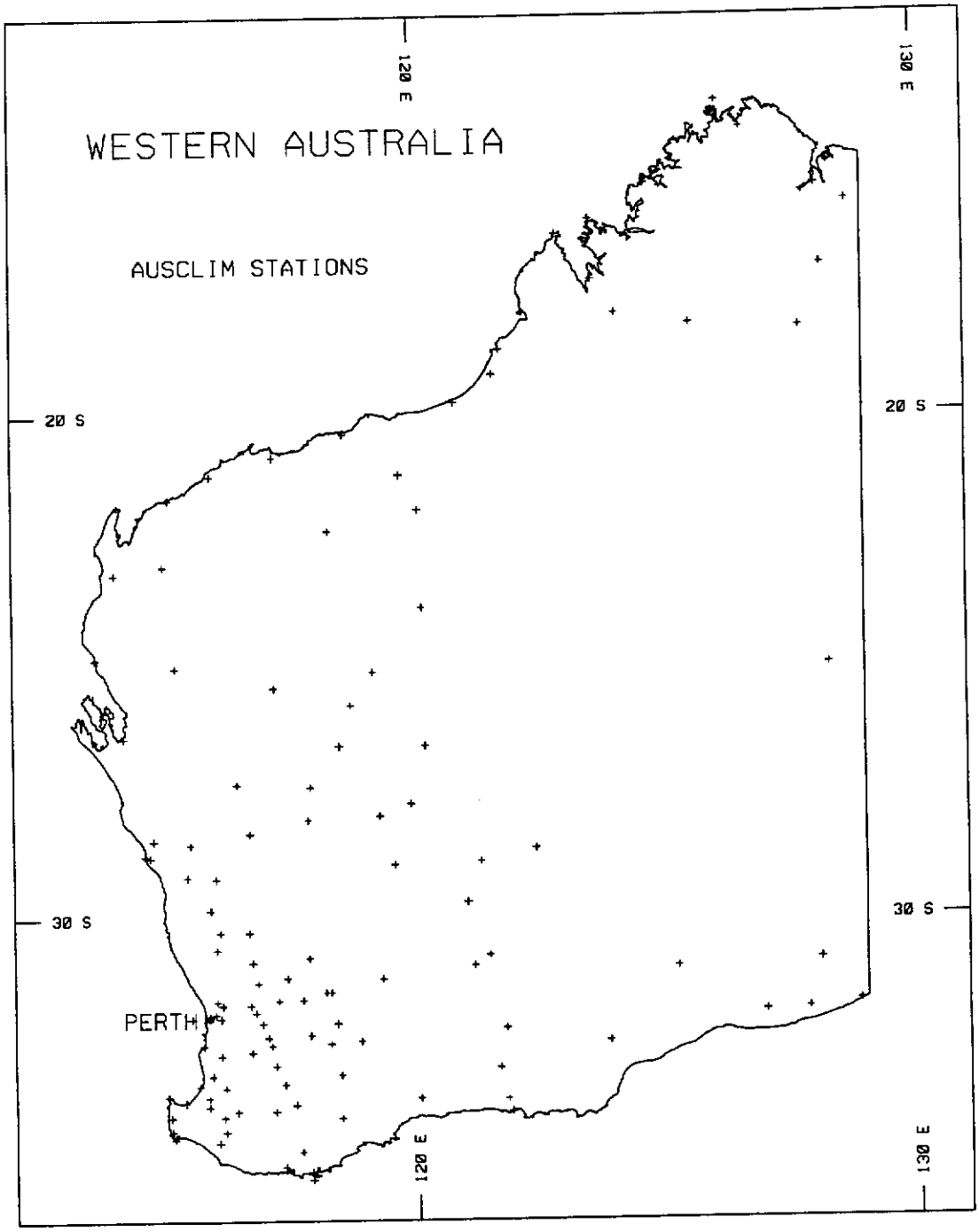

Figure 3.5 Stations having mean weekly climatic data

3.4.2 Rainfall Data

Monthly rainfall data to support this study was acquired from the Bureau of Meteorology. Measurements of total monthly rainfall were purchased for all recording stations within the State over the period January 1981 to June 1991. The location (latitude and longitude) of each station was also available from the Bureau of Meteorology. Figure 3.3 shows all stations which have recorded at least one measurement of monthly rainfall over the above period.

However, most stations have incomplete records over the period. Figure 3.4 shows those stations with no more than one missing monthly record during the 11 year period of data collection. Unfortunately, very few complete long term rainfall records exist in the pastoral areas.

3.4.3 Long Term Average Climatic Data

For water balance and plant growth modelling studies, the minimum data requirement is for pan evaporation, temperature and solar radiation data (Fitzpatrick and Nix, 1970). Actual observations of these climatic variables are not widely available. This study has used estimates (average) of these variables from long term records (10 to 15 years) available in the AUSCLIMMEANWK database. The data set was compiled under the guidance of Professor Henry Nix at the Australian National University. This database contains long term mean weekly values of selected climatic variables for a number of

primary climatic stations throughout Australia (Nix, 1982). The stations for which mean weekly data is available are shown in Figure 3.5. The weekly data is formulated using the so-called 52 standard weeks described in McCown (1981). The fields available in the AUSCLIMMEANWK database are shown below:

(a) Station name
(b) Latitude, Longitude and Elevation
(c) Day length
(d) Solar radiation
(e) Vapour pressure
(f) Max temp
(g) Min temp
(h) Mean temp ([max+min]/2)
(i) Day temp
(j) Night temp
(k) Rainfall
(l) Aust. Tank Evap
(m) % Rel Hum
(n) US Pan (Class A) Evap
(o) Penman Evap

3.5 Vegetation

In areas of predominantly natural vegetation, such as the pastoral and vacant areas indicated in Figure 3.1, vegetation mapping is a key requirement for interpretation of the satellite data. The NDVI has previously been shown to mean different things depending on the vegetation type (Townshend and Justice, 1986).

The most complete data set describing the vegetation of Western Australia has been compiled by Beard (Beard, 1974-1980). This project, begun in 1966, and completed in 1981 (Beard and Webb, 1974; Beard, 1990), mapped all vegetation within Western

Australia at a scale of 1:1000000 (total of seven sheets). Each map is accompanied by a detailed set of explanatory notes. Vegetation units were based primarily on community structure, with supporting floristic descriptions of the dominant species. This mapping forms the largest scale of complete map coverage of vegetation yet completed over the State. A broad scale vegetation map is shown in Figure 3.6 (Beard, 1990).

Land system surveys have been completed over approximately one half of the pastoral region by both CSIRO (e.g. Mabbutt et al., 1963) and the Western Australian Department of Agriculture (e.g. Payne et al., 1987). These surveys describe patterns of repeating landforms, soil and vegetation throughout their respective study areas, and are aimed at providing a broadly based inventory with some specific information on pastoral productivity.

Detailed vegetation species level information is also freely available through handbooks designed specifically for use in rangeland management and published by the Western Australian Department of Agriculture (e.g. Mitchell and Wilcox, 1988; Petheram and Kok, 1986).

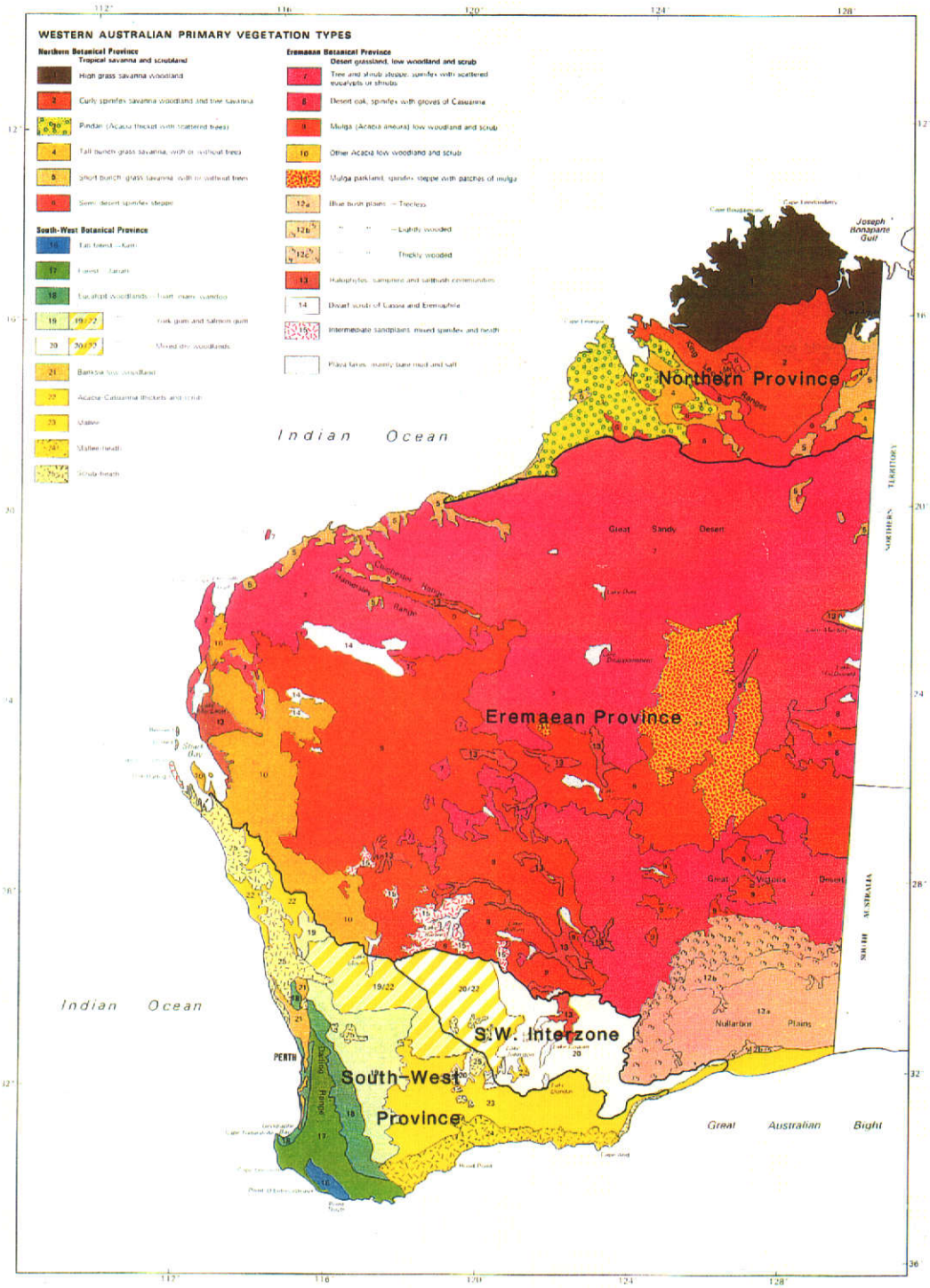

Figure 3.6 Vegetation of Western Australia (from Beard, 1990)

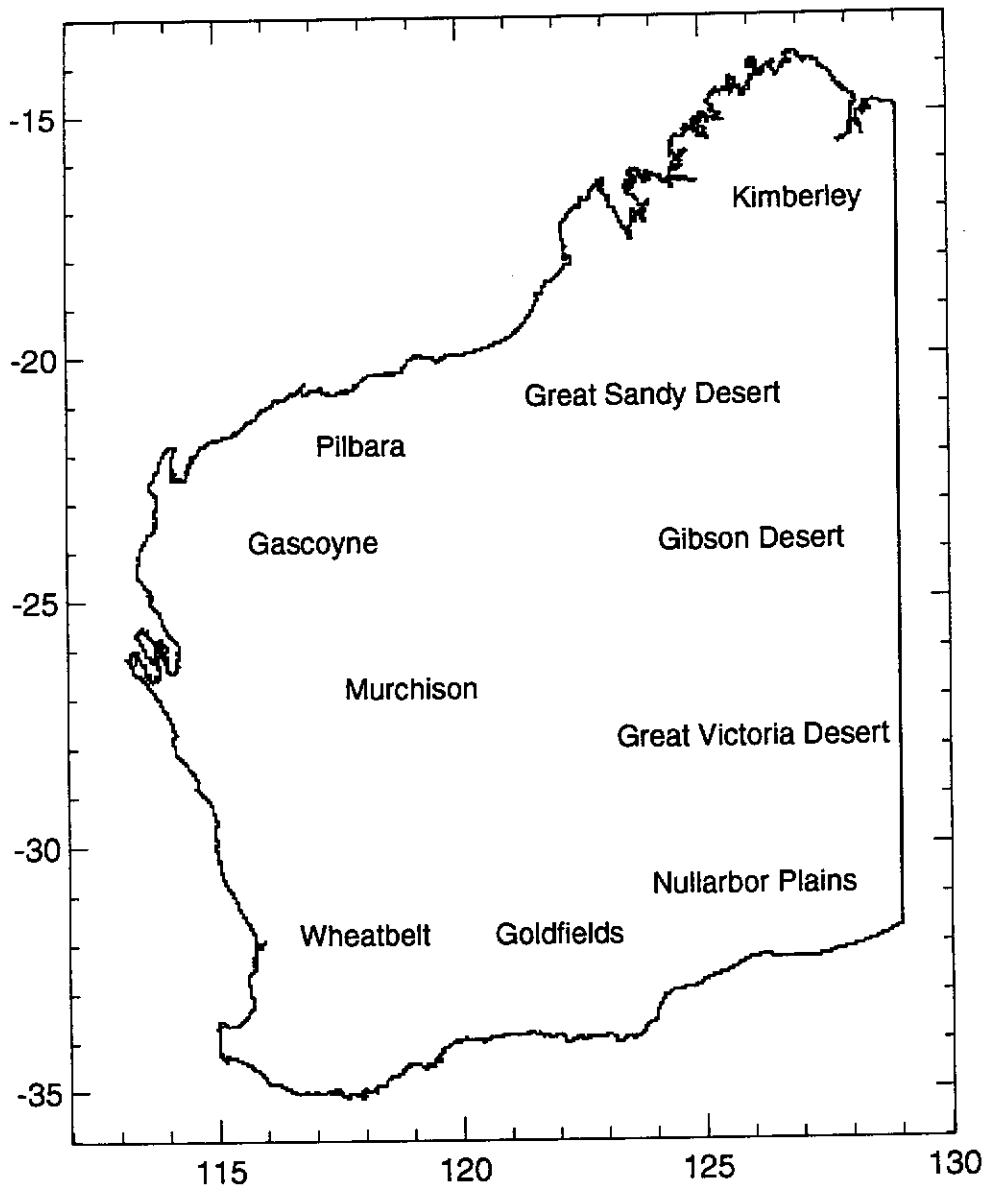

Figure 3.7 Broad scale regions of Western Australia

3.6 Regions

Regional areas in Western Australia which are in common usage are shown in Figure 3.7. These regions are referred to throughout the thesis, and are included for readers not familiar with

Western Australian geography. Boundaries are not shown, as there are no generally fixed boundaries defining these regions. Some of the regions refer to a geological feature such as the Nullarbor Plains, while others are a generic descriptor in common use such as the Kimberley.

3.7 Summary

Minimal data sets required for the effective interpretation of NDVI time series imagery (from NOAA-AVHRR) include land use, climatic data and vegetation mapping. Within Western Australia, all of these data sets are readily available. The climatic data include an extensive database of monthly rainfall (from the Bureau of Meteorology) for all stations in Western Australia, over the study period. This data are used (in Chapters 6, 7 and 8) as ground truth in the absence of biomass data.

Chapter 4

DETERMINING THE ACCURACY AND PRECISION OF THE NDVI

4.1 Introduction

The NDVI is a non linear index which transforms near infrared (N) and red (R) reflectances for the extraction of vegetation parameters. The formulation of the NDVI has been shown to be based on a soil line at N = R (see Section 2.4.5). The NDVI can be considered a quantity derived from individual measurements, which are each affected by errors.

The accuracy of the NDVI from NOAA AVHRR observations is a complex function of the entire data acquisition and processing system. This system includes image navigation (Townshend et al., 1992), atmospheric corrections (Paltridge and Mitchell, 1990), sensor calibration (Kaufman and Holben, 1993), soil line modelling (Huete and Tucker, 1991) and the impacts of bidirectional reflectance (Gutman, 1991). In addition, errors in the estimation of biophysical parameters from the NDVI also impact on the accuracy of the end product (Price, 1992; Huemmrich and Goward, 1992). Removal of systematic errors in N and R, such as those detailed above, will improve the accuracy of the NDVI. However, the precision of an NDVI estimate is primarily governed by the radiometric precision of the AVHRR. Radiometric precision is measured by the quantisation interval of the analogue to digital converter. Quantisation of the observations creates an absolute limit on the precision of any

vegetation index derived from those observations. The precision of radiometer observations and the subsequent effect on vegetation indices has received little attention in the literature.

One of the first studies demonstrating the importance of signal quantisation on the interpretation of multispectral satellite data was that of Tucker (1980). Tucker regressed various biological data (such as leaf water content) against simulated satellite signals (in bands three and four of Landsat TM) that were quantised at various levels of precision (i.e. 16, 32, 64, 128, 256, 512 classes). Tucker noted that the precision of a reflectance measurement was inversely related to the cosine of the solar zenith angle. Hence, at low sun angles, the precision was significantly worse. He concluded that radiometric precision of at least 128 levels was necessary for the estimation of biophysical parameters. While the simple ratio (N/R) was studied, no attempt was made to look at the effect of quantisation on that ratio.

In an Australian context, Graetz and Gentle (1982) simulated the reflectance characteristics of an Australian shrubland in the Landsat MSS bands, based on extensive field measurements, and simulation of the annual solar cycle. In winter, when solar zenith angles are low, the dynamic range of the MSS data was substantially reduced when compared to measurements taken in summer. They concluded that ecological changes would possibly be missed in winter imagery, due to this loss of precision in the signal.

Slater and Jackson (1982) investigated soil and atmospheric effects on spectral measurements of vegetation. As part of this study they noted that the simple ratio computed from the six bit data acquired by Landsat MSS was not sufficient to resolve differences between green and stressed vegetation. This is one of the few references on the effect of quantisation on vegetation indices that can be found in the literature. Goward et al. (1991) looked specifically at errors in NDVI computed from AVHRR measurements. They showed how NDVI was extremely sensitive to quantisation error at low reflectances. While simulated effects were computed for particular circumstances, no formal statistical framework was subsequently developed.

In developing vegetation monitoring applications using the NDVI computed from NOAA AVHRR observations, it is essential to understand the mathematical and statistical properties of that index. This chapter specifically addresses the mathematical nature of the NDVI function, and the precision which may be obtained, given quantisation errors in the N and R signals. To simplify the process, it is assumed that all other elements (such as sensor calibration and atmospheric effects) are controlled or known to infinite precision, and that the sensor is not affected by electrical noise. This will define an absolute limit for the precision of the NDVI.

In the light of this absolute limit, a suitable method for rescaling the NDVI for representation in integer based image

processing systems is proposed. Finally, comments about some other common vegetation indices are presented.

4.2 The NDVI Function

The NDVI is computed as:

$$NDVI=\frac{(N-R)}{(N+R)} \quad (when\ N > 0\ and/or\ R > 0) \qquad (4.1)$$

$$NDVI=0 \quad (when\ N,R = 0)$$

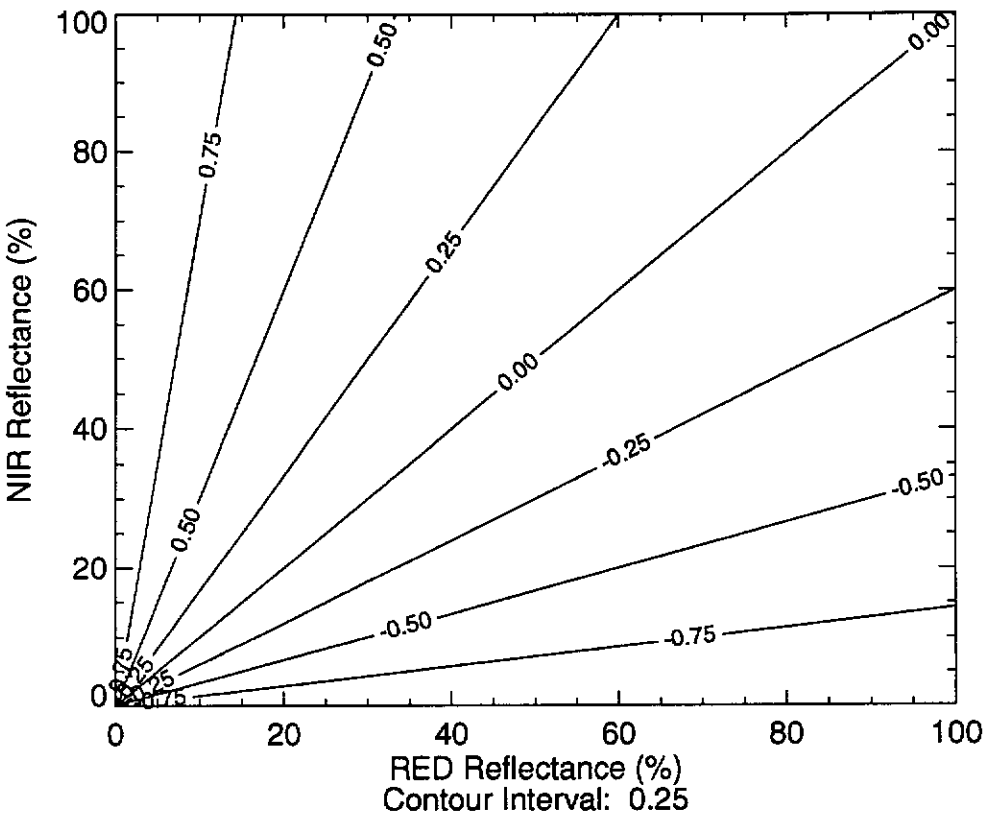

Figure 4.1 Contours of the NDVI function

A contour map of this function is shown in Figure 4.1. The NDVI varies from -1 to +1 but is undefined when N and R are zero. This discontinuity is overcome in the definition of the function. From the contours in Figure 4.1, it is evident that relatively small changes in either N or R, near the origin, can produce large changes in NDVI. This result was also demonstrated mathematically by Goward et al. (1991). Observations over dark soils could also be expected to be noisy. This is confirmed by the results of Huete and Tucker (1991). Clearly the precision will be better for larger values of N and R (i.e. brighter targets). On this basis high noise content in the NDVI can be expected over the ocean (i.e. dark targets).

Due to the non-linear nature of the NDVI, computation of NDVI from N and R, estimated using either digital counts, calibrated radiance, top of canopy or top of atmosphere reflectance, will give different values for NDVI (Price, 1987b; D'Iorio et al., 1991; Goward et al., 1991). This should be borne in mind when interpreting or using NDVI measurements from other researchers.

4.3 Precision of AVHRR Observations

The accuracy of the computed NDVI depends on how well the systematic errors in the individual bands (N and R) can be modelled and hence removed. The precision attainable in NDVI is governed by the radiometric precision of the AVHRR. The AVHRR instruments use a 10 bit analogue-to-digital converter to quantise the received

signal (L) into 1024 bins (0-1023). The reflectance is then calculated as (Goward et al. 1991):

$$\rho = \frac{L*\pi*d^2}{E_0*\cos\theta} \qquad (4.2)$$

where

ρ = *planetary reflectance* (0 - 100 %)

L = *reflected radiance*

d = *earth sun distance(AU)*

θ = *solar zenith angle*

E_0 = *solar irradiance (top of atmosphere) at* θ=0 *and* d=1

The reflected radiance (L) is quantised into 1024 bins, so the width of a bin in terms of reflectance units is given by:

$$\Delta p = \frac{\Delta L*\pi*d^2}{E_0*\cos\theta} \qquad (4.3)$$

where

ΔL = *bin width of radiance measurement*

Δp = *bin width of reflectance measurement*

The quantisation interval of the incoming radiance is a parameter of the instrument and theoretically should remain fixed. In reality, it will vary slightly as the calibration coefficient changes through time (Che and Price, 1992; Kaufman and Holben, 1993). If the solar irradiance is also considered to be constant, from Equation 4.3, it is evident that sensor precision (in reflectance units) varies with both solar zenith angle and earth-sun distance. The earth-sun

distance (d) varies from approximately 0.984 to 1.016 throughout the year and is 1 at the equinoxes (Roderick, 1993). In this context, it is reasonable to ignore the changes in d.

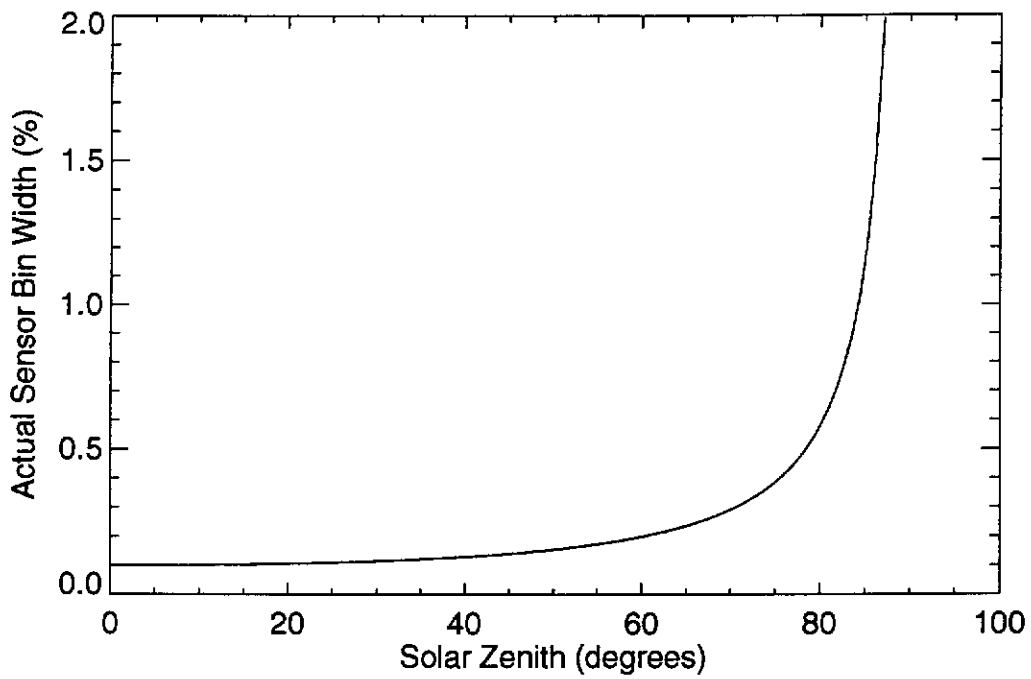

Figure 4.2 Sensor bin width (%) for AVHRR solar channels (as a function of solar zenith angle (for d=1); computed using Equation 4.4)

For the AVHRR, the nominal width of each bin is ~ 0.1 percent reflectance units (Price, 1987a). The nominal bin width assumes a solar zenith angle of zero degrees. The actual bin width for a particular observation of N or R, in reflectance units, is related to the nominal sensor bin width by (Goward et al. 1991):

$$\Delta p = \Delta p_0 * \frac{d^2}{\cos\theta} \qquad (4.4)$$

where

Δp = *actual sensor bin width*

Δp_0 = *nominal sensor bin width* (*ie.* θ=0,*d*=1)

The actual sensor bin width as a function of solar zenith is shown in Figure 4.2. Typically, precision is worse at high latitudes and in the winter months as the sun is lower in the sky. At a solar zenith angle of approximately 84 degrees, actual bin width of the AVHRR is greater than 1 percent.

Figure 4.3 indicates the solar zenith angle as a function of latitude (southern hemisphere) and time of the year (month) at 1430 and 1600 hrs WST (Western Standard Time). WST is the time zone used in Western Australia. The figure assumes a longitude of 120 degrees, which corresponds to the central meridian of the WST zone, and is broadly applicable to any latitude in the southern hemisphere. To apply the figure to a northern hemisphere equivalent, six needs to subtracted from the month number.

Graphs for both times were prepared taking into consideration the characteristic drift in the equatorial crossing times of the NOAA satellites (see Section 2.3.2 and Figure 2.3). At the end of the operational life of NOAA's 7 and 9, the local solar time of equatorial crossing was approximately 1600 hrs (see Figure 2.3). The solar

cycle was simulated using the technique of Roderick (1993).

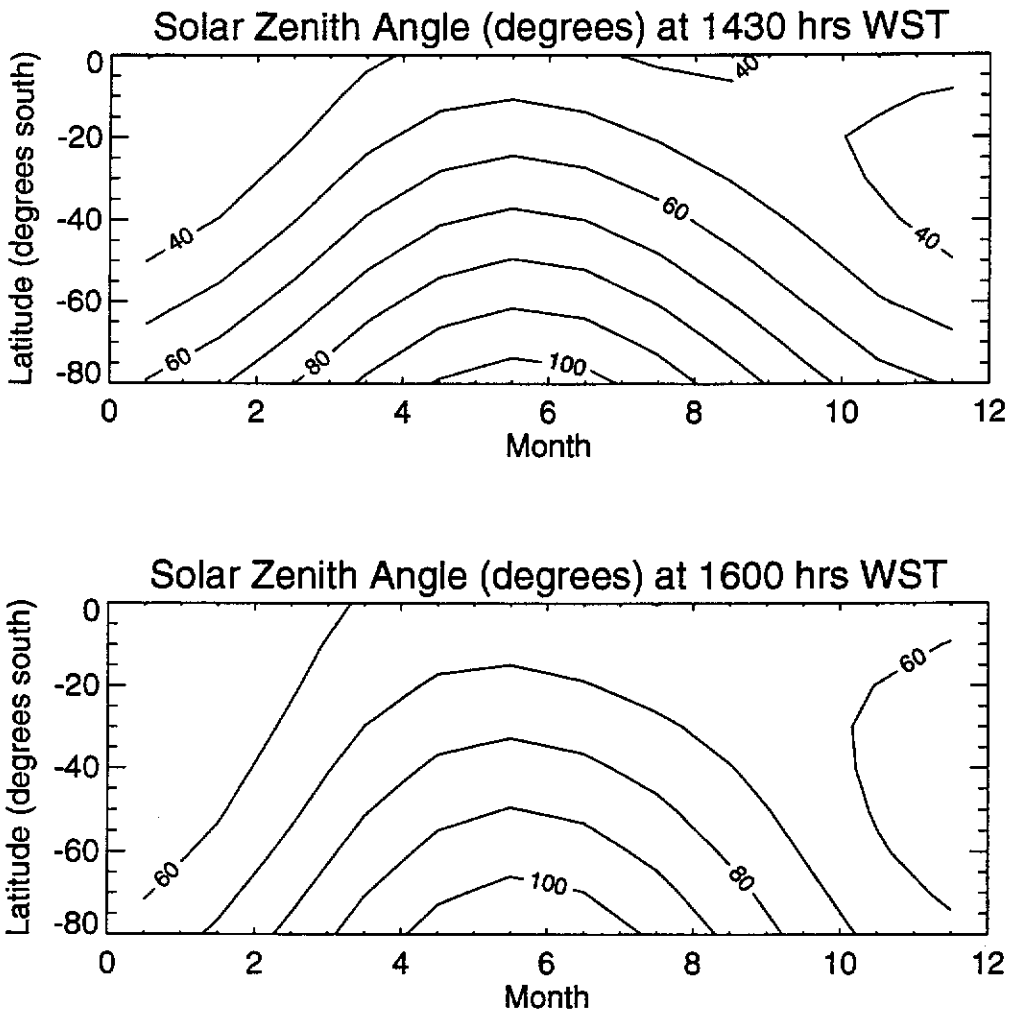

Figure 4.3 Solar zenith angle as a function of latitude and time (months of year for 1992 at a longitude of 120 degrees)

From Figure 4.3, for mid-latitude countries such as Australia and Africa (i.e. latitude less than 40 degrees), typical solar zenith angles do not exceed 70 degrees for the afternoon AVHRR overpass (NOAA-7, 9, 11) at WST of 1430 hrs. At 1600 hrs WST for the same window, solar zenith can be as large as 85 degrees (June). Using these data as a guide, average annual values of solar zenith angle for

latitudes from 40 degrees south to 0 degrees are 45 degrees at 1430 hrs WST and 64 degrees at 1600 hrs WST.

While there is a significant seasonal cycle in the sensor precision, the solar zenith will generally (although not always) be smaller than 70 degrees for latitudes less than 40 degrees. Using Equation 4.4, and assuming a nominal bin width of 0.1 precent, this equates to an actual bin width of approximately 0.3 percent. Note that, on occasions, the actual bin width will be significantly worse. For example, at a solar zenith of 85 degrees, the actual bin width is approximately 1.1 percent.

4.4 Precision of the NDVI

Using the previously derived estimates of precision in the individual observations (N and R), it is possible to derive an estimate of the precision of the NDVI. This is addressed in this section.

4.4.1 Quantisation Error

The probability density function appropriate to study quantisation or round-off errors is the rectangular (or uniform) distribution. This distribution ranges from -1/2 to 1/2 of the actual sensor bin width and is shown in Figure 4.4.

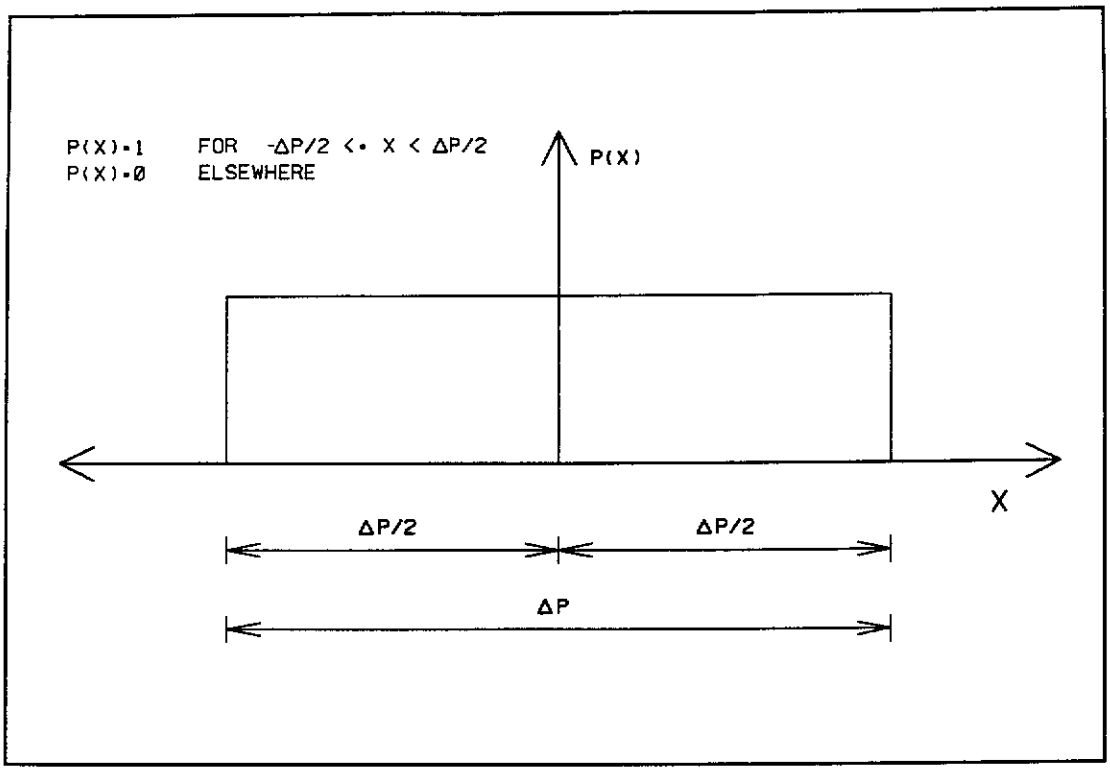

Figure 4.4 Probability density function for quantisation error

4.4.2 Uncertainty in NDVI

The error in NDVI, due to quantisation errors in N and R can be estimated using two basic approaches, a worst case (or 100 percent confidence interval) or some other confidence interval (such as 50, 75 or 90 percent). These two approaches are considered below.

4.4.2.1 Worst Case Error in NDVI

The true values of N and R will occur somewhere within the minimum and maximum values shown in Equation 4.5.

$$
\begin{aligned}
N_{min} &= N-(\Delta p_N/2) \\
N_{max} &= N+(\Delta p_N/2) \\
R_{min} &= R-(\Delta p_R/2) \\
R_{max} &= R+(\Delta p_R/2)
\end{aligned}
\qquad (4.5)
$$

The maximum possible NDVI ($NDVI_{MAX}$) occurs when N and R take the values N_{MAX} and R_{MIN} and the minimum possible NDVI ($NDVI_{MIN}$) occurs when N and R take the values N_{MIN} and R_{MAX} as shown in Equation 4.6.

$$
NDVI_{MAX} = \frac{(N_{MAX}-R_{MIN})}{(N_{MAX}+R_{MIN})} \quad and \quad NDVI_{MIN} = \frac{(N_{MIN}-R_{MAX})}{(N_{MIN}+R_{MAX})} \qquad (4.6)
$$

The maximum error in NDVI (due to quantisation in N and R) is thus given by:

$$
\begin{aligned}
&E_{MAX} = NDVI_{MAX} - NDVI \\
&or\ alternatively \\
&E_{MAX} = NDVI - NDVI_{MIN}
\end{aligned}
\qquad (4.7)
$$

Both results presented in Equation 4.7 are identical.

The quantisation error is approximately equal in both channels. Using this result, and rearranging Equations 4.5, 4.6 and 4.7, a general expression for the maximum error in NDVI, denoted E_{MAX} is obtained as follows:

$$E_{MAX} = \mp \frac{\Delta p}{N+R} \qquad (4.8)$$

The result in Equation 4.8 is a general result for the 100 percent confidence limit in NDVI, given quantisation errors only, and assuming equal quantisation errors in both N and R (which is nominally true with AVHRR). Note that the maximum possible error is symmetrical around NDVI.

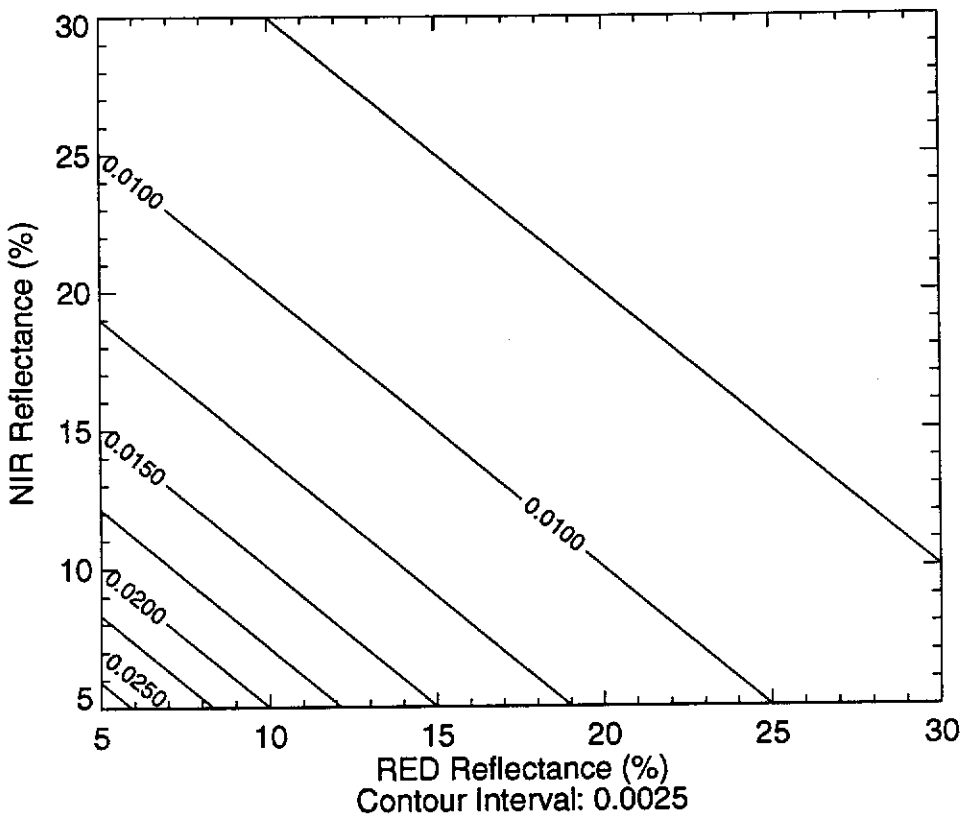

Figure 4.5 Maximum NDVI errors (E_{MAX}) for a sensor bin width of 0.3 % (in N and R)

Contours of the E_{MAX} function computed using Equation 4.8 are shown in Figure 4.5 using a typical sensor precision (for Australian latitudes) of 0.3 percent. These contours run approximately perpendicular to the original NDVI function and the sensitivity of the NDVI at low reflectances is clearly shown. If most land surface targets are assumed to have reflectances ranging from 5 to 45 percent in N and R (Rossow et al., 1989), then the precision of the NDVI, due to quantisation, varies substantially within a particular NDVI image, depending on the component reflectances N and R.

Assuming the approximate bounds of 5 to 45 percent for N and R noted above, Table 4.1 summarises the expected maximum error in NDVI for a few key positions in the graph at various quantisation errors. Note that at a reflectance precision of 1 percent, the quantisation error alone can generate errors of up to ± 0.1 NDVI units for low reflectances (i.e. N,R = 5 percent).

		Actual Sensor Bin Width		
		0.1 %	0.3 %	1.0 %
R (%)	N (%)	E_{MAX}	E_{MAX}	E_{MAX}
5	5	0.010	0.030	0.100
5	25	0.003	0.010	0.033
5	45	0.002	0.006	0.020
25	25	0.002	0.006	0.020
25	45	0.001	0.004	0.014
45	45	0.001	0.003	0.011

Table 4.1 Maximum NDVI errors (E_{MAX}) for various sensor bin widths (computed using Equation 4.8)

4.4.2.2 NDVI Distribution

The analysis presented in Section 4.4.2.1 is overly pessimistic, as it is unlikely that the worst case quantisation error will occur often. To estimate confidence intervals of the NDVI requires the estimation of the probability density function (PDF) of NDVI given the stochastic properties of N and R. Numerical simulation has been used to estimate the PDF, assuming N and R are uniformly distributed random variables. The method is as follows:

$$Let \quad N_i = N + n_i \quad and \quad R_i = R + r_i \tag{4.9}$$

where n_i and r_i are uniformly distributed random variables, and N and R are the observed (quantised) reflectances. The width of the distributions for n_i and r_i are set according to the actual sensor bin width.

Using a random number generator (for a uniform distribution) an array of random (uncorrelated) values for n_i and r_i are generated. The NDVI for a particular simulation (denoted i) is then given by:

$$NDVI_i = \frac{(N_i - R_i)}{(N_i + R_i)} \tag{4.10}$$

Thus a PDF of the NDVI can be generated numerically.

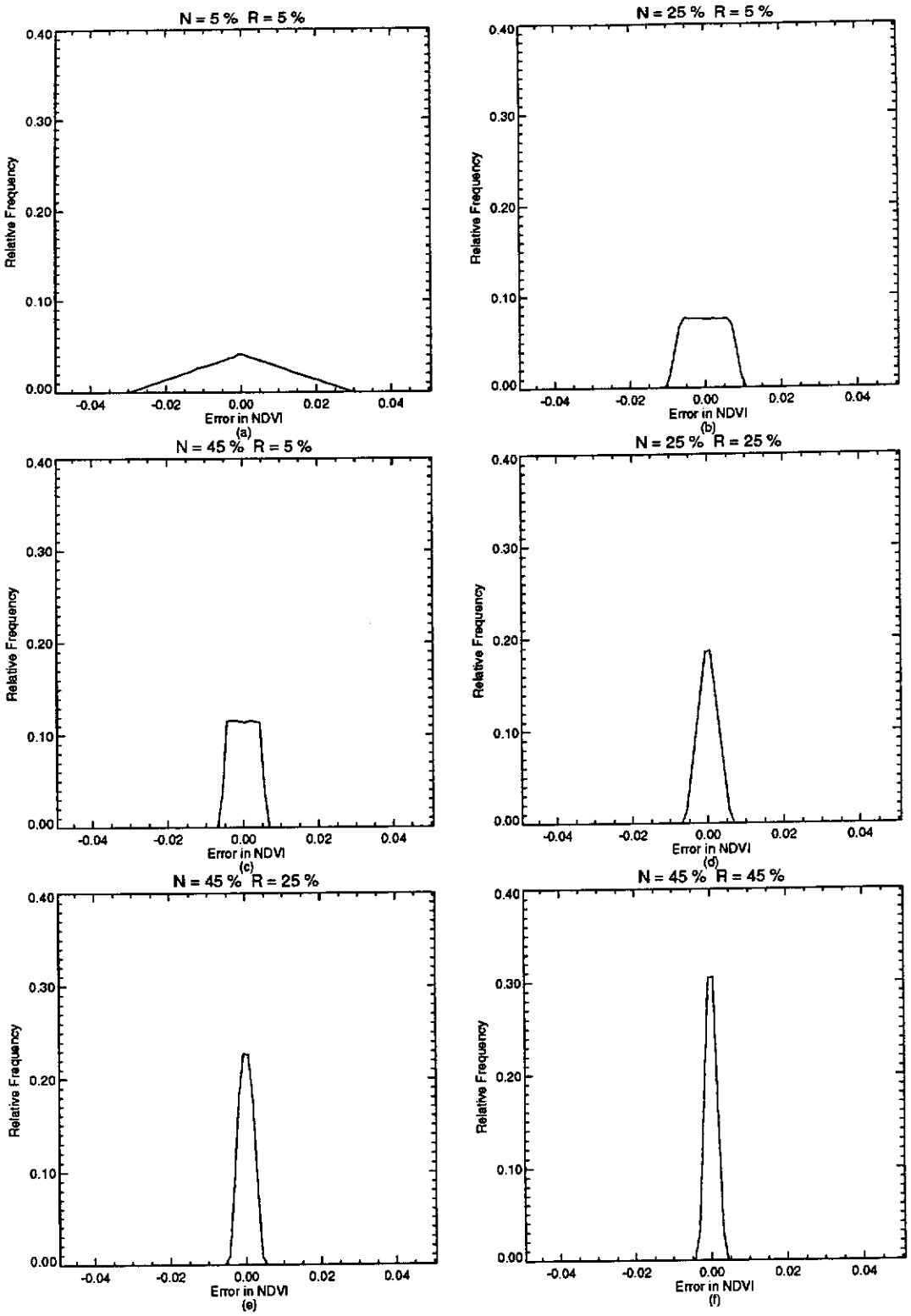

Figure 4.6 Various distributions (PDFs) for NDVI for a sensor bin width of 0.3 % (in N and R). (200,000 individual simulations were used to generate each PDF function)

The above technique has been used to generate a PDF for the NDVI at various key locations in the N-R space. The sensor bin width used was 0.3 percent. The simulation results are presented as histograms in Figure 4.6. Each of these histograms was generated using 200,000 randomly generated pairs of n_i and r_i. The nominal NDVI value (i.e. when n_i, r_i = 0) has been subtracted from each PDF to centre that PDF at zero for comparison purposes.

Inspection of Figure 4.6 indicates that the PDFs are unique for each combination of N and R. On the line N equals R (i.e. where NDVI=0), the PDF is triangular (Figure 4.5a, d and f) and, as the data point moves away from this line, the PDF becomes more rectangular (Figure 4.5b, c, e). This result is surprising and not intuitive. Given the different PDF functions for each combination of N and R, no simple computational technique is available which can estimate confidence intervals for errors in NDVI.

4.5 Rescaling the NDVI

The NDVI function varies from -1 to 1, and it is commonplace to rescale this value to a single or two byte integer for use in image processing systems. Various rescaling methods have been reported in the literature (e.g. Box et al., 1989; Eidenshink, 1992; Gupta, 1993). When rescaling the data, it is desirable to use the smallest number of bytes possible to minimise storage costs, whilst maintaining precision in the data.

As demonstrated, the error in NDVI due to signal quantisation varies according to the position of the original observations in the N-R space. Thus two points may have a similar NDVI, but completely different error characteristics. For typical land surface reflectances in the range 5 - 45 percent for N and R, and a quantisation error of 0.3 percent (suitable for latitudes less than 40 degrees), the maximum error in NDVI varies from 0.03 to 0.003 (see Table 4.1) depending on the values of N and R.

The NDVI varies from -1 to 1 and thus has a full range of two NDVI units. Using the previous assumptions, the smallest maximum NDVI error of ± 0.003 units equates to approximately 333 classes, i.e. 2 / (2 * 0.003), of unique information not subject to quantisation error. The storage of this number of classes will require a two byte integer value. For the largest (typical) maximum error of ± 0.03 NDVI units, there are 33 classes, ie. 2 / (2 * 0.03), of unique information available in the computed NDVI.

On this basis, the final scaling technique adopted was to rescale the NDVI from a theoretical range of -1 to 1 into an integer range of 0 to 200. This requires a single byte for storage of each pixel. The technique is expressed as:

$$I = (NDVI + 1) * 100 \qquad (4.11)$$

where I = scaled value

Thus an image pixel value of 105, equates to an NDVI of 0.05, i.e. (105/100)-1. While there will still be some noise due to quantisation error in the image data (particularly for targets with low reflectance), conversion back to the NDVI from the image data is simple compared to other techniques (e.g. Box et al., 1989; Gupta, 1993), and can be performed mentally. Equally as important, the NDVI can be stored in a single byte.

Evaluation of the proposed technique is necessary to establish how much noise will be present in the final image data (due to quantisation) and how much signal will be lost because of the compromise reached.

4.6 Evaluating the Rescaling Method

The suitability of the scaling technique proposed may be evaluated by calculating the probability of correct assignment to a particular bin. In this case the bin width of the proposed data storage technique is known to be ± 0.005 NDVI units (i.e. total width of 0.01 NDVI units). An example of these calculations is shown in Figure 4.7. By assuming that the value of NDVI falls in the centre of an output bin, then the required probabilities are the integrals of the PDF evaluated over the output bin width.

This technique was used to estimate the probability of correct assignment for various values of N and R (see Figure 4.8).

Simulation was used (n = 200000) to prepare a PDF for each N and R on a finite grid interval at a resolution of one percent (reflectance) in N and R. The probabilities derived are the confidence levels of the observed NDVI being put in the correct bin, having a width of 0.01 NDVI units, and assuming a quantisation error of 0.3 percent in N and R. The assumption of the NDVI value falling in the centre of a particular bin is unrealistic, and as such these probabilities are likely to be slightly optimistic. However, they do provide an understanding of the nature of the function.

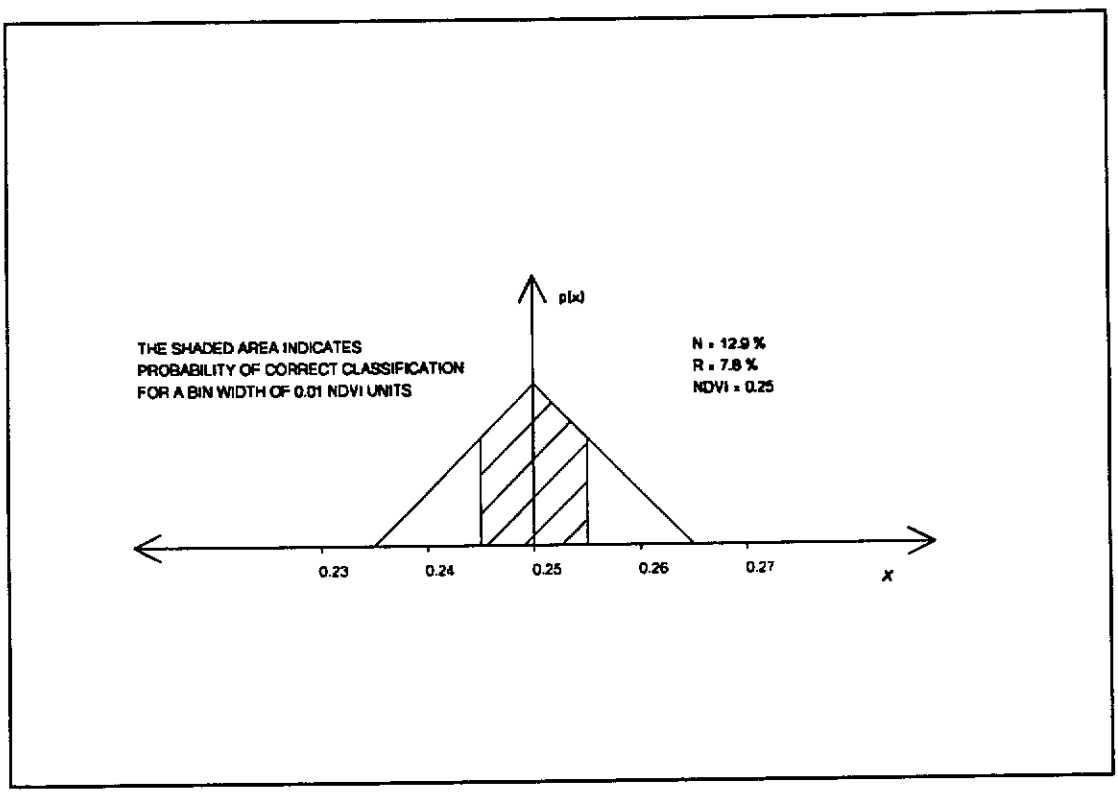

Figure 4.7 Calculation of the probability of correct assignment for NDVI

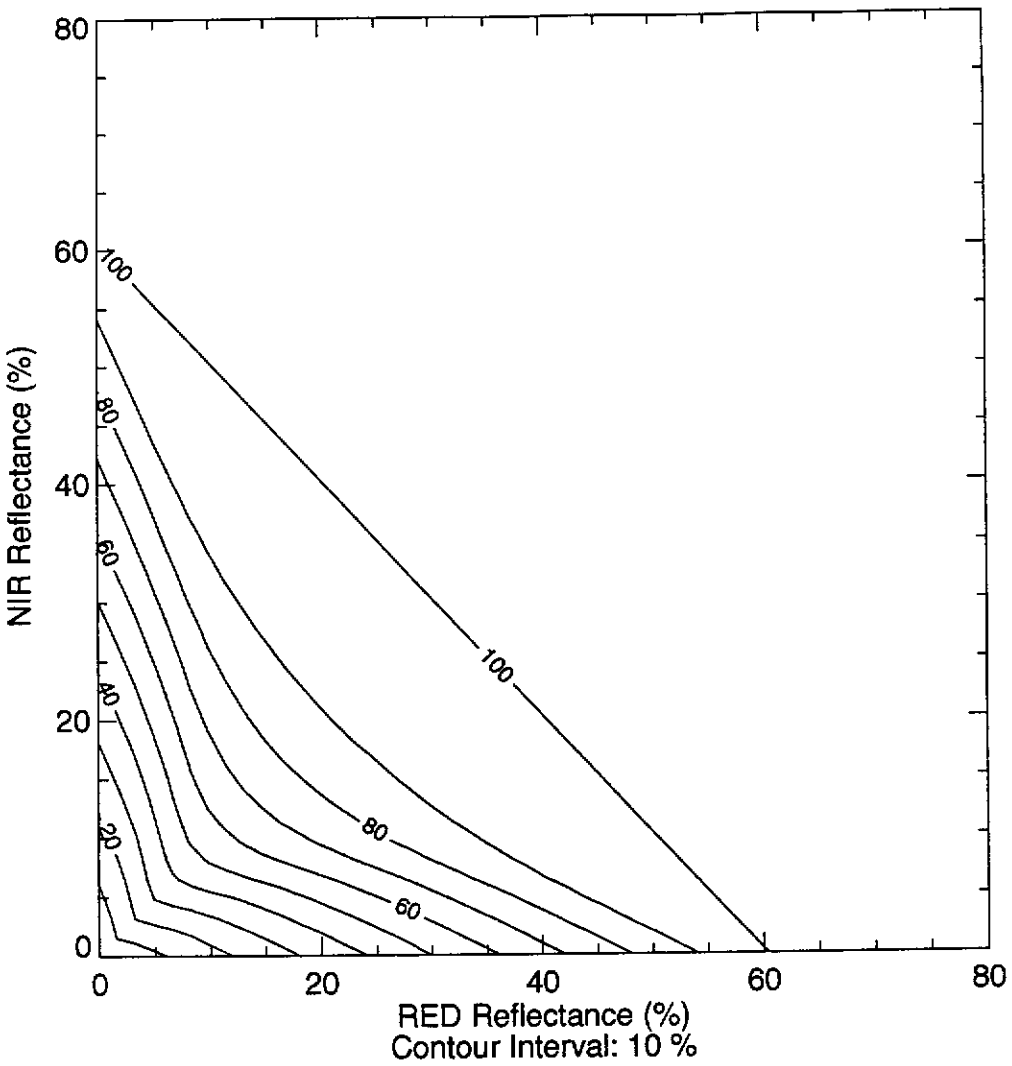

Figure 4.8 Probability of correct assignment for NDVI with a bin width of 0.01 NDVI units. (Sensor bin width assumed as 0.3 percent in both N and R)

Under the assumptions used to generate Figure 4.8, there is only 100 percent certainty of correctly assigning an NDVI value to the correct bin when N plus R is greater than 60 percent. For all other cases there will some uncertainty or noise in the NDVI due to quantisation error. At N, R equal to five percent, there is approximately 30 percent likelihood that the bin assigned is the correct bin.

In contrast to the straight line contours of maximum error presented earlier (see Figure 4.5), the contours shown in Figure 4.8 show a distinct pattern of decreasing confidence on departure (in a perpendicular direction) from the line N equals R. This is related to the shape of the PDF (see Figure 4.6). The triangular PDFs near the soil line (N=R) have more area under the PDF near the mean than rectangular PDFs.

Clearly, even using this relatively coarse rescaling procedure, there will still be some noise in the final NDVI due to quantisation. Differences of one or two DN (digital numbers) in the final image data (on the 0-200 scale) may not be significant depending on the original N and R reflectances.

4.7 Discussion

The mathematical (Figure 4.1) and statistical (Figures 4.3 - 4.8) properties of the NDVI are surprisingly complex for what is at first glance a seemingly simple function. The convergence of the NDVI isolines at the origin make the function very sensitive to small changes in N and R at low reflectances. This sensitivity has also been noted in the use of the simple ratio (N/R) (Crippen, 1988).

On this basis alone more noise would be anticipated in the NDVI over dark targets. This has been noted by Huete and Tucker (1991) over dark soils. Other likely dark targets which would be

affected include deep water bodies and dense forest. In addition, the effect of systematic errors such as atmospheric corrections will be greater over dark targets.

One major advantage of the NDVI is the potential ability to deal with varying amounts of shadow in image data. For many naturally vegetated scenes, shadow is a major cover component to be considered in remote sensing studies (Graetz and Gentle, 1982). The amount of shadow is dynamic, and is typically a maximum in winter as the sun is lower in the sky. If both an invariant soil line and unchanging vegetation are assumed, then as the amount of shadow increases, the resulting observation will track towards the pure shadow position in N-R space. Pure shadow will typically fall near the origin. The NDVI isolines mimic this behaviour, and thus provides at least a first order correction for the effects of shadow.

Due to the nature of the NDVI, the effect on the accuracy of the NDVI of various atmospheric correction schemes will depend on the position of the observation in N-R space. For bright targets, the NDVI is relatively insensitive to atmospheric and other disturbances. The converse is true for dark targets. When reporting results which indicate the effect on NDVI of various atmospheric effects (e.g. Soufflet et al., 1991) it is essential that those results be presented in a contour map of the NDVI function to enable effective use of the results.

The precision of N and R varies principally as a function of the cosine of the solar zenith angle. Thus, precision is not fixed, but has a seasonal component. Accordingly, the precision of the NDVI will also vary seasonally. The impact of errors in N and R on the NDVI is most easily dealt with using the maximum error approach. It is possible to compute a PDF function for the NDVI, and thus use a nominated confidence interval, to simulate the effect of quantisation on the NDVI. However, the PDF varies as a function of N and R.

For typical Australian conditions, the sensor bin width in AVHRR observations of N and R was estimated as approximately 0.3 percent, based on a solar zenith of 70 degrees. Using this figure, a worst case error in NDVI for a dark target (N, R = 5 percent) was calculated to be ± 0.03 NDVI units. For a bright target (N, R = 45 percent) the precision improved to ± 0.003 NDVI units. The error in NDVI can and will be worse for high latitudes in winter months. This is particularly the case at the end of the life for a NOAA satellite, due to drift in the time of equatorial crossing. It is recommended that observations of N and R acquired when the solar zenith is greater than 70 degrees not be used for computation of the NDVI.

Signal quantisation sets a finite limit on the precision possible in the NDVI. This "best possible precision" must be borne in mind, when considering the effects of various systematic errors such as atmospheric variability, sensor degradation and soil line variations on the calculation of NDVI. For dark targets, such as forest and

ocean, at high solar zenith angles, it is possible to have errors in NDVI up to ± 0.1 NDVI units (and greater) due to signal quantisation alone. In these cases, there will be little benefit in making other corrections. From an accuracy perspective, the nature of the NDVI function suggests that errors in estimation of N and R are more critical at low rather than high reflectances.

The maximum value composite technique is commonly used to select the least atmospherically contaminated observations from a time series of images (Holben, 1986). An interaction with the precision of the NDVI is thus likely. Over dark (and hence noisy) targets, selection of the maximum NDVI from a series of observations will bias the resulting NDVI values upwards. This will be particularly apparent over dark targets in winter.

The error in NDVI due to quantisation can be overcome to some extent by averaging a window of pixels. For relatively homogeneous surfaces, the precision improves as the number of observations used to estimate the mean increases. However, this does destroy spatial resolution. For future studies, it may be possible to specify a minimum number of pixels required to satisfy a given precision over a homogeneous target. It is also noted that some averaging of a pixel window is often used to reduce the effect of positional errors in time series image data.

Precision of the NDVI varies according to the position in N-R

space of the original observations. Given this fact, consideration should be given to a routine distribution of an error map with the NDVI data by production agencies. Given the difficulties in routinely estimating the PDF for a particular combination of N and R, the "maximum error" approach presented in Equation 4.8 may be used as an initial indicator of data quality. Users would thus receive the NDVI, and also an image of the likely errors due to quantisation. An alternative to this would be the distribution of the original N, R reflectance data, and allow users to calculate the likely NDVI precision. The latter course may be preferred by many, as it allows the data to be reprocessed, if sensor calibration values are modified in the future.

The methodology followed above allows a quantitative evaluation of the technique used to store the NDVI data. For the NDVI, a single byte is capable of storing all the necessary information. The original data acquired for this study were re-processed to a single byte format. This cut the storage requirement for the time series image data in half, a significant saving.

The behaviour of the NDVI (and simple ratio) can be contrasted with that expected in any of the orthogonal vegetation indices, such as the perpendicular vegetation index (PVI) (Richardson and Weigand, 1977) or alternative indices, such as the soil adjusted vegetation index, SAVI (Huete, 1988). While the SAVI is not an orthogonal transformation, for larger values of L (see Huete, 1988)

the sensitivity at low reflectances is largely removed. Contour maps of these functions (in N-R space) are published in Huete and Tucker (1991) and Huete (1989). The orthogonal nature of these transformations removes the sensitivity to small changes at low values of N and R. Preparing graphs of simple transformations such as vegetation indices is an essential step in understanding and hence predicting the expected behaviour of the function to various uncertainties.

The AVHRR instrument has greater radiometric precision than other earth resources satellites, such as Landsat and SPOT. The nominal precision of Landsat TM and SPOT is 0.25 percent, and for Landsat MSS, nominal precision is 0.5 percent for solar zenith angles of zero (Goward et al., 1991). This precision will also decrease as a function of the cosine of the solar zenith angle. Solar zenith angles at the time of overpass for these satellites are similar to those reported for NOAA above. As such, a typical loss in precision of a factor of three can be expected. Results presented in this chapter suggest that given these quantisation errors, users should be very cautious in using ratio based indices for data derived from these satellites, particularly for areas of low reflectance.

Given that all digital image data are quantised for representation in computer systems, an evaluation of the sensitivity of a particular data transformation technique to quantisation errors is a useful step in the comparison of alternative processing methods.

Simulation is a valuable technique in developing an understanding of the likely propagation of errors in a particular transformation.

4.8 Summary

Much of the expected behaviour of the NDVI under a variety of conditions, such as varying solar zenith angles, shadows, differing soil backgrounds and over various bright and dark targets, can be predicted from an understanding of the basic mathematics of the function. This was demonstrated using contour maps of the NDVI and from previous findings reported in the literature.

The NDVI is computed from reflectance observations of N and R. As such, it is affected by errors in N and R. Significant efforts have been made to improve the accuracy of the NDVI by making various atmospheric corrections to N and R. However, a more fundamental relationship is the limit to precision in the NDVI due to quantisation of the original observations. Quantisation is a fundamental component of any digital system.

The precision of the original observations (N, R) was shown to vary as a function of the cosine of the solar zenith angle. For large solar zenith angles, the precision rapidly deteriorates due to the non-linear nature of the cosine function. For typical Australian conditions, each digital count output from the AVHRR refers to a change of 0.3 percent in reflectance.

Two techniques were developed to estimate the precision in the NDVI as a function of the precision in N and R. The first proved simple, and was based on a worst possible error in NDVI approach. The second was based on the derivation of a PDF for the NDVI using numerical simulation. This approach generated results that were both surprising and somewhat counter-intuitive. The PDF was found to vary as a function of N and R. While some pattern was detected in the various PDF functions, the approach is expensive on computer resources. Under this scenario, the worst case approach is proposed as a simple technique to rapidly estimate the likely effect of quantisation on the NDVI.

Using these results it was found that the NDVI derived from AVHRR observations could be stored with suitable precision in a single byte format. The original data purchased for this study were subsequently re-processed from the two byte integer format to a single byte. A significant saving in disk space resulted. This process also removes noise from the NDVI, which may complicate future interpretations of the image data.

The underlying complexity of the mathematical and stochastic properties of the NDVI came as a surprise. Despite this, significant insights into the use of the NDVI in particular, and vegetation indices in general were gained. In particular, the strong relationship between solar position and observational precision is of utmost importance in vegetation monitoring programs using remotely sensed

data. Techniques were developed in this chapter to quantify these relationships.

Having re-processed the data into a byte range, and gained an in-depth understanding of the NDVI, the next step is to investigate the calibration of the NDVI time series imagery. This is known to be a problem (see Section 2.4.1) and is addressed in the following chapter.

Chapter 5

CALIBRATION OF THE SATELLITE DATA

5.1 Introduction

Instrument calibration is an essential task for any measurement program, and particularly for long term monitoring studies. Conversion of satellite digital counts to physical quantities has traditionally not been seen as an important component of satellite based remote sensing studies. However, with increasing interest in long term monitoring studies, using satellite data, conversion of the digital counts to physical quantities and subsequent calibration is essential (Price, 1987a, 1987b).

The AVHRR instrument (carried on NOAA satellites) does not have a complete on-board calibration facility for the solar channels (one and two). Thus, scientists have previously used the pre-flight calibration data for AVHRR solar channels determined by NOAA prior to launch. Subsequent studies have shown this approach to be incorrect (Frouin and Gatier, 1987; Slater et al., 1987; Holben et al., 1990; Brest and Rossow, 1992; Che and Price, 1992; Kaufman and Holben, 1993). Calibration coefficients of the AVHRR solar channels are now known to be different from their pre-flight values by up to 30 percent and drift in time (Che and Price, 1992). This introduces error into the estimation of reflectances (N and R) which subsequently affects the value of the NDVI.

The satellite data used in this study have been derived from three successive NOAA satellites (7, 9 and 11) using the pre-flight calibration coefficients (see Table 3.1). In addition to the drift in calibration for each satellite, there is also the problem of cross (i.e. absolute) calibration between successive satellite platforms. Another obvious possible error source which may have affected the NDVI is the trend in equatorial crossing time of the NOAA satellites (see Figure 2.3).

The image data used in this study were supplied by NASA in NDVI format without the original component reflectances (N and R) used to calculate the NDVI. Thus it is not possible to apply a rigorous correction to the NDVI data set. Attempts have been made (Kaufman and Holben, 1993; Los, 1993; Che and Price, 1992) to apply simple additive corrections to the NDVI based on the time elapsed since launch. These techniques are evaluated against a new technique developed by the author, which uses the data set and time series modelling to derive appropriate corrections.

In this chapter, the actual calibration coefficients as determined by several post-flight studies are used to estimate theoretical corrections to the NDVI. These corrections are then compared to estimates derived both from other studies and also directly from the data set using a new technique. Finally, a set of corrections are proposed which create a consistently calibrated NDVI data set for use in further studies.

The values τ_i, δ_i are provided by NOAA and are known as the pre-flight calibration coefficients. The equivalent spectral albedo (A_i) is defined as (Price, 1987b):

$$A_i = \frac{L_i}{S_i} \times 100 \ (\%)$$

where (5.4)

$$S_i = \frac{E_{0i}}{\pi} \qquad (\textit{termed solar radiance})$$

and $\theta = 0$, $d = 1$

The solar radiance (S) is derived by convolving the spectral response filter of each channel over known global solar radiance spectra such as Thekaekara (1973) or Neckel and Labs (1981, 1984).

As a check on the count output at zero radiance, the AVHRR records the digital counts (in N and R) from observations of deep space (NOAA, 1987). The above formulation does not consider the possible use of observed deep space counts in the conversion from digital counts to radiance (Equation 5.1). Equation 5.1 can be modified to explicitly consider the observed deep space counts ($C0_i$) in each channel as follows:

$$L_i = \alpha_i \times (DN_i - C0_i)$$

where $C0_i = -\frac{\beta_i}{\alpha_i}$ (5.5)

By substituting Equation 5.5 into Equation 5.4 expressions for τ_i and δ_i in terms of α_i, $C0_i$ and S_i can be derived as follows:

$$\tau_i = \frac{\alpha_i}{S_i} \times 100$$
$$\delta_i = \frac{-\alpha_i \times C0_i}{S_i} \times 100 \qquad (5.6)$$

Since the deep space counts are actual observations, it makes sense to use them in the computation of radiance from the DN. Thus Equation 5.5 can be used to convert the digital counts (DN) to radiance (L), and Equation 5.4 can be used to compute the equivalent spectral albedo (A). Equation 5.6 can be used to convert NOAA pre-flight calibration data (τ and δ) to this alternative formulation (α, C0, S).

Price (1987b) noted that A will only equal the reflectance when the sun is overhead, and the earth-sun distance is one. While the solar zenith in particular has a major impact on reflectance, for a lambertian target (and no atmosphere) there is no subsequent effect on the NDVI. Due to the ratio nature of the NDVI, both solar zenith and earth sun distance cancel out in the computation of NDVI. This is the major advantage of using a ratio vegetation index such as NDVI. This of course assumes a lambertian target and no atmospheric effect on the signal.

5.3 Previous AVHRR Calibration Results

To be able to estimate the likely error in NDVI caused by incorrect pre-flight calibration information, it is necessary to know firstly, what calibration parameters were actually used to process the data and secondly, what calibration data should have been used. The GAC data tapes supplied by NOAA (to NASA) and subsequently used to create these data have the pre-flight data recorded on a header. This section documents both the pre-flight calibration and post-flight calibration results to date, from the two major studies reported in the literature.

5.3.1 Pre-Flight Calibration

Pre-flight data used to process the data set (compiled from the literature) are shown in Table 5.1.

The solar constant (S) varies on each AVHRR instrument depending on the exact band pass function of that instrument. A further difficulty is the use of different solar spectra to compute the solar constant for the pre-flight calibration data issued by NOAA. The solar constant (S) for NOAA 7 and 9 was taken from the data of Thekaekara (1973) (noted in Price, 1987b, 1988). For NOAA 11 the solar constant was derived from the more recent data of Neckel and Labs (1984) (Abel, 1990). The NOAA 11 pre-flight calibration was also modified on 27 September 1990 (Abel, 1990), after a re-evaluation of the original calibration methodology and results.

NOAA	Ch.	α	τ	δ	S	C0 c-calc s-spec	Ref
7	1	.532	.1068	-3.44	498	32.21c	[1]
7	2	.347	.1069	-3.488	325	32.63c	[1]
9	1	.523	.1063	-3.8464	492	36.18c	[1]
9	2	.350	.1075	-3.877	326	36.07c	[1]
Launch -> 27 Sep 1990							
11	1	.470	.0906	-3.73	518.7	41.17c	[2]
11	2	.277	.0827	-3.39	335.2	40.99c	[2]
27 Sep 1990 -> ongoing							
11	1	.490	.095	-3.78	518.6	40s	[2]
11	2	.301	.090	-3.6	334.8	40s	[2]

[1] Kidwell (1991), NOAA (1987) and Price (1987b, 1988)
[2] Abel (1990)

Table 5.1 AVHRR pre-flight calibration data for NOAA 7, 9 and 11. (Where deep space counts (C0) were not specified in the reference, they were computed using Equation 5.6)

The solar constant (S) for each instrument, derived from the Neckel and Labs (1984) data set, and the appropriate band pass filter has been prepared by Kidwell (1991, pp. 3-19) and is shown in Table 5.2. The relationship between the quantities (F and W) shown in Kidwell (1991) and S is:

$$S_i = \frac{F_i}{W_i \times \pi} \qquad (5.7)$$

where

F_i = *integrated solar spectral irradiancein bandpass*(Wm^{-2})

W_i = *equivalent width of band pass* (μm)

Differences of up to five percent in S (e.g. on NOAA 7 Channel 1, S goes from 498 to 523.1) result from the change in data source for solar radiance spectra.

NOAA	S (Ch.1)	S (Ch.2)
7	523.1	334.8
9	520.5	335.4
11	518.6	335.1

Table 5.2 Solar constant (S) for AVHRR (NOAA 7, 9 and 11) (per Neckel and Labs (1984) Solar Radiance Spectra - from Kidwell, 1991, page 3-19)

The AVHRR instrument uses 10 bit quantisation (0-1023) to digitise the incoming radiance and was designed to respond linearly to input radiance over the entire solar range, whilst maintaining a buffer of approximately 40 counts at either end of the scale. This buffer was designed to allow for possible sensor drift (Goward et al., 1991). A calculation example of the conversion from digital number (DN) to equivalent albedo (A) is given in Example 5.1.

Example 5.1:
Conversion of digital counts to radiance (NOAA 7 Channel 1)

DN = 223
L = .532 * (223 - 32.21)
= 101.5
A = 101.5 / 498 * 100
= 20.38 %

By inspection of the above example, when the recorded DN is 32, A is zero, and when DN is 968, A is 100 percent. These two values (32, 968) represent the minimum and maximum responses of the instrument (NOAA 7) based on the pre-flight calibration data. The extra counts (i.e. < 32 and > 968) on the ten bit scale are the buffer mentioned above. Note that this formulation does not consider the solar zenith angle.

5.3.2 Post-Flight Calibration

The estimation of post-flight calibration coefficients involves estimation of α and C0 for both channels as a function of time since launch. This section documents reported results from the literature.

5.3.2.1 Deep Space Counts

Observed deep space counts have been reported by Holben et al. (1990) and Kaufman and Holben (1993). These papers both result from the one ongoing study and the results reported in the second paper have been adopted and are shown in Table 5.3.

The deep space observations for NOAA 11 agree with the pre-flight data for NOAA 11 (after 27 September 1990) shown in Table 5.1. However, the deep space values for all other satellites disagree (by up to six digital counts). Supporting evidence for NOAA 11 is reported by Mitchell et al. (1992, p. 64) who report the observed deep space counts as 40 with a standard deviation of ± 0.2 counts.

Independent confirmation of the observed deep space counts for the other satellites was not available in the literature.

Satellite	Ch. 1 (R)	Ch. 2 (N)	Date Observed
NOAA 7	36	38	August 1981
NOAA 7	36	37.7	August 1982
NOAA 7	35.8	37.4	August 1983
NOAA 7	35.4	37.2	August 1984
NOAA 7 MEAN SD	35.80 ± 0.28	37.58 ± 0.35	
NOAA 9	38	39.9	August 1985
NOAA 9	37.9	39.3	August 1986
NOAA 9	37.8	39.1	August 1987
NOAA 9	37.8	39	August 1988
NOAA 9 MEAN SD	37.88 ± 0.10	39.33 ± 0.40	
NOAA 11	40	40	Feb-Mar 1989
NOAA 11	40	40	August 1990
NOAA 11	40	40	August 1991
NOAA 11 MEAN SD	40.00 ± 0.00	40.00 ± 0.00	

Table 5.3 Observed deep space counts for NOAA 7, 9 and 11 (from Kaufman and Holben, 1993)

The data presented in Table 5.3 indicate a slight change (decrease) in deep space counts over the life of a particular satellite mission. However, as quantisation error will be present in the deep space count measurement, this change is not considered significant and it can be assumed that the deep space counts for each channel remain essentially fixed in time but are different from the pre-flight

values given by NOAA. A mean value for deep space counts over the mission life of each satellite has been computed, and is also shown in Table 5.3.

5.3.2.2 Sensor Gain

A number of studies have been conducted to estimate the gain of the AVHRR instruments. Che and Price (1992) summarised all existing calibration work (to 1992) and plotted estimates of the gain derived from numerous studies as a function of time (months) since launch for NOAA 7, 9 and 11. The data from this study have been used to prepare Figure 5.1. By pooling all data for each satellite, Che and Price (1992) proposed a regression relationship for the gain, based on the time (months) since launch. This regression is shown in Figure 5.1 (dotted line).

The actual sensor gain determined by numerous studies is clearly larger (i.e. less sensitive) than the pre-flight value. This indicates a loss of sensitivity in the instrument since launch. The drift in gain over time is relatively minor (typically 4-6 percent per year), and the various AVHRR instruments appear relatively stable. However, the gain is clearly different from the pre-flight values adopted by NOAA. Che and Price (1992) attribute this to the long storage period prior to launch, and/or the outgassing of the instrument in space.

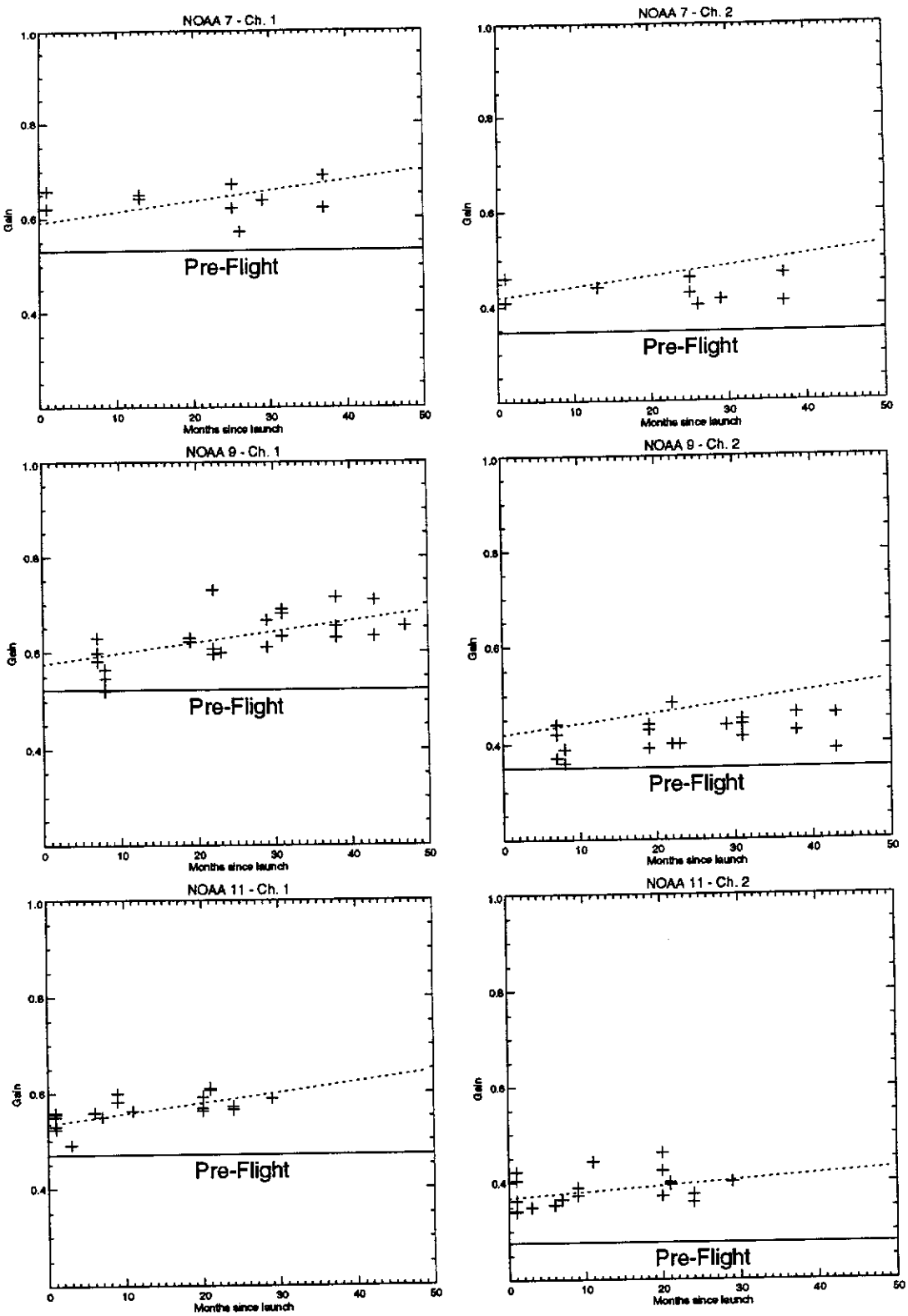

Figure 5.1 Sensor gain since launch for NOAA 7, 9 and 11 (from Che and Price, 1992). Solid line is pre-flight gain. Dotted line indicates regression by Che and Price (1992)

Satellite	Channel	Regression for Gain
7	1	.591 + 0.00223 x M
9	1	.576 + 0.00223 x M
11	1	.534 + 0.00223 x M
7	2	.420 + 0.00223 x M
9	2	.420 + 0.00223 x M
11	2	.369 + 0.00120 x M

Table 5.4 Regressions of time dependence versus sensor gain. M is months since launch (per Che and Price (1992), Table 5, p. 24)

The linear regression parameters proposed by Che and Price (1992) to describe the change in gain over time are shown in Table 5.4. They derived this relationship by pooling all data for each channel across all satellites. Rather than adopt a statistical estimate for each satellite, they assumed that the instruments were behaving similarly (except Channel 2 on NOAA-11) and calculated a mean value for the loss of sensitivity. As a consequence of this approach, the regression models for channel 2 (NOAA's 7 and 9) do not follow the observations (see Figure 5.1).

Kaufman and Holben (1993) have also conducted an extensive series of tests on the calibration of the AVHRR instruments on NOAA 7, 9 and 11. Their results are currently recommended by the IGBP (Townshend, 1992) for the construction of a global one km resolution data set. The estimates of sensor gain derived by Kaufman and Holben (1993) using stable desert targets are shown in Table 5.5 and Figure 5.2. Using their data, linear regressions for each channel on

each satellite have been calculated and are shown in Table 5.6.

Satellite	Channel	Gain	Date (August of that year)
7	1 2	0.62 0.40	1981
7	1 2	0.65 0.44	1982
7	1 2	0.67 0.45	1983
7	1 2	0.69 0.47	1984
9	1 2	0.60 0.42	1985
9	1 2	0.63 0.43	1986
9	1 2	0.67 0.45	1987
9	1 2	0.71 0.46	1988
11	1 2	0.60 0.41	1989
11	1 2	0.59 0.41	1990
11	1 2	0.59 0.41	1991

Table 5.5 Sensor calibration coefficients using stable desert target method (from Kaufman and Holben, 1993)

Satellite	Channel	Regression for Gain
7	1	0.620 + 0.00191 x M (R^2=0.99, n=4)
9	1	0.572 + 0.00307 x M (R^2=1.00, n=4)
11	1	0.603 - 0.00043 x M (R^2=0.75, n=3)
7	2	0.411 + 0.00158 x M (R^2=0.96, n=4)
9	2	0.410 + 0.00116 x M (R^2=0.98, n=4)
11	2	0.410 + 0.00000 x M (R^2=1.00, n=3)

Table 5.6 Regressions of time dependence versus sensor gain. M is months since launch (data from Kaufman and Holben, 1993) (see Table 5.5)

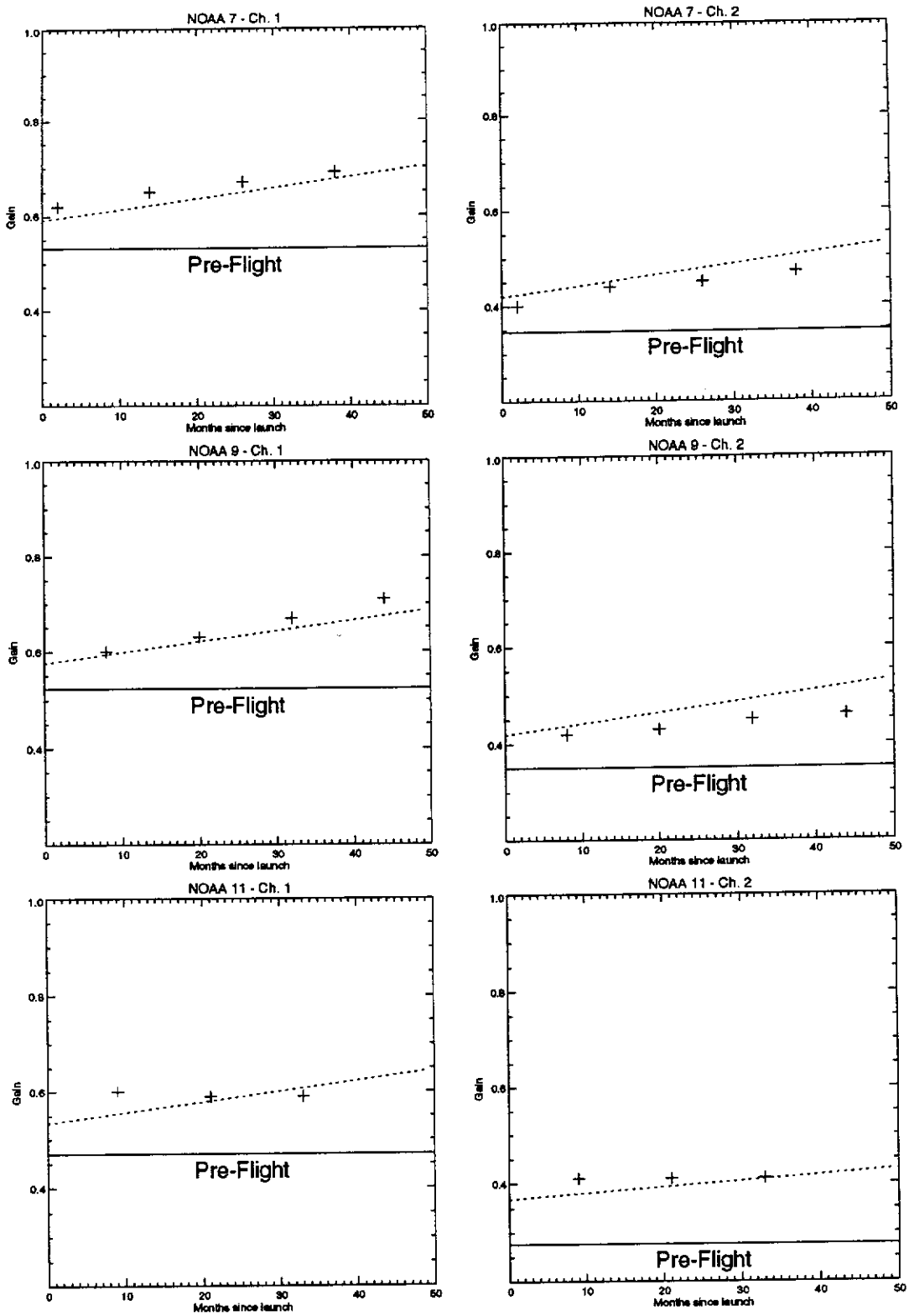

Figure 5.2 Sensor calibration results using stable desert target method (from Kaufman and Holben, 1993). The dotted lines indicate regression from Che and Price (1992) for comparison with Figure 5.1

Kaufman and Holben (1993) claim a precision of ± 0.02 for the determination of calibration coefficients using the 'desert' method. Clearly the regression of Che and Price (1992) is not within a 0.02 error tolerance of the data of Kaufman and Holben (1993). Che and Price (1992) used the results of Kaufman and Holben (1993) (with many others) in their determination of suitable regressions. The only conclusion that can be drawn from this is that calibration of satellite radiometers is as yet an uncertain science. Che and Price (1992) estimate that an absolute accuracy in calibration of ± 10 percent is currently possible using post-flight methods.

5.4 Effect of Calibration Errors on NDVI

Errors in the calibration coefficients used to recover reflectance (or equivalent spectral albedo) from digital counts for N and R, lead to errors in the NDVI in cases where the calibration coefficients do not change in the same proportions for each channel. An example calculation to determine error in NDVI due to changes in the calibration data is presented in Example 5.2.

Example 5.2, shows that the expected error in NDVI is a complex function of differences in pre-flight and post-flight values of S, C0, α. Due to the mathematical nature of the NDVI (see Chapter 4), the effect of these changes will vary depending on the original reflectances. This is a similar situation to the quantisation error being a function of the original reflectances (see Figures 4.5 and 4.6).

Example 5.2:

Error in NDVI due to Calibration Errors for NOAA 7 at Launch

	Ch. 1 (R)	Ch.2 (N)	
DN	234	267	[in 0-1023 range]
Pre-flight data			
α	0.532	0.347	[Table 5.1]
C0	32.21	32.63	[Table 5.1]
S	498	325	[Table 5.1]
A_{pre}	21.56 %	25.02%	[Equation 5.4, 5.5]
$NDVI_{pre}$	0.074		
Post-flight data			
α	0.591	0.420	[Table 5.4]
C0	35.80	37.58	[Table 5.3]
S	523.1	334.8	[Table 5.2]
A_{post}	22.39%	28.78%	[Equation 5.4, 5.5]
$NDVI_{post}$	0.125		
$Error_{NDVI}$	0.051		[Error = $NDVI_{post}$ - $NDVI_{pre}$]

5.4.1 Theoretical Simulations

The range of possible digital counts (N and R) varies from 0 to 1023. The error in NDVI due to errors in the calibration coefficients can be simulated at each possible combination of digital count values to give a global overview of the likely impact of calibration errors on the NDVI. Figures 5.3, 5.4 and 5.5 show the error in NDVI (Error = $NDVI_{post}$ - $NDVI_{pre}$) over a range of digital counts from 50 to 900 for the NOAA 7, 9 and 11 satellites respectively. In each case the pre-flight calibration data are from Table 5.1. Post-flight calibration data are from Table 5.3 (deep space counts), Table 5.2 (solar constant) and Table 5.6. The gains were assumed to be as per the regression from the data of Kaufman and Holben (1993) for the launch date of each satellite (Table 5.6).

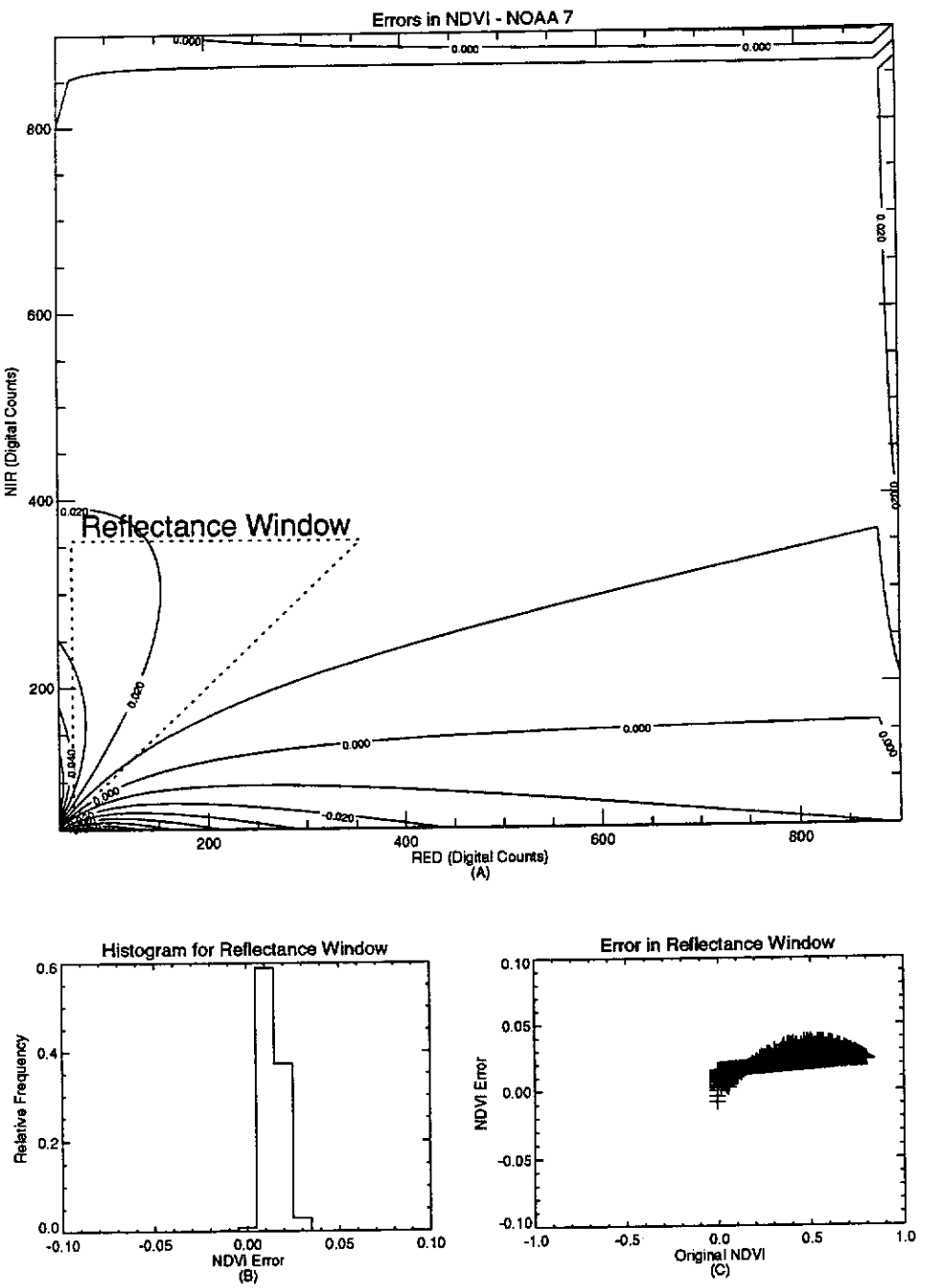

Figure 5.3 NDVI error due to pre-flight calibration error for NOAA 7. Pre-flight data per Table 5.1.
Post-flight data (α_1=0.620, $C0_1$=35.80, S_1=523.1, α_2=0.411, $C0_2$=37.58, S_2=334.8).
(a) NDVI error contours as a function of digital counts
(b) Histogram of NDVI errors for reflectance window
(c) NDVI error as a function of the original NDVI for reflectance window

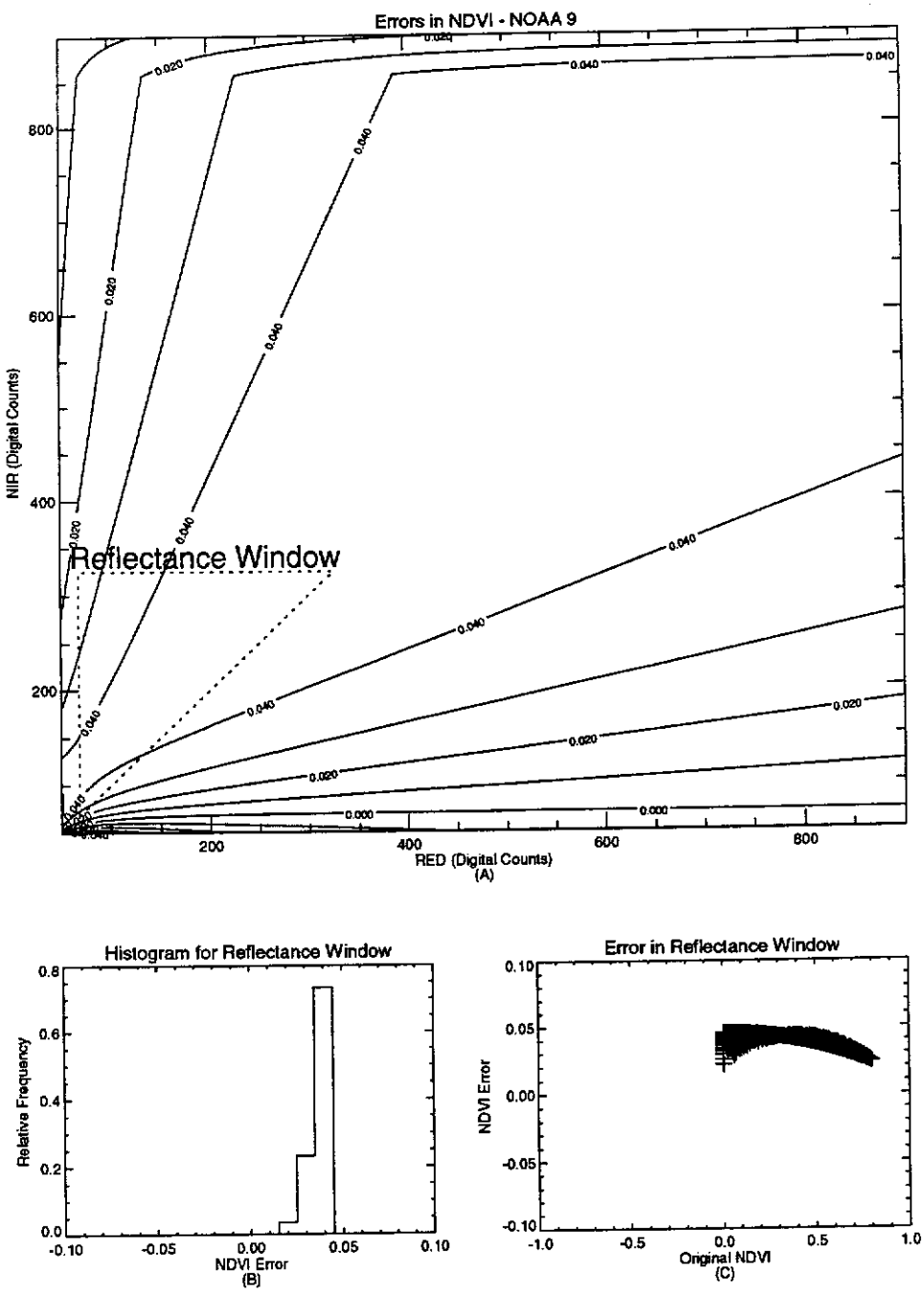

Figure 5.4 NDVI error due to pre-flight calibration error for NOAA 9. Pre-flight data per Table 5.1.
Post-flight data (α_1=0.572, $C0_1$=37.88, S_1=520.5, α_2=0.410, $C0_2$=39.33, S_2=335.4).
(a) NDVI error contours as a function of digital counts
(b) Histogram of NDVI errors for reflectance window
(c) NDVI error as a function of the original NDVI for reflectance window

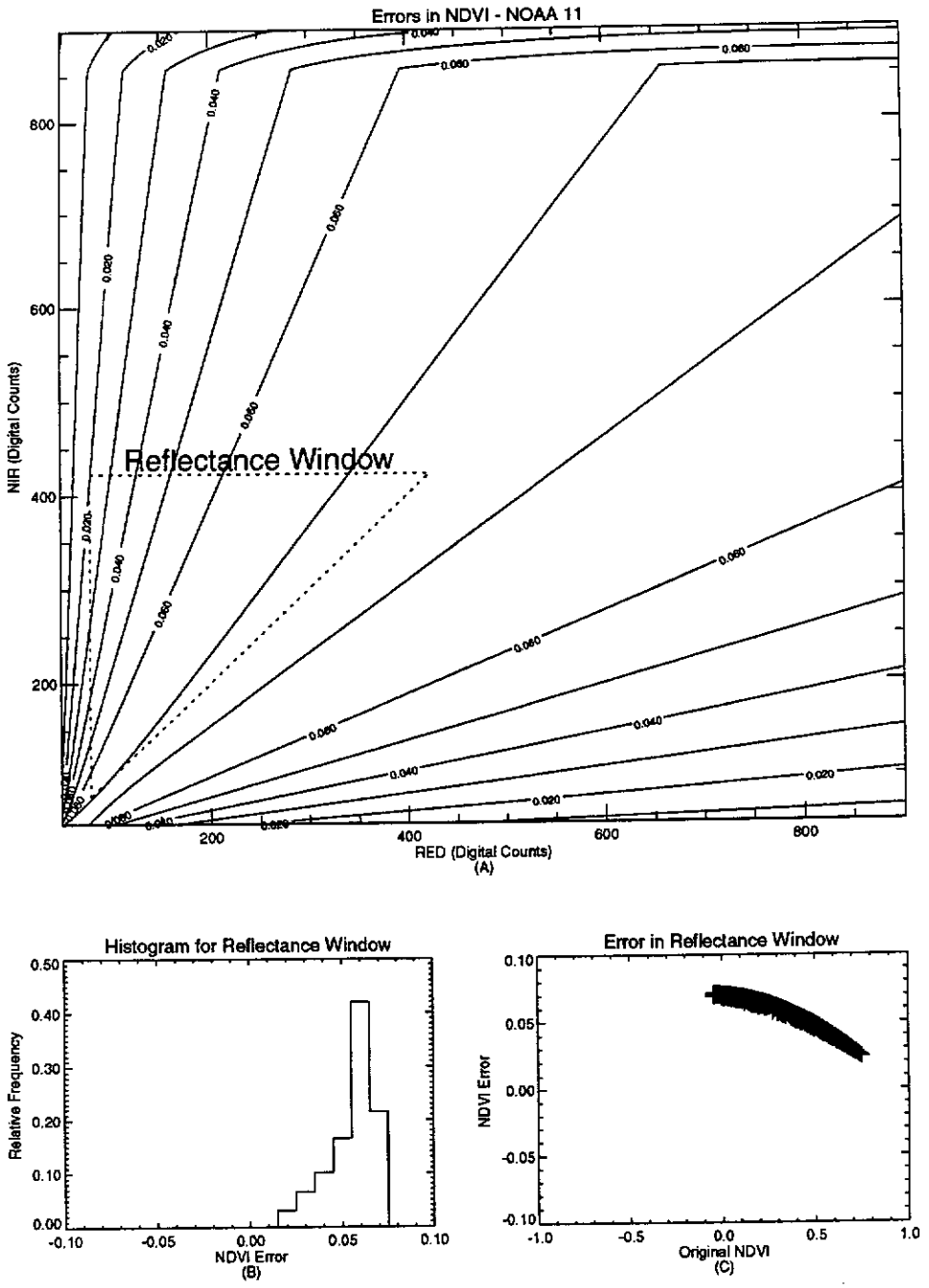

Figure 5.5 NDVI error due to pre-flight calibration error for NOAA 11. Pre-flight data per Table 5.1.
Post-flight data (α_1=0.603, $C0_1$=40.00, S_1=518.6, α_2=0.410, $C0_2$=40.00, S_2=335.1).
(a) NDVI error contours as a function of digital counts
(b) Histogram of NDVI errors for reflectance window
(c) NDVI error as a function of the original NDVI for reflectance window

In each Figure (5.3, 5.4, 5.5) part (a) shows a contour plot of error in NDVI at each possible combination of digital counts in the range 50 to 900. The error clearly varies with reflectance in the individual bands. Thus it is necessary to know the original digital counts recorded for a particular pixel to estimate the error in NDVI due to errors in the pre-flight calibration. In this study, this is not possible, as the data were distributed as NDVI only. This problem is not unique, as many users receive NDVI data only (Los, 1993; Hutchinson, 1991).

An alternative approach is to use prior knowledge to estimate the approximate location of the digital counts that would have been imaged. While this is clearly dynamic, a static window has been assumed. Each plot shows a 'reflectance window' which is an estimate of the data range for Australian conditions and assumes a range of reflectance from 10 percent (at solar zenith of 70 degrees) up to 40 percent (at solar zenith of 30 degrees). For this reflectance window, part (b) of each Figure (5.3, 5.4, 5.5) is a histogram of all errors inside the reflectance window, and part (c) plots the error in NDVI as a function of the original NDVI. Table 5.7 summarises the error in NDVI within each of the reflectance windows, for each particular simulation.

Satellite	Mean	SD	Min	Max
7	.0196	.0044	-.0080	.0373
9	.0411	.0043	.0219	.0456
11	.0600	.0122	.0194	.0712

Table 5.7 Summary of NDVI errors in the specified reflectance window for NOAA 7, 9 and 11 (from Figures 5.3, 5.4, 5.5)

The overall pattern in each figure indicates that the worst error in NDVI is for very bright and dark targets. Given that very bright targets such as snow, ice and cloud are not of interest here, the worst error is for dark targets. Note that the effects of signal quantisation (Chapter 4) are also worse for dark targets, which is due to the mathematical nature of the NDVI. Despite this overall similarity, the plots for each satellite clearly indicate that the error structure is different for each satellite, depending on the exact differences between the pre-flight and post-flight calibration data. This error structure will also be dynamic, as the gains change over time.

For NOAA 7 and 9, the error in the window of interest (Figure 5.3b) is almost constant and could be approximated by a simple additive correction. It is important to recall the effect of quantisation error on the NDVI from Chapter 4. Figure 4.8 shows the probability of correct assignment of a computed NDVI value to a final scale, with bin width of 0.01 NDVI units for typical Australian conditions. For low reflectances (i.e. 5-10 percent) the probability of correct assignment is in the range 30-50 percent. Given the standard

deviation of the error within the window (~0.005, see Table 5.7), a simple additive correction is clearly applicable.

For NOAA 11, Figure 5.5c shows the error in NDVI is related to the original NDVI value. Thus it would be possible for this satellite, using the indicated post-flight for Figure 5.5, to model the error in NDVI with a quadratic curve, and estimate the correction as a function of the original NDVI. However, the standard deviation (0.013, Table 5.7) of the error for NOAA 11 is not sufficient to justify the extra effort to make such a correction when the effect of quantisation on the NDVI is also considered.

The results presented above are surprising and again show the complicated mathematical nature of the NDVI.

5.4.2 Discussion of Theoretical Results

Conceptually, the NDVI is sensitive to error in the deep space counts at low reflectance counts, and sensitive to instrument gain at high reflectance. While the deep space counts are measured quantities in space, the pre-flight calibration coefficients provided by NOAA do not make use of them. The differences between pre- flight and post-flight deep space counts (Tables 5.1 and 5.3) will clearly have a major impact on NDVI over dark targets. Che and Price (1992) recommend the use of measured deep space counts rather than the pre-flight values.

Los (1993) has used a similar technique to that in the previous section to estimate error in the NDVI due to error in the pre-flight calibration data. The key difference is that Los had access to parts of the original reflectance data from which the NDVI was computed. He thus used these data to define a region of interest from which an average correction for the entire data set was estimated. Che and Price (1992) also present a graph depicting error in NDVI as a function of the original NDVI (Che and Price, 1992, Figure 4, p. 25). This graph assumes the data were processed with the observed deep space counts. For NDVI data from NOAA (or NASA) this is not the case, and these results must be ignored. Kaufman and Holben (1993) simulated the error in NDVI as a function of the original digital counts (Kaufman and Holben, 1993, Table 6, p. 45) for different targets in terms of reflectance. These targets are effectively the corners of the cover triangle depicted in Figure 5.3. They recommend the use of an simple global additive correction and have tabulated values on an annual basis from 1981 to 1990.

The technique adopted above is based on a brute force simulation, and is clearly appropriate under the circumstances. The technique can be improved by refining the window for which error estimates are computed. This could be done using observed data, or global average reflectance data (Rossow et al., 1989). Obviously the ideal technique would be always to preserve the observed digital counts, which could then be reprocessed when more accurate calibration data become available.

5.5 Corrections to NDVI Time Series

The gain of the AVHRR instrument changes (loses sensitivity) with time. Time dependent estimates of the gain, and the simulation technique (of Section 5.4) can be used to compute an average error in the NDVI due to calibration errors for each month of the data set used in this study. For validation, the results of such a simulation can be compared against a NDVI time trace derived over a stable target from the image data.

5.5.1 Computational Approach

Estimates of the average (global) error in NDVI have been computed using:

(a) Pre-flight calibration data (Table 5.1) assuming all NOAA 11 data were processed using the original pre-flight calibration (i.e. launch to 27 Sep 1990),

(b) Post-flight calibration data as follows:

  (i) Solar radiance data from Neckel and Labs (1984) (Table 5.2),

  (ii) Mean observed deep space count for each satellite (Table 5.3),

  (iii) Estimates of the gain from the regressions of Che and Price (1992) (Table 5.4) and the computed regressions (Table 5.6) from the data of Kaufman and Holben (1993).

For the GAC data set used in this study, the platforms from which each monthly image was derived are shown in Table 5.8. These dates were derived from the launch dates and operational phases of each satellite (see Table 3.1) and inspection of the several NDVI time traces.

Satellite	Start Date	End Date	Total Months
NOAA 7	Jul 1981	Feb 1985	44
NOAA 9	Mar 1985	Nov 1988	45
NOAA 11	Dec 1988	Mar 1991	28

Table 5.8 Satellite platforms for NOAA GAC data used in this study

At each month, the time dependant regressions for gain were used to estimate the current values of the AVHRR gain (in each channel). These estimates were used to compute the average NDVI error for a reflectance window corresponding to a minimum of 10 percent (at solar zenith of 70 degrees) to a maximum of 40 percent (at solar zenith of 30 degrees). This window would cover most of the expected reflectances over the Australian land surface (Rossow et al., 1989). Software was developed to automate the production of these calibration reports. Separate reports are presented in Appendix A, for both the gain data of Kaufman and Holben (1993) and Che and Price (1992). These reports also include a (quadratic) regression to relate the error in NDVI to the original NDVI for comparison purposes. The average error and standard deviation of that error for the above reflectance window is shown as a time series in Figure 5.6.

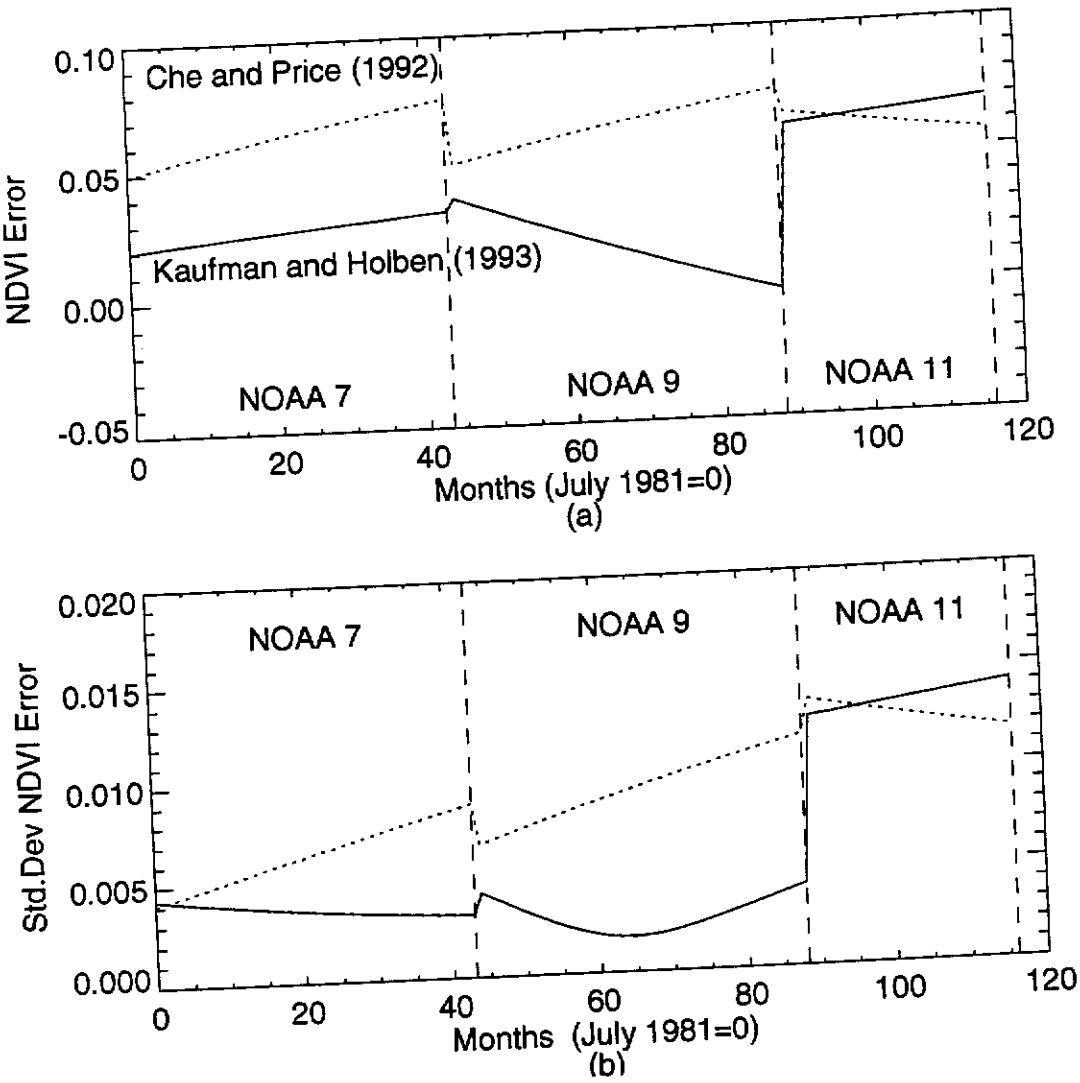

Figure 5.6 Simulated NDVI errors due to errors in gain, deep space count and solar constant

From Figure 5.6, the changeover between satellites is clearly visible in the plot. The gain estimates from both data sets generate similar results for NOAA 11. For NOAA 7, while the trend is similar, the magnitude is approximately 0.03-0.04 NDVI units different. For NOAA 9, the trend is in the opposite direction. Another major feature is the large step between NOAA 9 and 11 (approximately 0.07 NDVI units) generated using the gain estimates from Kaufman and Holben (1993).

The standard deviations of the average error for each reflectance window, do not agree for the different data sets but are less than 0.014 NDVI units in all cases for both data sets. For NOAA 11, the standard deviation of the error estimate is significantly greater than for NOAA 7 and 9, echoing the previous results for single date simulations. Given the effect of quantisation errors on the NDVI, the average error approach is clearly applicable for all image dates in the NDVI (GAC) data set, for the adopted reflectance window.

The estimates of sensor gain for NOAA 9 (see Figures 5.1 and 5.2) by Che and Price (1992) and Kaufman and Holben (1993) are both plausible given the possible absolute calibration errors quoted by Che and Price (1992) of ± 10 percent. Despite this, the trend in simulated error in the NDVI for NOAA 9 (Figure 5.6) is in the opposite direction. At the end of the NOAA 9 mission the error estimates were different by 0.07 NDVI units.

Overall, the results of the simulations are conflicting, and not encouraging. While the overall methodology has been proven, the data used to estimate gain, from the two most complete calibration studies to date, generated significantly different results. Given the general difficulties with post-flight calibration (Che and Price, 1992), this situation will likely remain until on board calibration facilities are provided on the next generation of satellites. To resolve these difficulties, a new technique has been developed to estimate

corrections to the NDVI from the data set itself. This technique and the assumptions it is based on are described below.

5.5.2 Broad Area Invariant Target Approach

An alternative method to estimate NDVI error due to error in the pre-flight calibration data is to extract a time series of observations from an invariant target in the image. If the NDVI of such a target changed, it could be assumed that some of those changes were calibration related. After extensive searching (using computer based techniques) through the image data base, no truly invariant targets were found to exist in the data set. While the ocean is immediately attractive conceptually (i.e. no green vegetation), the low precision of the NDVI at low reflectances which occur over the ocean negated this approach.

An alternative hypothesis was thus generated:

Hypothesis: *Any trend in the time series of the mean NDVI from a large area would indicate changes in the post-flight calibration. While this may have a strong seasonal component, it may be possible to remove this component using standard signal processing techniques.*

This hypothesis assumes;

(a) That error in NDVI due to calibration error is (approximately) additive,

(b) That the proportions of major cover types (i.e. land, water) are the same for each image in the time series,

(c) That seasonal influences occur at (approximately) the same time and are of similar magnitude each year.

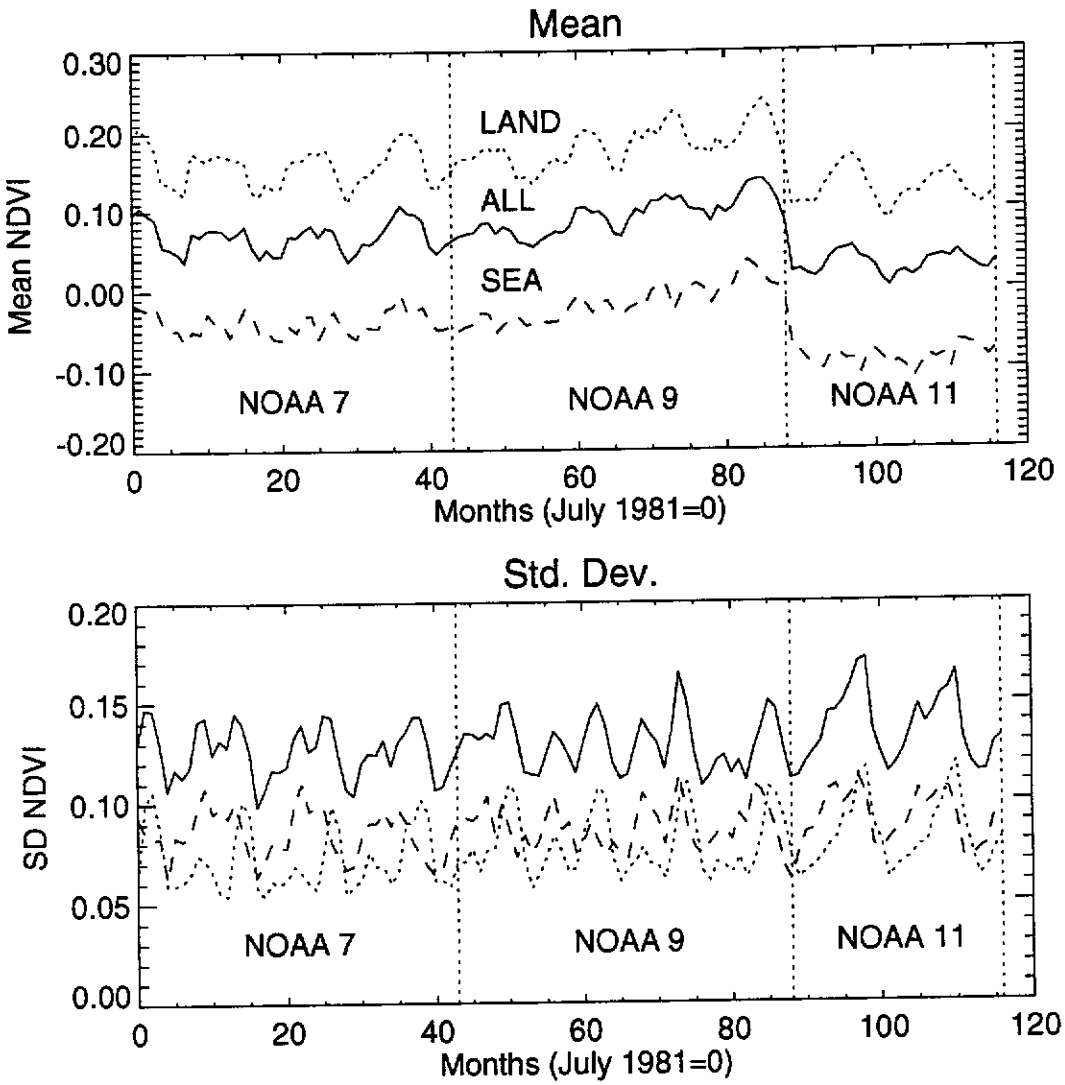

Figure 5.7 Time series of means and standard deviations of NDVI (for entire image, land pixels only, and ocean pixels only)

Using a land/ocean mask, the global mean NDVI, and means for both land and ocean pixels were extracted from each individual monthly image in the time series (see Table 3.1). In addition, the standard deviation of each was also extracted. The resulting time series is presented in Figure 5.7.

A strong seasonal signal (with period of 12 months) is clearly evident in both the mean and standard deviation of all surface types (see Figure 5.7). As expected, the mean NDVI over land is consistently higher than that over the ocean, and the global average NDVI (both land and ocean) sits in the middle of these two major surface types. The global average shows no trend during NOAA 7 observations, a slight increasing trend during NOAA 9, followed by a large drop when NOAA 11 observations commenced. This mirrors the results of the previous section, using gain values from Kaufman and Holben (1993), although does not agree with the results using gains from Che and Price (1992). All that is now required is a technique to extract the assumed calibration error from the time series. For this purpose all data were pooled, and the global average was used.

The global average NDVI time series is assumed to be represented by the following model:

$$X_t = T_t + S_t + R_t \tag{5.8}$$

where

X_t = *original data*
T_t = *trend component*
S_t = *seasonal component*
R_t = *random component*

The error in NDVI due to changes in the sensor calibration are assumed equal to the trend component (T_t). Estimation of the various components is a standard topic in time series textbooks, and will be only briefly given here. The trend component is recovered from the original series, by filtering with a running average filter of length p, where p is the length of the seasonal period (Brockwell and Davis, 1987). For the monthly data shown in figure 5.7, there is a clear seasonal period of 12 months. For the general case, trend estimates (by smoothing) of the time series using a moving average of length p can be obtained from Brockwell and Davis (1987):

$$T_t = \frac{\sum_{t=t-q}^{t+q} x_t}{(2 \times q) + 1} \qquad (5.9)$$

where $p = (2 \times q) + 1$ *(i.e. p is odd)*

When the seasonal period (p) is even (i.e. p=12), Equation 5.8 is modified as follows:

$$T_t = \frac{0.5x_{t-q} + x_{t-q+1} + \ldots + x_{t+q-1} + 0.5x_{t+q}}{2 \times q} \qquad (5.10)$$

where $p = 2 \times q$ *(i.e. p is even)*

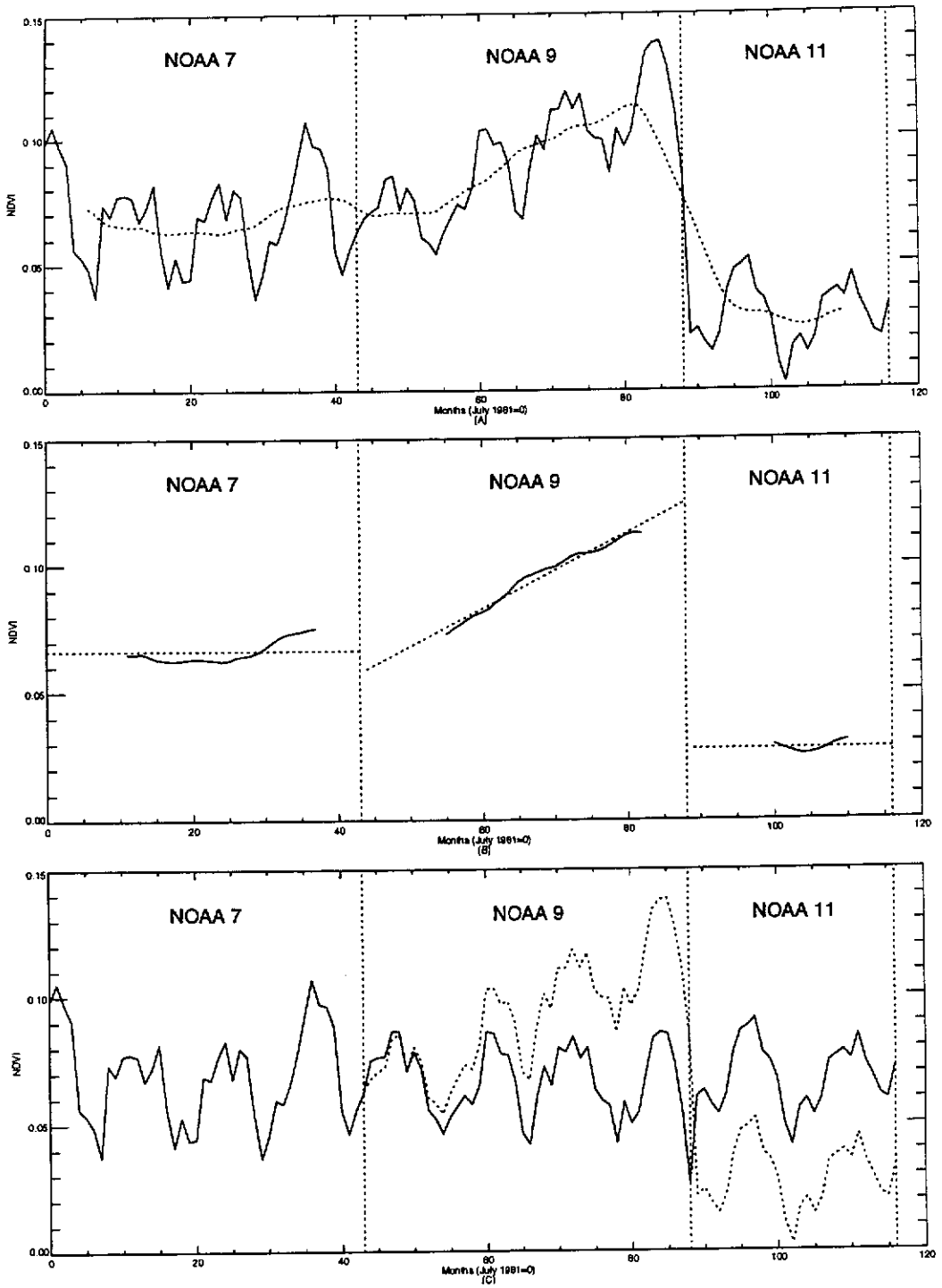

Figure 5.8 Trend estimates from global time series

(a) Global mean NDVI (all pixels) (solid) and 12 point running average filter indicating trend (dotted)

(b) Filtered estimates of trend composed of measurements from a single satellite (solid) and assumed model (dotted)

(c) Detrended global mean NDVI (solid) using trend estimates from (b) original data (dotted)

Figure 5.8a shows the global average NDVI smoothed with a 12 point running average filter (per Equation 5.10). It is known from the previous results that the calibration error in NDVI has a different error structure for each satellite. In Figure 5.8a, when the satellites change over, the running average will be computed using measurements from two different satellites, which is not desirable for error estimation. Figure 5.8b extracts the results from the running average, where that average is composed of measurements taken from a single satellite. The dotted line in Figure 5.8b, is a fitted model to describe the error, and subsequently extrapolate to the start and end of the measurement periods for each satellite. The fitted models are detailed in Table 5.9.

Satellite	Trend Estimate
NOAA 7	Error = 0.06628
NOAA 9	Error = -0.00602 + 0.0014805 x M where M = months (July 1981=0)
NOAA 11	Error = 0.02735

Table 5.9 Assumed trend estimate for each satellite (derived from Figure 5.8b)

A constant error was chosen as a suitable model for NOAA 7 and 11 by inspection of Figure 5.8b. For NOAA-9 a linear trend was chosen again based on inspection. The quality of fit in all cases is excellent. The trend for NOAA 7 appears from Figure 5.8b to be rising slightly at the end of the mission. This has been caused by an very wet season in the arid parts of Western Australia during 1984

(see Chapters 6 and 8). This season caused higher values of NDVI in this time period. This represents a problem for the technique and violates one of the basic assumptions. The effect could be removed by inspection of the image data for any particularly good seasons, and removing this area from the analysis. Fortunately, in this case the season had minimal impact on the trend estimate, as it occurred during a change over from NOAA 7 to 9. This will not always be the case, and careful inspection of the image data is necessary to remove any area that experiences an atypical season.

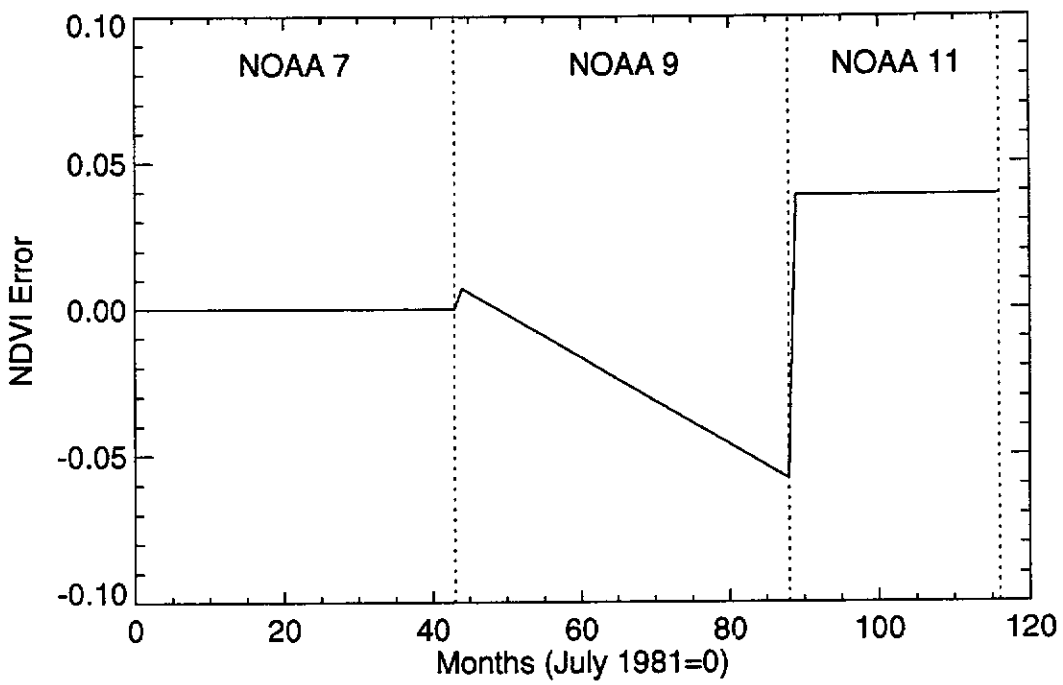

Figure 5.9 Estimates of error in NDVI of the GAC data set (assuming no error in NOAA 7 measurements) (Error=$NDVI_{post}$-$NDVI_{pre}$)

Using the models proposed in Figure 5.8b (see Table 5.9), the error in NDVI, due to calibration errors, is the value that when added to the series would result in no trend being evident. Absolute calibration is not possible, and the only available option is to anchor the calibration to one particular observation in the time series. For this purpose, it was tentatively assumed that the NDVI measurements from NOAA 7 were correct, and all others were adjusted to reflect this assumption. The error in NDVI (based on these assumptions) is presented in Figure 5.9. These data reflect a correction added to each monthly image in the original data set, to create a relative calibration for the data set.

The resulting detrended time series is shown in Figure 5.8c. This was created by adding the error estimates shown in Figure 5.9 to the original time series of Figure 5.8a. Clearly, this detrended data set is a visual improvement on the original time series.

5.6 Comparison of Results

Two alternative techniques have been used (Figures 5.6, 5.9) for the estimation of error in NDVI due to calibration errors in the measurements from each AVHRR. The first, based on knowledge of both the pre-flight and post-flight calibration, gives estimates which are absolute. The second was developed due to dissatisfaction with the results of the first method, and uses the data set to estimate trend (using classical time series analysis methods), which is

assumed to be solely due to calibration errors. This second technique provides relative calibration information only. This section compares the results from the two techniques and proposes an absolute calibration based on the comparison.

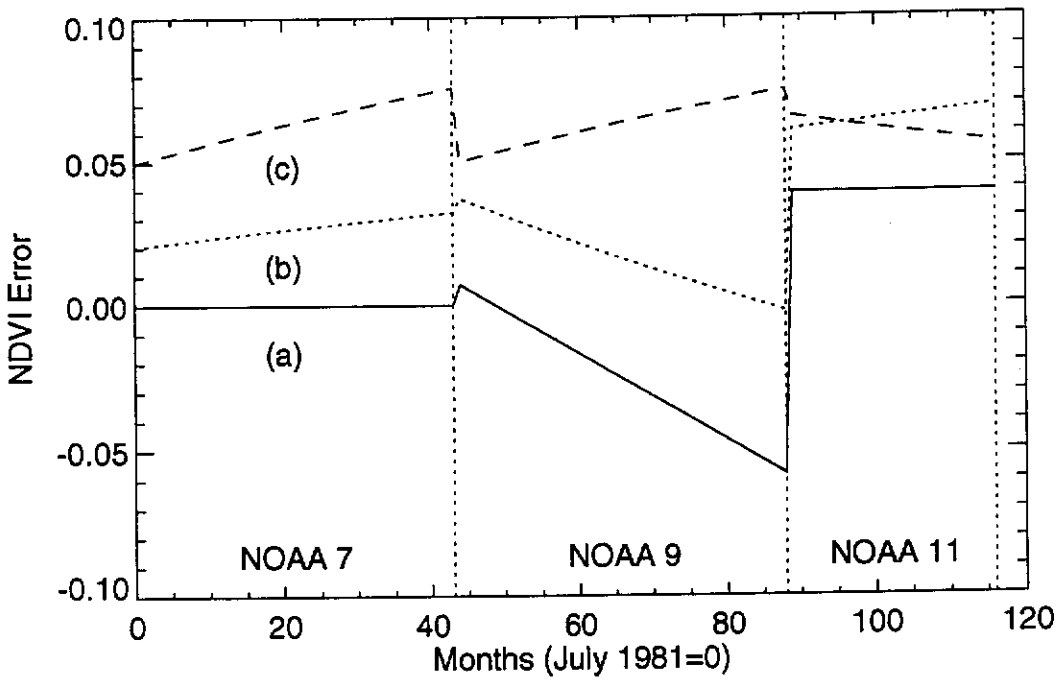

Figure 5.10 Comparison of error estimates (a) Time series analysis technique (b) gain data from Kaufman and Holben (1993) (c) gain data from Che and Price (1992)

Figure 5.10 shows a comparison between the results derived using the time series approach with the computational technique. The agreement between (a) and (b) is very good (under the circumstances), if the constant difference is ignored. The results from the gain estimates of Che and Price (1992) do not agree with either of the other two.

The constant difference (noted above) between (a) and (b) is of no consequence, as the time series technique can only provide a relative calibration for the NDVI data, whereas the computational approach is capable of delivering an absolute calibration. On this basis, the error derived from the time series data (a) has been adjusted by the mean difference between (a) and (b) of Figure 5.10 to provide an absolute calibration. The mean difference was 0.032 NDVI units. The new corrections from the time series data set are shown plotted in Figure 5.11a, against the data of Kaufman of Holben (1993) (b) (repeated from Figure 5.10). The root mean square error (RMS) of the difference is 0.0093 NDVI units.

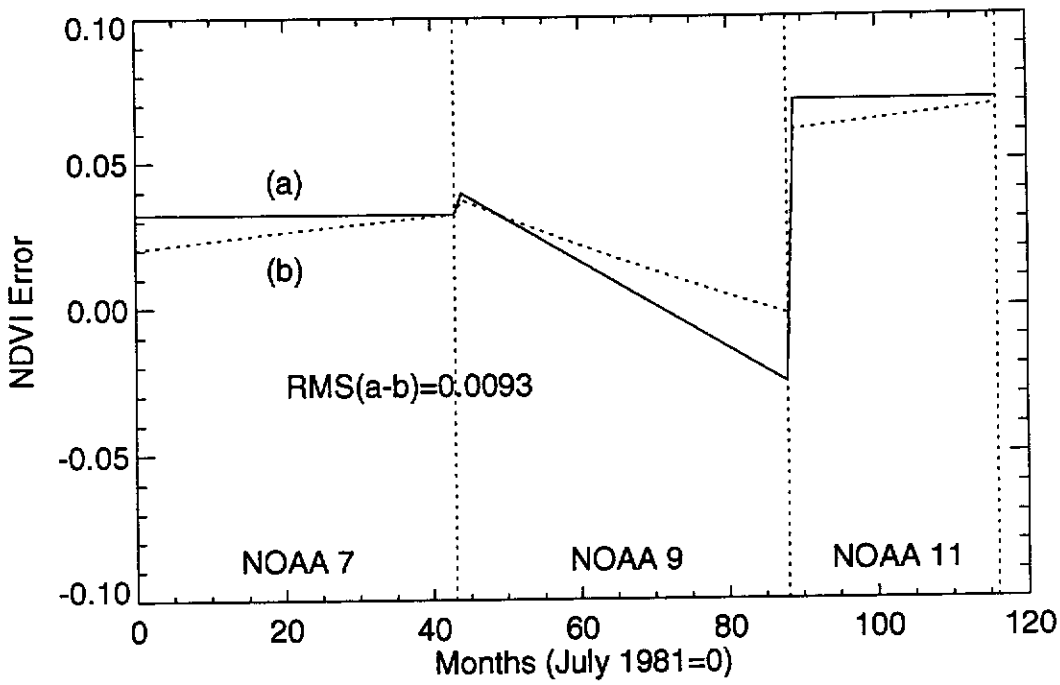

Figure 5.11 NDVI error estimates (a) Time series adjusted for mean difference with data of Kaufman and Holben (1993) (b) Kaufman and Holben (1993)

The close agreement evident in Figure 5.11 is an excellent result given that they were derived using independent techniques. The data derived from the time series technique shown in Figure 5.11 have been adopted as a post-flight calibration for the NDVI data used in this study. The corrections added to each monthly image in the GAC data set are listed in appendix B.

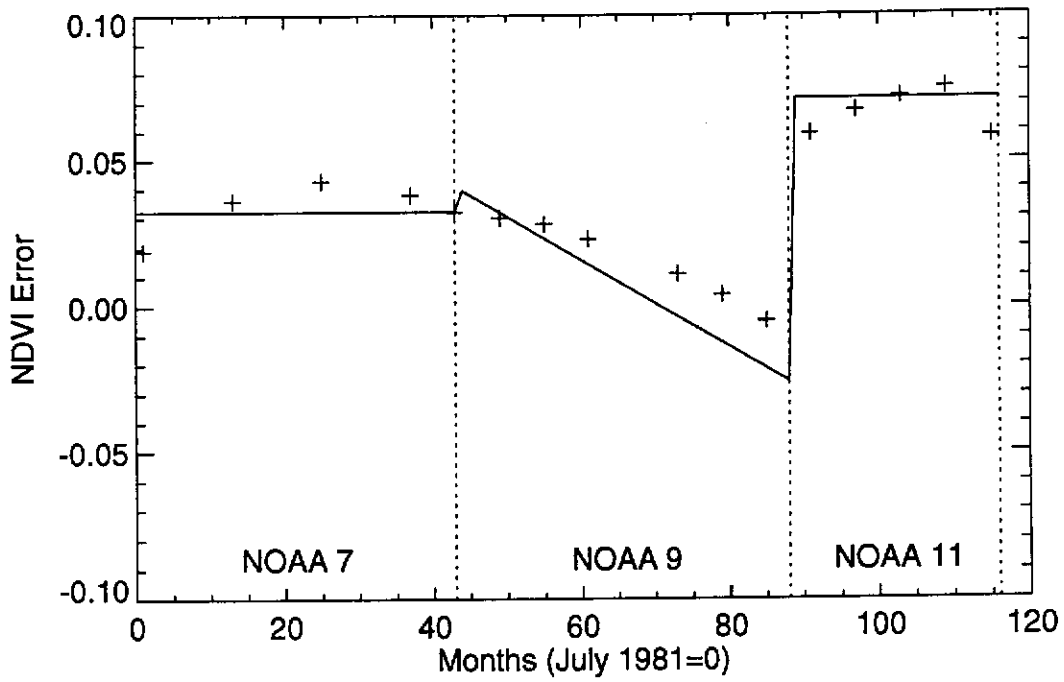

Figure 5.12 Adopted NDVI error estimates compared with error estimates of Los (1993)

Los (1993) used a similar approach to that outlined in Section 5.5.1 to estimate a single additive correction to NDVI for a particular image date. Table 1 of his paper provides estimates of error for 17 months spread over the period 1981-1991, and these are plotted in Figure 5.12. Also shown in Figure 5.12 is the adopted calibration corrections to NDVI (from above) for comparison purposes. Los

(1993) used estimates of the sensor gain from a series of studies most recently reported by Kaufman and Holben (1993). Given the agreement between the proposed time series technique and the results of a theoretical approach using the data of Kaufman and Holben (1993), the results of Los (1993) should be similar to those reported in this study. Figure 5.12 shows this to be the case. While small differences are noted, they relate primarily to the selection of a reflectance window from which errors are estimated. The close agreement is further verification of the proposed (time series) technique.

5.7 Discussion

A linear calibration problem, such as that posed by the solar channels on AVHRR, requires the estimate of both a gain and an offset. Measurements from the literature (Mitchell et al., 1992; Kaufman and Holben, 1993) show the deep space counts (i.e. offset) are very stable over time, but are different to the pre-flight values. Che and Price (1992) also found this and recommend the use of deep space count measurements for the recovery of reflectance information.

Despite this, the calibration equations for AVHRR channels one and two have been formulated by NOAA with no facility to use this observed (and apparently reliable) information. An alternative formulation is presented in this study (Equations 5.2 and 5.5) which

is recommended for use when recovering radiance and reflectance from AVHRR observations. Users of vegetation indices are typically involved in the study of the terrestrial surfaces and, in Australia, reflectances in the range 10 to 40 percent can be expected (Rossow et al., 1989). Since this is at the lower end of the 0 to 100 percent scale, deep space counts represent a key data item for reflectance estimation. For users studying very bright targets, such as ice, snow and clouds, sensor gain will be more important.

Painstaking documentation of the calibration data used to process a particular data set is essential. For example, even if the NDVI data used in this study had been processed using the correct gains and deep space counts, there would still be a calibration problem. This is due to the change of the solar data source used to derive the solar constant from NOAA 7 and 9 to NOAA 11 (i.e. Thekaekara, 1973 to Neckel and Labs, 1984). Clearly successful long term calibration requires both accurate data and documentation of all the steps undertaken.

It was demonstrated theoretically that the error in NDVI due to errors in the calibration data is a function of the original reflectances N and R. In this study, the original reflectance information was not available, and an approximate technique was developed to estimate corrections to the NDVI, based on knowledge of the pre-flight and post-flight calibration data. A key element of the methodology is to estimate the typical range of reflectances that would have been

observed. A lower limit of 10 percent (in both channels) was used for this window. While some terrestrial targets such as dense forest may have lower reflectances than this, the NDVI is an unstable quantity at these lower reflectances (see Chapter 4).

Estimates of the NDVI error derived using the two most complete studies published to date (Che and Price, 1992; Kaufman and Holben, 1993) did not agree. This prompted the development of a new approach to post-flight calibration of NDVI (AVHRR) imagery. The new approach is based on the fundamental assumption that any long term trend in the NDVI is error caused by calibration errors. The results derived using this technique agreed remarkably well with those derived theoretically using the observations of Holben and Kaufman (1993).

The apparent lack of precision in many post-flight calibration studies is a significant problem for users of AVHRR data. The paper of Che and Price (1992) presents data from numerous calibration studies conducted since 1987, which are shown in Figure 5.1. The scatter in the gain estimates does not appear promising. Che and Price (1992) estimate that absolute calibration is possible within ± 10 percent of the correct values. In this context, the estimates of sensor gain for NOAA 9 (see Figure 5.2) by Che and Price (1992) and Kaufman and Holben (1993) are both plausible. Despite this, the trend in the simulated error in NDVI for NOAA 9 (Figure 5.6) was in opposite directions. In essence it becomes an issue of which study to

believe. In this context, the time series technique developed in this chapter is preferable, as it is derived from the data set.

The likely error in absolute calibration suggested by Che and Price (1992) (i.e. ± 10 percent) suggests that calibration data alone will not be sufficient to successfully post calibrate NDVI time series data. The time series approach based on filtering is a tool which can be used and is based on sound assumptions for scientists studying the terrestrial surface. One potential problem in this approach is the presence of residual cloud in the image data. To use the technique with cloud affected data would require the cloud areas to be masked out, and adjustments made to the computed mean, depending on the area of land and ocean included in the calculation of the mean for each monthly image. In the GAC data used in this study, approximately 30 images were used to create each monthly composite, and there are no signs in any image of cloud contamination.

Another potential difficulty is the requirement for at least 12 months of data (to remove seasonal influences) before a single trend estimate can be calculated. For real time monitoring, this is clearly not suitable, particularly when a satellite changeover occurs. Targets that were invariant over extended periods could not be identified in this study from the image data. Even the numerous large salt lakes in Western Australia periodically fill with water, which alters the NDVI. However, over shorter periods (say three

months) it is likely that suitable invariant targets can be located. In the event of a satellite changeover, these targets could be located and used to make an additive correction to the NDVI data from the new satellite. Extreme care in target selection would be necessary. For example, inspection of Figure 5.8a shows that the changeover from NOAA 9 to NOAA 11 coincided with the natural seasonal decline in the series. In time, as more data become available, these corrections could be refined using the technique developed in this study. This would require sophisticated data management systems to be able to keep track of the original and updated calibration error estimates over time.

5.8 Summary

Several studies have confirmed that the AVHRR solar channels are not stable over time. Two distinct errors have been recognised:

(a) Large change following launch,

(b) Slow drift over time.

Errors in the calibration data for individual AVHRR channels (N and R) subsequently lead to errors in NDVI.

If the original observations are available, then it is a simple matter to reprocess the entire data set using the updated calibration data. However, many users receive the NDVI, and do not have access to the original observations. This was the case in this research. A theoretical framework was developed to estimate

corrections to the NDVI based on assumptions about the range of reflectances likely for the study area. It was found that, in general, a simple additive correction can be applied to the entire image.

Observations of the post-flight calibration data from the two most complete studies to date were used to estimate corrections to the NDVI. Unfortunately, the NDVI error estimates did not agree. It should be possible to resolve such a difficulty using invariant targets selected from the imagery. However, no truly invariant targets could be located.

To resolve this difficultly, a new technique was investigated, based on the assumption that the mean NDVI from a large area (i.e. the entire image) should be constant. It was assumed that any trend observed in such a time series would be error due to calibration and should be removed.

By taking the mean of the entire image, and filtering out a seasonal signal (of 12 months period), an estimate of the error in NDVI due to calibration errors was derived. Estimates were derived separately for each satellite (i.e. NOAA 7, 9 and 11). This estimate agreed remarkably well with one of the previous studies. This agreement provided confidence in the proposed technique, which was subsequently adopted. Corrections which are added to each image were derived to create a consistent NDVI data set for further analysis.

Chapter 6

STATISTICAL ANALYSIS OF NDVI IMAGERY

6.1 Introduction

The highly frequent time series image data available from the NOAA-AVHRR sensor have challenged existing data analysis techniques, such as classification, principal components analysis and image differencing (Davis et al., 1991). In particular, the limited temporal frequency of high resolution remotely sensed data has not encouraged research into temporal processing techniques (Ehrlich et al., 1994). Given the lack of guidance in available data processing methodologies, this section describes techniques used to explore the character of the image data sets in view of previous theoretical discussions. This exploration will assist the development of guidelines for the design of information extraction techniques from the data set.

A key data set in this initial data exploration is the monthly rainfall data available from the Bureau of Meteorology at various locations over the entire state. These sites span a number of bioclimates, vegetation types and land use regions. Time series plots incorporating rainfall and NDVI are used to describe the nature of the image data.

Statistical summaries of the data have also been presented. These summaries are computed on a pixel by pixel basis, and allow a

rapid appraisal of the dynamic nature of the data. Computation of these statistical summaries also provides a means of verifying the calibration technique adopted in Chapter 5. Sites with a low dynamic range of NDVI, are relatively invariant and present an opportunity to visually assess the adopted calibration results across a number of land cover types.

6.2 Rainfall NDVI Time Traces

Monthly rainfall was acquired from the Bureau of Meteorology for all stations in Western Australia. Time series NDVI data (mean and standard deviation) were extracted from the imagery for a five by five pixel window (i.e. 15 minutes square) surrounding eight well spaced meteorological stations within the State. Taking the mean value over a local window will tend to lessen the effect of any positional error in the data. The criterion used for selection was that the meteorological station have both a continuous monthly rainfall record and mean weekly climatic data (see Section 3.4.3).

This approach could be criticised since cultural features, such as buildings and roads surrounding these meteorological sites, would theoretically affect the NDVI. However, the size of the pixels (i.e. three minutes), the sampling scheme used to create the GAC data, and the maximum value compositing (MVC) procedure all tend to lessen these influences. Thus, the presence of cultural features is not expected to be a problem. The standard deviation (SD) over the

local window is a measure of the spatial variability in the land surface (green) cover. The SD may also be used to detect anomalous data in the local neighbourhood. Details of the stations are shown in Table 6.1 and Figure 6.1. The extracted time series data are shown in Figure 6.2.

SITE NO.	SITE NAME	LONG, LAT	LAND USE	VEGETATION TYPE
002032	Turkey Creek	128.22°E, 17.02°S	P	Grass savanna and low tree savanna (Beard, 1979)
004006	Bonney Downs	119.93°E, 22.19°S	P	Shrub steppe (scattered shrubs and spinifex) (Beard, 1975b)
007020	Annean	118.17°E, 26.87°S	P	Mulga (Acacia Aneura) low woodland and scrub (Beard, 1976, 1990)
012065	Norseman Post Office	121.78°E, 32.20°S	P	Sclerophyll (Euc.) woodland (Beard, 1975a)
011004	Forrest A.M.O.	128.10°E, 30.83°E	P	Unwooded succulent steppe (Beard, 1975a)
013017	Giles M.O.	128.30°E, 25.03°S	V	Mulga low woodland (Beard, 1974b)
010536	Corrigin Post Office	117.87°E, 32.33°S	A	Cereal (wheat) and sheep farming [1]
009512	Springfields	115.93°E, 34.40°S	F	Tall forest (mainly Karri) (Beard, 1981)

[1] Native vegetation all cleared for mediterranean type agriculture

Table 6.1 Meteorological sites used for NDVI time series extraction. Land use codes per Figure 3.1. Site number is the standard Bureau of Meteorology identification

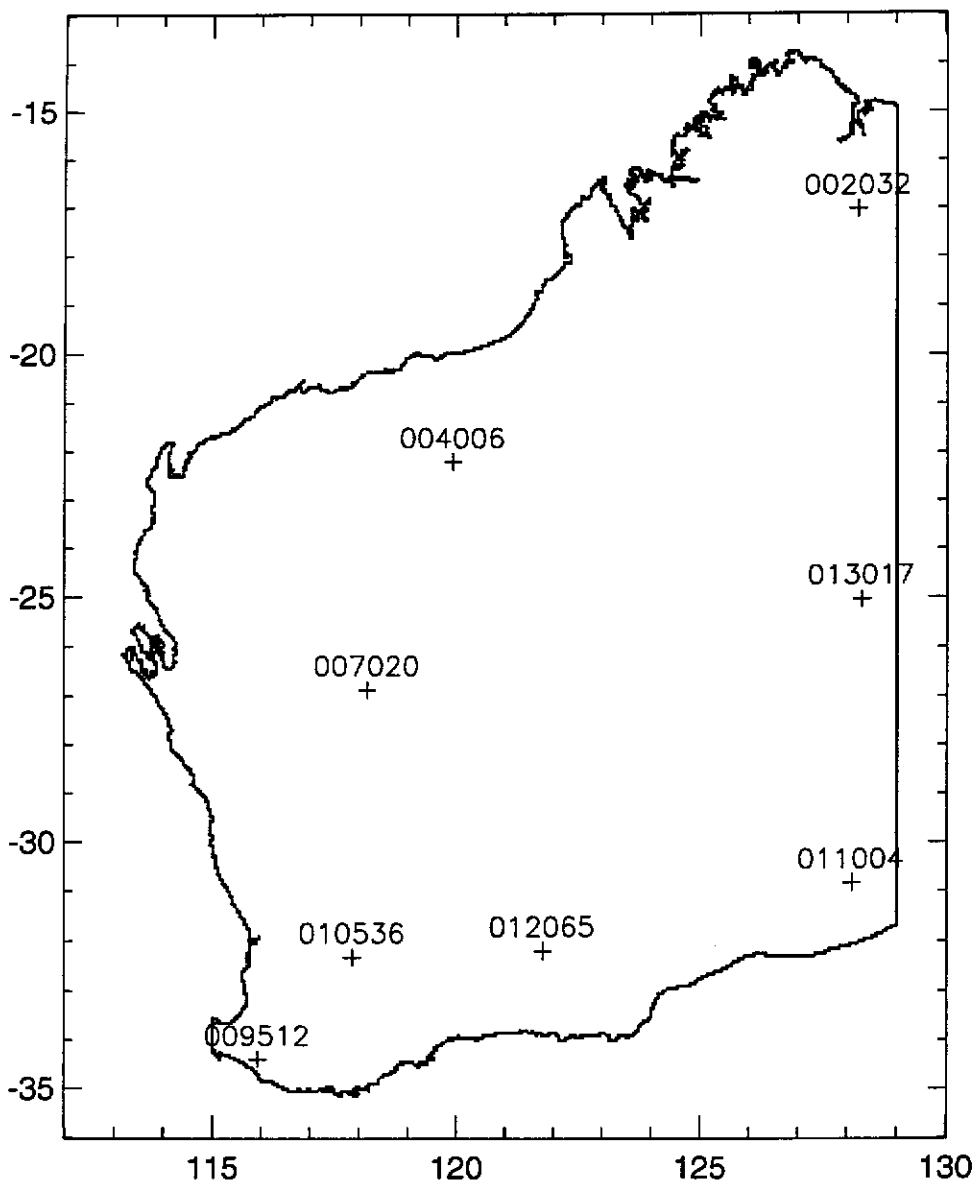

Figure 6.1 Meteorological stations used for extraction of time series NDVI data (see Table 6.1)

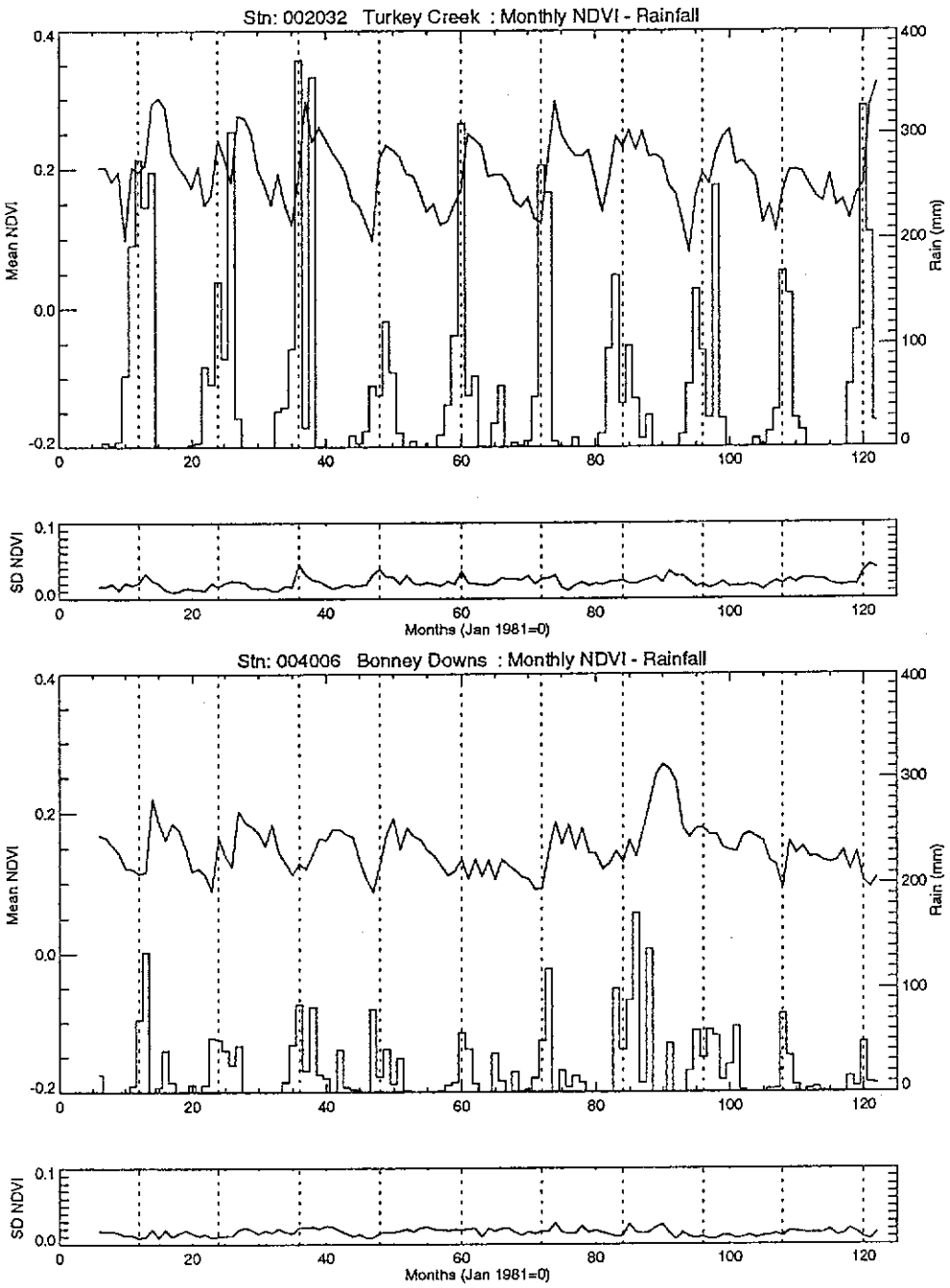

Figure 6.2 Monthly NDVI-rainfall time series (1981-1991). Mean and Standard Deviation (SD) are for 5 x 5 pixel window centred on meteorological station

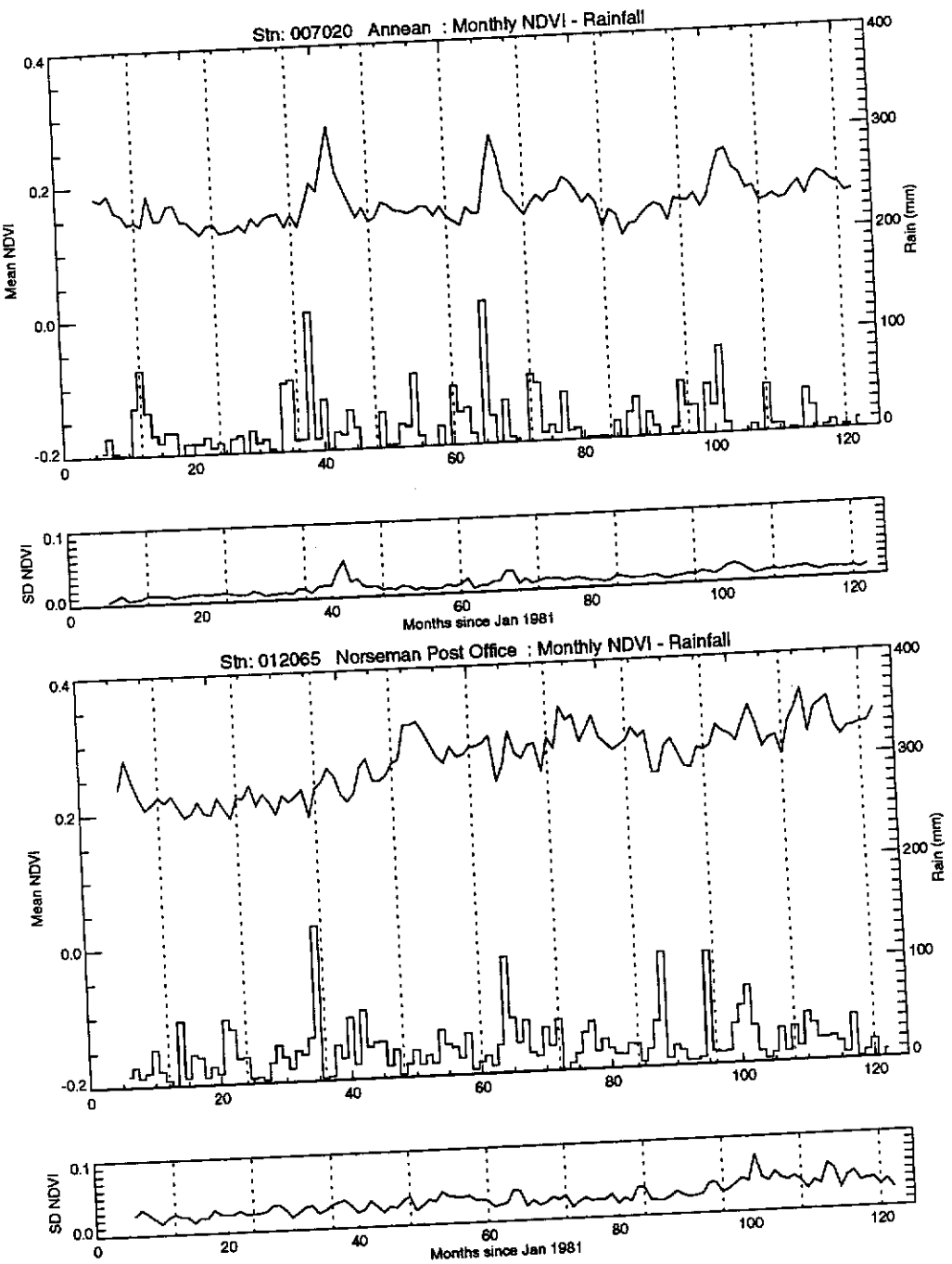

Figure 6.2 Monthly NDVI-rainfall time series (1981-1991) (continued)

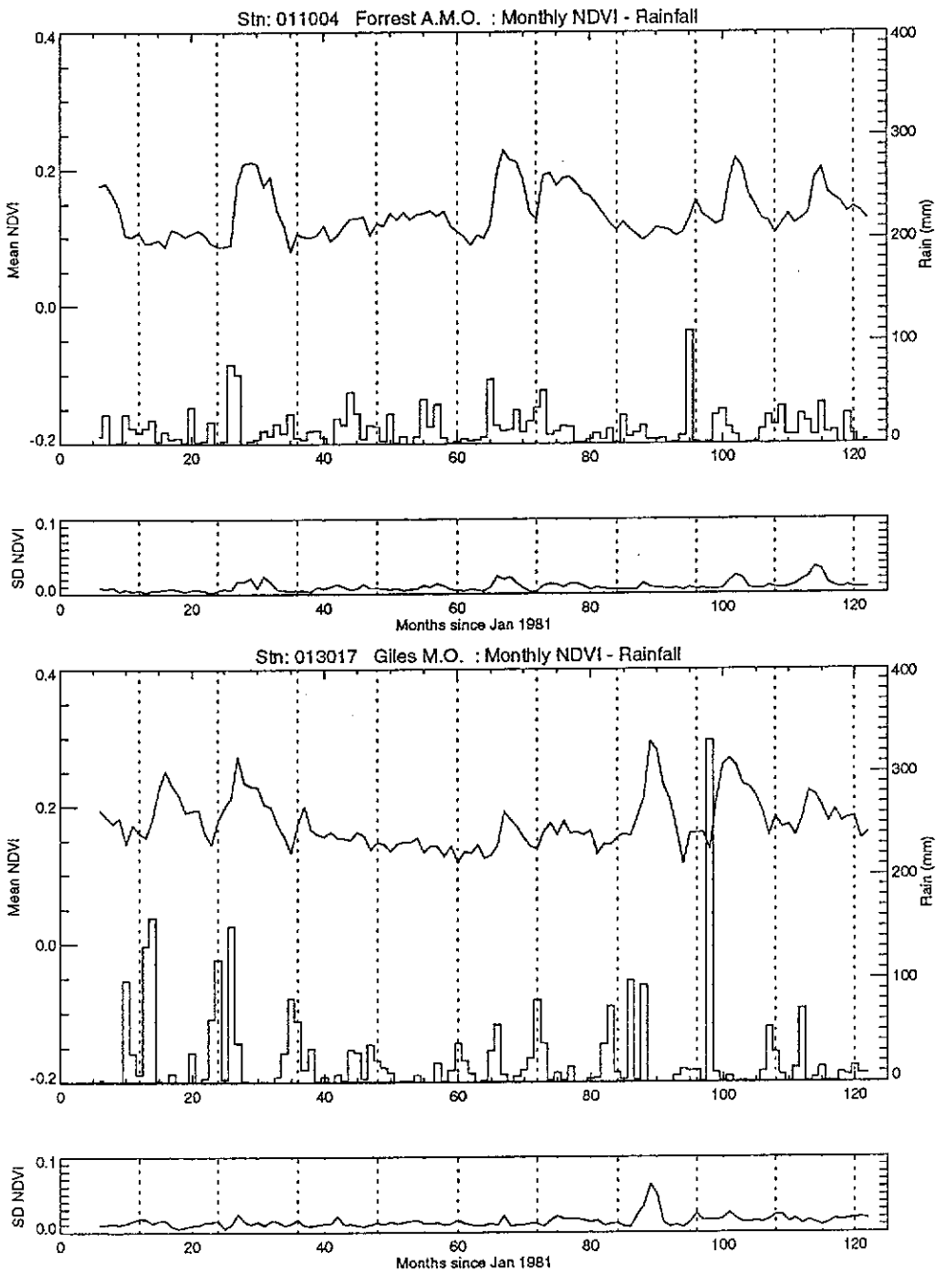

Figure 6.2 Monthly NDVI-rainfall time series (1981-1991) (continued)

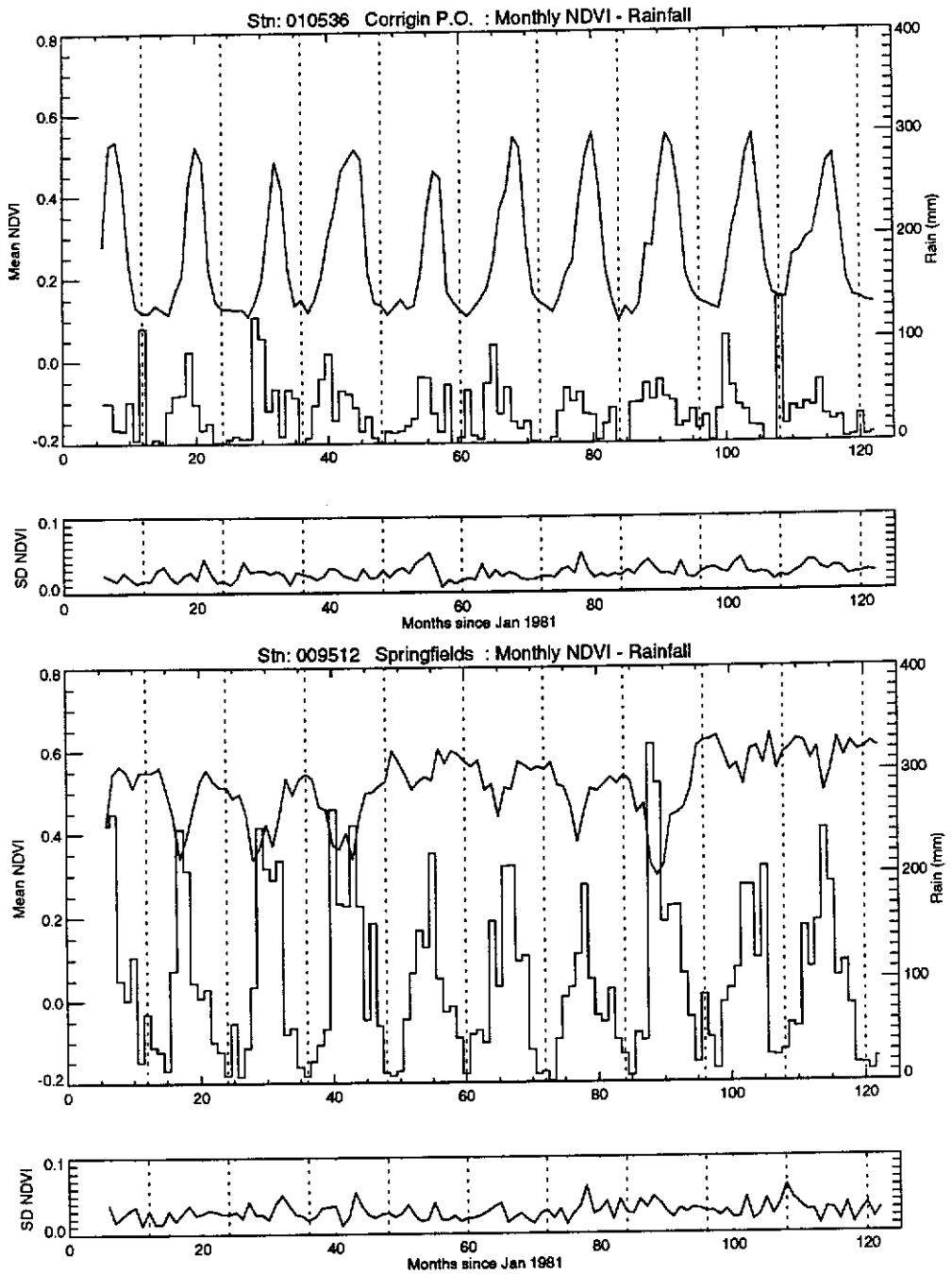

Figure 6.2 Monthly NDVI-rainfall time series (1981-1991) (continued)

The most striking feature of Figure 6.2 is the time series plot of an agricultural site (see Stn 010536, Corrigin Post Office). The regular winter growth, typical of mediterranean agriculture is clearly evident. All rangeland sites (except Stn 012065, Norseman Post Office) show a clear relationship to the rainfall graph, with either regular or spasmodic growth pulses evident. Each of the graphs will now be discussed in turn.

6.2.1 Stn 002032 - Turkey Creek

The relatively regular summer rains in this area (i.e. December-March) produce a characteristic pulse-decay pattern in the NDVI signal. The SD shows that spatial variation tends to be higher in the growth period. The pattern is as expected for a semi-arid savanna grassland.

6.2.2 Stn 004006 - Bonney Downs

This graph is similar in nature to the previous graph with a definite summer bias for rainfall. However the magnitude of the seasonal growth is considerably less than that for the previous station. A total failed season is evident in 1986. In 1988, summer-autumn rainfall produced a large growth pulse, which appears to have carried through 1989 to 1990, when a failed season occurred. This seasonal variability is symptomatic of the arid lands (Stafford Smith and Morton, 1990).

6.2.3 Stn 007020 - Annean

This site shows several growth pulses (1984, 1986, 1989) which all follow late summer or autumn rain. Autumn rain would tend to be more effective than summer rain due to the lower evaporative demand of the atmosphere (Payne et al., 1987). The SD is clearly related to the seasonal conditions, and follows the mean NDVI closely. Failed seasons are clearly evident in both the NDVI signal and the rainfall data.

6.2.4 Stn 012065 - Norseman Post Office

This graph is the only rangeland site not to show a clear relationship to the rainfall trace. The rainfall does not appear seasonal and even following good rains (i.e. December 1983, winter 1986 and 1988) no large pulse is obvious. Despite this, the plot indicates a rise in the NDVI following good rainfall in December 1983. The NDVI rose from a previous value of approximately 0.2 to a new value of 0.3, over a period of one year following this large rainfall. At the end of the trace (1991), the NDVI had not returned to its previous level of 0.2.

The vegetation of this area is Sclerophyll Woodland (mainly Euc.) and the high canopy cover (see Beard, 1975a) may not allow the satellite to sense the herbaceous layer. This vegetation is ever-green and net leaf loss is minimal, even in adverse seasons (Specht, 1981). Presumably, the rise in NDVI following summer rainfall,

relates to a major germination event. Note that the minimum NDVI is higher than that for the previous grassland and shrubland sites. This is possibly related to a higher standing perennial plant biomass. The SD does not appear related to either the NDVI signal or rainfall, but is consistently higher than that for the previous rangeland sites.

6.2.5 Stn 011004 - Forrest A.M.O.

This site at the eastern end of the Nullarbor Plains (Beard, 1975a) shows the characteristic growth pulse related to rainfall. Summer rainfall appears ineffective (e.g. December 1988) as would be expected due to the higher evaporation at that time. The SD is very strongly related to rainfall. A feature of this graph is the growth pulse following rainfall in June 1986. The NDVI trace shows a good season in the winter of 1986 extending through 1987, despite low rainfall to a subsequent poor season in 1988. This could be related to the maintenance of annual plants following the well distributed rainfall over this period.

6.2.6 Stn 013017 - Giles M.O.

This area, in the Great Sandy Desert, is the site of a permanently staffed meteorological station. It shows the typical growth pulse following rainfall in arid areas. A run of good seasons in the early 1980's was followed by several poor years (1984-1987). The rainfall shows a summer dominance over this period. A large monthly rainfall in March 1989 (~ 300 mm) did not seem to generate

a significantly different pulse from other wet periods. Presumably, this was due to large amounts of run off following intense rainfall. The 1988 rainfall generated a large SD pulse, indicating high spatial variability in the immediate area. The reason for this is unknown, although the pattern of rainfall in 1988 was excellent for general plant growth. The initial rainfall in March 1988 would have germinated many plants, and the follow up rainfall two months later would have provided ideal growth conditions.

6.2.7 Stn 010536 - Corrigin Post Office

This site, in the wheat belt region, shows a large and regular pulse peaking in spring. This pattern reflects the agricultural land use, and the dominance of mediterranean annual species. The NDVI reaches a higher peak than for any of the rangeland sites previously discussed. For wheat crops, maximum leaf area index typically occurs in late September each year (Arbrecht, 1994). The rainfall is winter dominant, and this is clearly seen in the NDVI plot. Some other relationships with the rainfall are also noted. In 1983 and 1985, poor rainfall at the start of the season is shown by a delayed NDVI, presumably reflecting the delayed planting of crops. Summer rainfall (January 1982, 1990) does not appear to produce a growth pulse. This is a function of both the summer dormancy of the mediterranean species, and possible management intervention. While unplanted seeds (such as weeds, etc.) could have germinated after summer rain, they are often controlled by ploughing, or the use

of herbicides for weed control. Clearly, in an area of permanent agriculture, the nature of the species and management factors will control periods of plant growth.

6.2.8 Stn 009512 - Springfields

This area is in the midst of the wettest area in Western Australia, and is heavily forested. While rainfall shows a clear winter dominance, the NDVI indicates growth periods tending to occur over summer (particularly 1981-1984 period). This may be related to temperature controlling growth in the absence of water deficit over summer. Water deficit may be avoided by the deep root systems of trees common throughout the region (Stuart Crombie, 1992). The minimum NDVI recorded (~0.4) is significantly higher than that at any of the other sites, possibly confirming that the minimum NDVI value is related to perennial standing biomass. The SD trace is noisy by comparison with all others. This may indicate the effect of variable viewing geometry and bidirectional reflectance on the NDVI.

6.2.9 Review

The graphs presented clearly show the NDVI responding as expected to vegetation growth. In the rangeland areas, the response to rainfall varies from a relatively regular seasonal pattern to the classic growth pulse and irregular rainfall of arid areas described by Noy-Meir (1973). Local spatial variation (in a 15 minute window) often increases following rainfall (particularly in the pulse dominated

systems). The size of the growth pulse (in NDVI) seems to be related to the pattern of rainfall, as much as the amount of the rainfall. For this reason, water balance techniques are often preferred in the estimation of periods of plant growth, as they can account for both the pattern of rainfall and the evaporative demand of the atmosphere (Fitzpatrick et al., 1967; McAlpine, 1970).

The minimum NDVI appears to be related to the permanent (or perennial) standing biomass. The interpretation of the NDVI signal is more difficult at sites with a high perennial biomass, as there is no obvious relationship with rainfall. This may be due in part to the canopy obscuring the herbaceous layer of plants.

6.3 Image Summaries

To investigate the spatial nature of the imagery, summary statistics were computed on a pixel by pixel basis over the whole image. While this approach explicitly ignores the time series nature of the data, as an initial stage it is clearly appropriate to develop simple summaries. In particular, it is necessary to confirm some of the observations made in Section 6.2 over the entire data set. To accomplish this, statistics (minimum, maximum, range, median and standard deviation) were computed on a pixel by pixel basis over the entire 117 months (July 1981 - March 1991). These images are presented in Figures 6.3 - 6.8.

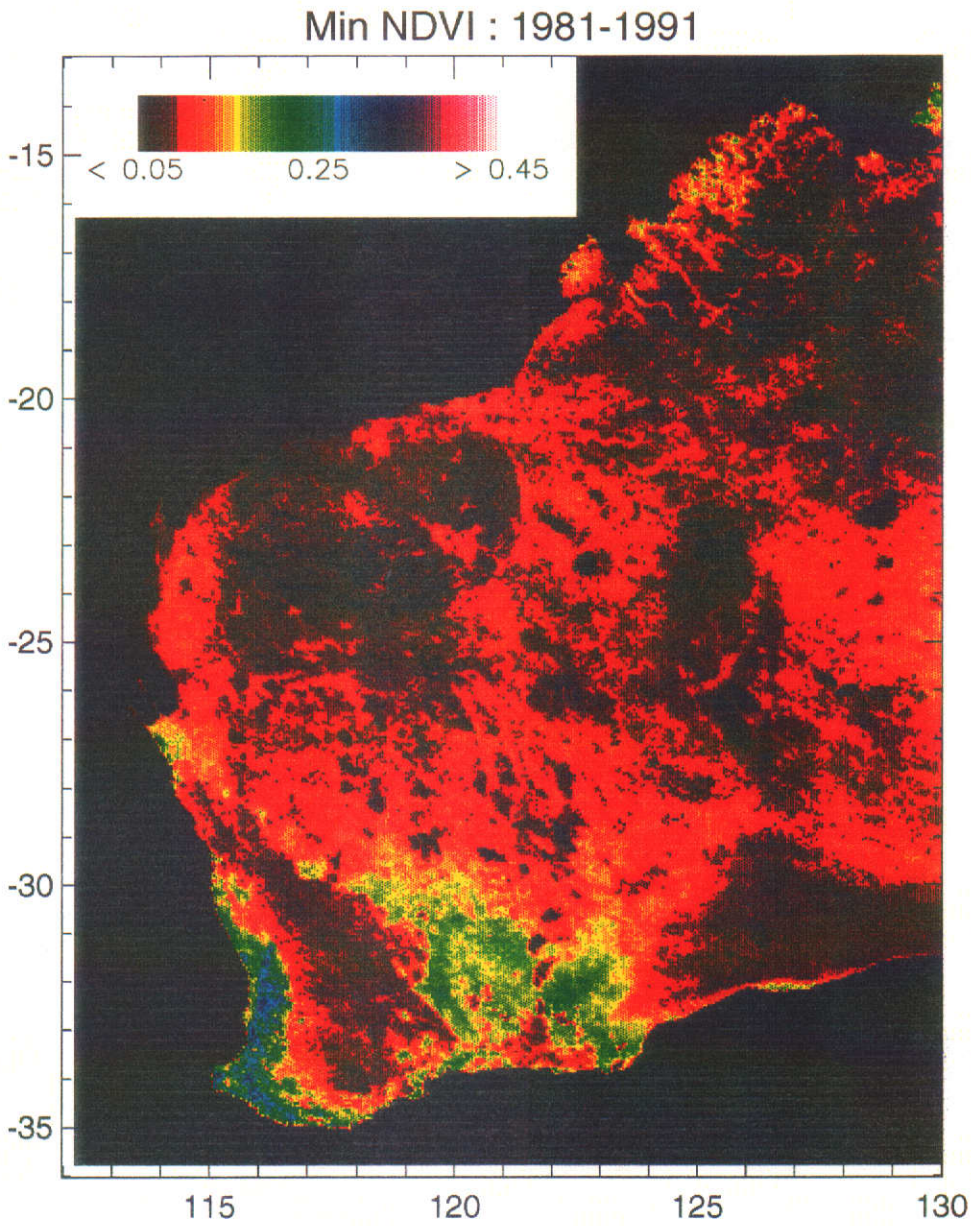

Figure 6.3 Minimum NDVI for each pixel over period July 1981 - March 1991

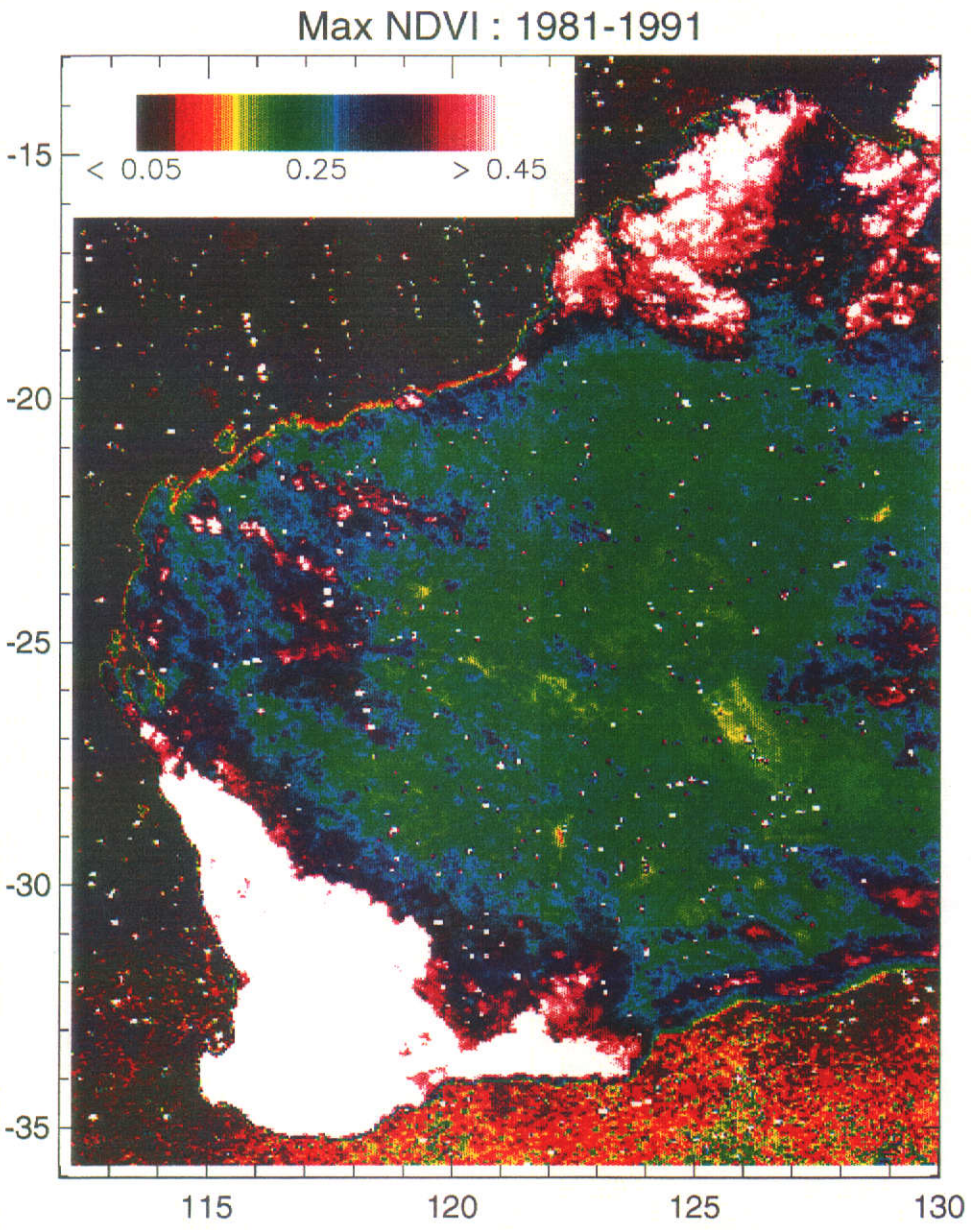

Figure 6.4 Maximum NDVI for each pixel over period July 1981 - March 1991

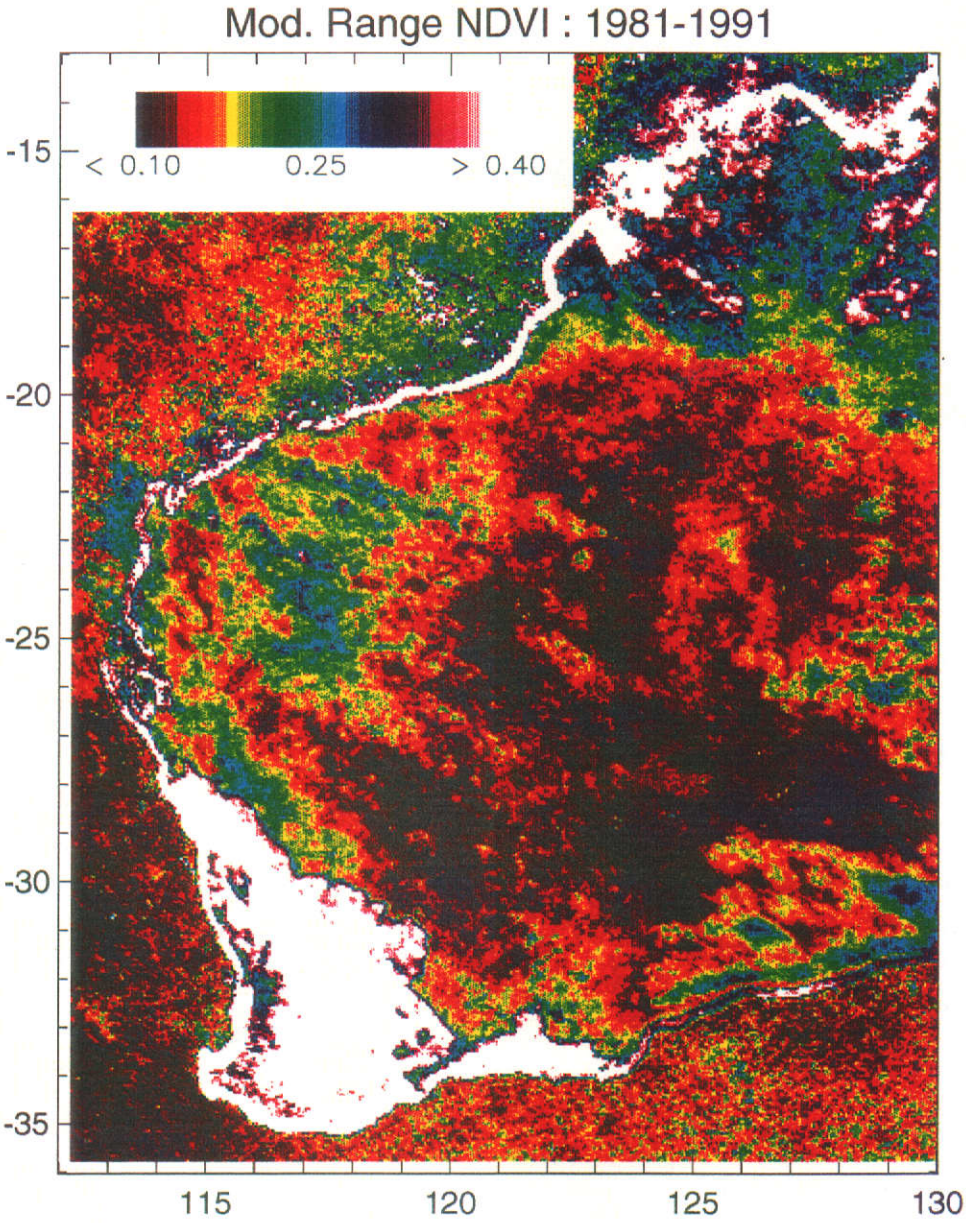

Figure 6.5 Modified range in NDVI for each pixel over period July 1981 - March 1991. (The modified range is computed by dropping of the maximum NDVI recorded prior to computing the range. This avoids the 'dropouts' evident in Figure 6.4)

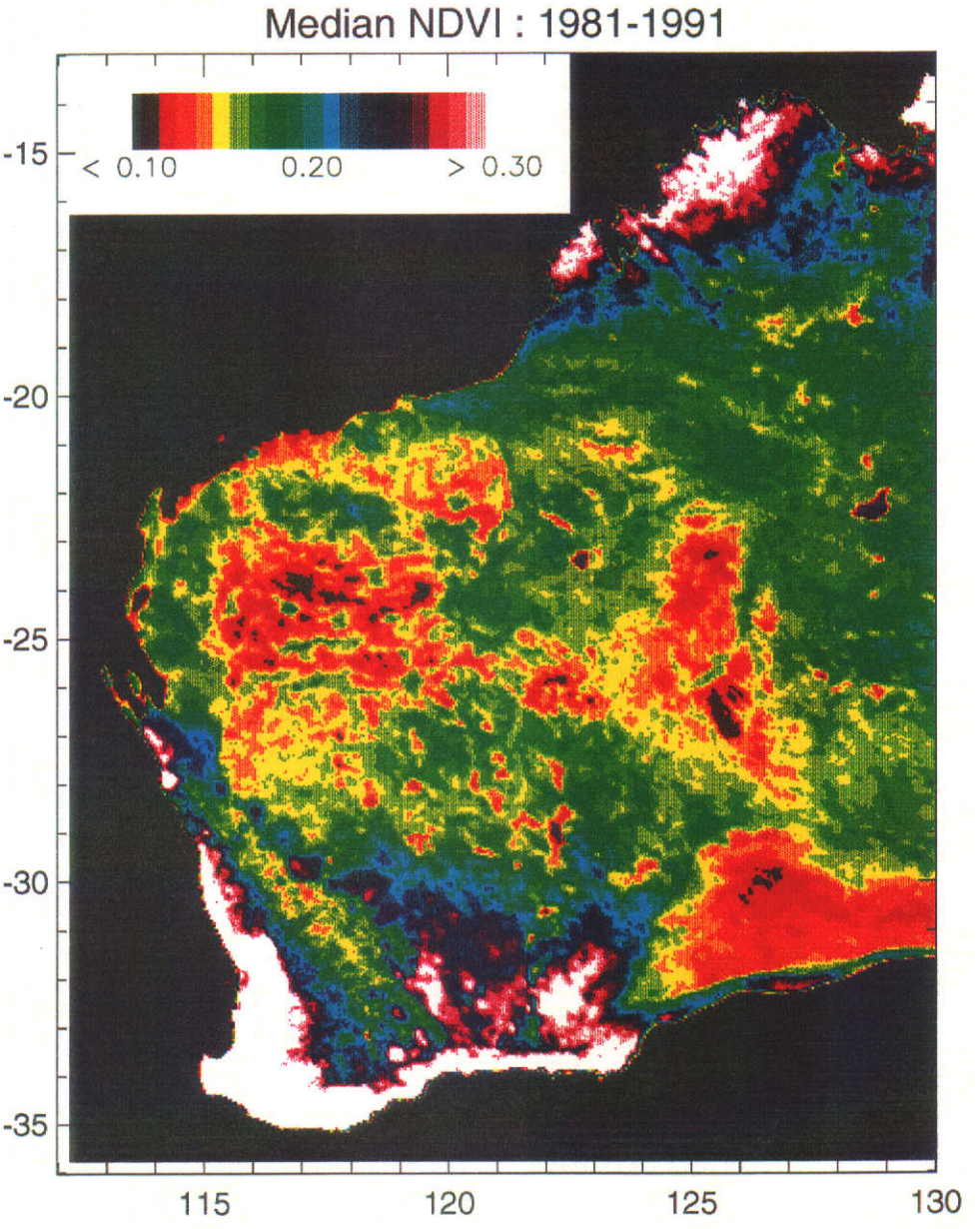

Figure 6.6 Median NDVI for each pixel over period July 1981 - March 1991

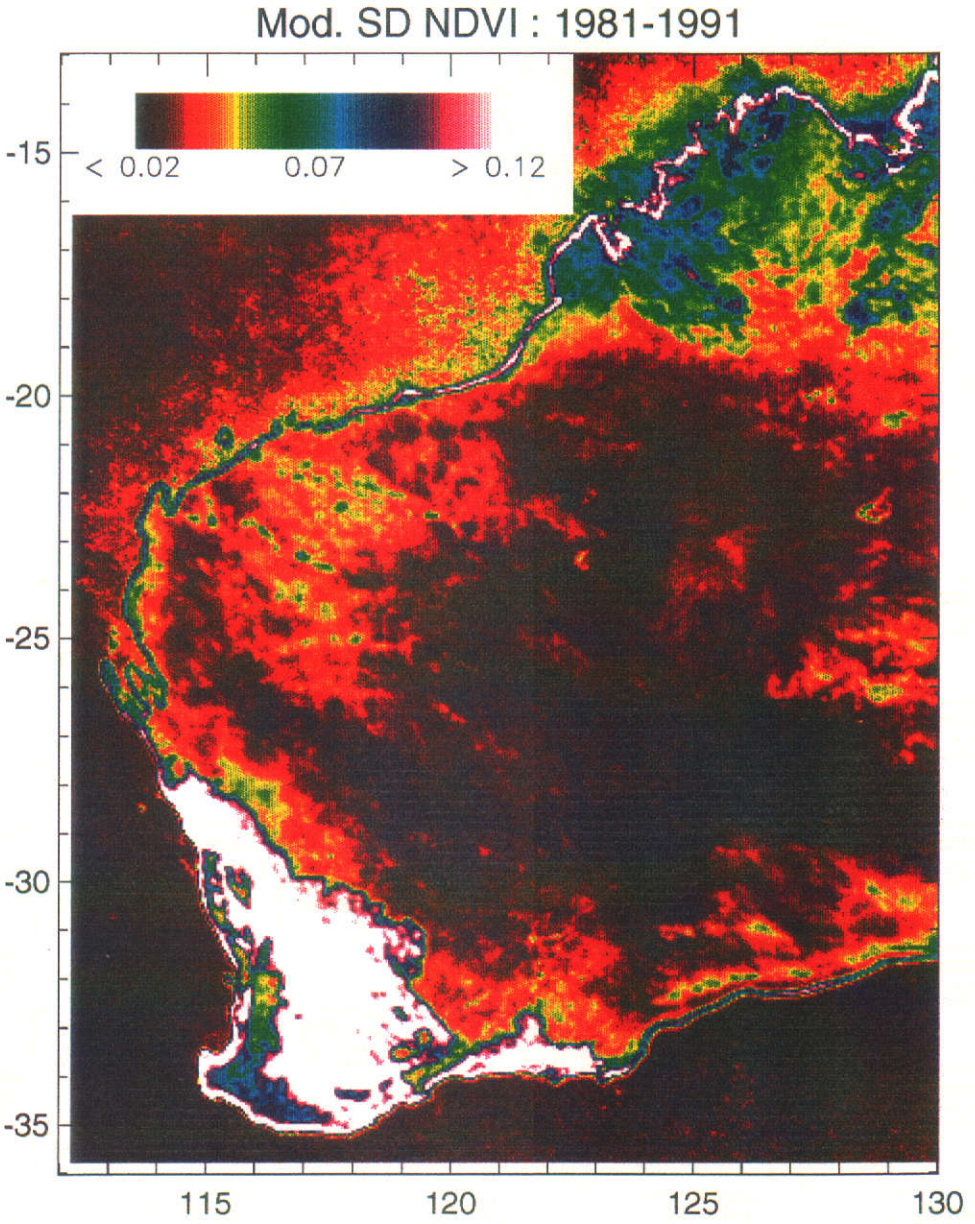

Figure 6.7 Modified standard deviation (SD) in NDVI for each pixel over period July 1981 - March 1991. (The modified SD is computed by dropping of the maximum NDVI recorded prior to computing the SD. This avoids the 'dropouts' in Figure 6.4)

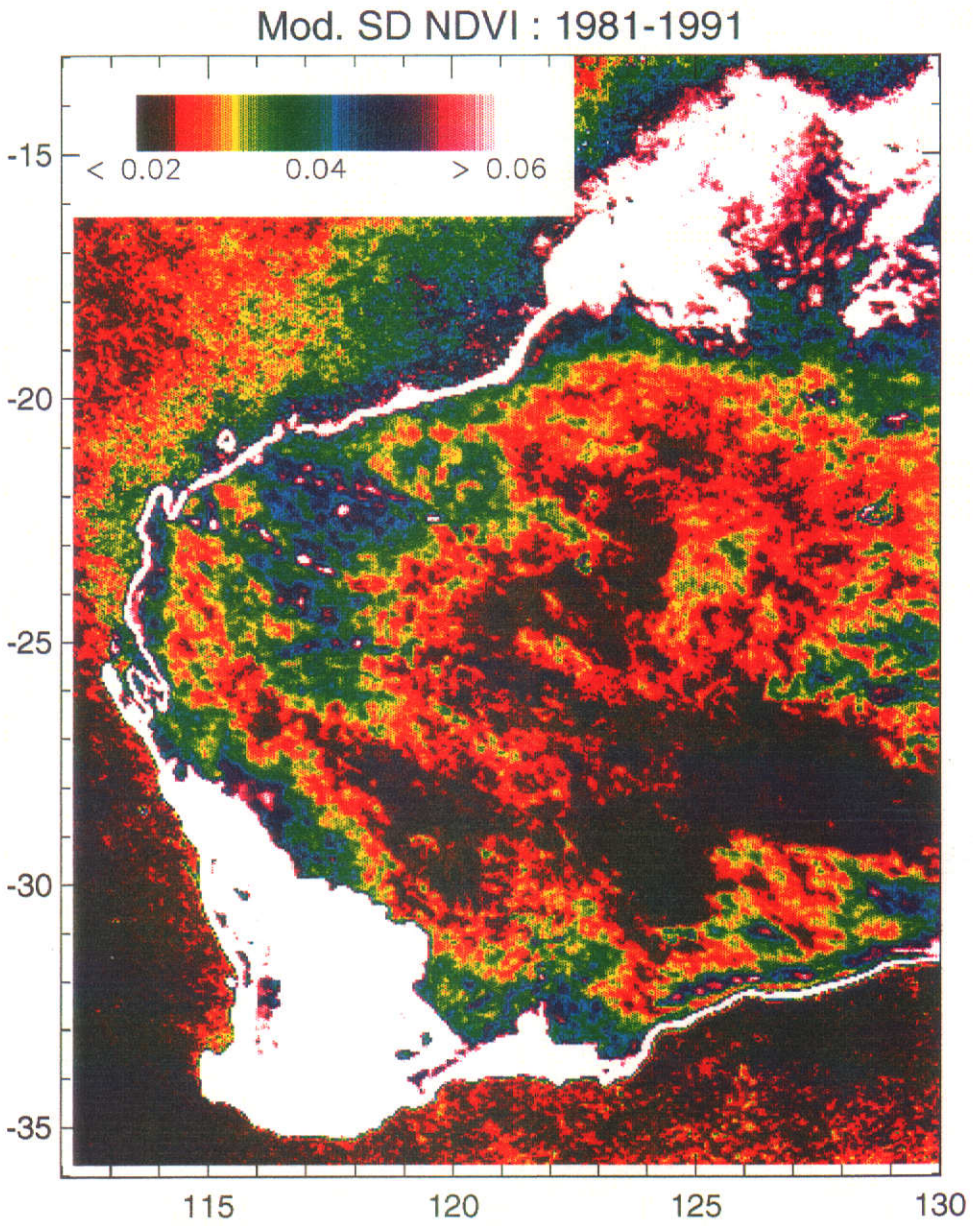

Figure 6.8 Modified standard deviation (SD) (modified colour scale) in NDVI for each pixel over period July 1981 - March 1991 (Colour change from Figure 6.7 to highlight arid zones of Western Australia)

6.3.1 Minimum Image

The minimum NDVI (Figure 6.3) clearly shows a distinct spatial structure, and the broad agreement with the small scale mapping of Beard (1990) (Figure 3.6) is striking. The forested areas of the southwest show a much higher minimum NDVI than other parts of the State. The so-called Southwest Interzone described by Beard (1990) is also clearly visible as an area of higher NDVI east of the agricultural area. The agricultural area has a lower minimum NDVI than the surrounding perennial native vegetation. This clearly is appropriate, as wheat and other crops are harvested, and annual pastures senesce over summer, leaving the paddocks relatively bare. The Nullarbor Plains (Beard, 1990) is also clearly visible in the image.

Theoretical arguments indicate that the minimum NDVI could also reflect the underlying soil colour. In addition, the minimum NDVI is clearly a function of vegetation structure and, in particular, standing perennial biomass. This confirms the observations from Section 6.2. In particular, areas of higher rainfall typically support higher amounts of perennial biomass, which is subsequently reflected in a higher minimum NDVI.

6.3.2 Maximum Image

For comparison purposes the maximum image (Figure 6.4) was printed with the same colour scale as the minimum image. The

presence of dropouts in the data set is clear. The agricultural area, dominated by annual crops and pasture, is clearly differentiated from the native vegetation. Areas of higher NDVI in the rangelands may be related to variability in rainfall over the period, vegetation type and soil colour. The maximum NDVI over the southern ocean is greater than the northern ocean areas. This is possibly due to lower sun angles at the southerly latitudes, causing greater variability in NDVI at low reflectances (see Chapter 4). The compositing procedure used (MVC) selects the largest NDVI over any particular month.

The typical maximum NDVI values recorded in this data set are over the agricultural area in the southwest and are in the range 0.65 - 0.7. Box et al. (1989), in a global study using the global vegetation index (GVI) product from NOAA (Tarpley et al., 1984), found a maximum value of 0.4 for NDVI globally. The apparent difference with the result in this study is possibly due to the different pixel sizes of the data sets. The GVI pixels are typically 15 km opposed to the (approximately) 5 km pixels in the GAC data. Price (1993) has shown that, as the pixel size gets larger, the NIR and RED reflectances (and subsequently the NDVI) converge to a single point. This smooths spatial variation, but also reduces the data range in NDVI which is observed.

6.3.3 Range Image

The range (i.e. maximum-minimum) for each pixel is clearly

affected by the dropouts evident in the maximum image. Due to the compositing procedure, high values of NDVI resulting from processing errors will be retained in the data set. To avoid these dropout values, a modified range (MR) was used, defined as:

$$MR = \textit{second largest value of NDVI} - \textit{minimum NDVI} \qquad (6.1)$$

Clearly, as shown in Figure 6.5, much of the arid lands has a limited range in NDVI, while the agricultural areas in the southwest and the northern grasslands tend to have a higher range. The forest areas of the southwest have a lower range than the surrounding agricultural areas.

Positional errors in the image data will tend to obscure the land/ocean boundary due to the MVC process (see Section 2.4.4). The white band along the coast, in the range image (see Figure 6.5) is partly due to positional error in the image data. Where the land/ocean boundary is sharp, such as cliffs, the width of the boundary indicates the worst case positional error in the data. The width of the boundary in a region of large cliffs between latitudes 27.5°S and 26.5°S is approximately ± 2 pixels. The boundary is wider in the north, presumably due to a larger tidal range. This is an absolute worst case scenario, as along boundaries the compositing procedure will always select observations with the worst positional error.

6.3.4 Median Image

The median was chosen over the mean to represent the central tendency as it is relatively unaffected by dropouts and positional error when compared to the arithmetic mean. This image (Figure 6.6) clearly shows some vegetation structural detail (e.g. Nullarbor Plains), although it could be expected to be confounded by the particular seasonal conditions over the period of the data. Numerous salt lakes in the central southern area of the arid zone are also clearly visible in the median image.

6.3.5 Standard Deviation Image

The presence of dropouts also affects the standard deviation (SD). For this reason, a modified SD was computed by dropping the maximum NDVI value prior to the computation of the SD. Two images are presented on different colour scales to highlight different regional information. The agricultural area has a large SD by comparison and known areas of native vegetation are clearly shown within the agricultural area. The forest areas are clearly differentiated using this statistic from the agricultural area (Figure 6.7). In the northwest region of the Kimberley (125°E, 20°S), a boundary clearly differentiates between desert to the south and grassland to the north. A number of small 'spots' are evident in the Pilbara region (115°E, 23°S). These are possibly related to extreme rainfall events over the period of the data set.

The effect of positional error and subsequent compositing along the coastline is again evident, although they are not highlighted as much as the range image presented previously. The Kimberley coast (125°E, 17°S) shows greater SD probably due to the large tidal range in this area.

A second colour image was required to show detail in the arid area (Figure 6.8). Large areas of the arid lands show limited change in NDVI, even over such a long time frame. Such areas may be useful for post-flight calibration of the AVHRR radiometers.

6.3.6 Review

While summary statistics of the type presented above ignore the time series nature of the data, they are an essential preliminary step in developing an understanding of the image data. Different statistics highlight different global characteristics of the NDVI over varying land cover and land use areas. In imagery with a land/ocean boundary, the range in NDVI is an excellent statistic to rapidly assess the positional accuracy of that imagery. The standard deviation clearly indicates broad scale difference in seasonal conditions over the period studied. In addition, the minimum NDVI value is globally related to the biomass of perennial species.

6.4 Calibration Verification

The images of standard deviation (Figures 6.7, 6.8) offer an opportunity to select relatively invariant targets to provide further validation on the calibration results adopted in Chapter 5. Three sites were selected, one over the land (desert) immediately north of the Nullarbor Plains, and the others over the ocean. Large windows were used in all cases (441 pixels over land, 1681 pixels over each of the ocean sites) and the mean and standard deviation of that window computed for each image in the time series. The NDVI time series from pre-flight data, and the calibrated data (using the corrections listed in Appendix B) are shown in Figure 6.9.

It was shown in Chapter 4 that the NDVI computed from surfaces with low reflectance (such as the ocean) is very noisy due to quantisation error. Despite this, by selecting a large number of pixels over the ocean, a reliable estimate of the NDVI can still be obtained for a large area. Thus, by using the ocean, the entire surface is assumed to be relatively invariant. Clearly, none of these sites can be regarded as invariant from these plots (see Figure 6.9). The desert and northern ocean sites are both more stable than the southern ocean site, which shows considerable pulses at the end of NOAA-7 and 9 respectively. Such pulses are possibly related to atmospheric conditions, and the relatively smooth nature of the pulse, indicates that it is not related to the noise in the NDVI at low reflectances, which is suppressed by averaging over a large window.

The mean NDVI time series shows a dip when observations from NOAA-11 commenced, and the slight upward trend in NDVI during NOAA-9 confirms the previous results from Chapter 5. The standard deviation traces are typically less than 0.02 units, reflecting the large number of pixels used to compute the statistics. Small spikes in the SD traces indicate the presence of dropouts in the window. These traces further demonstrate that calibration is feasible using long time traces and assuming any trends evident are instrument related. However, they also show the difficulty of finding invariant sites in image data.

6.5 Oceanic Time Series

In Chapter 4, it was shown that the error in NDVI was a non-linear function of the original reflectances and that, at low reflectances, the NDVI is sensitive to quantisation error. In this section, time series derived from three sites centred over the ocean are used to demonstrate that this is the case. These series are shown in Figure 6.10. All the series have been calibrated.

The standard deviation of these oceanic plots is typically less than 0.02 NDVI units, which is significantly less than most of the land surface plots. This indicates low spatial variation exists in a local window from the composited monthly data. However, the time series of mean NDVI is significantly noisier than the land surface plots, which tends to show a highly smooth nature. From a

calibration point of view, the high frequency noise present in the oceanic time series would make it difficult to use ocean based sites as short term calibration targets. These results confirm earlier theoretical results (see Section 4.4).

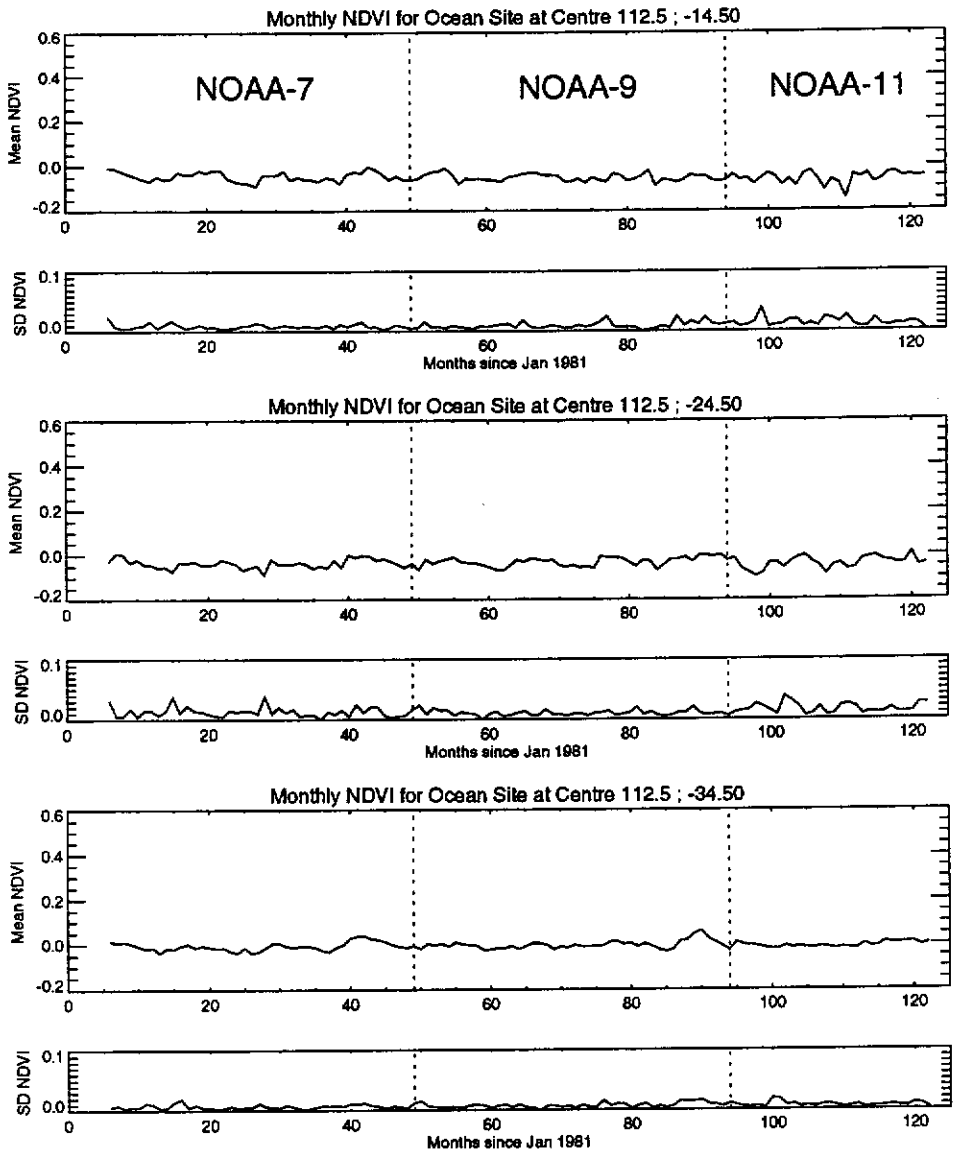

Figure 6.10 NDVI time series plots for three ocean sites. Mean and standard deviation are for a 5 by 5 pixel window centred at coordinates shown

6.6 Gross NDVI - Rainfall Relationships

As discussed in Section 6.3, the minimum NDVI image (Figure 6.3) is clearly related to standing perennial (above ground) biomass. A glance at any rainfall map over Western Australia (Bureau of Meteorology, 1989), and subsequent comparison to a broad scale vegetation map (Beard, 1990) indicates that the native perennial plant biomass is globally related to spatial patterns of annual rainfall in Western Australia. This basic approach has also been used in several large scale bio-geographic studies (Pittock and Nix, 1986; Box et al., 1989).

Previous studies have related annual integrals of NDVI from NOAA-AVHRR to annual rainfall totals (Lo Seen Chong et al., 1993; Davenport and Nicholson, 1993) over Africa. However, annually integrating the NDVI also integrates the minimum (or base) NDVI value. Assuming that this base NDVI value already reflects rainfall differences (through perennial biomass), this approach will mask inter-seasonal differences.

Conceptually, the minimum rainfall at a site can set a threshold for the existence and growth of perennial plants. To demonstrate the utility of this approach, the minimum annual rainfall over a nine year period (1982-1990) has been related to the minimum NDVI over a similar period.

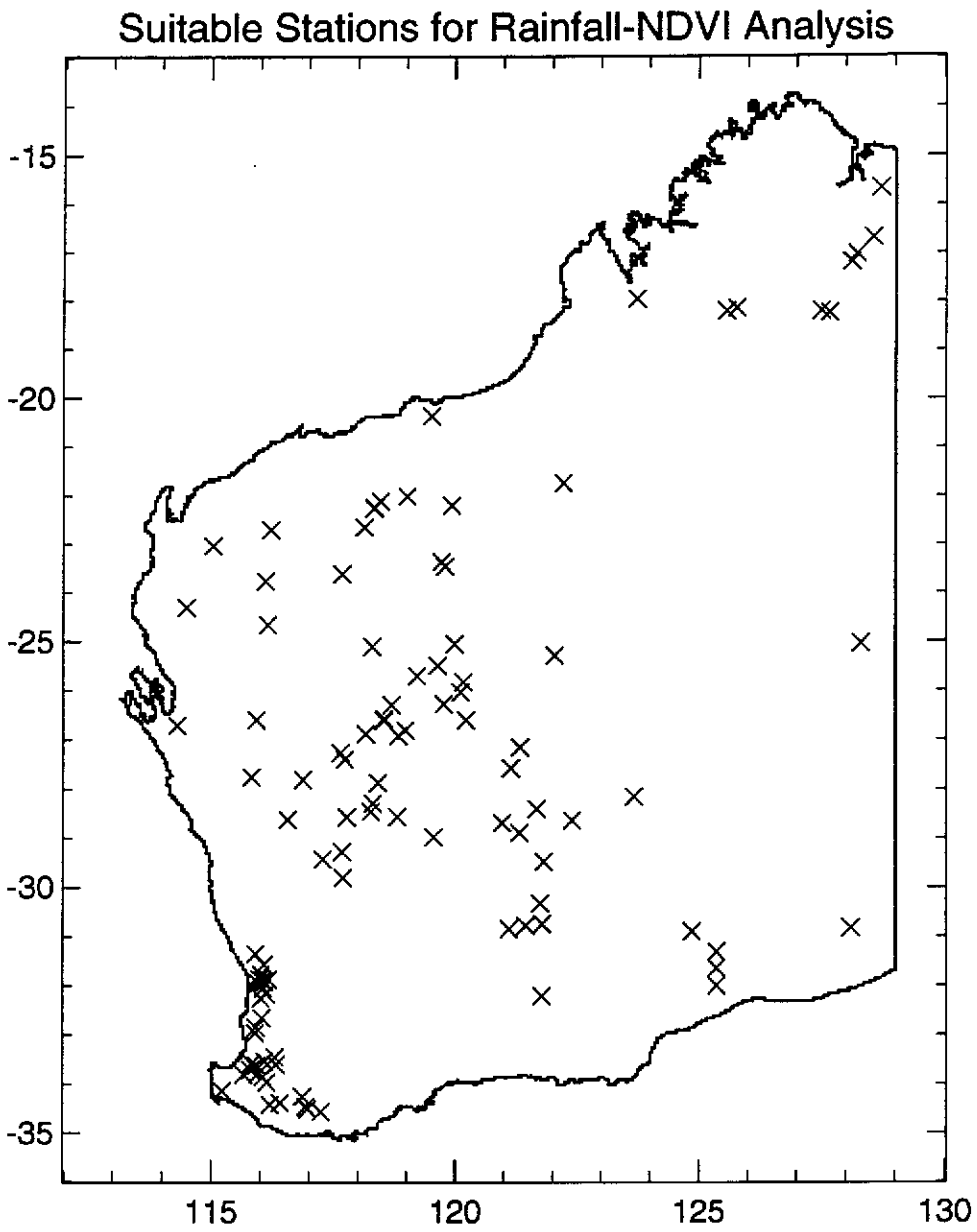

Figure 6.11 Suitable meteorological stations selected for rainfall-NDVI analysis. All stations have a continuous record of monthly rainfall over period July 1981 - March 1991

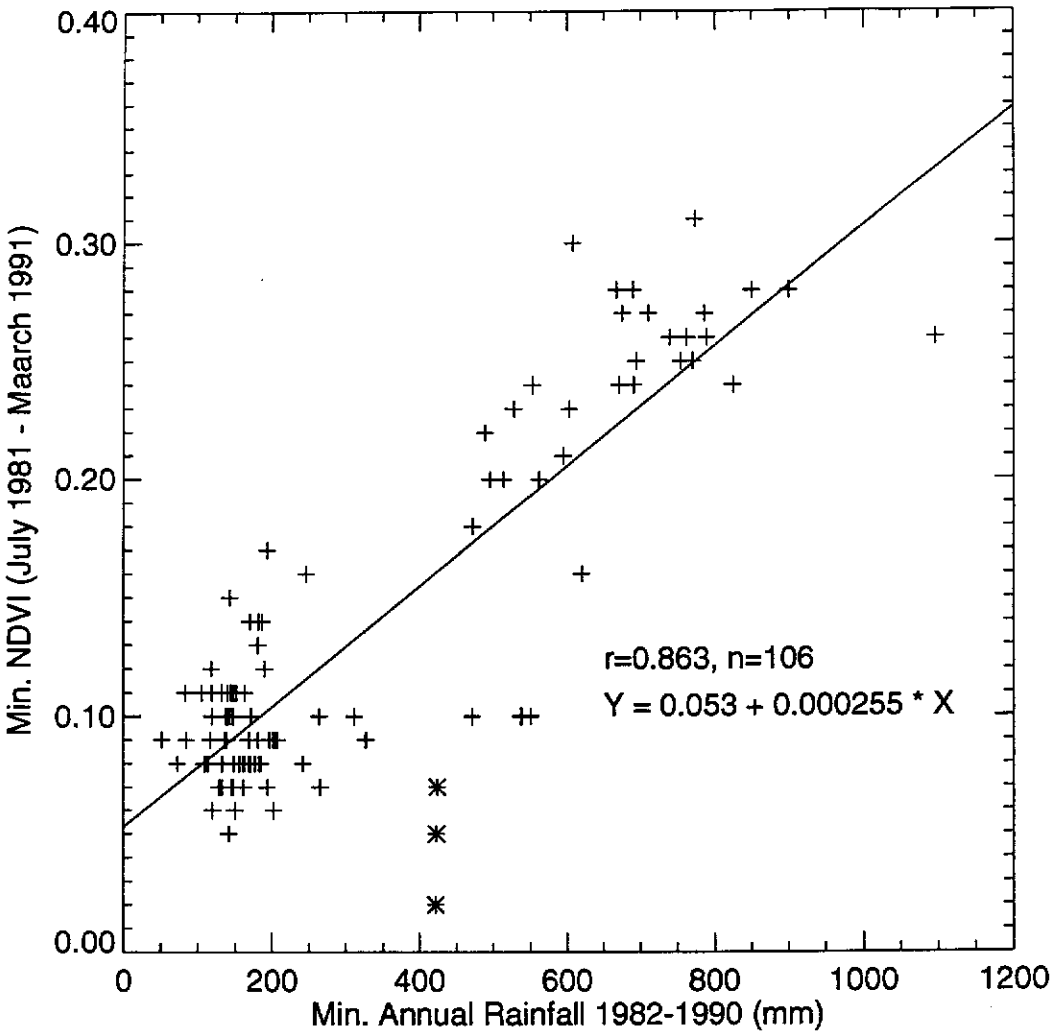

Figure 6.12 Relationship between minimum annual rainfall and minimum NDVI for period 1981-1991. Sites marked * are discussed in text

Continuous monthly rainfall data are available at some 410 meteorological stations over Western Australia (see Figure 3.4). It would be inappropriate to include sites from the agricultural area in the analysis, since virtually all the perennial biomass has been removed for agricultural activities. In addition, the slight positional errors in the data set precludes using coastal stations, as the minimum NDVI could have been observed over the ocean.

Meteorological stations that were away from the coast, and not in the agricultural area, were selected for the analysis and are shown in Figure 6.11. Some 106 stations satisfied this criteria. For each station the minimum annual rainfall total over the 1982-1990 period was selected. These annual rainfall totals ranged from approximately 50 to 1100 mm. The minimum NDVIs for these stations over the period were extracted from the image data and have been plotted against the corresponding rainfall data in Figure 6.12.

While it may be argued that such an approach ignores the time series nature of the data, as previously described, areas of high perennial cover do not show a clear relationship to the rainfall trace (see Section 6.2). In this context the approach adopted is a useful indicator of the strength of the proposed relationship.

The graph (Figure 6.12) indicates a strong positive correlation between minimum annual rainfall and minimum NDVI on a global basis. The cluster of points in the 50-200 mm rainfall are all arid zone sites, and this scatter indicates that other site specific factors, such as run-off and local soil conditions, also play a part in determining water availability and perennial biomass (Graetz et al., 1988b). Variations in soil colour and canopy architecture could also affect the minimum NDVI (Huete and Tucker, 1991; Williamson, 1989; Begue, 1993). Similarly, the sites from the forest region (minimum rainfall greater than 500 mm) all occupy a discrete portion of the graph.

Three outliers away from the main groups are marked in the graph by an asterisk. These sites are all spatially grouped within the semi-arid savanna grasslands in the Kimberley area (at 128.1°E, 17.2°S; 128.2°E, 17.0°S; 128.6°E, 16.7°S). Perennial biomass will on occasion be limited on these grassland sites due to seasonal conditions and fires. In addition, given seasonality in rainfall, Westoby (1980) has outlined several scenarios where grasses could dominate over woody plants despite a high annual rainfall. The rainfall in this area is highly seasonal (see Section 6.2.1). As such, rainfall is not always a good estimator of perennial biomass.

6.7 Discussion

The image-based statistical summaries largely confirm the insights gained from studying a wide variety of NDVI-rainfall time series plots. The relationship between minimum NDVI and perennial biomass is an important one for the design of information extraction techniques. Annual integration of the NDVI without considering this minimum value will generally give a strong relationship to rainfall via the link with perennial biomass. Bonifaco et al. (1993) used an annual integration above this minimum NDVI value to reduce the effect of calibration errors. This will also reduce the differences due to background effects, in addition to the calibration problem. The concept of a minimum and maximum NDVI, which is related to individual site conditions, was proposed by Kogan (1990), who rescaled the current value of NDVI into the range observed at that

site. This technique has also been used in Western Australia by Cridland et al. (1994), to remove some of the background effects, which can make spatial comparisons of raw NDVI values difficult.

Maselli et al. (1992) rejected the rescaling proposed by Kogan (1990), claiming the selection of minimum and maximum values was statistically unstable. They proposed transforming the data to a standardised normal ordinate (i.e. Z-score) using the mean and standard deviation on a pixel by pixel basis. While this technique may be viable over a homogeneous land type, such as an agricultural area, over a large area with a diversity of vegetation types, valuable information will be lost. The minimum NDVI value in particular reflects real differences in the perennial plant cover.

For practical use of the above techniques, the other issue of importance is the temporal variability of rainfall. The maximum value implicitly assumes that it is the best (or highest) NDVI that a particular site can get. In arid and semi-arid areas the reliable estimate of a minimum value should not pose similar problems as poor seasons are regular occurrences. However, in some cases it may take 10 or more years to observe an area under excellent seasonal conditions, and thus obtain an estimate of the maximum value for that site.

One possible technique to overcome this problem would be to use existing maps of vegetation structure (Beard, 1974a; Carnahan,

1981) to estimate the best value for a particular vegetation type somewhere over the temporal record of the data. While this method would substantially shorten the length of record required to get an estimate of the maximum value, it also assumes that the structure of the vegetation will not change. Some form of iterative updating of both the base map data and the maximum NDVI value would be required.

6.8 Summary

This chapter has shown that the NDVI is clearly related to seasonal conditions across nearly all the rangeland and agricultural areas of Western Australia. The use of rainfall NDVI time series plots is a valuable exploratory technique for developing an understanding of the dynamic information inherent in the data. The classic irregular growth pulse following rainfall is evident in nearly all the arid and semi-arid zone time series plots.

The statistical image summaries deliberately ignore the time series nature in the data, and concentrate on developing a gross understanding of the behaviour of the NDVI over large regions of diverse bioclimatic conditions and vegetation types. Specific time series studies are undertaken later. The minimum and maximum NDVI are clearly capable of physical interpretation in terms of the worst and best seasonal conditions at a particular site. At a broad scale, spatial differences in the minimum NDVI are clearly related to

perennial biomass via broad scale difference in rainfall. Some exceptions were noted in the tropical savanna grasslands, where fire also regularly impacts on the vegetation. However at a local scale, other factors also need to be considered, such as runoff, soil type, canopy structure of the vegetation and soil colour.

The range in NDVI is an excellent technique to rapidly estimate the worst case positional error in NDVI time series imagery. The image of standard deviation gives a valuable measure of the variability of the NDVI across broad regions. One major use for the standard deviation image is the selection of potential post-flight calibration sites. Simple statistical summaries, such as those used above, have previously been used to classify broad land cover types. In this type of application, care must be taken, as it is possible that many of the spatial differences noted are really differences in the rainfall over the sampling period. The minimum NDVI is an excellent statistic for use in this type of study.

From the standard deviation images, potential calibration sites were selected, and the calibration methodology developed in Chapter 5 evaluated. All the chosen sites agreed qualitatively. However, all sites showed high frequency noise in the traces, which will make rapid calibration following the launch of a new satellite difficult. The calibration technique developed in Chapter 5 is better suited to using long time series to get a good statistical estimate of the trend. The global relationship between minimum NDVI and minimum annual

rainfall was surprisingly strong. This minimum NDVI value should always be considered in any NDVI-rainfall study.

Chapter 7

DERIVATION OF RAINFALL-NDVI RELATIONSHIPS

7.1 Introduction

An essential component of any remote sensing study is the verification of the results using an independent data set. Several studies have verified the theoretical relationships between NDVI and NPP using field measurements of biomass and green cover in arid and semi-arid environments (Tucker et al., 1985b; Foran and Pearce, 1990; Filet et al., 1990; Prince, 1991a).

Field based sampling for calibration of NDVI estimates of growth is a highly labour intensive process. The difficulty in acquiring field based data to relate to the satellite information has led a number of researchers to use rainfall as a surrogate of plant growth in arid and semi-arid regions (Hielkema et al., 1986). In this context rainfall has been used as 'quasi' ground truth. The basis for such an approach is a linear relationship between NPP and rainfall in arid and semi-arid areas (Foran et al., 1982; Le Houerou, 1984).

Several studies have shown relationships between total seasonal rainfall and integrated NDVI (Kerr et al., 1989; Seguin et al., 1989; Maselli et al., 1992; Bonifacio et al., 1993). The best linear relationship typically shows a lag between rainfall and NDVI of one month (Maselli et al., 1992; Cihlar et al., 1991). This lag represents the time for vegetation to respond to rainfall. The relationships have

often been treated as global, without considering differing vegetation types. Davenport and Nicholson (1993) looked at the relationship between rainfall and NDVI across various vegetation types in eastern Africa. They found that the lag between rainfall and NDVI varied depending on the type of vegetation.

Not all long term studies have used satellite imagery. Noble (1977) looked at the relationship between biomass and rainfall in an arid zone site in South Australia over some 50 years (1926-1974). A technique was developed to rank biomass by species using photographs taken at annual intervals. These biomass ranks were found to be highly correlated with rainfall over varying periods depending on the species type. For annual plants, the current biomass was correlated with the previous 12 months rainfall. In contrast, the biomass of saltbush (Atriplex vesicaria), a perennial species, was found to be highly correlated with rainfall from the previous 42 months.

The 10 year sequence of monthly satellite imagery available in this study offers a unique opportunity to investigate the relationship between NDVI and rainfall across varying vegetation types in the arid zone of Western Australia.

7.2 Conceptual Approach

The NDVI time traces presented in Chapter 6 indicate qualitatively the strong relationship that exists between rainfall and NDVI in the arid and semi-arid zones. The previous studies reported above have focussed on annual or seasonal relationships in seeking a relationship between rainfall and NDVI. In the arid and semi-arid zones of Australia, the rainfall is more noted for its variability than seasonality (Stafford Smith and Morton, 1990). In these cases there is no clear time each year for establishing a seasonal relationship.

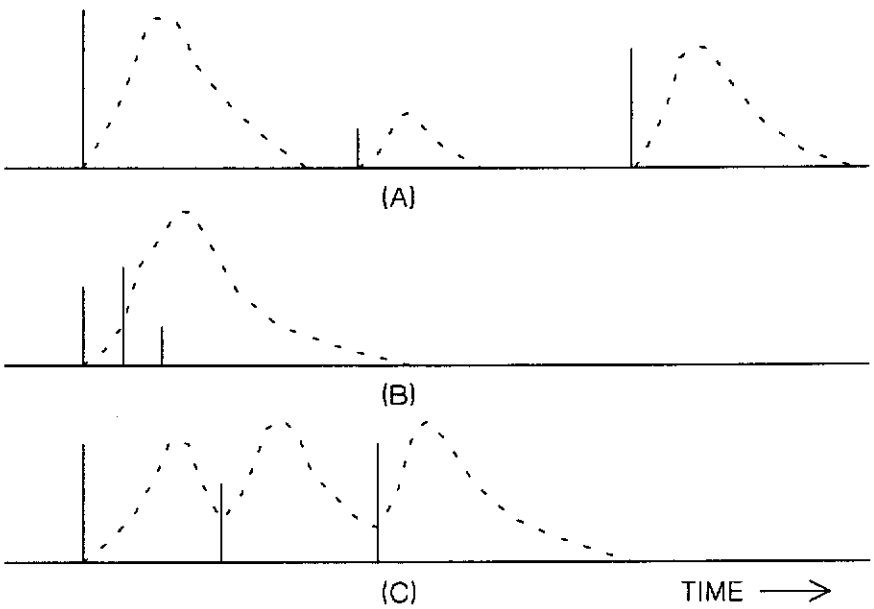

Figure 7.1 Plant growth response to rainfall inputs (Noy-Meir, 1973)
(a) widely separated inputs
(b) clustered inputs
(c) intermediate spacing between inputs

An alternative view of the rainfall-plant growth relationship in arid and semi-arid lands was proposed by Noy-Meir (1973). He argued that rainfall was the dominant factor in arid ecosystems and that it was linearly related to NPP. Rainfall in these arid zones is essentially discontinuous and must be viewed as a series of discrete inputs to which the system responds. Plant growth responses are thus a series of pulses. These pulses may overlap in cases of clustered rainfall to produce a composite output pulse as shown in Figure 7.1. The growth pulses described above are evident in the time series plots of NDVI and rainfall for arid zone sites presented in Chapter 6. Noy-Meir (1973) proposed that the concepts and techniques used to establish the impulse response in engineering may be applicable to the study of such systems.

The conceptual basis of a system transfer function is shown in Figure 7.2. The input(s) excite the system to produce some response which is measured. The input is said to be 'transferred' by a system transfer function to an output sequence. In this study the input and output signals can be measured but the transfer function is essentially unknown. The derivation of the (linear) function relating the input to the output is known as transfer function modelling (Brockwell and Davis, 1987). Such an approach offers a rigorous technique for establishing an empirical relationship between the two signals (i.e. rainfall and NDVI).

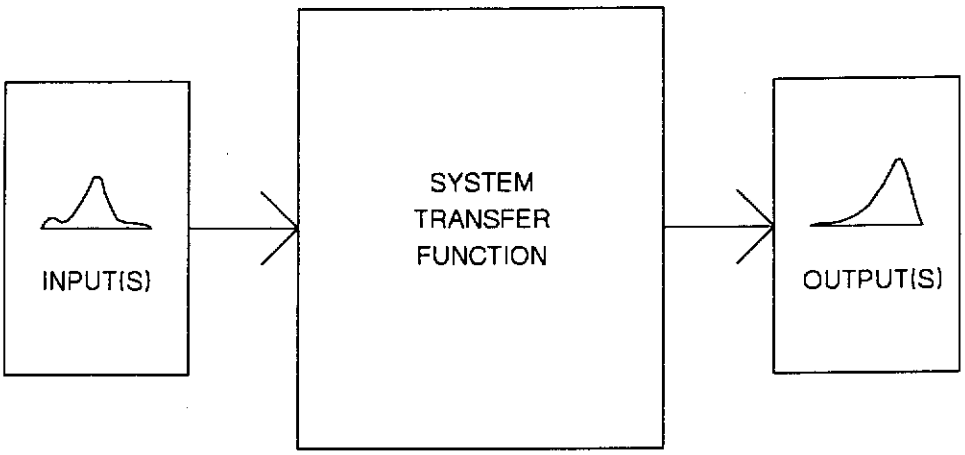

Figure 7.2 Concept of a system transfer function

It can be argued that other processes, such as solar radiation, temperature and germination, also impact on the amount of plant growth (Fitzpatrick and Nix, 1970; Mott, 1973; Mott, 1974; Mott, 1975). However, rainfall is known to be the controlling input (Noy-Meir, 1973). The strength of the relationship between rainfall and NDVI may also indicate how important these other factors are in regulating plant growth in various regions.

7.3 Transfer Function Modelling

Transfer function modelling is a standard technique in systems engineering and many standard text books cover the topic in detail (Cooper and McGillem, 1986; Haykin, 1989; Bennett, 1979). A brief overview is presented below, following the terminology of Brockwell

and Davis (1987).

7.3.1 Theoretical Background

The essential task is to establish a linear relationship between the input (X_t) and output (Y_t), where the measured output is corrupted by noise (N_t) as follows (Brockwell and Davis, 1987):

$$Y_t = \sum_{i=0}^{n} t_i X_{t-i} + N_t \qquad (7.1)$$

The noise (N_t) is assumed to be a zero mean stationary process which is uncorrelated with the input process. The requirement of transfer function modelling is to identify the coefficients (t_i). The relationship between the input and output sequences can be expressed using the cross-covariance (C_{YX}) between the input and output and the auto-covariance (C_{XX}) of the input as follows (Brockwell and Davis, 1987):

$$C_{YX}(k) = \sum_{i=0}^{n} t_i C_{XX}(k-i) \qquad (7.2)$$

The auto-covariance (C_{XX}) is a measure of the linear dependence in a signal as a function of time. The difference in time is measured as a lag (k). The auto-covariance at lag k is defined as (Brockwell and Davis, 1987):

$$C_{XX}(k) = \frac{1}{N} \sum_{i=0}^{N-k} (X_{i+k}-\bar{X})\ (X_i-\bar{X}) \qquad (7.3)$$

where

k = *lag*

$C_{XX}(k)$ = *autocovariance at lag k*

The auto-correlation function (A_{XX}) reduces the auto-covariance to a bounded range from -1 to 1 and is given by (Brockwell and Davis, 1987):

$$A_{XX}(k) = \frac{C_{XX}(k)}{C_{XX}(0)} \qquad (7.4)$$

Similarly, the cross-covariance (C_{YX}) is defined as (Brockwell and Davis, 1987):

$$C_{YX}(k) = \frac{1}{N} \sum_{i=0}^{N-k} (X_i-\bar{X})\ (Y_{i+k}-\bar{Y}) \qquad (7.5)$$

The cross-covariance is computed by sliding the output at various lags across the input signal, and computing the covariance at each of these lags.

The cross-correlation (A_{YX}) between the input and output is given by (Brockwell and Davis, 1987):

$$A_{YX}(k) = \frac{C_{YX}(k)}{\sigma_X \sigma_Y} \qquad (7.6)$$

To solve for the coefficients (t_i) it is necessary to solve Equation 7.2. Equation 7.2 is simplified if the input process (X) can be assumed to represent a random process. Such a process is known as 'white noise' (Brockwell and Davis, 1987). The term white noise is borrowed from physics, where white light refers to light composed of equal combinations of all frequencies. Under this assumption, the auto-covariance function of the input becomes:

$$C_{XX}(k) = \sigma_X^2 \quad (k=0)$$
$$C_{XX}(k) = 0 \quad (k\neq 0) \tag{7.7}$$

Substituting Equation 7.7 into Equation 7.2 leads to a general solution for the coefficients t_i under the assumption of a random input process (Brockwell and Davis, 1987):

$$t_i = A_{YX}(i)\frac{\sigma_Y}{\sigma_X} \tag{7.8}$$

If the input cannot be modelled as white noise, then filters can be designed to pre-process the input to convert the signal to white noise. In this case, the output signal is also pre-processed using the same filter. This process is commonly described as 'pre-whitening' (Brockwell and Davis, 1987).

7.3.2 Example

The above theoretical framework is demonstrated using an example. A transfer function modelling package available within the

ITSM package (Brockwell and Davis, 1991) has been used for all computations in the following example. Data for the example comprise the time series for Giles meteorological station (Stn 013017) originally presented in Chapter 6 (see Figure 6.2). The input sequence is monthly rainfall, and the output sequence is monthly NDVI.

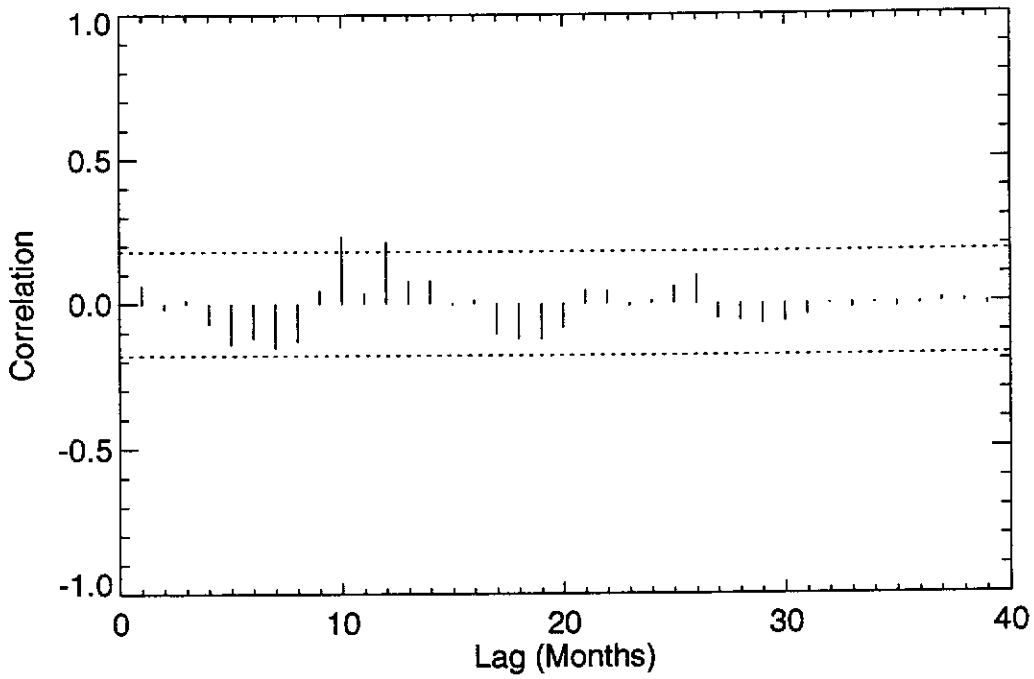

Figure 7.3 Autocorrelation function for monthly rainfall recorded at Stn 013017 (Giles) lags (1-40). Dotted lines indicate 95 % confidence interval

The autocorrelation of the input (rainfall) is shown in Figure 7.3. An estimate of the 95 percent confidence limit for the sample auto-correlation and cross-correlation functions is given by Brockwell and Davis (1987) as $\pm$ 1.96 $N^{-1/2}$ where N is the number of observations in the time series. Correlations which are outside this limit are assumed to be significantly different from zero. The

autocorrelation at lags 10 and 12 is slightly larger than the 95 percent significance limit. They will be ignored, and the process is assumed to represent white noise (Bennett, 1979).

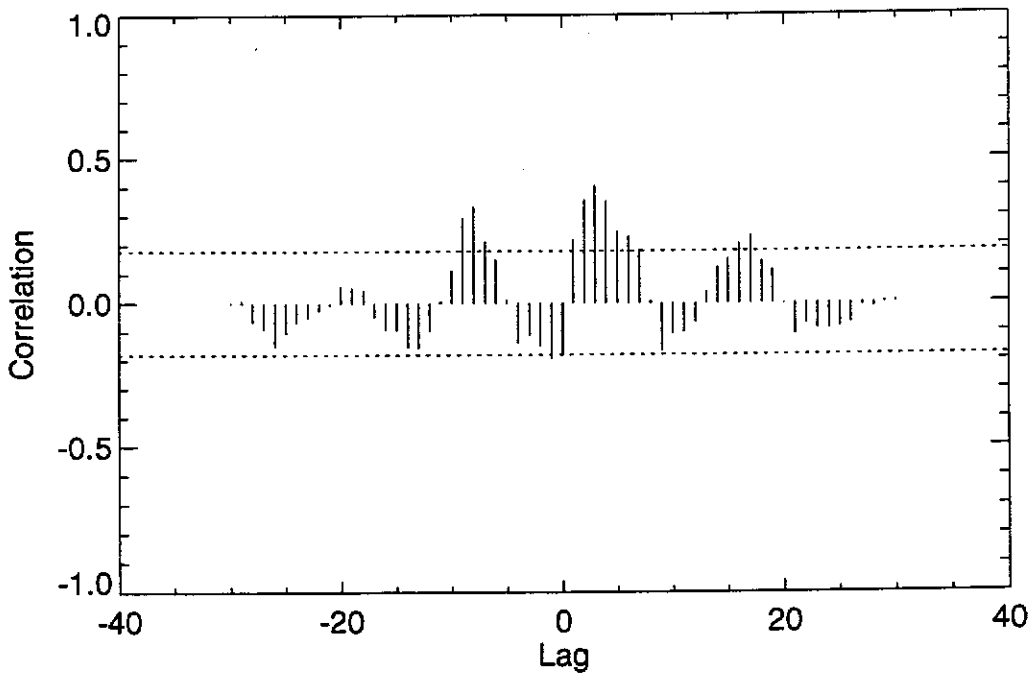

Figure 7.4 Cross-correlation function between input (rainfall) and output (NDVI). Dotted lines indicate 95 % confidence limit

The cross-correlation between rainfall and NDVI (Figure 7.4), indicates the rainfall has an effect on the NDVI at lag one, and this effect continues for some seven months. Correlations after seven months are outside the 95 percent confidence limit, and thus are assumed to be zero. The small (and significant) correlations at lags 16 and 17 have again been ignored. These are an artefact of ignoring the correlations at lags 10 and 12 in the input. The correlations at negative lags (i.e. ~ 12 months) are also a result of ignoring the autocorrelation in the input. Thus a tentative model relating the

NDVI to previous values of rainfall (R) is as follows:

$$NDVI_t = B + t(1)R_{t-1} + t(2)R_{t-2} + \ldots\ldots + t(7)R_{t-7} \quad (7.9)$$

The constant B is conceptualised as the base or minimum NDVI. This was shown to have ecological meaning in Chapter 6 (see Sections 6.3.1 and 6.6). According to the hypothesised model, this is the NDVI value that would be measured if there were no rainfall for seven months. The order of the model is the length of non-zero coefficients following the lag. The initial estimates of the coefficients for the tentative model are made using Equation 7.8 and these are shown in Table 7.1.

	σ_X = 42.9 (Rainfall) σ_Y = 0.037 (NDVI)		
i	$A_{YX}(i)$	t(i) [initial estimate]	t(i) [final estimate]
1	0.2164	0.00019	0.000254
2	0.3565	0.00031	0.000341
3	0.4054	0.00035	0.000339
4	0.3535	0.00030	0.000279
5	0.2456	0.00021	0.000209
6	0.2308	0.00020	0.000237
7	0.1838	0.00016	0.000255

Table 7.1 Estimates of transfer function coefficients. Initial estimates are from Equation 7.8. Final estimates are made using optimisation routines in ITSM package (Brockwell and Davis, 1991)

The ITSM package computes the final estimates of the coefficients (t_i) using an iterative maximum likelihood approach. The

model is seeded with the initial estimates. The structure of the model (i.e. lag and order) is not altered in this final estimation phase.

To estimate the constant B, an initial prediction of the NDVI is made using rainfall and the transfer function coefficients, assuming B is zero. The mean difference between the prediction and the measured output is adopted as the constant B. Using this technique the final model specified for the example is:

$$NDVI_t = 0.1327 + 0.000254\ R_{t-1} + 0.000341\ R_{t-2} + 0.000339\ R_{t-3} + 0.000279\ R_{t-4} + 0.000209\ R_{t-5} + 0.000237\ R_{t-6} + 0.000255\ R_{t-7} \quad (7.9)$$

The final model indicates that the NDVI 'remembers' rainfall from some seven months ago. Beyond this there is no memory according to the model. The predicted and measured values of NDVI are shown in Figure 7.5. The quality of the model may be assessed both visually, and statistically using the coefficient of determination (R^2).

The impulse response is the response of the system to a single input pulse. Figure 7.6 indicates the impulse response to a discrete input of 100 mm of rainfall. The response function is clearly plausible and demonstrates the utility of this approach.

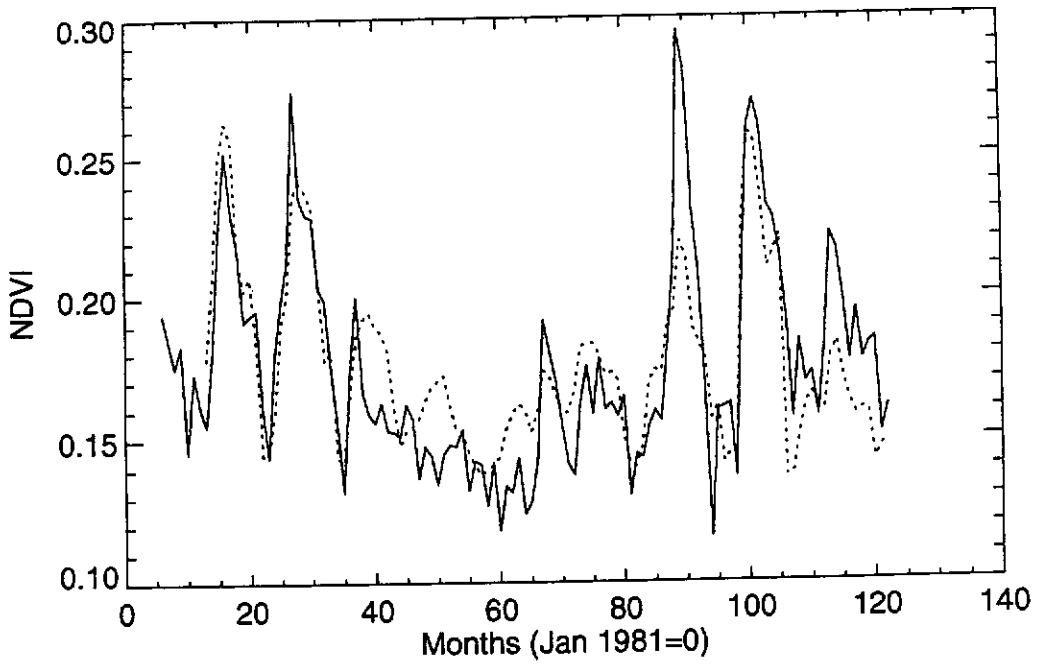

Figure 7.5 Measured (full) and predicted (dotted) NDVI for Stn 013017 (Giles). Prediction uses monthly rainfall data and Equation 7.10 (R^2=0.66, n=110)

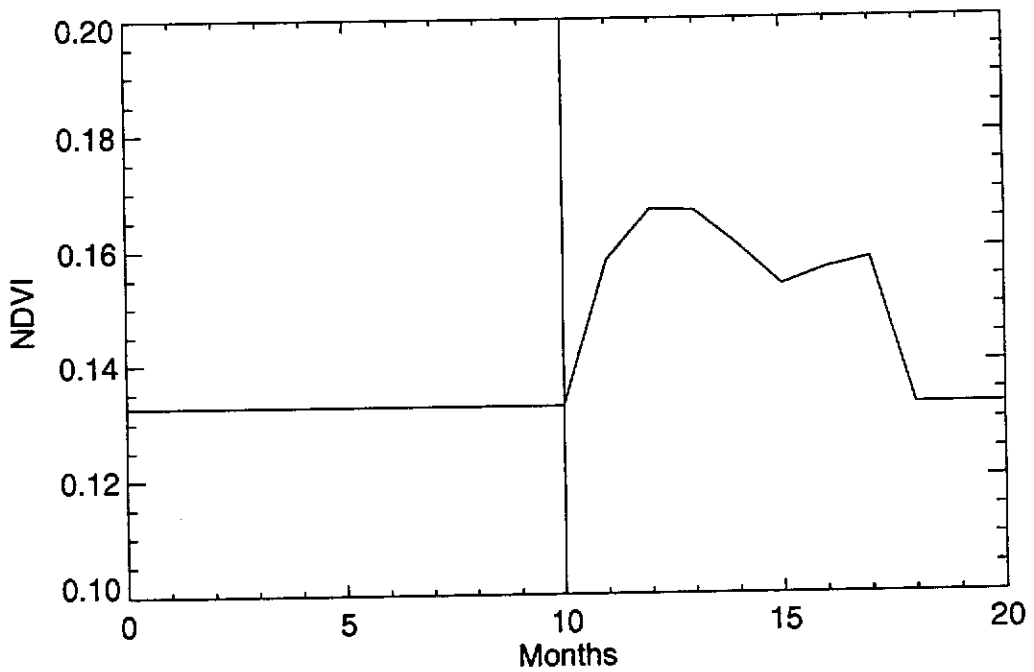

Figure 7.6 NDVI response to 100 mm rainfall input (impulse) for Stn 013017 (derived using Equation 7.10)

7.3.3 Review

While the transfer function methodology is involved, it offers a rigorous technique to establish a suitable model between an input and output sequence which are theoretically related. Previous work by Davenport and Nicholson (1993) has demonstrated that the relationship between rainfall and NDVI varies according to the vegetation type. By adopting a transfer function approach, it is possible to identify both the lag and order of the linear relationship between rainfall and NDVI.

The transfer function approach can also be described as a time invariant linear filter (Brockwell and Davis, 1987). This means that the filter coefficients do not change through time. Seasonal changes in environmental conditions, such as solar radiation and temperature, are ignored. In addition, the filter does not respond to previous values of the output. While this may appear a problem, the transfer function approach is consistent with the original hypothesis of Noy-Meir (1973) regarding the effects of rainfall in arid and semi-arid regions.

One potential drawback of the approach is the need for interpretation of intermediate results. The auto-correlation and cross-correlation functions both require skill and judgment to interpret and hence specify a tentative model linking the input and output sequences. This tends to make the procedure difficult to

program in a suitable algorithm. However, once a tentative model has been established, the final solution can proceed automatically.

Despite these drawbacks, the transfer function approach clearly offers promise. The prediction of the NDVI for Station 013017, presented as an example above, is outstanding, considering it was achieved using monthly rainfall values alone. The approach contrasts with use of linear relationships between the NDVI and rainfall for the previous one or two months, and is a diagnostic of the system behaviour. Given the initial success, it was decided to establish links between the rainfall and NDVI for all suitable stations presented in Chapter 6.

7.4 Application

Monthly rainfall and NDVI time series were presented in Chapter 6 for several stations covering a variety of climatic conditions and vegetation types across Western Australia. However the methodology proposed above is not suitable for all stations. To establish links between the rainfall and NDVI time traces there has to be a clear relationship between rainfall and NDVI.

In the forest areas of the extreme southwest of Western Australia, the NDVI indicates that growth cycles follow solar radiation, rather than rainfall (see Figure 6.2, Stn 009512 and Section 6.2.8). Presumably, the deep root systems of the vegetation

in this region allow the vegetation to draw stored water from the soil during summer periods with typically low rainfall. As such, it is not appropriate to study the links between rainfall and NDVI for this station. In the wheatbelt areas, management of the agricultural system is designed to avoid significant growth over summer periods (Smith, 1993). Thus a linear relationship between rainfall and plant growth cannot be expected at all times. A more appropriate input in this case would be seasonal (winter) rainfall, or the use of some other rainfall weighting scheme (Stephens et al., 1994).

Six of the stations presented in Chapter 6 were selected for further analysis. All stations come from either the pastoral region, or the area of currently vacant crown lands. They span all typical climatic conditions encountered in the arid and semi-arid regions of Western Australia. Those stations used are listed below (for details of stations see Figures 6.1 and 6.2, Table 6.1, and relevant discussions in Chapter 6):

(a)	Stn 002032	Turkey Creek
(b)	Stn 004006	Bonney Downs
(c)	Stn 007020	Annean
(d)	Stn 012065	Norseman
(e)	Stn 011004	Forrest
(f)	Stn 013017	Giles

7.5 Results

7.5.1 Transfer Functions

Transfer functions relating rainfall to NDVI were derived using the methodology given in Section 7.3 for the stations listed in Section 7.4. The resulting transfer functions and the quality of the prediction (R^2) are shown in Table 7.2. Plots depicting the predicted and measured NDVI, and the associated monthly rainfall are shown in Figure 7.7. The results for each station are discussed below.

Met. Stn.	Model Lag	Model Order	Model relating NDVI to rainfall	R^2
002032	1	2	0.1718 + 0.000203 R_{t-1}+0.000200 R_{t-2}	0.49
004006	1	8	0.1064 + 0.000253 R_{t-1}+0.000235 R_{t-2}+ 0.000228 R_{t-3}+0.000283 R_{t-4}+ 0.000337 R_{t-5}+0.000214 R_{t-6}+ 0.000133 R_{t-7}+0.000209 R_{t-8}	0.64
007020	1	7	0.1193 + 0.000199 R_{t-1}+0.000328 R_{t-2}+ 0.000306 R_{t-3}+0.000329 R_{t-4}+ 0.000275 R_{t-5}+0.000254 R_{t-6}+ 0.000211 R_{t-7}	0.51
012065	15	2	0.2515 + 0.000375 R_{t-15}+ 0.000290 R_{t-16}	0.11
011004	1	4	0.0993 + 0.000697 R_{t-1}+0.000637 R_{t-2}+ 0.000517 R_{t-3}+0.000484 R_{t-4}	0.29
013017	1	7	0.1327 + 0.000254 R_{t-1}+0.000341 R_{t-2}+ 0.000339 R_{t-3}+0.000279 R_{t-4}+ 0.000209 R_{t-5}+0.000237 R_{t-6}+ 0.000255 R_{t-7}	0.66

Table 7.2 Transfer function models relating NDVI to rainfall. Derived using ITSM package (Brockwell and Davis, 1991) for six arid and semi-arid zone sites

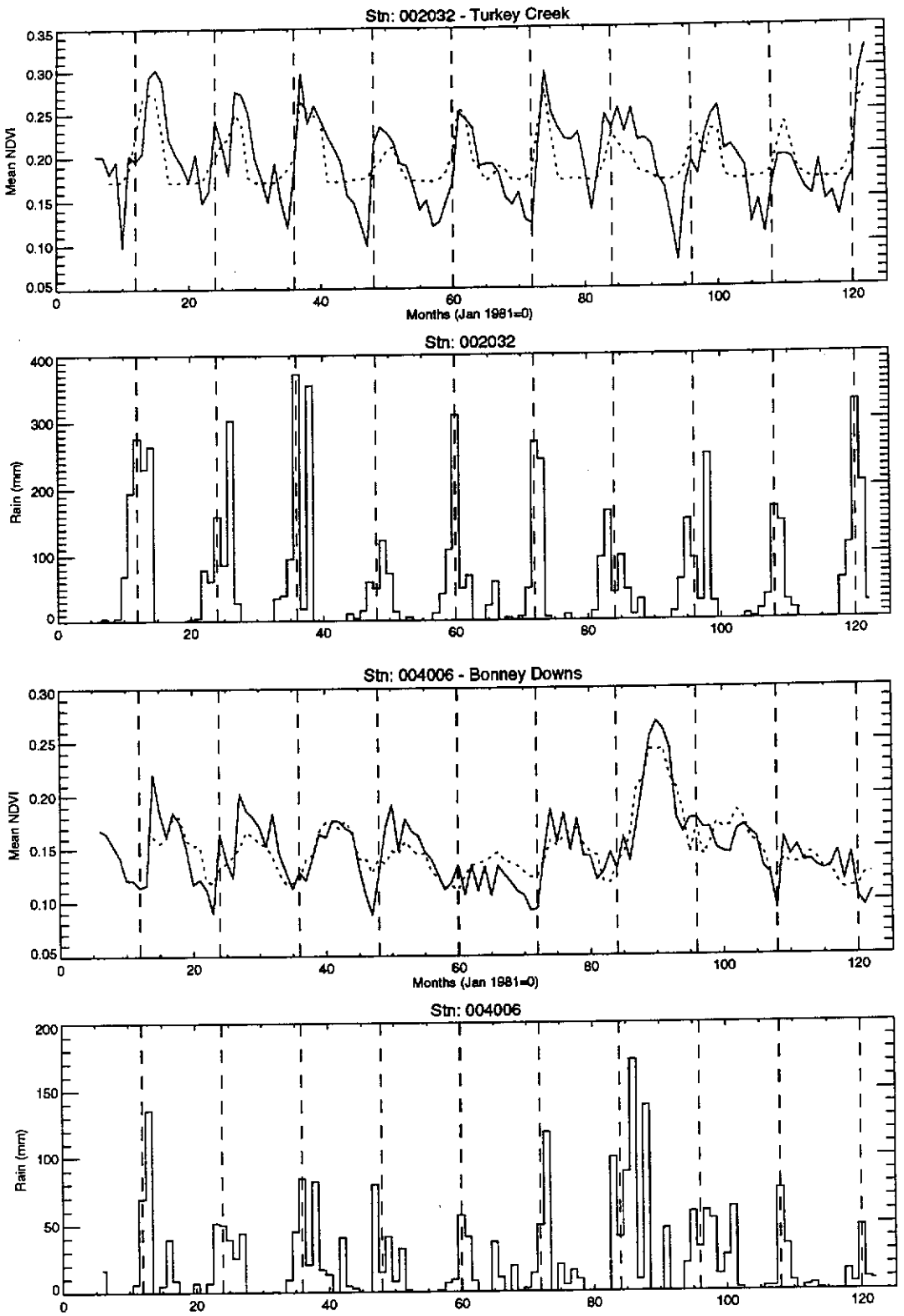

Figure 7.7 NDVI predictions (dotted) and NDVI measurements (full). Predictions are computed using transfer functions from Table 7.2. Rainfall is reproduced for convenience

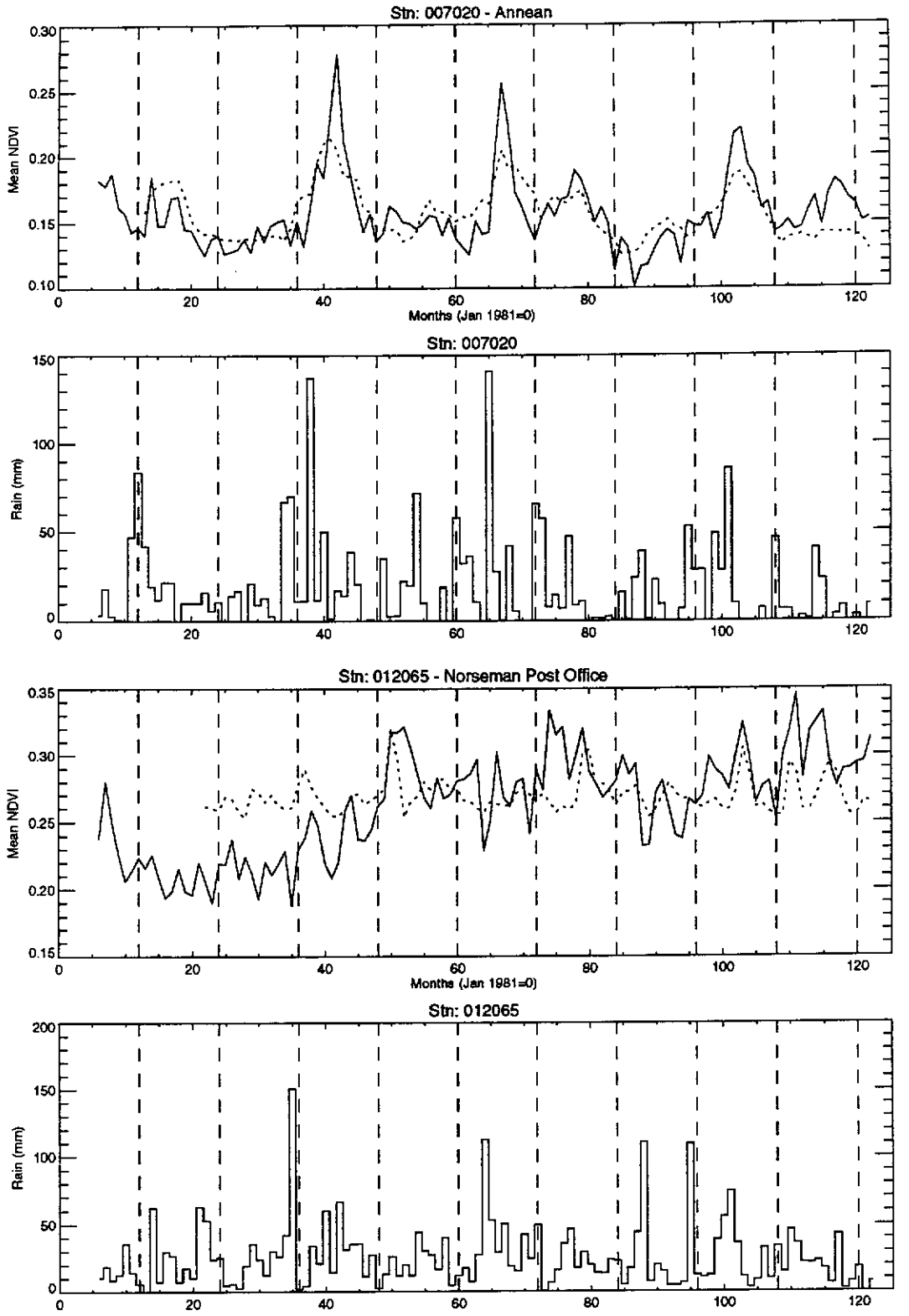

Figure 7.7 NDVI predictions and NDVI measurements (continued)

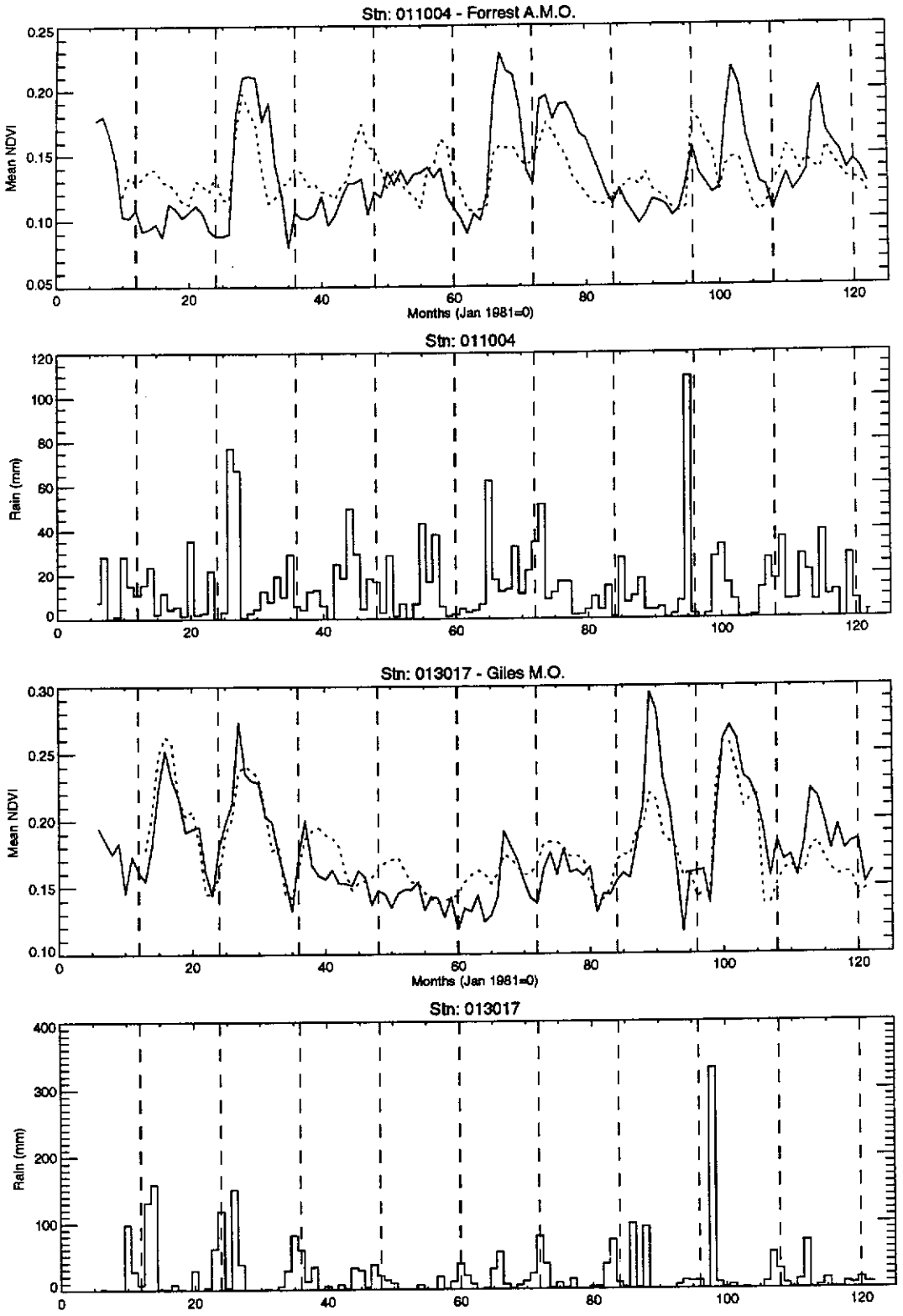

Figure 7.7 NDVI predictions and NDVI measurements (continued)

7.5.1.1 Stn 002032 - Turkey Creek

The transfer function approach is clearly not appropriate with this station. Despite poor rainfall over the November 1984-March 1985 season, the NDVI still shows a rapid rise, which the predicted value does not follow. While the quality of fit (R^2=0.49) is reasonable, the plot is clearly unreasonable. A more sophisticated approach will be required to relate rainfall to the NDVI in this environment. The short order of the model indicates that the system responds very quickly to rainfall, in contrast to other sites.

7.5.1.2 Stn 004006 - Bonney Downs

The quality of the fit is excellent (R^2=0.64) and the time series plot verifies this. In this case, the transfer function is clearly an appropriate model. The model indicates the current value of the NDVI is related to the previous eight months rainfall. The coefficients of the model are remarkably constant, indicating a virtual linear relationship.

7.5.1.3 Stn 007020 - Annean

The time series plot indicates the model is unable to account for large rainfall events. Despite this, the fit is still reasonable both statistically (R^2=0.51) and visually.

7.5.1.4 Stn 012065 - Norseman Post Office

Visual inspection of the NDVI and rainfall demonstrates that no clear relationship exists. The high perennial cover (see Section 6.2) may obscure observation off the herbaceous layer by the satellite. A large summer rainfall event in December 1983 is clearly implicated in the rising NDVI values in the following year. However, the transfer function approach assumes a linear relationship between the rainfall and NDVI at all times. This assumption is not valid for this station.

7.5.1.5 Stn 011004 - Forrest A.M.O.

While the NDVI prediction does follow a similar path to the measured value, the predicted values are less than measured values in all the major growth events. In addition, the prediction tends to overestimate the value of smaller rainfalls, such as the spring (September to November) falls in 1984 and 1985. The high latitude of this site (i.e. 30.83 degrees, see Table 6.1) will introduce a marked seasonality in evaporation and temperature. The changes in the external environment may be responsible for the lack of performance of the transfer function technique. The excellent run of rainfall from June 1986 to June 1987 has maintained growth throughout the summer period. Presumably, the predominantly annual species were able to persist and effectively use the rainfall as their root systems were maintained. The prediction of these circumstances was poor. This effect is essentially non-linear, in that the effectiveness of

rainfall was highly dependant on the existing vegetation (Le Houerou, 1984).

7.5.1.6 Stn 013017 - Giles M.O.

This station was used as the example in Section 7.3.2. The fit between predicted and observed NDVI is excellent both statistically (R^2=0.66) and visually. The prediction was poor following two rainfall events one month apart in the late summer of 1988. This is possibly due to the same non-linear effects discussed in 7.5.1.5 above.

7.5.1.7 Review

The transfer function approach is clearly appropriate for the arid zone sites in the more northerly regions (i.e. Stations 004006, 007020, 013017). For Station 012065, there is no clear relationship to rainfall, possibly due to high perennial cover.

The rainfall at Station 002032, a tropical savanna grassland site, is markedly seasonal. This extreme seasonality is not modelled adequately using the transfer function approach. It may also be possible that regular fires have an impact on the vegetation, which is not captured by the rainfall sequence, but is present in the NDVI.

The high latitude of station 011004, creates a marked seasonal regime in both evaporation and temperature. Thus the external factors affecting plant growth cannot be considered constant

throughout the year. It is possible that a better prediction of the NDVI would be obtained by converting the rainfall to a moisture index, which accounts for varying evaporation throughout the year (Fitzpatrick and Nix, 1970). In addition, a non-linear element was also identified, where plant growth can be highly dependant on the current status of the vegetation (Le Houerou, 1984).

7.5.2 Impulse Response Functions

The impulse response of each system to a discrete rainfall input of 100 mm is shown in Figure 7.8, for those stations where the approach has been successful (i.e. stations 004006, 007020, 013017).

The impulse pulse functions are similar for all stations except for a difference in the base NDVI value. The variation in the base NDVI could be related to variations in perennial vegetation, canopy architecture or soil colour (see Sections 2.4.5, 6.6, 6.7) amongst others. The coefficients of the transfer function are very similar, and indicate an almost linear relationship with the previous seven or eight months rainfall total.

The similarities between the impulse response function (Figure 7.8), and the transfer function models (Table 7.2) are striking. This is despite variation in rainfall, land use, vegetation type and latitude.

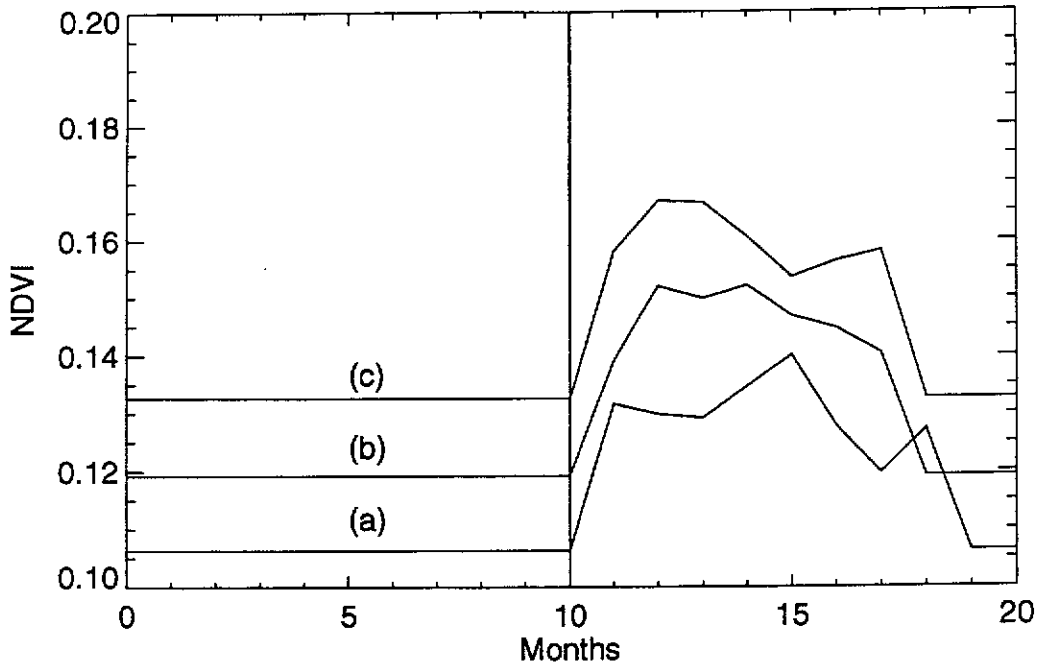

Figure 7.8 Impulse response in NDVI to 100 mm rainfall pulse. (a) Stn 004006 (b) Stn 007020 (c) Stn 013017. Impulse is derived from models in Table 7.2

7.6 Discussion

Transfer functions are a technique in common use in engineering for system analysis, monitoring and control tasks. Despite their common use in this field, their use in ecological and biological fields has been limited. Only one example of their application outside the systems engineering field could be found. This application was in deriving catchment hydrographs from rainfall records (Bennett, 1979).

Despite the lack of application, this study has demonstrated that rainfall can be quantitatively related to NDVI in the arid zone through the use of transfer functions. In particular, it is feasible to

reproduce the NDVI time series for the entire decade (at monthly intervals) using rainfall alone. While previous studies have looked at the relationship between rainfall and NDVI, no attempts have been made to reproduce the NDVI signal from rainfall alone.

The models derived for the three arid zone sites were found to be remarkably similar, with a settling time of seven to eight months after a discrete rainfall input to the system. From a practical viewpoint, the green vegetation cover standing at those sites studied is linearly related to rainfall received over the previous seven or eight months.

This study confirms the hypothesis proposed by Noy-Meir (1973) that NPP in the arid zones may be conceptualised as a number of discrete growth pulses which are linear combinations of rainfall inputs. However, the relationships do not hold over all arid zones sites. It is noted that Noy-Meir (1973) did not claim the results would be universal. In particular, highly seasonal rainfall, or highly seasonal temperature (and evaporation) appear to invalidate the linear relationship with rainfall.

Noble (1977) sought to relate rainfall to annual estimates of biomass taken from site photographs over a 50 year span at Koonamore reserve in South Australia. It was not possible to use the transfer function approach in his study as the biomass data were ranked (rather than measured). Despite these difficulties a tentative

relationship was established between rainfall and biomass which varied by species. The annual species were found to be correlated with the previous 12 months rainfall. The biomass of perennial species was related to much longer totals of monthly rainfall.

For satellite based studies this represents a problem as the separation of species is not possible. The green cover of all plant forms is recorded in a single pixel. This leads to a focus on the annual species which respond quickly to favourable moisture conditions in the arid zone. The response signal for the perennial plants will be masked by the larger and faster response of annual plants. Under these conditions the transfer function model implicitly assumes a constant perennial component. This limitation cannot be overcome, and is a parameter of the satellite measurement system.

It is likely that variations in perennial ground cover could also cause the coefficients of the transfer function to change. Thus care is required in interpreting the coefficients derived from the models. In many areas of the arid zone this will not present a problem as the perennial cover is very low (typically less than 10 percent) (Holm, 1994).

The results indicate that it is not possible to compare the output of the system (i.e. vegetation) without reference to the corresponding inputs. This led Le Houerou (1984) to propose the concept of rain use efficiency as a means of comparing the system

output across varying vegetation communities. The rain use efficiency (RUE) is a measure of the primary production expressed per mm of rainfall.

The measurement of the current status of vegetation is a major aim of earth resource satellite programs. For management purposes, a warning signal may be required when major change in the behaviour of the system has occurred. This could be inferred from changes in the transfer function through time and would potentially allow monitoring to be independent of the rainfall. One approach to this problem is the use of Kalman filters to dynamically estimate the parameters of the transfer function. Changes in the coefficients will signal a change in system behaviour.

Bennett (1979) has termed this task parameter mapping, and has presented an example of changes in the transfer function describing catchment runoff, as land use in the catchment changes (Bennett, 1979, p. 383). Such an approach is not viable in this study as rainfall is only measured at a small number of discrete sites. It may be possible in the future to derive spatially comprehensive estimates of rainfall using satellite measurements (Snijders, 1991) and derive dynamic transfer functions using the parameter mapping techniques proposed above. Such a system could potentially offer a monitoring technique that was independent of seasonal effects.

7.7 Summary

Transfer function modelling, a technique in common use in engineering disciplines, has been used to establish linear relationships between rainfall and NDVI. This technique was originally proposed as a possibility some 20 years ago. Despite this proposal, field verification of this hypothesis appears not to have been carried out, presumably due to the difficultly in collecting the necessary data.

Inspection of the original NDVI-rainfall time series plots indicates that rainfall is the controlling factor in plant growth for five of the six arid sites studied in this Chapter. The exception, Station 012065, is in a heavily wooded eucalypt woodland.

Of the remaining five sites, reasonable linear relationships were established between rainfall and NDVI for three of these sites (Stations 004006, 007020, 013017). The two sites where rainfall was not sufficient to predict the NDVI occurred in the extreme north and south of the State (Stations 002032, 011004). In the north, the highly seasonal pattern of rainfall has affected the relationship between NDVI and rainfall. The short memory of two months indicated for this site (Station 002032), may also indicate that the monthly sampling is too coarse to establish a relationship between rainfall and NDVI.

In the south, the higher seasonality in temperature and evaporation possibly invalidates the assumption of a constant external environment, required for a linear relationship to be established with rainfall. Improved predictions may be attained by relating estimated water use to the NDVI via an appropriate water balance model. This hypothesis needs to be tested in future studies.

The transfer functions successfully established for three arid zone sites (Stations 004006, 007020, 013017) were remarkably similar. This was despite variations in rainfall, land use, vegetation type and climatic conditions.

The transfer function is indicative of the operation of the system in processing rainfall, through transpiration to become dry matter. It is proposed that it may be possible to monitor changes in the transfer function coefficients through time using Kalman filtering. Such a technique would permit changes in the behaviour of the system through time to be identified which are virtually independent of seasonal influences. Practical application of such a technique would require satellite measurements of rainfall on a spatially comprehensive grid.

Chapter 8

DEVELOPMENT OF SEASONAL SUMMARIES

8.1 Introduction

The inspection of time series plots of NDVI and rainfall provides an understanding of the nature of plant growth responses to rainfall in various regions. However these plots ignore the spatial aspect of the satellite imagery, which is the major advantage over point based data sets. In essence, the understanding gained from the point-based data needs to be synthesised to produce ecologically meaningful information products from the satellite imagery (Millington, 1992).

One simple technique to visualise the seasonal information inherent in the time series imagery is to produce annual summaries which depict plant growth. Such summaries should permit a broad appreciation of the seasonal activity on an annual basis. This is currently done by interpolating annual rainfall data measured at discrete stations and subsequent presentation as either contours of annual and/or seasonal rainfall or regions of rainfall deciles (Gibbs, 1984). In either case, rainfall is used as a surrogate indicator of seasonal plant growth. The use of a measure such as the NDVI avoids the need for the interpolation of surrogate measures from sparse measurement stations to create a spatially comprehensive coverage.

Such an approach has been adopted by Tucker et al. (1991). They used NDVI GAC data to produce images depicting the mean and coefficient of variation (CV) of the growing season for Northern Africa over the period 1981-1991. Using GAC imagery they integrated raw NDVI values for the July-October period on a pixel by pixel basis for each year. The integrated NDVI values were then summarised by taking the mean and CV of the 11 annual images to produce a decadal summary of growing conditions. The CV was chosen to represent annual seasonal variability rather than the standard deviation, to sharpen the boundary between the desert and savanna lands. By restricting the geographic coverage, they were able to apply a fixed integration period (i.e. July-October) each year.

In Western Australia the growing season varies from summer in the north, to winter in the south. Thus a fixed integration period for all regions is clearly not appropriate. In addition, in the arid regions which cover most of the State (and Australia), seasonal growth occurs at variable times from year to year. Clearly a technique is required which can identify the growing season on a pixel by pixel basis each year.

This chapter describes simple techniques which summarise the annual growing conditions over Western Australia both annually and over the entire decade (1982-1990).

8.2 Conceptual Approach

Time series plots of NDVI show two distinct pieces of information:

(a) Magnitude of seasonal activity,

(b) Time of occurrence.

Previous studies have shown that the integral of NDVI over the growing season is related to NPP (see Section 2.5 for a full discussion). The timing of rainfall (i.e. summer or winter) is also an important ecological consideration and has been shown to affect the germination and growth of various species in Australia (Austin, 1980; Mott, 1973).

Thus the proposed annual summaries should seek to answer three basic questions:

(a) Where did the plant growth occur ?

(b) When did the major growth period occur ?

(c) How much growth occurred ?

The time series images can be processed on a pixel by pixel basis, so (a) can be answered by making an image of the result. This leaves (b) and (c) to be defined.

An ideal situation would be to identify the start and end of each growth period and subsequently integrate the NDVI over that period. Based on theoretical relationships (see Equations 2.4, 2.5,

2.6), this integral should be linearly related to NPP. To convert the integral to an actual production measurement (kg/ha) requires knowledge of the efficiency of conversion of solar energy to dry matter for each pixel (see Equation 2.4).

Water balance techniques have been used extensively to identify the start and end of growing seasons (Fitzpatrick et al., 1967; McAlpine, 1970). Using these techniques the start and end points of a growth period are identified based on some objective criteria. This criterion is usually based on the ratio of soil moisture storage to potential evapotranspiration being above some threshold value (McAlpine, 1970; McCown, 1973). In a study of the effect of variation in soil storage capacity on growing season length, McCown (1973) found that relatively small differences in growing season length often lead to large differences in final dry matter production. This study, conducted at a Northern Queensland grassland site, demonstrates the importance of accurate definitions of the start and end of the growing season. This is primarily due to the exponential nature of plant growth (Charles-Edwards et al., 1986).

Water balance techniques have also been used to identify the start and end of the growing season on NDVI time traces. Henricksen and Durkin (1986), working in Northern Africa, used a simple water balance technique requiring monthly inputs of rainfall and potential evapotranspiration to define the start and end of the growing season. The NDVI time series was derived from GAC data

sampled at various intervals ranging from one to three weeks. Spline-based interpolation methods were used to resample the soil water and NDVI data to common time periods. Broad agreement was obtained between the two series once the lag between soil water and growth was accounted for.

In a similar study, Bonifacio et al. (1993) defined the beginning and end of the growing season using characteristics of the NDVI time series measured at ten day intervals. These estimates were compared to those derived from water balance techniques in common use throughout the region. The agreement between the definitions was generally good, with the estimates being within one sampling period of each other (i.e. ten days) at 62 percent of sites. The worst agreement between the two series was found in the arid regions. Poor agreement was also found by Henricksen and Durkin (1986) in arid regions.

Both the above studies used NDVI image data sampled at a finer interval than the monthly data available for this study. A further complication is the maximum value compositing (MVC) procedure used to generate the data. By selecting the maximum value for each month, a bias is introduced into the time series curve. At the start of the growing season, the pixels will tend to come from the end of the month, and vice-versa at the end of the growing season. Clearly, any attempt to define the start and end of the growing season from monthly NDVI data would be very coarse. In

view of these difficulties an alternative scheme was investigated.

Inspections of numerous NDVI time series traces over various regions of Western Australia during this study, show that all are essentially unimodal on an annual basis. While bimodal rainfall patterns can and do occur within one year (e.g. summer and winter), these patterns do not seem to produce bimodal growth curves in Western Australia. Typically, it appears that, if two separate periods of effective soil water occurred during the year, then the second period reinforces the first to produce a better overall season during the second period. This is to be expected, as the opening rains germinate seeds, and the follow-up rains allow growth to occur. However, bimodal NDVI time series can be seen in the literature. Justice et al. (1985) show areas in both India and Pakistan, which display annual NDVI time series that are bimodal (Justice et al., 1985, see Figure 17, pp. 1312-1313). Irrigated regions would also show multi-modal growth periods throughout a year.

Given the limitations on defining the start and end of a growing season, an alternative technique for summarising the annual series was adopted. This technique is based on a fixed length growing season each year and is appropriate for any region where the majority of any annual seasonal growth occurs in one distinct period.

The nature of growing seasons in Australia has been

investigated by Nix (1982). He used long term mean climatic data and a simple plant growth model (Fitzpatrick and Nix, 1970) to determine average lengths of growing seasons across Australia. This study shows that only in the extreme southwest and northwest corners of the State does the mean growing season extend beyond six months (Nix, 1982, Figure 4, p. 52). For an area roughly corresponding to that used for pastoral activities (see Figure 3.1) the mean growing season length was between 13 and 26 weeks. For the area approximately indicated as vacant in Figure 3.1, Nix reports a mean annual growing season length of less than 13 weeks.

On this basis, the growing season was assumed to be five months. In some years this will tend to underestimate the growth, and in others an overestimate will occur. By assuming a fixed growing season that is longer than the actual growing season, the integration of NDVI will tend to be overestimated. This is preferred in these circumstances, as it takes a conservative approach.

An annual production index (API) was defined as the maximum contiguous five monthly integral of the NDVI occurring over a 12 month period. This integral was normalised for the minimum NDVI value that had occurred over the entire time series for each pixel. The subtraction of a base value has also been used by Bonifacio et al. (1993), and avoids integrating the base value which is highly correlated with long term rainfall patterns (see Figure 6.12).

The season was deemed to have occurred at the central month of this five month moving integral. The integration was performed over each calendar year. To avoid the possibility of splitting one growth period into two successive years, a biological year should be defined for each region. However, it was found by inspection that virtually no regions in the study area have a growth peak in the December/January period, which avoids the problem of splitting a contiguous growth period. An integration over the calendar year is also simple to report. The integral was approximated by summing the NDVI value over five successive months. This concept is shown in Figure 8.1.

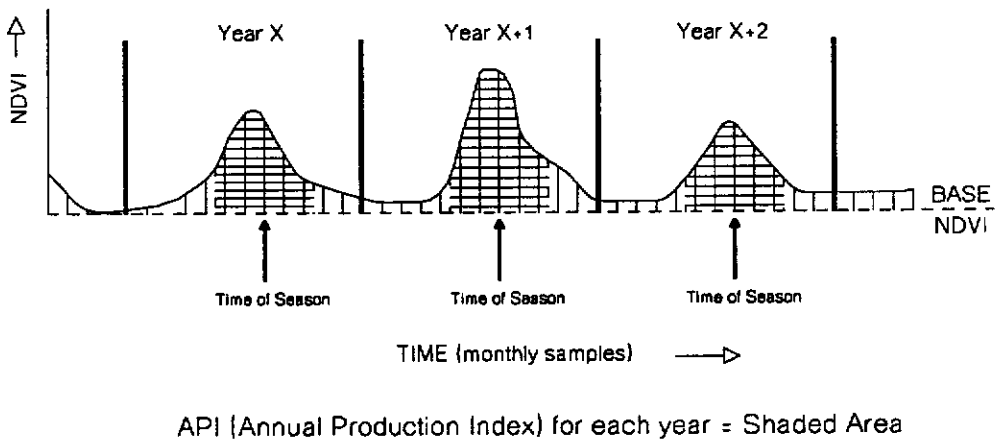

Figure 8.1 Method for extraction of annual seasonal information from continuous NDVI trace

8.3 Annual Summary Images

Using the technique described above, the API was computed for each full year of the series. The value of the API and the central month of the integration period chosen were written as images on a pixel by pixel basis. The images are shown in Figures 8.2 and 8.3. The scale of the API is NDVI months.

The images of API for each year clearly show the extraordinary spatial variation in seasonal activity over the arid zone. The images were scaled to highlight differences in the arid zones, and hence the API over agricultural zone saturates on the colour scale. In addition to the spatial variability in API, there is also large variation in the timing of the API over the decade. The agricultural areas of the southwest show an annual cycle peaking in August-September each year, which agrees with the current cropping practices. In all years, large parts of the arid zone do not show periods of seasonal growth. However, these regions typically change from year to year, presumably following changes in rainfall. In some years (such as 1986) very 'patchy' seasonal growth is evident. Various aspects of the seasonal growth during each year are briefly discussed below.

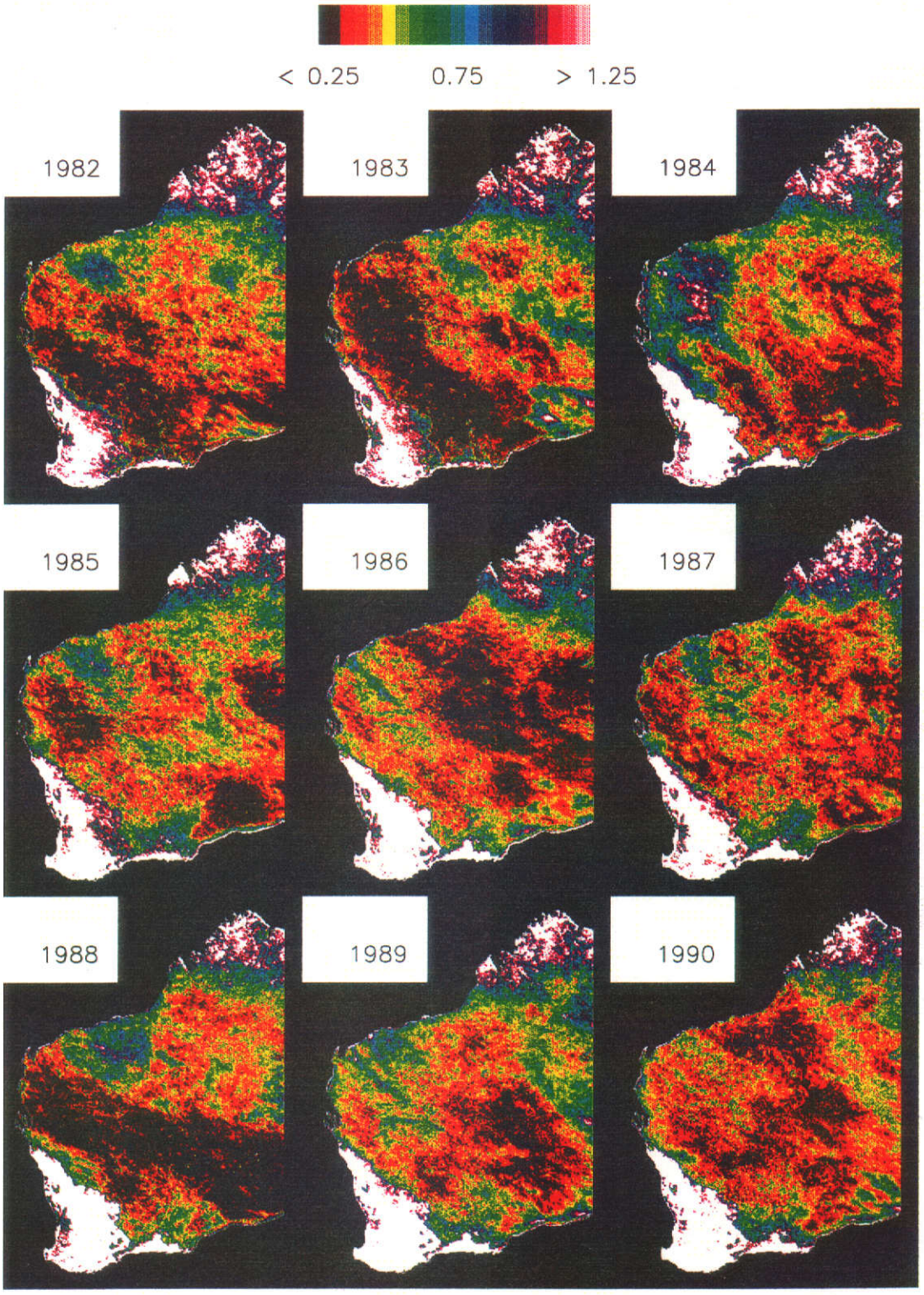

Figure 8.2 API (in NDVI months) for each year of NDVI time series

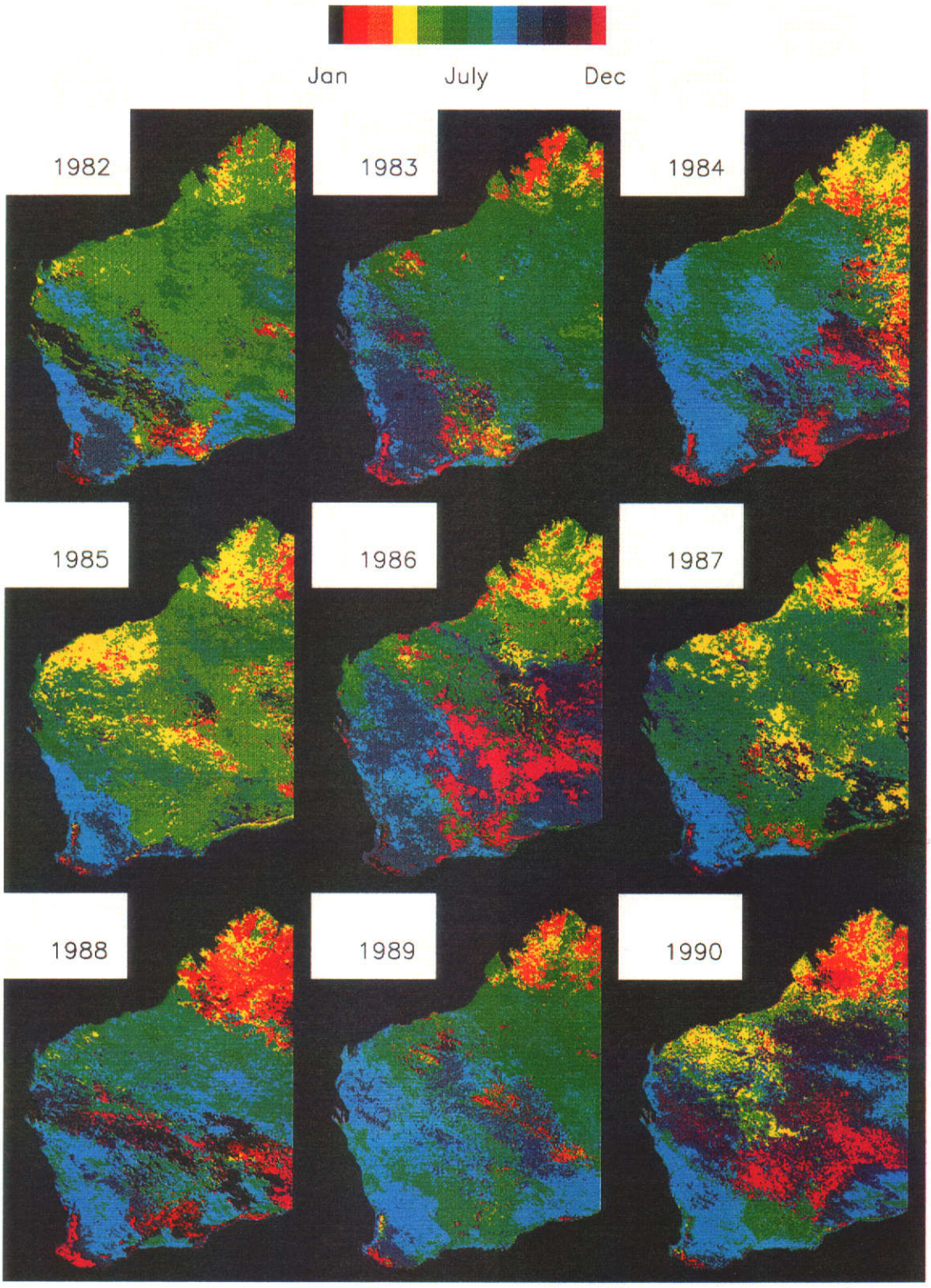

Figure 8.3 Month of maximum Annual Production Index for each year of NDVI time series

8.3.1 1982 Seasonal Summary

An excellent season in parts of the Pilbara is evident. The time image indicates that the peak in this region occurred in April/May. The Murchison region shows no indication of any significant growth periods. A region of vegetation growth is evident in the desert (126°E, 22°S).

8.3.2 1983 Seasonal Summary

An excellent season is evident on the Nullarbor Plains, with a peak in June/July. Note that spatial variation still exists and some areas have responded, while an area through the centre of the Nullarbor Plains appears to have missed out on a growth period, presumably due to lack of rain.

8.3.3 1984 Seasonal Summary

An excellent year in a large area of the east Gascoyne and Pilbara regions, peaking in July/August. A small isolated area in the southern Gascoyne appears to have missed a growth period, presumably due to missing rainfall. A very distinct boundary appears in the time of seasonal growth in the West Kimberley region. This boundary is a persistent feature throughout the images. Note that a small area on the western edge of the Nullarbor Plains, which missed out in 1983, has shown a seasonal response.

8.3.4 1985 Seasonal Summary

A region in the Pilbara indicates growth has occurred, and the time of peak growth was April. This region is almost identical to the area of growth in 1982. The other distinguishing feature is the patchiness of the growth over the arid regions of the State.

8.3.5 1986 Seasonal Summary

Very patchy growth is evident on the Nullarbor Plains, predominantly occurring in September. Another band of patchy growth is evident through the Murchison region occurring in September.

8.3.6 1987 Seasonal Summary

Very patchy growth again over much of the arid areas. Note that small areas of growth on the eastern end of the Nullarbor Plains were evident in April, indicating summer/autumn rainfalls, in contrast to previous winter dominance.

8.3.7 1988 Seasonal Summary

This image contains the outstanding feature of the series. The band of poor seasonal growth separating the northern and southern parts of the State is clearly related to the dominant weather patterns in Western Australia (Payne et al., 1987). Winter frontal activity from the south, and summer monsoonal activity from the north have not

overlapped, leaving a band of the State without seasonal growth for the year.

8.3.8 1989 Seasonal Summary

A small area of the central Kimberley has not shown a seasonal response in 1989. The image indicating time of growth shows a band across the State indicating a June peak to the north and a September peak to the south. This corresponds to a boundary of growth/no growth in the API image. Good seasonal growth is evident in the Pilbara.

8.3.9 1990 Seasonal Summary

The Pilbara region shows very patchy areas of seasonal growth, and the image of peak time shows the peaks were in April, indicating summer rainfall. Perhaps the patchy growth is related to convective thunderstorm activity. The eastern end of the Nullarbor Plains also shows seasonal growth peaking in September.

8.3.10 Review

The series of images indicates the extreme spatial and temporal variability in the pastoral and vacant areas of Western Australia. One can imagine the land surface being in a constant state of flux, depending on how long it has been since a period of plant growth.

In some years the API indicates a strong regional influence, such as the good seasons in the Pilbara region in 1982 and 1988, and the excellent season extending from the Gascoyne into the Pilbara in 1984. This regional influence is presumably related to a regional weather pattern of the time. In contrast, other years show very patchy seasonal growth. Despite this, some small areas have still shown a good seasonal response in these patchy years.

8.4 Decadal Summary Images (1982-1990)

Answers were sought to three basic questions proposed in Section 8.2 as follows:

(a) Where did the plant growth occur ?

(b) When did the major growth period occur ?

(c) How much growth occurred ?

The annual summaries have been designed to specifically address the above issues. However, for scientific and management purposes, it is also important to know how regular the growth periods were in both time and space. Traditional approaches to such a problem have used average meteorological data measured at discrete sites over extensive periods of time (e.g. 100 years). Such a scheme has been proposed for Western Australia by Beard (1990). He proposed a bioclimatic classification (see Figure 3.2) based on the season of dominant rainfall and length of the dry spell each year.

Classification schemes, such as the one discussed above, do not indicate the variability expected within a particular class. The NDVI image-based time series offers a unique opportunity to summarise the seasonal information and focus on the variability of the growth through space and time.

The annual summary images computed can themselves be summarised into a decadal summary of both the magnitude and timing of seasonal growth. For the API, the average and standard deviation over the decade have been computed on a pixel by pixel basis from the nine annual summaries.

Summarising the timing of seasonal growth requires the use of circular statistics (Zar, 1984). Such statistics are not commonly used, so a brief review is presented, as well as the method used to apply them to this task. Finally, images are presented of the mean time of a seasonal peak and (approximate) 95 percent confidence limits for that mean time.

8.4.1 Summary of Seasonal Growth

The mean and standard deviation of the API were computed on a pixel by pixel basis for the nine annual observations available at each pixel. The resulting images are shown in Figures 8.4 and 8.5.

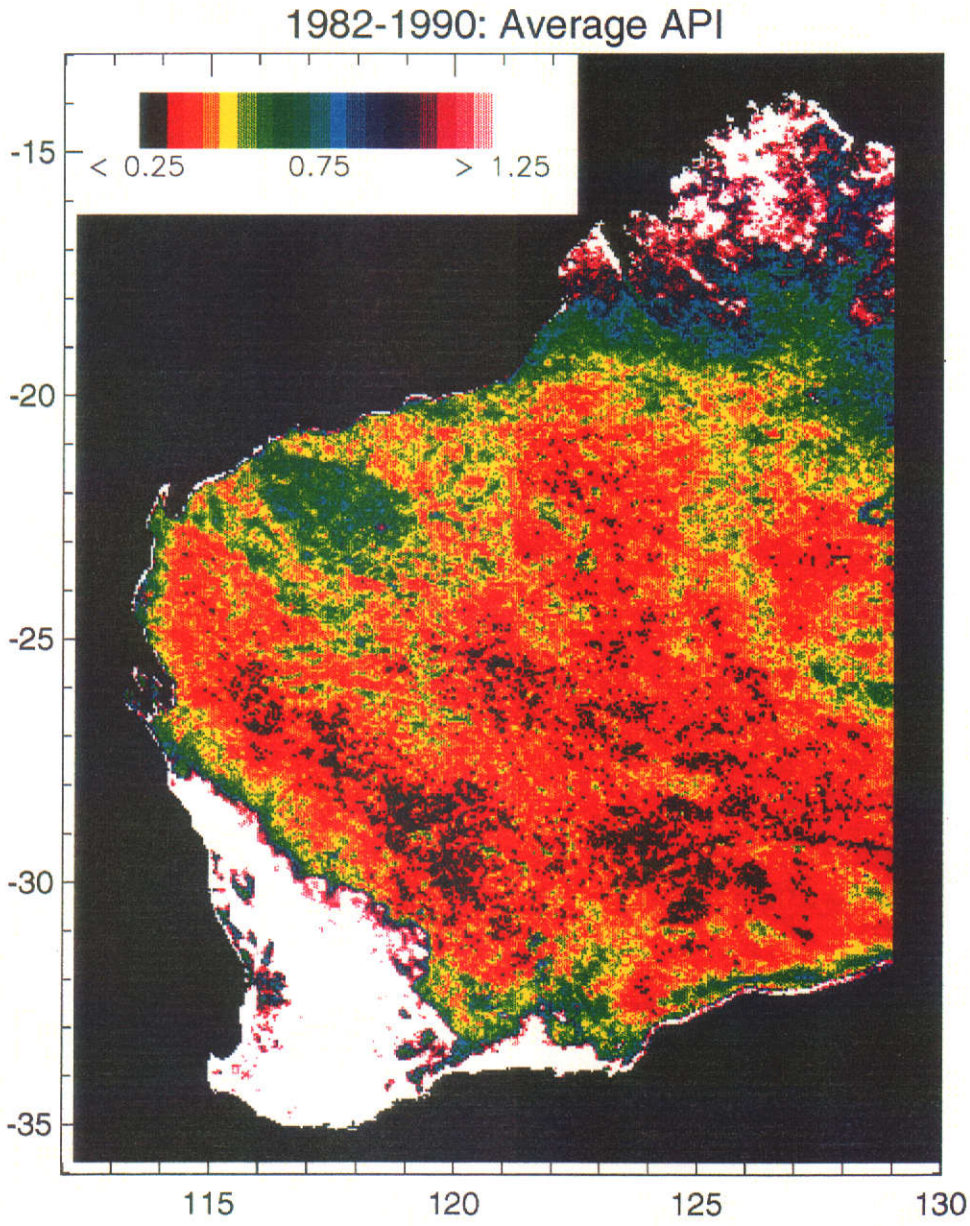

Figure 8.4 Mean Annual Production Index (1982-1990)

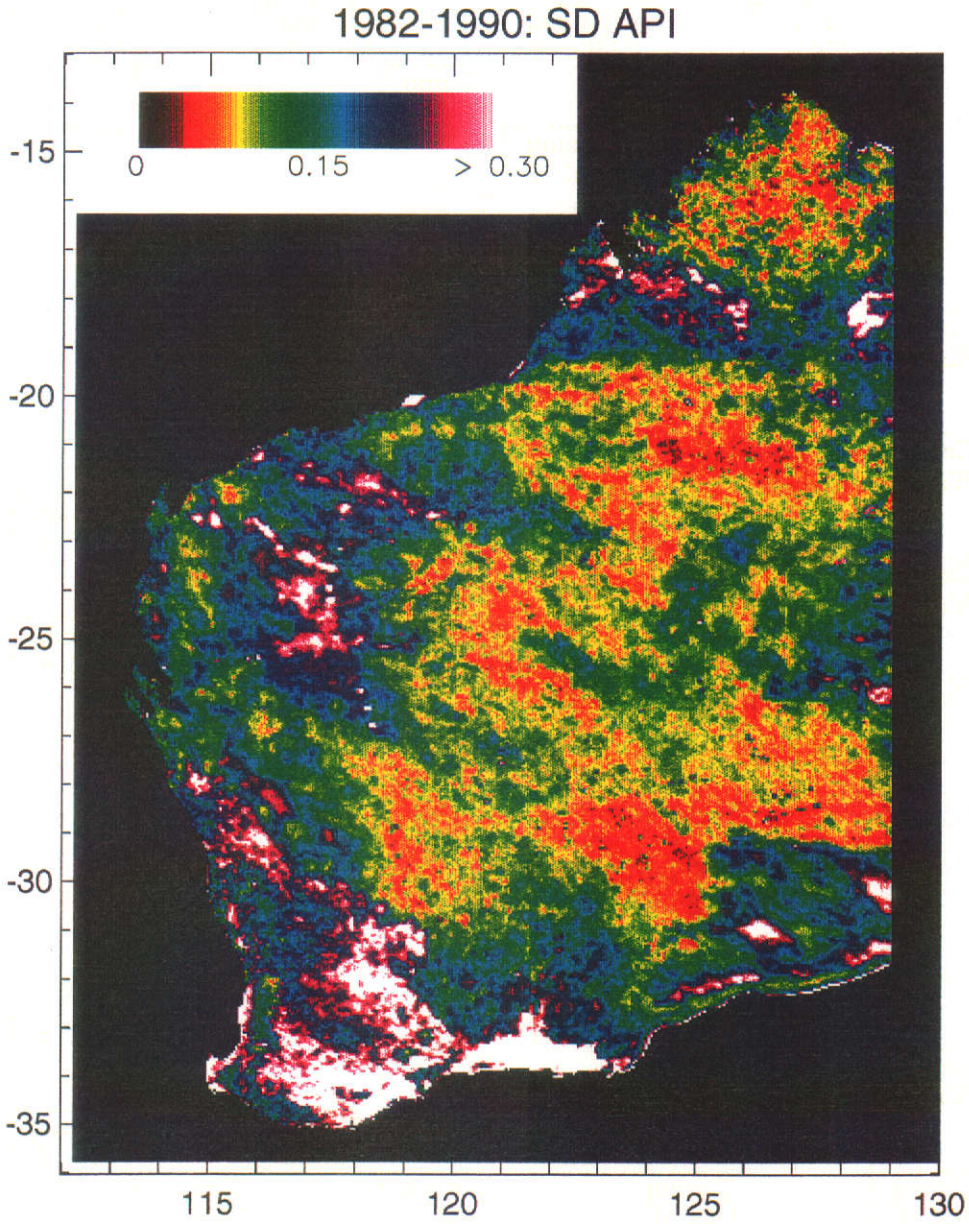

Figure 8.5 Standard deviation of API (1982-1990)

The average API over the decade shows expected patterns. A region in the Pilbara (118°E, 22°S) shows a higher mean than the surrounding lands, presumably reflecting greater rainfall during the decade. Most of the pastoral and vacant areas show a very low mean API for the decade.

The standard deviation in API shows significantly more information. Note that this image shows similar detail to the modified range image (Figure 6.5) described in Chapter 6. Areas of the west and east Kimberley show large variation in the API from year to year. These are grassland areas. The excellent season noted in 1984 has been outlined in the Gascoyne area. The standard deviation indicates a sharp boundary to the north of the Nullarbor Plains. This boundary was not generally evident in the annual API images, and presumably reflects response differences in vegetation type. Within the wheat belt area of the southwest, the eastern and northern areas show greater variation in API than the central area. This reflects greater year to year variation in rainfall and hence wheat yields (Arbrecht, 1994).

8.4.2 Time-Based Decadal Summary

The summary images of the time of seasonal growth make use of circular statistics (Zar, 1984). A brief overview of these statistics is presented, as well at their application in this work.

8.4.2.1 Statistical Background

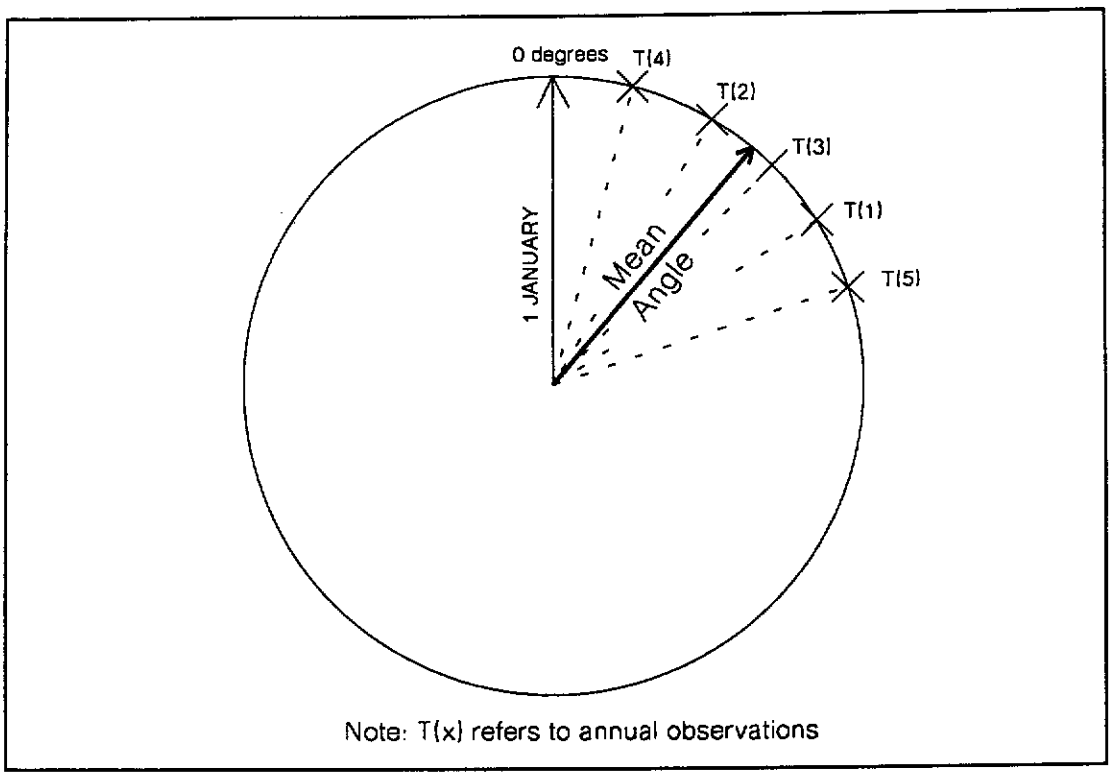

Figure 8.6 Concept of mean time of seasonal growth

The time of peak API for each year is conceptualised as a vector of unit length, on a circle where that circle represents one full year. The vector defining the start of the year is assumed to be at the 12 o'clock position. These relationships are shown for several observations in Figure 8.6. Assuming that the time occurs in the centre of each month, then the monthly observations can be converted to angles on a scale of 0 to 360 degrees, based on the relation that one complete year is 360 degrees and commences in January as follows:

$$\alpha = (M+0.5)/12 \times 360 \qquad (8.1)$$

where

M = month of the year (ie. 0=Jan, 1=Feb, ..., 11=Dec)

α = angular equivalent of M (degrees)

Each vector is assumed to have equal length and can be decomposed into an X and Y component using standard trigonometry as follows:

$$X_i = \frac{\sin \alpha_i}{n} \quad \textit{and} \quad Y_i = \frac{\cos \alpha_i}{n} \qquad (8.2)$$

where

n = number of angular observations in data set

The mean angle (A) is given by summing all the individual X and Y components as follows:

$$A_i = \tan (\Sigma X_i / \Sigma Y_i) \qquad (8.3)$$

Dispersion of circular data is assessed based on the length of the final vector (r) defined as (Zar, 1984):

$$r = \sqrt{(\Sigma X_i)^2 + (\Sigma Y_i)^2} \qquad (8.4)$$

For a data set of n observations, all with the same angle α, r would thus equal one. As the angular dispersion in the data increases, the value of r approaches zero. Zar (1984, pp. 665-666)

presents tables to convert values of r to a confidence limit around the mean at both the 95 and 99 percent levels. Data from these tables (95 percent level) are shown in Figure 8.7.

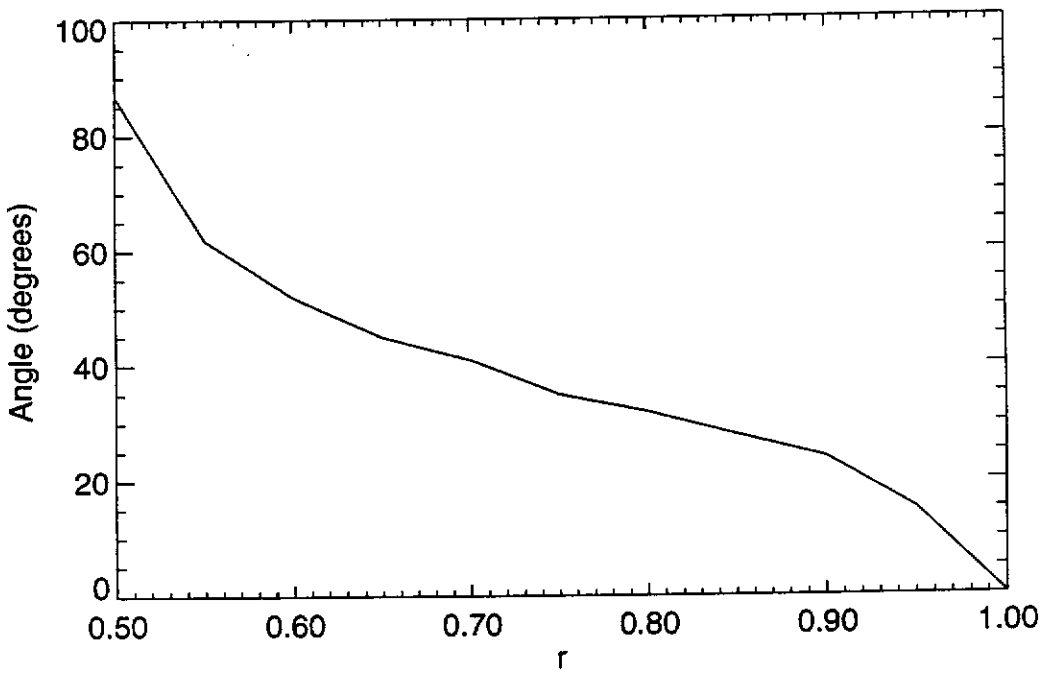

Figure 8.7 95 % confidence limits (degrees) for mean angle as a function of r given eight observations (Zar, 1984, p. 665)

For example, if r of 0.8 is calculated from eight observations, then from Figure 8.7 the 95 percent confidence limit around the mean is approximately ± 32 degrees. For values of r less than 0.5, there is virtually no confidence in the mean. While the 95 percent confidence interval is presented in degrees, since the original data are in years, then one degree is approximately equal to one day (i.e. 360 degrees = 365 days of the year). Such an approximation is useful, as it gives the mean time in months with a confidence limit in days around the mean.

8.4.2.2 Example Calculation

To illustrate the above statistical framework a worked example is presented in Table 8.1.

n	M	α (degrees)	X_i	Y_i
1	3	105	0.121	-0.032
2	4	135	0.088	-0.088
3	5	165	0.032	-0.121
4	3	105	0.121	-0.032
5	6	195	-0.032	-0.121
6	4	135	0.088	-0.088
7	5	165	0.032	-0.121
8	3	105	0.121	-0.032
		SUM	**0.571**	**-0.636**
		A (mean angle)	**138.1** (degrees)	
		r	**0.855**	
		95 % confidence interval	**± 28** (degrees)	

Table 8.1 Circular statistics for summarising seasonal growth over eight years. M is month of seasonal peak and α is equivalent angle. For other symbols, see text

From the example, over eight years the peak season can be observed to range from April (M=3) to July (M=6). The mean angle derived for this data set is 138 ± 28 (degrees). Converting back to a monthly scale indicates a peak season in early May. There is 95 percent certainty sure that the peak season will occur within one month either side of this date (i.e. ± 28 degrees).

8.4.2.3 Results

While a formal methodology has been described above, one problem still remains. For many areas in the arid zones of Western Australia, significant seasonal growth as measured by the NDVI does not occur on an annual basis. Dregne and Tucker (1988) reported that integrated NDVI was not sensitive for values of annual production below 400-550 kg/ha/year dry matter production in Northern Africa. It is also noted that they did not subtract a base value prior to integrating the NDVI. The failure to subtract a base value may have produced more scatter in the relationship between integrated NDVI and dry matter production. Subsequently it is not clear whether the threshold is a real biological concept, due to the use of raw NDVI values, or a general lack of sensitivity in the NDVI for areas of low production.

To identify an approximate season/no season threshold, histograms were taken for the large regions of no growth indicated on each of the annual summary images. In each case, monthly rainfall records were also inspected to ensure that the threshold was a valid concept. Typically, the 95 percent upper limit for the API within these regions was in the range 0.40 to 0.45 NDVI months. This was consistent over various vegetation types, and in different years. A value of 0.40 NDVI months was subsequently chosen. Thus a season was only deemed to have occurred at a particular pixel if the API for that year was greater then 0.40 NDVI months.

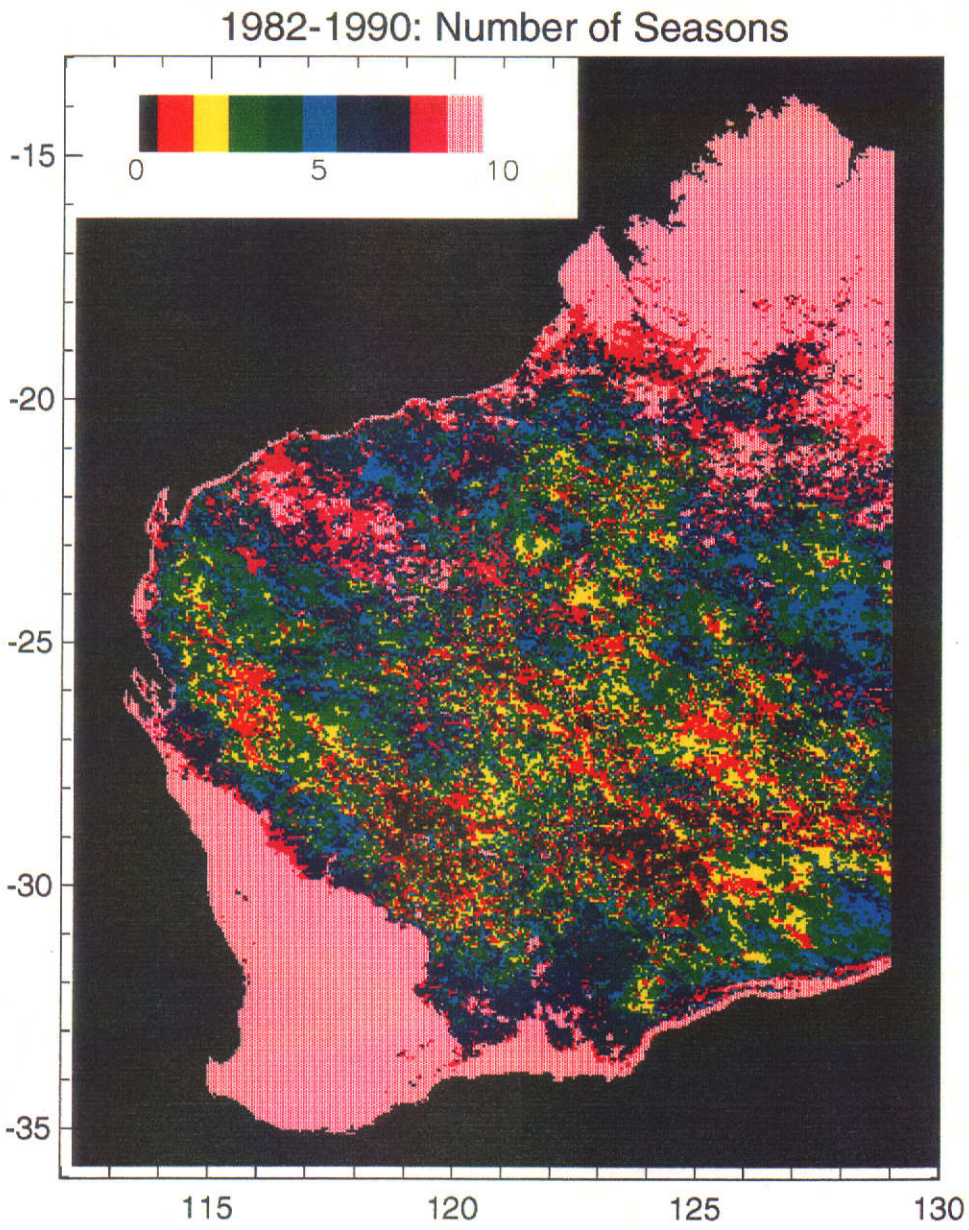

Figure 8.8 Number of seasons over period 1982-1990. API threshold of 0.40 was used to determine if a season had occurred

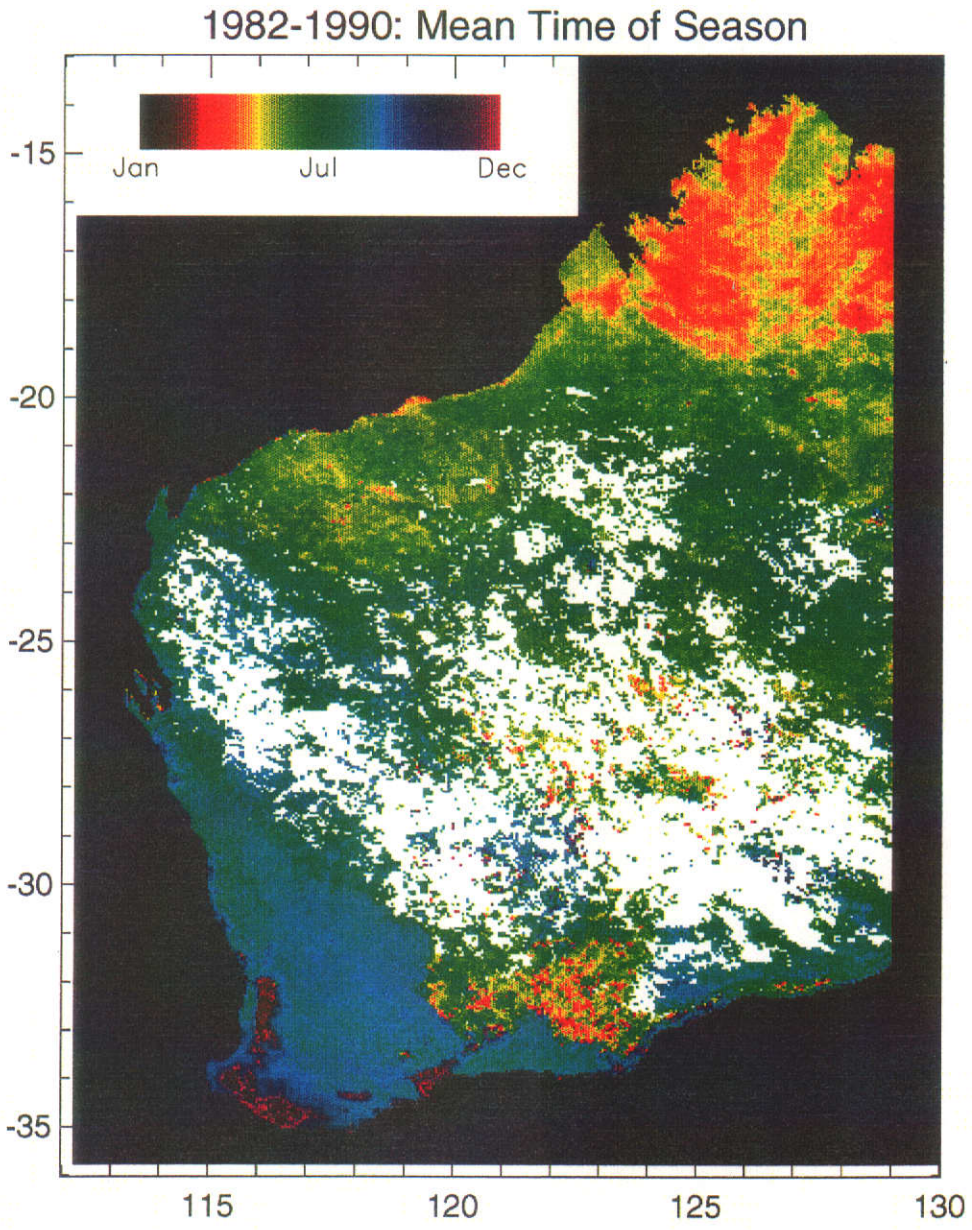

Figure 8.9 Mean time of seasonal growth over period 1982-1990. White pixels have less than four seasons during the period, and no statistics were calculated for them

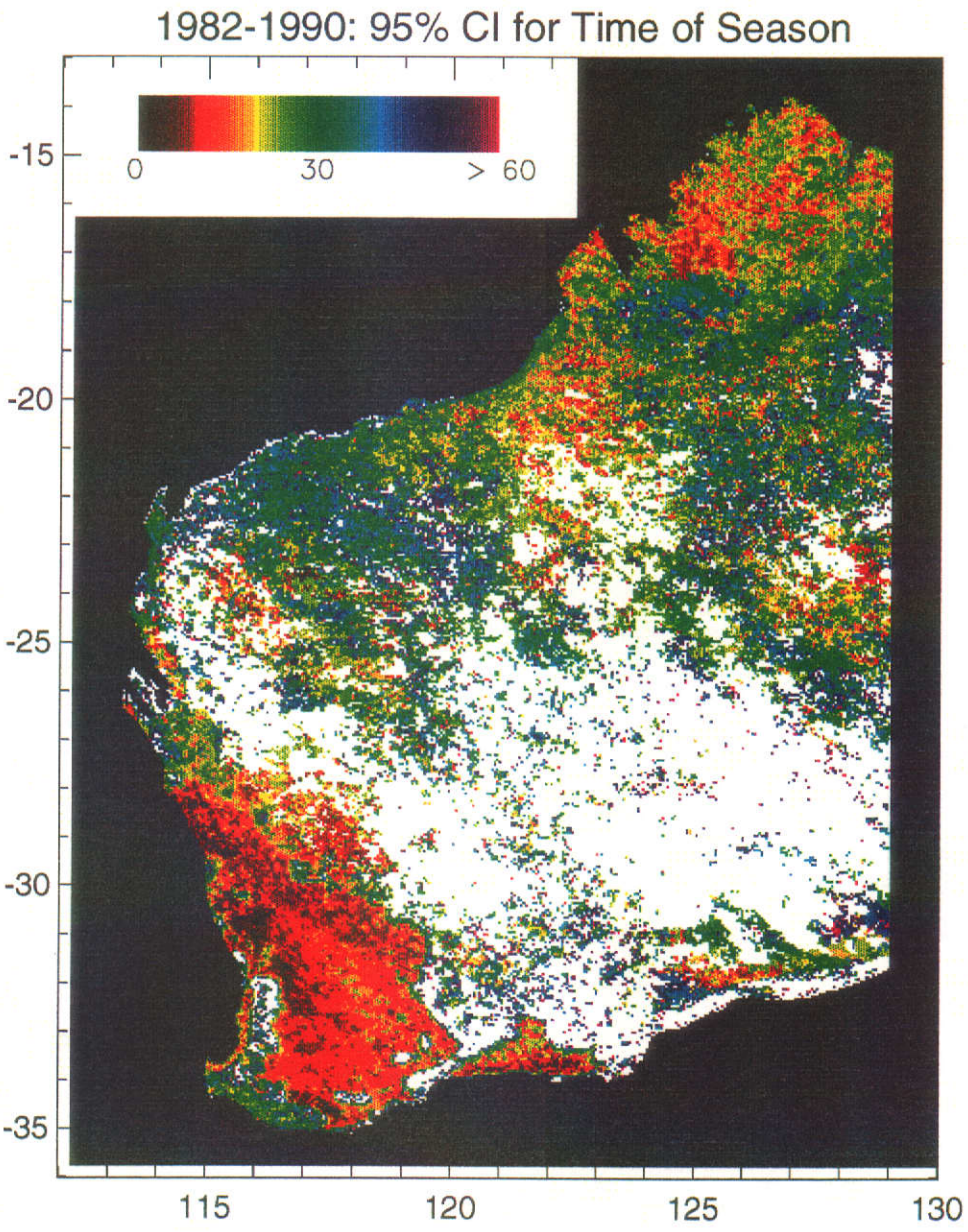

Figure 8.10 95 % confidence interval for mean time of season. White pixels include those described for Figure 8.9 and where the 95 % interval was greater than 60 degrees

Using this threshold, the number of seasons experienced over the nine years was calculated for each pixel. The resultant image is displayed in Figure 8.8. Inspection of this figure reveals that both the southwest agricultural region, and the Kimberley region experienced a season in each year as expected. Also a small region in the Pilbara indicates at least eight seasons occurred over the nine year period. However, throughout much of the arid zone, the frequency of seasons varied from one up to five out of a possible nine. Statistics were only calculated to describe the time of a season at a particular pixel if that pixel had experienced at least four seasons during the nine years.

The image indicating the mean time of season according to the above criterion is shown in Figure 8.9. Those pixels which did not experience at least four seasons (out of nine possible) have been set as white on the image. In addition, for the confidence interval about the mean (Figure 8.10), any pixels that had a confidence interval greater than 60 degrees (i.e. approximately ± 2 months) were also set as white. Some regions (particularly on the Nullarbor Plains) did have sufficient pixels to calculate a mean seasonal time, but the confidence limit around the mean was greater than two months.

Tables were not available for the 95 percent confidence interval around the mean for a given number of observations less than eight. Thus, the values given for eight observations (Figure 8.7) were used to compute an approximate 95 percent confidence interval about the

mean for all pixels, regardless of the number of observations used. The result is shown in Figure 8.10. For pixels where there were less than eight seasons over the nine year period, the confidence interval is indicative only.

8.4.2.4 Review

For areas indicated as white on Figure 8.10, there is no confidence concerning any time based summary information. According to this image, seasonal timing in the wheatbelt region has a 95 percent confidence of approximately ± 15 degrees (or 2 weeks). The mean time of peak growth for this area (Figure 8.9) is September. Similar confidence levels are apparent in the Kimberley region, with a mean time of peak growth of March/April. A sharp line in the southwest Kimberley region (125°E, 19°S) divides that region from a desert area to the south. The presence of a line indicates a change in the basic phenology of the vegetation, as there is no corresponding line in the summary images of API (Figures 8.4 and 8.5), indicating that rainfall falls over both sides of the 'line'.

For much of the Pilbara region, the 95 percent confidence limit is approximately ± 30 degrees (i.e. four weeks). Inspection of the mean indicates a peak season in July, with confidence that this occurred within one month (i.e. June to August) at the 95 percent level.

8.5 Discussion

The annual summary images clearly show the spatial variation that exists in seasonal growth in arid areas. To derive these annual summaries, a fixed length growing season of five months was adopted as a basis for the API. This is a useful and necessary approximation, given the monthly sampling interval is not sufficient to resolve the start and end of the growing season. While it is possible that for some regions, the growing season may be of greater length, in the majority of the arid zone this would rarely occur. Given this necessary limitation, the API should be used as a summary technique, and not for establishing correlation based relationships.

The API has been formed by subtracting the minimum NDVI over the decade from the series prior to integration. This technique was also used by Bonifacio et al. (1993). This contrasts with the method of Kogan (1990) who rescaled the NDVI into the maximum range observed for each pixel. Such a technique would potentially normalise the NDVI observations for different vegetation types and express the NDVI value as a percentage of the 'best it can get'. While this is an attractive concept, for much of the arid zone this would enhance noise in the image for this data set. As an approximation, the noise expected in the NDVI due to quantisation alone is about 0.01 NDVI units (see Chapter 4). For large areas of the arid zone, the standard deviation of the NDVI over the decade is approximately

0.02 NDVI units (see Figures 6.7 and 6.8). By rescaling using the method of Kogan (1990), the noise content of the series will be enhanced for areas of low variation in NDVI. For this reason, this method was rejected as a suitable global analysis technique.

The aim of the decadal summary images was to extract information of scientific and management importance. While some areas show elements of predicability, in the arid and semi-arid areas variability dominates. The time based summary information in particular provides complementary information on the nature of seasonal growth patterns and is an important addition to the production estimates commonly employed.

Lloyd (1989a, 1989b, 1990) has proposed a classification of vegetation phenology based on extracting significant elements from the time series. The variability in time and space of seasonal activity in the arid lands of Western Australia would make such a classification scheme very difficult to use for a decadal data set. For the period 1982-1990, the only constant over much of the arid lands was extreme variability.

Eastman and Fulk (1993) used principal components analysis (PCA) to describe a 36 month NDVI time series of image data over the African continent. While major elements of the time series were evident in the factor loadings (Eastman and Fulk, 1993, Figure 1, p. 993), the major problem relates to interpretation. The PCA technique

functions as a black box, from which regions which are identified as having similar characteristics have to be labelled after the analysis. This contrasts with the approach taken above, where at each stage of the analysis a direct physical interpretation can be made of the results. Lloyd (1990) noted that direct physical interpretation was a feature which guided the development of his classification system also.

An alternative technique of summarising NDVI time series images from NOAA was proposed by Menenti et al. (1991). They used Fast Fourier Transform (FFT) techniques to convert the NDVI time series into the frequency domain. The use of FFT techniques in summarising NDVI time series are evaluated in Chapter 9 of this thesis.

Comparison of the decadal summary images to the bioclimatic classification proposed by Beard (see Figure 3.2) shows broad scale similarities, with the northern grasslands experiencing a summer season, progressing to winter seasons in the southwest of the State. Beard's Class 2b is similar to the area in the Pilbara having a higher annual seasonal influence. However, Beard's Class 1c is indicated as having dominant summer rainfall. During the period 1982-1990, Figures 8.9 and 8.10 show this region to have growth peaks in July (± one month). This difference may possibly be due to peculiar weather conditions over this decadal period. Whatever the reason for the differences noted, it does clearly indicate the difficulty in working

with classification schemes based on average data, when variability is more a feature of the system than the average.

Recent research interest in the dynamics of arid zone ecology have focussed on the dynamics of the system (Noy-Meir, 1973; Noy-Meir and Walker, 1986; Westoby, 1980; Westoby et al., 1989) to both internal and external inputs. In all cases, temporal variation in rainfall is identified as a driving force in the system dynamics. In areas where the climate is more noted for its variability than any central tendency, sequences of events become an important factor in the dynamics of the system, rather than measures of long term averages. The run of events also has a major impact on commercial and ecological aspects of pastoral enterprises in the arid and semi-arid regions of Australia (Stafford Smith and Foran, 1992). The spatial and temporal coverage available from NOAA-AVHRR can be used to monitor the particular run of seasons over continental sized regions.

8.6 Summary

A technique was developed to summarise seasonal growth on an annual basis using both magnitude and timing as descriptors of that growth. The technique is limited to describing one growth period per year. While a few examples of bimodal NDVI time series have been noted in the literature, they are not generally common. The technique required an assumption about the length of the

growing season, which was fixed. Five months was chosen for this study. The measure used to compare growth between years was the API (annual production index).

Using these assumptions, annual summaries were created for the years 1982-1990 which depicted the amount and growth and the time of peak growth. These summaries indicated the enormous seasonal variability which occurs over the arid and semi-arid lands of Western Australia in both space and time.

These annual summaries were themselves summarised to create a decadal seasonal summary (1982-1990), which indicated the mean and variability about the mean of both the amount of growth and the timing of that growth. For handling the time-based information, the use of circular statistics was required.

In many years a seasonal growth period was not evident for large areas in the arid zone. A threshold for a season/no season switch was identified from inspection of both monthly rainfall records and the image data. Using this threshold, some areas of the arid zone were found to have experienced only one or two seasonal growth periods throughout the decade, and an image depicting the number of annual growth periods over the decade was created.

An image indicating the mean time of seasonal growth with appropriate confidence limits was also written. Over much of the

arid zone (particularly in the south), there were insufficient seasons over the nine year period to warrant a mean time being calculated, and these areas were excluded from the analysis.

In dealing with only nine years of data, it is difficult to ascertain whether the patterns seen in the decadal summaries are a reflection of the long term patterns or not. What is clear is that there are areas of both Western Australia, and presumably over the entire earth, for which a traditional bioclimatic classification is not possible due to the variability of seasonal growth. This variability, and associated impact on ecological systems is the feature that one should seek to understand.

The overriding impression from the analysis is the extreme variability in seasonal growth periods. In some years (such as 1984) large regional events are evident, while in others 'patchy' growth is more typical. The ability to identify these regions and summarise the activity will in time lead to increased understanding of the dynamics of arid zone systems, and the dominant role of variable rainfall in those systems.

Chapter 9

STRUCTURAL ANALYSIS OF TIME SERIES IMAGERY

9.1 Introduction

The NDVI time series plots presented in previous chapters demonstrate three broad classes of behaviour as follows:

(a) Trend related,

(b) Highly seasonal,

(c) Irregular pulses.

Measurement noise contaminates all the time series, although it is generally only significant for those systems dominated by trend. These classes of behaviour can be easily recognised by inspection of the time series data, and may be termed the nature or character of the time series.

This character has important implications for the design of more sophisticated analysis techniques. For example, Kogan (1990) proposed rescaling the NDVI into the range that had occurred historically for a particular pixel. Thus the current NDVI value is expressed as a percentage of the 'best it can get'. This technique was rejected as unsuitable for the development of annual summaries (see Chapter 8) as it enhances noise in the NDVI over areas with low NDVI variability. However, there is ample evidence (Kogan, 1990; Cridland et al., 1994) that when used in appropriate areas, it can be an efficient technique for reducing the effect of variation in soil colour and plant canopy attributes on the NDVI and allow spatial

comparison. This example clearly demonstrates that there is unlikely to be one data analysis method suitable for all applications.

The analysis of time varying signals is a central task in many areas of engineering and economics. Over the years these disciplines have developed a comprehensive statistical framework (Box and Jenkins, 1976; Makridakis and Wheelwright, 1989) for dealing with signals common in their respective domains. The selection of an analysis method is driven by:

(a) The nature or character of the data,

(b) The purpose of the analysis.

In this case, there is a measured output series. Only at discrete rainfall sites is the dominant input (i.e. rainfall) measured. This generally limits the applications to those which only require an output sequence, such as forecasting or statistical summaries. In forecasting applications, the data analysis method is often chosen, based solely on the nature of the data (for examples, see Chapter 15 of Makridakis and Wheelwright, 1989; Chapter 1 of Brockwell and Davis, 1987).

While the system character is immediately apparent from a time series plot, the issue is to synthesise this knowledge into a spatial framework. The phenological classification proposed by Lloyd (1990) was the first attempt to look specifically at details of the NDVI time series data (see Section 2.6 for review). However, this

classification scheme does not specifically extract information on the structure of the time series. For example, an NDVI time series that displays a long term trend, with a base NDVI above 0.1 (see Station 012065 in Sections 6.2.4 and 7.5.1.4) would not be adequately described under the scheme proposed by Lloyd.

Menenti et al. (1991) adopted a different approach by using the fast fourier transform (FFT) to decompose NDVI time series data into a series of harmonic curves. Images were then written of the information contained in the various harmonics. These harmonics were then used to interpret growth cycles in the data.

The work presented in Chapters 6, 7 and 8 of this thesis all demonstrate that the structural content of NDVI time series does vary spatially. This spatial variation is due to changes in vegetation type, variable rainfall regimes and land use, amongst others. However, none of the analysis techniques previously used were specifically designed to address this issue. In this chapter, three methods suitable for the identification of system structure are evaluated. One of these is chosen as suitable for this purpose and images which describe the structural content of the NDVI time series are presented using that method.

9.2 Conceptual Approach

The overall methodology adopted is similar to that used in Chapter 8. By developing appropriate measures of the structure of the time series, the time series imagery can be processed on a pixel by pixel basis to create one or more images of the proposed structural measures.

Ideally, the measures adopted should show the nature of the time series, independent of the input sequence over the sampling period. That is, the prime interest is the generic structure and not the particulars over the sampling period. This contrasts with the approach taken in Chapter 8 where the particular details of each year were the objective of the analysis. While this an ideal, it is not likely to be achievable. The linear relationships between rainfall and NDVI established in Chapter 7 indicate that it is not possible to view the output without reference to the system input. The structural content of the NDVI time series will vary depending on the particular details of the input over the sampling period. It is possible, perhaps, to become virtually independent of the input sequence by collecting longer time series. In addition, the structural measures adopted should be capable of direct interpretation.

The structural measures will be subsequently used to identify regions where forecasting and other sophisticated summary techniques might be applicable. In addition, these measures might

also provide bio-geographic information of scientific interest. It is anticipated that for some regions the best forecast may be the mean, and some measure of the variability around that mean. However, in some areas there is a very regular signal, which could be exploited for forecasting purposes.

9.3 NDVI Signal Characterisation

The structure of time varying signals may be analysed in either the frequency or time domains (Bennett, 1979). Engineers have typically worked in the frequency domain using the FFT as a central tool to transfer their data from the time domain to the frequency domain and vice-versa. In the frequency domain the structure of the time series is typically analysed by looking at the energy content of the signal as a function of frequency. The relationship between energy and frequency is typically displayed as a power spectrum (Burroughs, 1992). This technique has been used by Menenti et al. (1991) to analyse NDVI time series.

However, not all engineering time series are displayed in the frequency domain. A technique which is commonly used in control system engineering is the so-called ARMA (autoregressive moving average) models (Box and Jenkins, 1976). Using this technique, the time series is conceptualised as a process where the next value observed in the series depends on the previous value or values. The model is essentially formulated as a Markov chain (Burroughs,

1992). The degree of dependence, and hence the structure of the time series, is measured using the autocorrelation function (Brockwell and Davis, 1987). This technique has also been used in other environmental applications (Macchiato et al., 1993; Burroughs, 1992), although not for NDVI based time series.

In contrast to the above examples, typical time series models used in economics have remained relatively simple. Perhaps this is due to the smaller data sets which are typical of economic time series. For example, engineers may sample a system at 50 Hz, generating 50 samples a second. Economic time series tend to be sampled at monthly, quarterly or annual intervals. Some of the engineering techniques have been applied to economic time series, but the results have often been poor (Makridakis and Wheelwright, 1989).

Typically, economic time series are formulated as a function of trend, season and random influences as described in Equation 5.8. The estimation of these three elements from the original series is commonly known as classical decomposition (Brockwell and Davis, 1987). Clearly there is a synergy between classical decomposition and the description of the NDVI time series proposed above. The techniques are essentially empirical, but have proved successful in numerous practical applications (Makridakis and Wheelwright, 1989).

The three techniques described above, FFT, ARMA models and classical decomposition, have been evaluated as a means of describing the structure of NDVI time series data. For the evaluation of the most appropriate technique, NDVI time series data originally presented in Chapter 6 have been used.

9.3.1 Fast Fourier Transform

The FFT is a technique for decomposing any function into a set of harmonics. It is important to note that any function, no matter what form it takes, can be exactly reproduced by these harmonic terms (excluding round off error) at the sample points. The theory underlying the use of the FFT and an example of its application to NDVI time series is described in the following sections.

9.3.1.1 Theory

The FFT decomposes a time series X of P observations into a series of harmonics of the form (Burroughs, 1992):

$$f(X) = A_0 + \sum_{i=1}^{\frac{P}{2}} A_i \cos\frac{2\times\pi\times i}{P} + \sum_{i=1}^{\frac{P}{2}} B_i \sin\frac{2\times\pi\times i}{P} \qquad (9.1)$$

where

A_0 = *mean of the original series*

P = *number of samples*

$\frac{i}{P}$ = *frequency of the harmonic*

A_i = *amplitude of cosine function*

B_i = *amplitude of sine function*

The number of harmonics computed is half the number of observations in the original series due to the phenomena known as aliasing (Hamming, 1989). For example, for a series with 100 observations at monthly intervals, only 50 harmonics can be uniquely defined. Thus the smallest period that can be resolved is twice the sampling interval. Assuming the data are sampled monthly, this corresponds to a period of two months. The cut off point is known as the Nyquist frequency (Hamming, 1989). The expression in Equation 9.1 may be further simplified by combining the cosine and sine functions into a single expression as follows:

$$f(X) = A_0 + \sum_{i=1}^{\frac{P}{2}} C_i \cos \frac{2\times\pi\times(i - i_0)}{P} \qquad (9.2)$$

where

C_i = *Amplitude*

$= \sqrt{A_i^2+B_i^2}$

i_0 = *phase offset*

The variance (σ^2) of any sinusoidal signal with an amplitude C_i, when computed over one or more complete periods, is given by (Weidner and Sells, 1973):

$$\sigma_i^2 = \frac{C_i^2}{2} \tag{9.3}$$

Since the harmonics are all uncorrelated (Burroughs, 1992) the sum of the variance of all harmonics is the variance of the entire signal (σ_X^2) as follows:

$$\sigma_X^2 = \sum_{i=1}^{\frac{P}{2}} \frac{C_i^2}{2} \tag{9.4}$$

Thus the contribution of each harmonic to the overall variance may be expressed using Equations 9.3 and 9.4. A plot of the contribution of each harmonic against frequency is commonly known as the spectrum. The term power spectrum, as used by engineers, is a plot of the amplitude squared against frequency. The power (square of the amplitude) and variance are thus linearly related. The phase of each harmonic (i_0) can also be plotted against frequency in a phase spectrum (Hamming, 1989) although this is not common.

9.3.1.2 Results

The IDL package (Research Systems Inc., 1993) has been used to compute the FFT of an NDVI time series for a wheatbelt site. The site is the Corrigin Post Office (Station 010536). The time series was

originally presented and discussed in Chapter 6 (see Section 6.2.7) and further details can be found in that chapter.

When computing the spectrum of a data set with a known (or suspected) periodicity, if the number of observations in the time series (P) is not an integer multiple of that period, then spectral leakage occurs (Hamming, 1989). One technique often used to minimise the impact of leakage is the use of window functions (Hamming, 1989). In this case there are 117 monthly observations in the NDVI time series. By inspection (Figure 9.1a), it is clear that the annual cycle is dominant. To avoid leakage, the last nine observations were dropped from the series prior to computing the FFT. This left 108 observations in the series, which is an integer multiple of 12.

From Figure 9.1 (b, c), there are three clear spikes in the spectrum. These occur at periods of 12, 6 and 4 months respectively. The first two harmonics (12 and 6 month periods) account for approximately 85 percent of the variance of the total signal.

Despite the apparent success in describing the signal, no clear physical reason is available to describe there being cycles at 6 and 4 months in addition to the annual cycle. These cycles are not a physical feature but rather an artefact resulting from the use of the FFT. While the FFT can describe any signal uniquely, the

interpretation of the resulting spectrum must be done in light of the basic assumption of sinusoidal input signals. In many engineering tasks, the signals are known to be sinusoidal prior to the analysis. This will not generally be true of environmental time series (Hamming, 1989; Bennett, 1979).

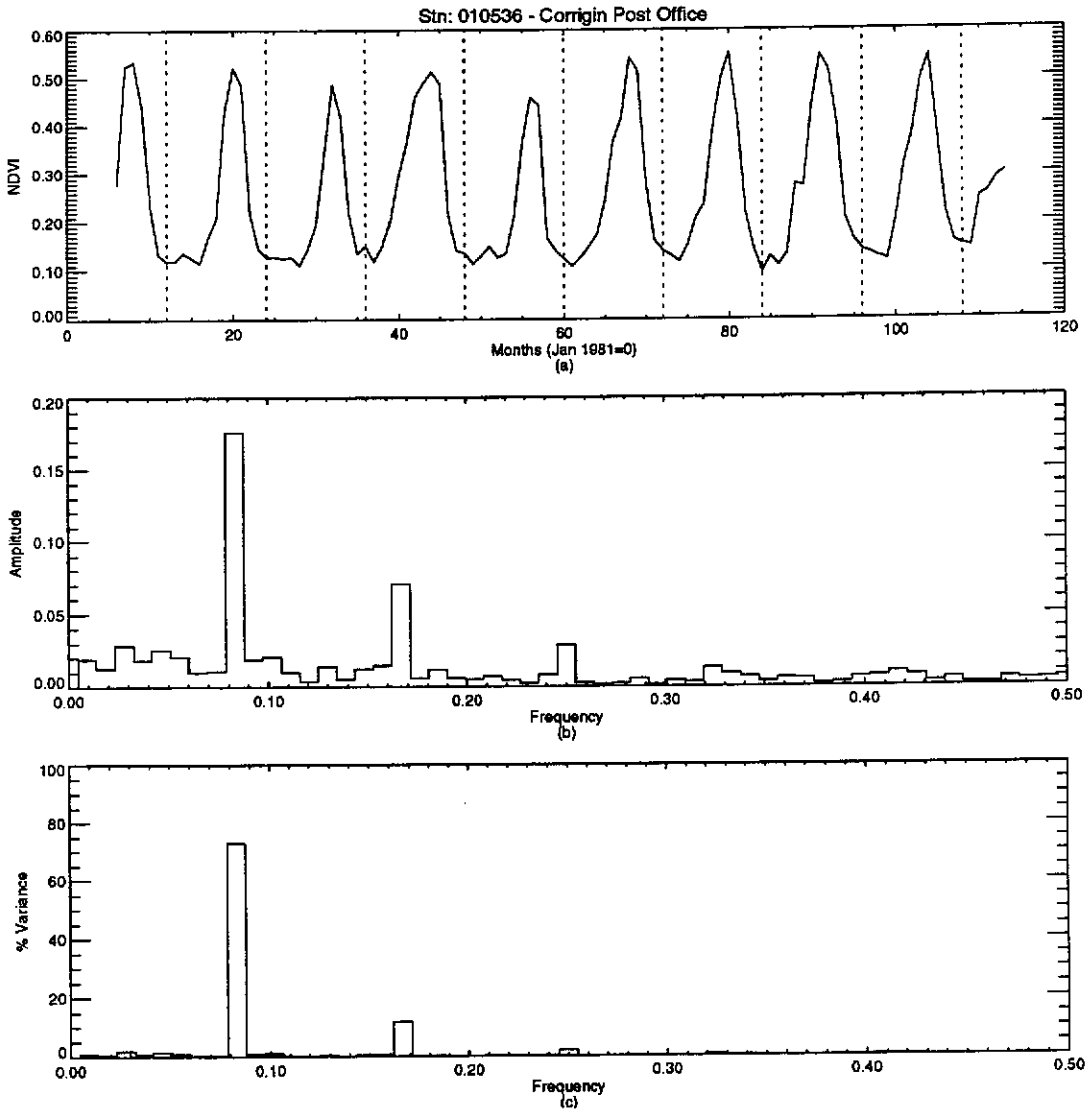

Figure 9.1 NDVI time series and Spectrum for Stn 010536 (Corrigin Post Office)
(a) NDVI time series
(b) Amplitude v frequency
(c) Percentage variance v frequency

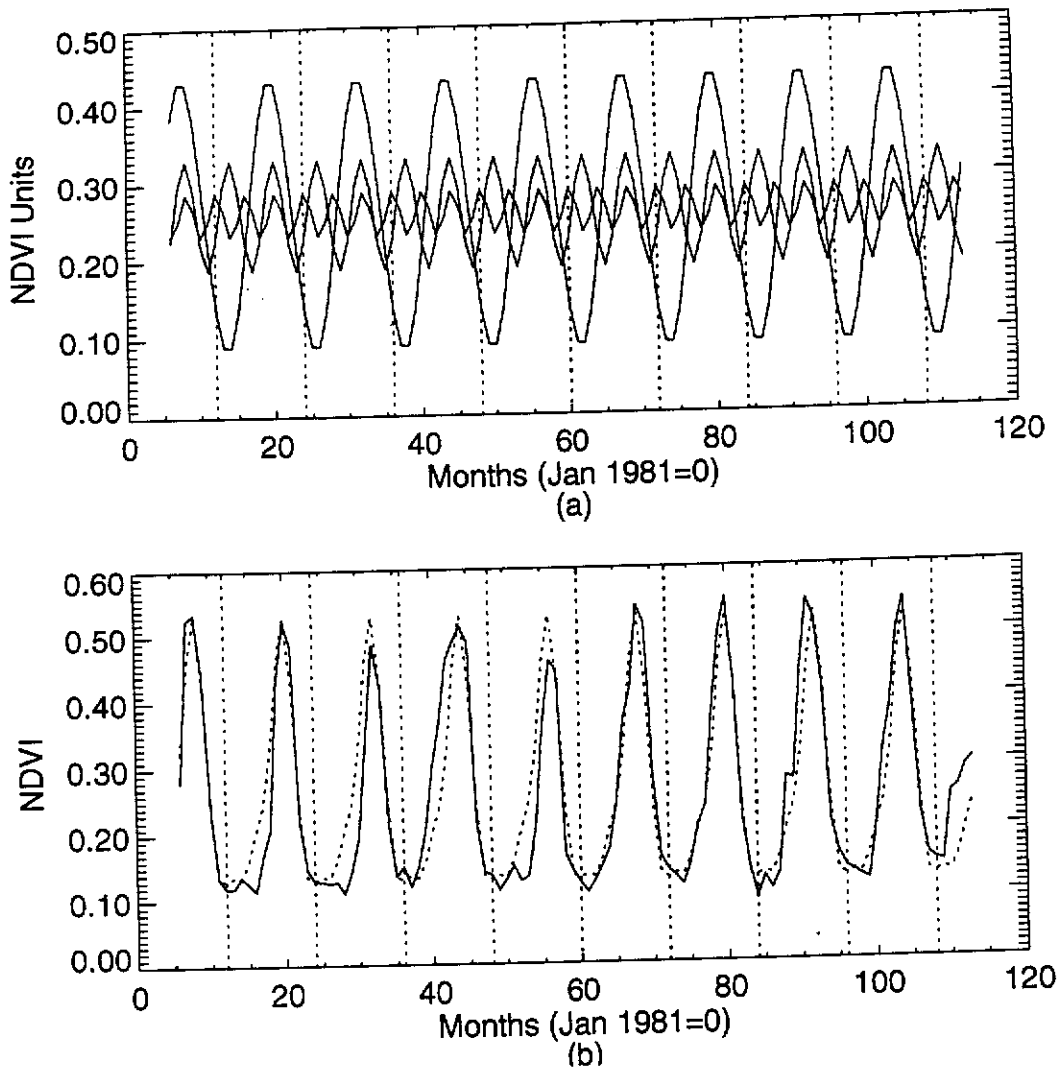

Figure 9.2 FFT of NDVI time series for Stn 010536
(a) Harmonic terms
(b) Original signal (full) and prediction (dotted)

To develop further understanding of this problem, the actual coefficients were recovered from the FFT coefficients for the 12, 6 and 4 month harmonics using Equation 9.2. The resulting equation for this time series is shown in Equation 9.5. These harmonics (Equation 9.5) and their final sum are compared to the original series in Figure 9.2.

$$X_i = 0.259 + 0.176\cos\left(\frac{2\pi(i-1.508)}{12}\right) + 0.071\cos\left(\frac{2\pi(i-1.970)}{6}\right) + 0.029\cos\left(\frac{2\pi(i+1.802)}{4}\right) \quad (9.5)$$

From Figure 9.2, the harmonics at 12 and 6 months are clearly in phase, which allow the FFT coefficients to describe a slightly non-sinusoidal signal. Growth functions are typically sigmoidal in shape rather than sinusoidal (Byrne, 1973; Noble, 1977; Honey and Tapley, 1981). To demonstrate the result of using non-sinusoidal inputs, a Rayleigh function has been used as an approximation to a sigmoidal curve. Rayleigh functions are commonly used as probability distributions in a variety of physical situations and are defined as (Cooper and McGillem, 1986):

$$f(r) = \frac{r}{\sigma^2} e^{-\frac{r^2}{2\sigma^2}} \quad (9.6)$$

In this case, r corresponds to the time dimension, and σ is a variable describing the distribution. Here, a σ of 3 was chosen to generate 12 values of f(r). These were then replicated nine times to simulate a 108 element time series. While this time series is perfectly regular, it is not sinusoidal. The plot and the corresponding power spectrum are shown in Figure 9.3.

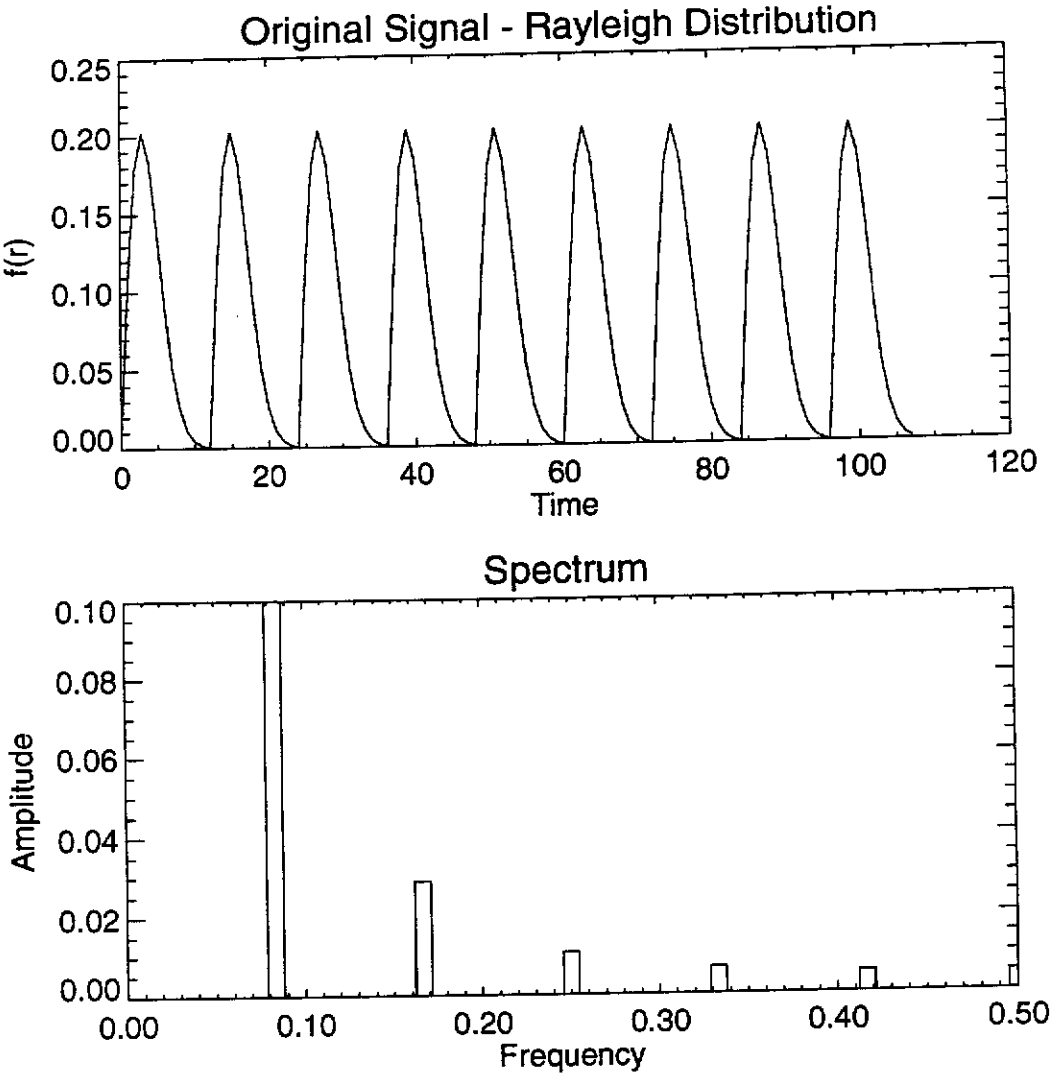

Figure 9.3 FFT of a simulated periodic Rayleigh function
(a) Replicated nine times to simulate nine year time series
(b) Spectrum of curve in (a)

Figure 9.3 clearly indicates the difficulty in interpretation of Fourier series when the input signal is not sinusoidal. Ecological interpretation, and subsequent comparison of these results is virtually impossible. Given the stated requirement for a clear interpretation of the results, the use of FFT based methods was not pursued further.

9.3.2 Autocorrelation

The autocorrelation function is the central tool used in ARMA modelling (Box and Jenkins, 1976). It essentially describes the degree of dependence of two measurements from the one time series separated by some time (which is called a lag). The autocorrelation varies from -1 to 1 in an identical fashion to linear correlation. Importantly, no prior assumptions are required about the nature of the signal being studied.

9.3.2.1 Theory

The autocorrelation function A(h) of a time series X_j of N observations is defined as (Brockwell and Davis, 1987):

$$C(h) = \frac{1}{N} \sum_{j=1}^{N-h} (x_{j+h}-\bar{x})\ (x_j-\bar{x}) \tag{9.7}$$

$$A(h) = \frac{C(h)}{C(0)} \tag{9.8}$$

where

h = *lag*

$C(h)$ = *autocovariance at lag h*

At lag zero, the autocovariance (C) of a time series is the variance of that series. The autocorrelation is derived from the autocovariance using Equation 9.8. Note that the autocovariance is derived by division by N (rather than N-h). This avoids a bias in the estimate of A(h) as h becomes large. Typically h should not exceed

one third of the length of the series (Brockwell and Davis, 1987). The measure is used extensively in ARMA modelling and an extensive literature exists to assist in the interpretation of the autocorrelation function in this context.

9.3.2.2 Results

The autocorrelation functions of the test data are shown in Figure 9.4. The time series data have been repeated here for convenience. Full details of the stations are available in Table 6.1. The autocorrelation functions are all smooth, which is a result of the averaging procedure used in the computation.

The autocorrelation function identifies distinct differences in temporal behaviour between the series. The highly regular series (Stations 002032 and 010536) show seasonal dominance. Station 012065 shows significantly different behaviour from the rest. The long term trending nature of this time series is highlighted in the autocorrelation function. It takes some 36 months for the autocorrelation to reach zero. This site is a woodland, with high perennial (evergreen) cover. Contrast this with the autocorrelation for Station 011004. The system in this latter case has a memory lasting some four months (time to fall to zero). Beyond this, there is no clear correlation.

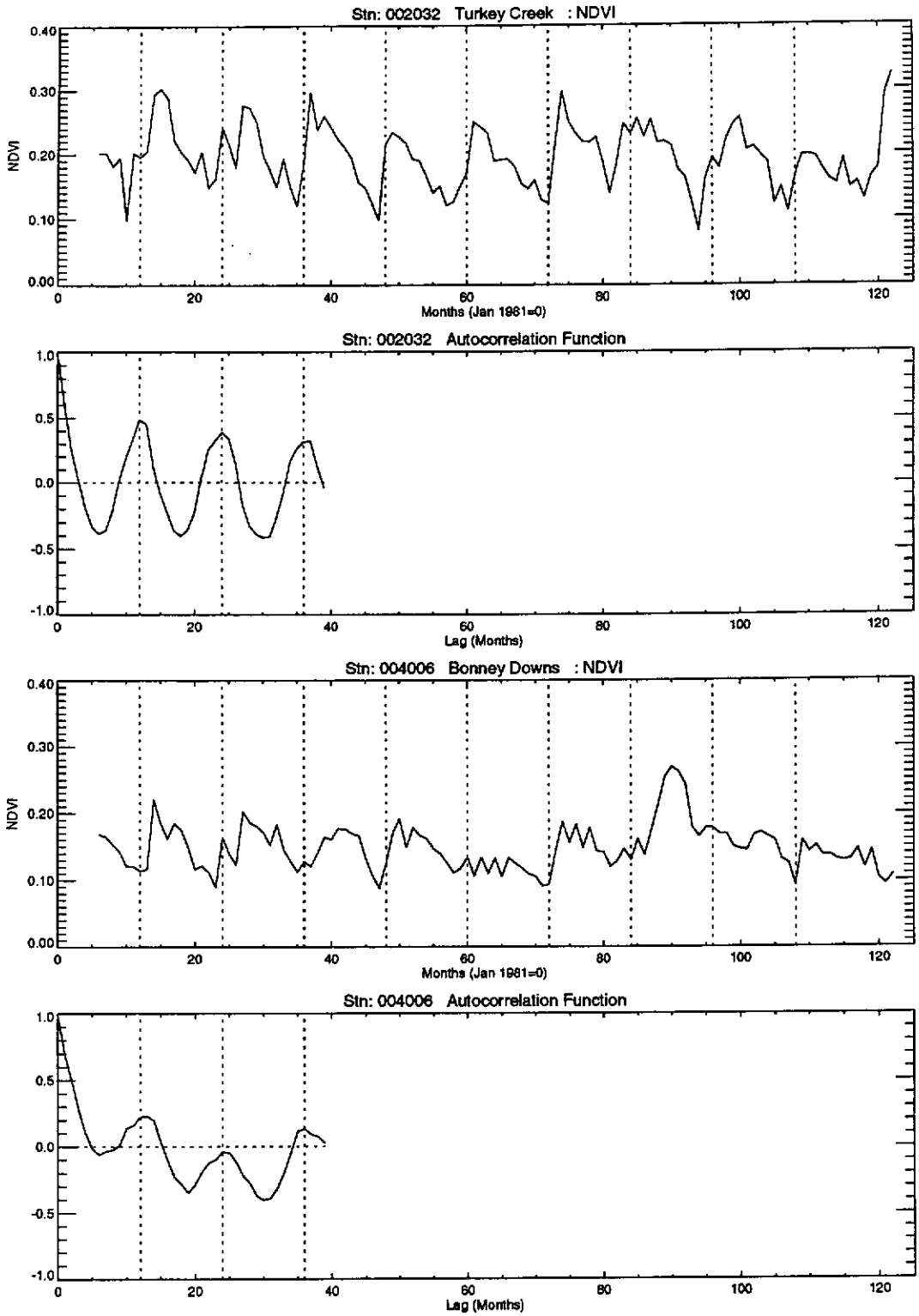

Figure 9.4 NDVI time series and associated autocorrelation function (For details of stations see Table 6.1)

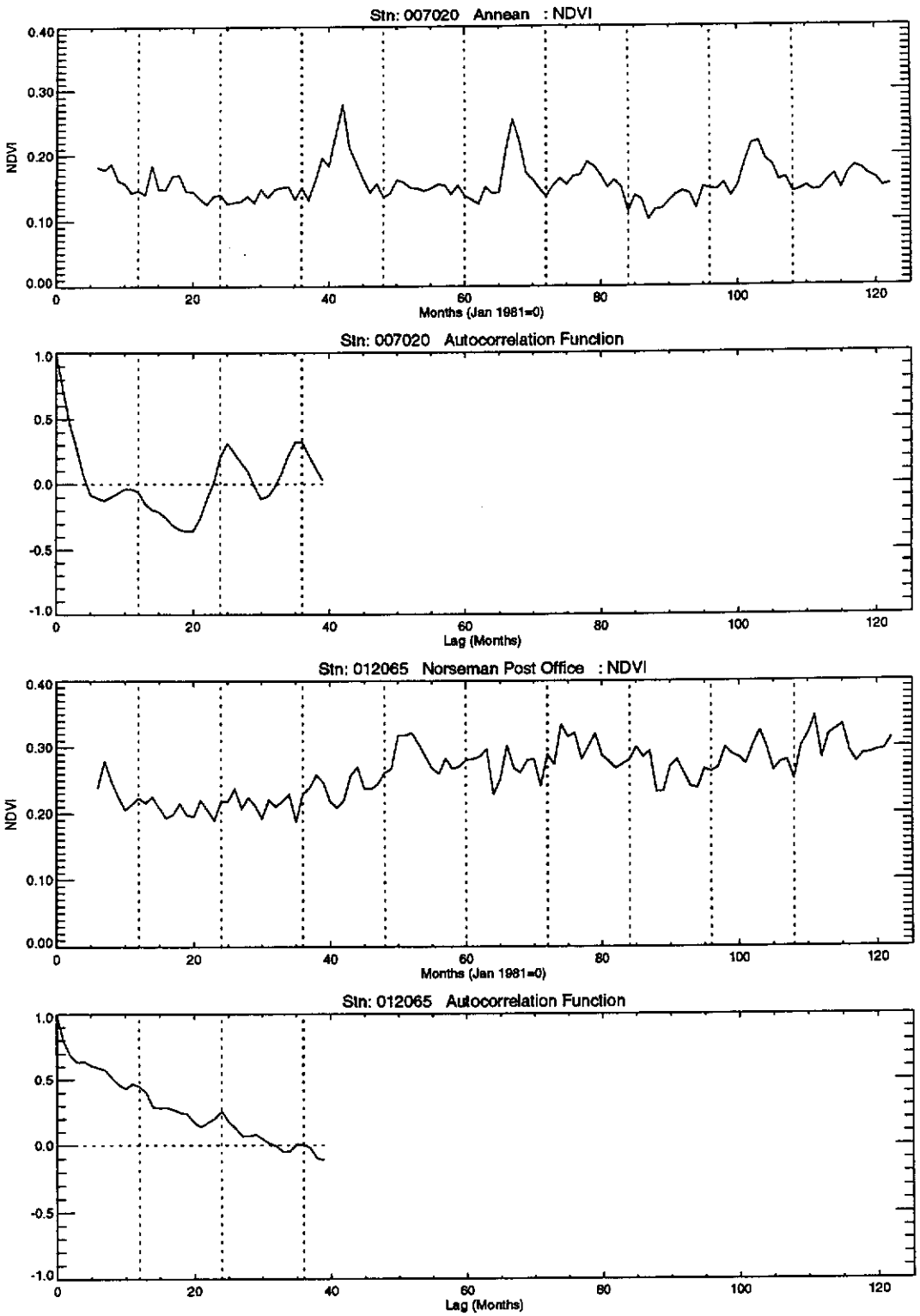

Figure 9.4 NDVI time series and associated autocorrelation function (continued)

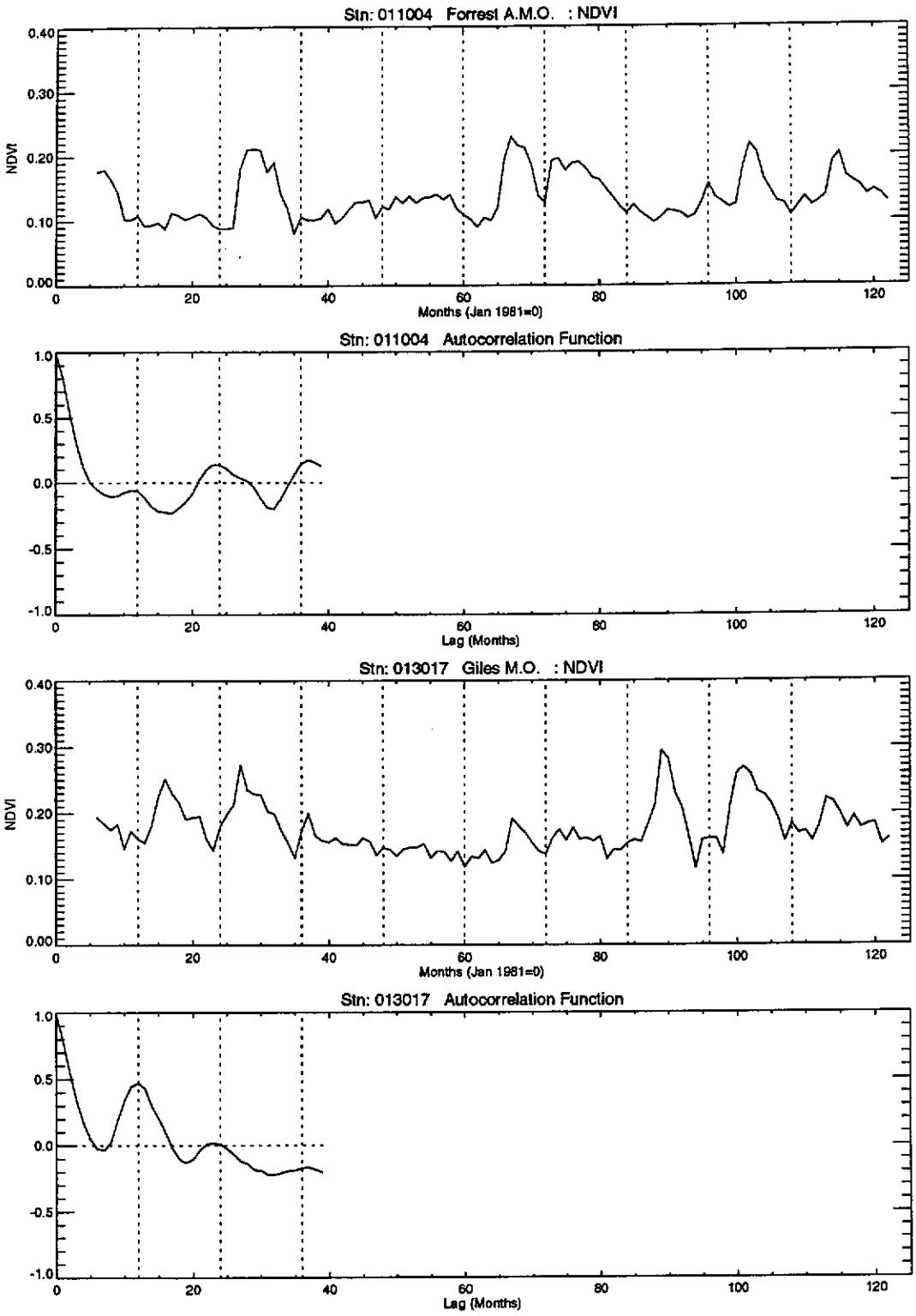

Figure 9.4 NDVI time series and associated autocorrelation function (continued)

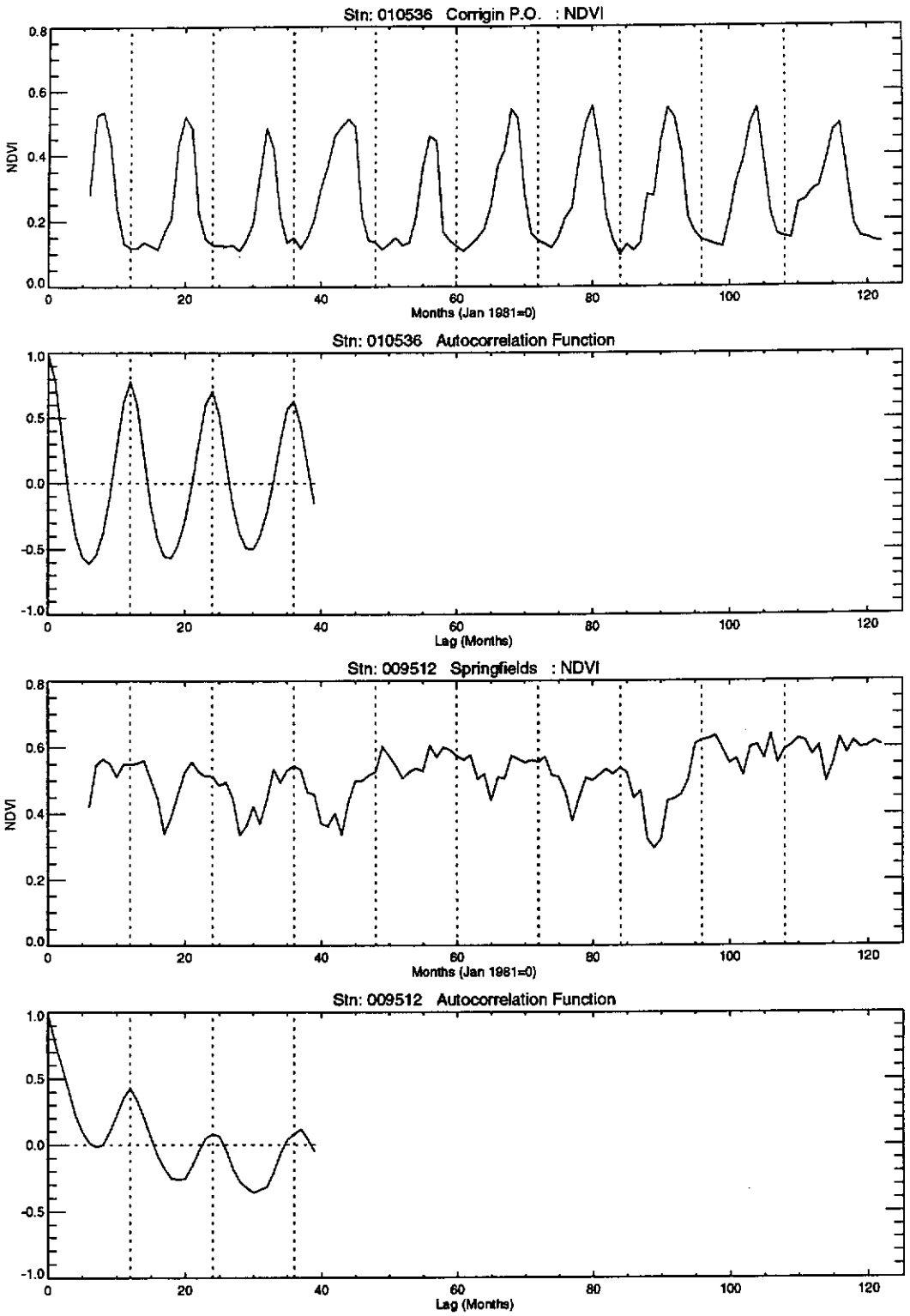

Figure 9.4 NDVI time series and associated autocorrelation function (continued)

The balance of the stations show behaviour that is somewhat seasonal (i.e. peak at 12 months in the autocorrelation), but with some 'wandering' also. This wandering is a tendency of non-stationary data sets (Brockwell and Davis, 1987). Some key elements of the autocorrelation function, which could be used to infer the structural content of the NDVI time series, include:

(a) Lag when zero autocorrelation is first reached,

(b) Autocorrelation at lags 12 and 24,

(c) Non-stationarity of the autocorrelation on an annual basis.

9.3.3 Classical Decomposition

Classical decomposition is a popular technique used with economic time series. The technique is based on an assumption that any series X can be adequately described by trend, seasonal and random components in the series. This is described in Equation 9.9 (Brockwell and Davis, 1987):

$$X_t = T_t + S_t + R_t \qquad (9.9)$$

where

X = *original data*

T = *trend estimate*

S = *seasonal component*

R = *random component*

The model is empirical, and has been successful in a number of economic applications (Makridakis and Wheelwright, 1989).

9.3.3.1 Theory

The procedures for estimating T, S and R are covered in many standard time series textbooks, and will only be briefly given here in algorithmic form (Brockwell and Davis, 1987, pp. 23-24) assuming monthly sampling, and a seasonal component at 12 months:

(a) Make an initial estimate of the trend (TE) using a moving average of order 12 (see Equation 5.10)

(b) S+R=X-TE (subtract the trend estimate from original series)

(c) Take the mean of S+R for each month to estimate the mean S

(d) T+R=X-S (subtract the seasonal estimate from original series)

(e) Fit a moving average of order 12 to the series T+R to estimate T

(f) R=X-T-S

At the conclusion there are 12 monthly values which describe the seasonal effect S. For forecasting purposes, a suitable model can be fitted to the trend term T. The algorithm described above was programmed in the IDL environment (Research Systems Inc., 1993) and used to decompose the NDVI time series.

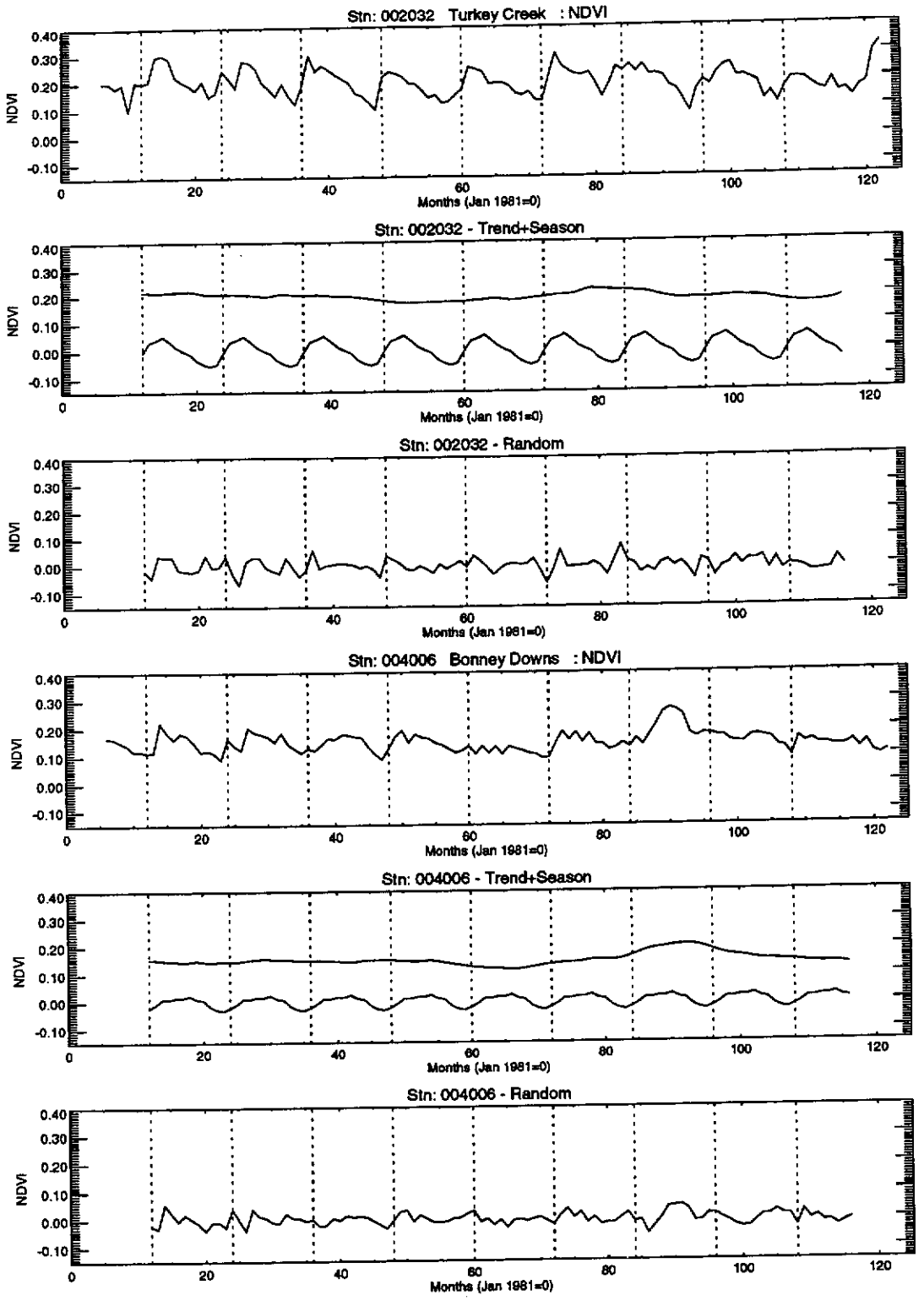

Figure 9.5 NDVI time series and resulting decomposition (For details of stations see Table 6.1)

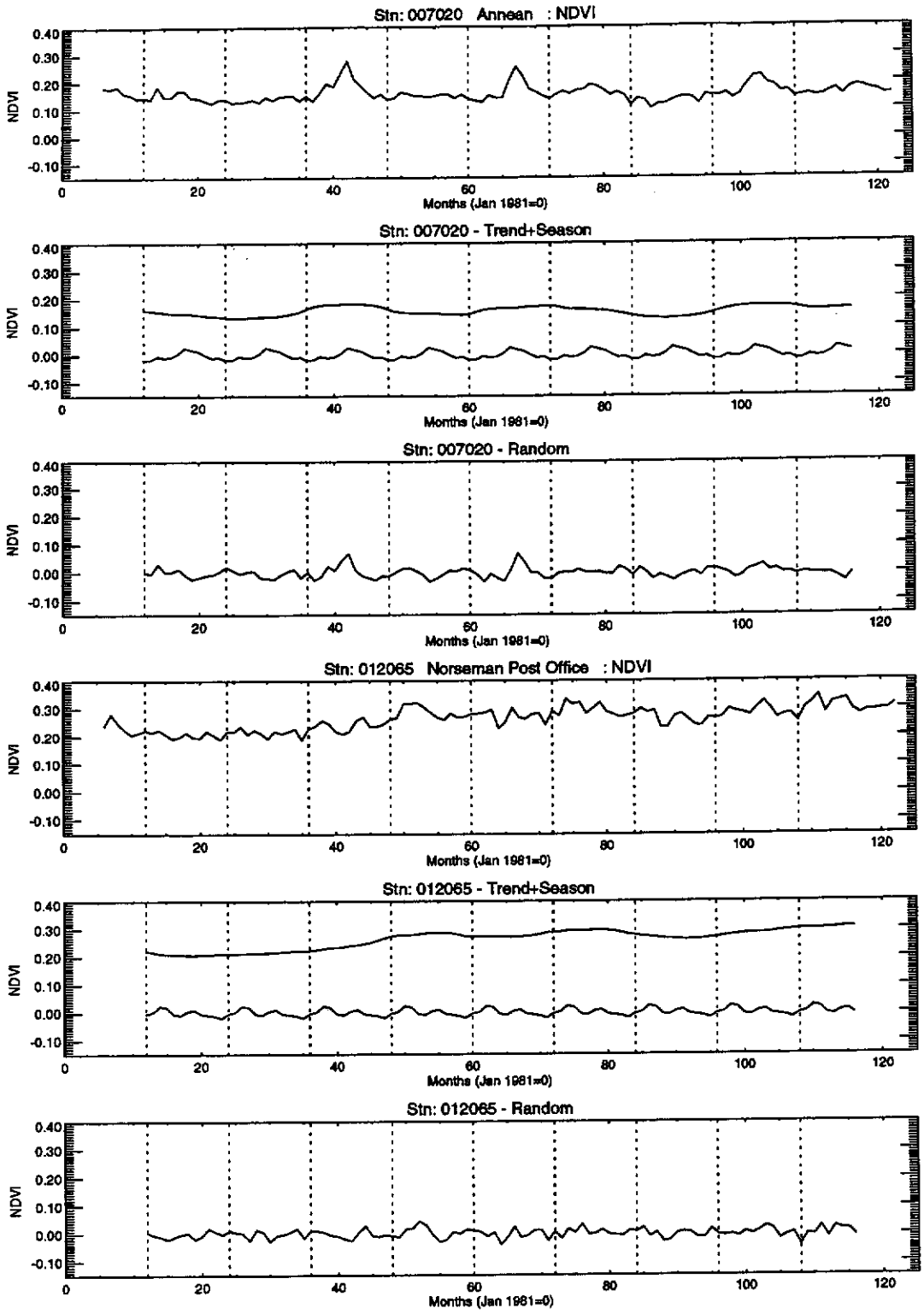

Figure 9.5 NDVI time series and resulting decomposition (continued)

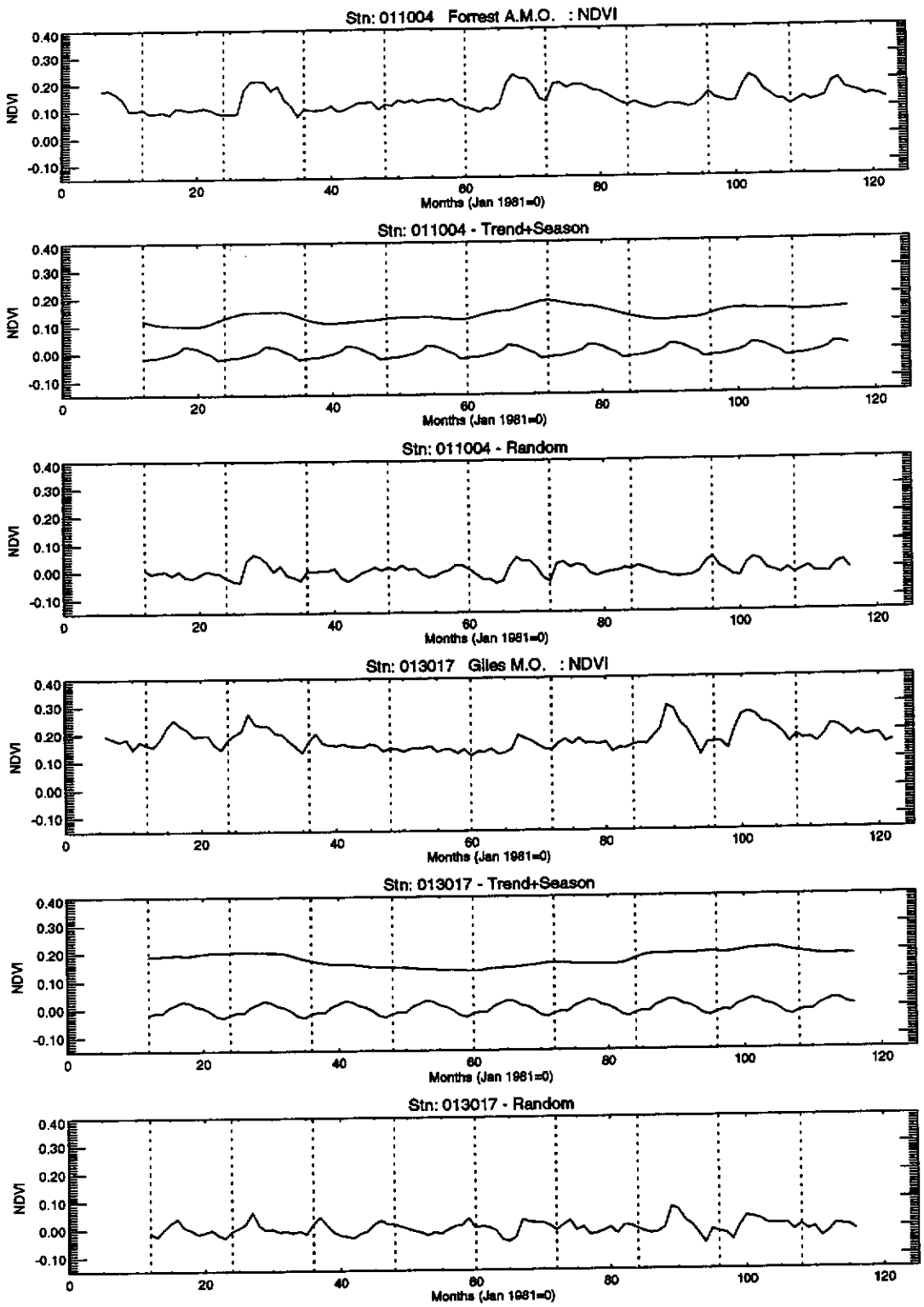

Figure 9.5 NDVI time series and resulting decomposition (continued)

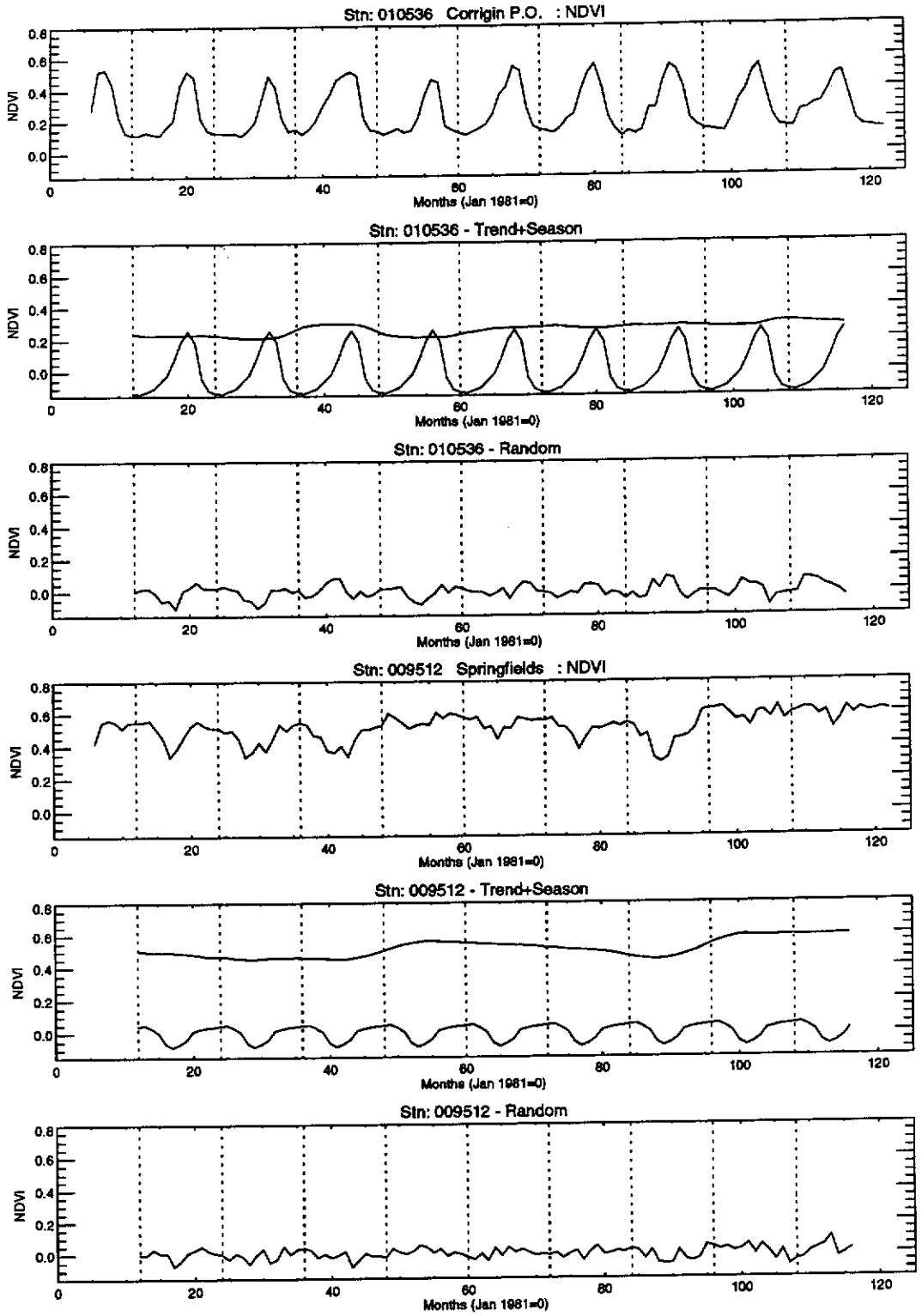

Figure 9.5 NDVI time series and resulting decomposition (continued). (Note change of scale in plots)

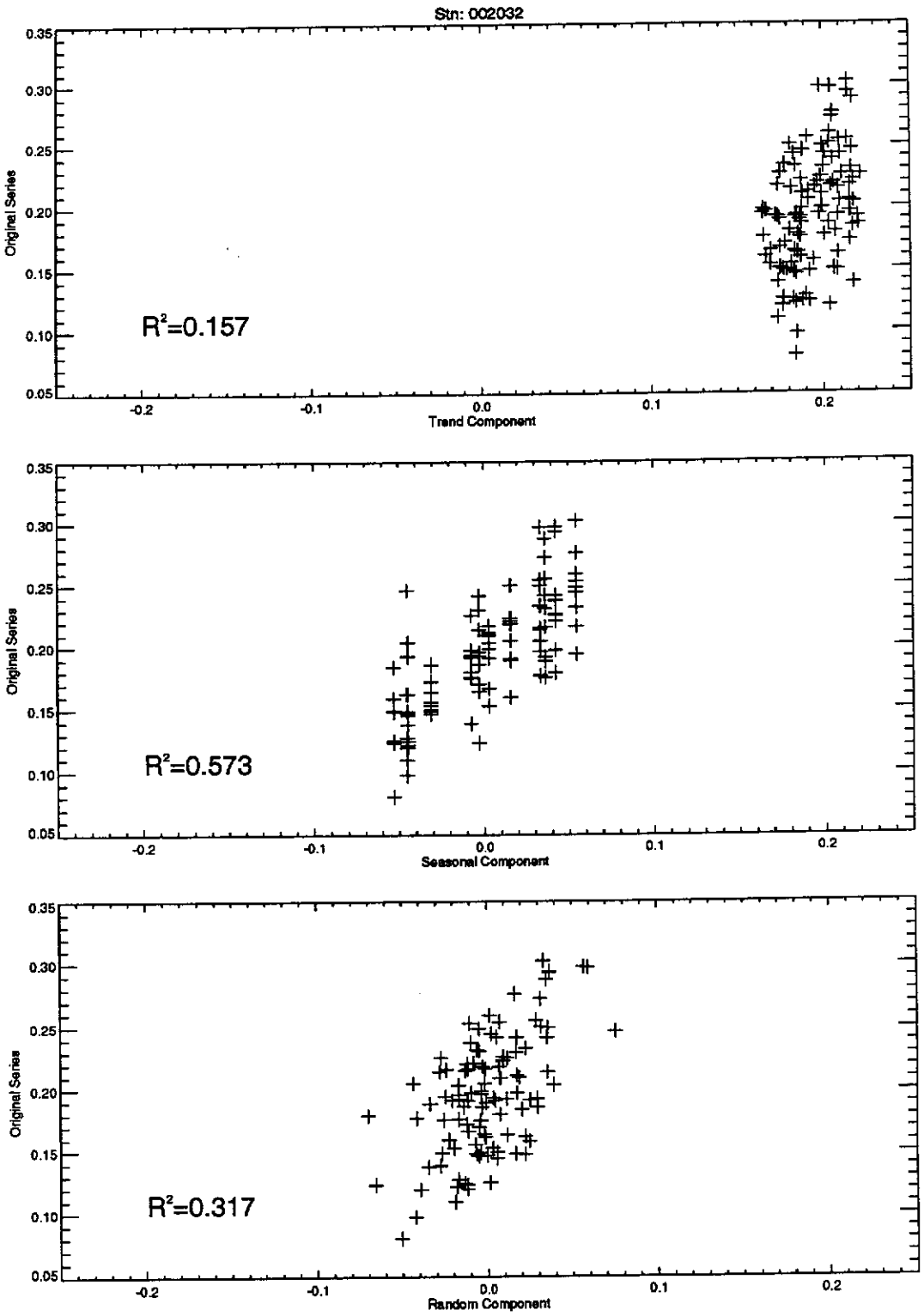

Figure 9.6 Contribution of various components to overall variance for Station 002032. (See Table 6.1 for details of Station 002032)

9.3.3.2 Results

Results of the decomposition are shown in Figure 9.5. The decomposition approach is clearly appropriate for those sites with a regular seasonal pattern (Stations 002032, 010536 and 004006). For those sites showing irregular pulses, the description is not entirely satisfactory. For example, the time series for Station 011004 indicates that the 'average' seasonal component has been lifted by the irregular influences. The random component virtually reproduces the original series. Similar results are seen for Station 013017. Despite these difficulties, the description looks promising. For Station 012065, which shows a long term trend, the decomposition is an excellent description of that series.

The underlying premise of classical decomposition is to spilt the time series into three uncorrelated components. Each component effectively describes a range of frequencies in the spectrum, but no assumption of sinusoidal behaviour is required. The trend is composed of frequencies lower than the seasonal component. Conversely the random component is composed of frequencies higher than this component. As such, one method to describe the various decompositions is to look at the contribution of each component to the overall variance of the series in a manner akin to analysis of variance. Graphs which demonstrate this proposal are shown in Figure 9.6.

If the components are uncorrelated, then the variance of each is added together to derive the variance of the original series as follows:

$$\sigma_X^2 = \sigma_T^2 + \sigma_S^2 + \sigma_R^2 \qquad (9.10)$$

The correlation matrix for the various components of the decomposition for Station 002032 is shown in Table 9.1.

Correlation Matrix			
	T	S	R
T	1	0.0066	0.1117
S	0.0066	1	-1.18E-9
R	0.1117	-1.18E-9	1

Table 9.1 Correlation matrix for decomposition of the NDVI time series for Station 002032 (trend, seasonal and random components)

Note that in Figure 9.6, the sum of the R^2 values for each component is 1.047, not one that would be expected for uncorrelated variables. The reason is clear from Table 9.1. The trend and random components are slightly positively correlated (0.1117). This correlation means the sum of the R^2 values will not equal one. The correlation matrices for all other stations were inspected and are virtually identical to the result shown above. This is caused by the formulation of the algorithm. The subtraction of S from X in the algorithm, and subsequent smoothing of the balance to recover T and R, leaves T and R correlated. An alternative would be to

subtract a constant value for T over each seasonal period. This technique is described by Brockwell and Davis (1987, p. 21) as the 'small trend method'. This approach was rejected, as there are some sites where this is clearly not appropriate. Despite this difficultly, the correlation between T and R is generally small, and will not bias the results.

Three elements were chosen to describe the structural differences between sites based on their decomposition as follows:

(a) R^2 value for S and the original series (X),

(b) R^2 value for T and the original series (X),

(c) Overall variance (σ_X^2) of the series.

The three pieces of information above summarise the entire data set. While they do not indicate the shape of the trend and seasonal curves, it needs to be remembered that the aim is to define the structure, and not the details. The R^2 value for the seasonal component is a direct measure of the predictability of the series using a seasonal correction. In contrast, the value for trend is an indicator of the variance due to trend only. To form a predictive model for applications such as forecasting, it is still necessary to model the trend component. To demonstrate the utility of this approach, Table 9.2 shows the (three) proposed descriptors for all the time series presented in Figure 9.5.

Station	R^2 for S v X	R^2 for T v X	σ_X^2
002032	0.573	0.157	0.00221
004006	0.254	0.391	0.00124
007020	0.241	0.386	0.00081
012065	0.094	0.732	0.00150
011004	0.201	0.480	0.00137
013017	0.240	0.438	0.00151
010536	0.870	0.045	0.02117
009512	0.325	0.481	0.00621

Table 9.2 Summary measures of decomposition structural characteristics for all NDVI time series

The relative rankings from Table 9.2 demonstrate the merit of the proposed approach. Station 010536 is clearly the most seasonal, and this is evident in the table. By the result above, 87 percent of the variance in this series can be predicted using a seasonal component. In contrast to this, the time series for Station 012065 is trend dominated, and approximately 73 percent of the variance in this series is accounted for by the trend component.

9.3.4 Review

Three techniques were reviewed as potential indicators of the time series structure of NDVI images. The FFT technique was not found to be useful due to difficulties in the interpretation of the results. This was due to the non-sinusoidal nature of vegetation growth in the study area. This premise is also borne out after inspection of the seasonal components in Figure 9.5. Very few of these show a strict sinusoidal shape.

The autocorrelation function was found to be useful in interpreting structure in the NDVI time series data. The annual cycles are clearly evident in the autocorrelation functions. However, the non-stationarity evident in many of the time series causes a 'wandering' of the autocorrelation function. Of particular interest is the 'memory' of the system. Autocorrelation is interpreted as memory in ARMA modelling, and some of the time series presented show distinct examples of memory in the system.

The presence of memory in biological systems has been proposed by Mott (1973) for a region in the Murchison area of Western Australia. Mott demonstrated that the pattern of seasons could impact on the seed bank supplies, and thus affect future seasons. In particular, for communities dominated by annual plants, once an annual germinates, it must survive for sufficient time to set seed. If it does not, the seed bank is not replenished. Seed bank dynamics are a form of memory in the system.

The decomposition method clearly indicates the structure in the data. For areas dominated by either seasonal or trend influences, the descriptors proposed distinguish these clearly. For stations dominated by irregular pulses of growth, the measure is not as good. In particular, the seasonal component is enhanced by averaging over several years. Despite this, the characteristic of these systems is the higher trend and seasonal estimate to describe the series.

Due to the succinct summary available and ease of interpretation, the decomposition method was chosen as the best technique to highlight structural characteristics of the NDVI time series. Another advantage was that virtually all the information could be described by three variables. Despite this choice, it is noted that the autocorrelation still shows information relating to system memory, which is not available in the decomposition method.

9.4 Classical Decomposition Images

Images of the variance are best presented as standard deviation, as the scale is more linear, and hence easier to interpret. These images were calculated as part of the image summaries in Chapter 6 (Figures 6.7 and 6.8). Images depicting the percentage of the variance explained by seasonal and trend components are shown in Figures 9.7, 9.8, 9.9 and 9.10.

The seasonal component explains some 90 percent of the variance in the southwest agricultural region, and approximately 70 percent in the north Kimberley region. Throughout much of the arid pastoral lands the seasonal component is in the range of 30-50 percent. In much of the arid lands not used for pastoralism, the seasonal signal is virtually zero.

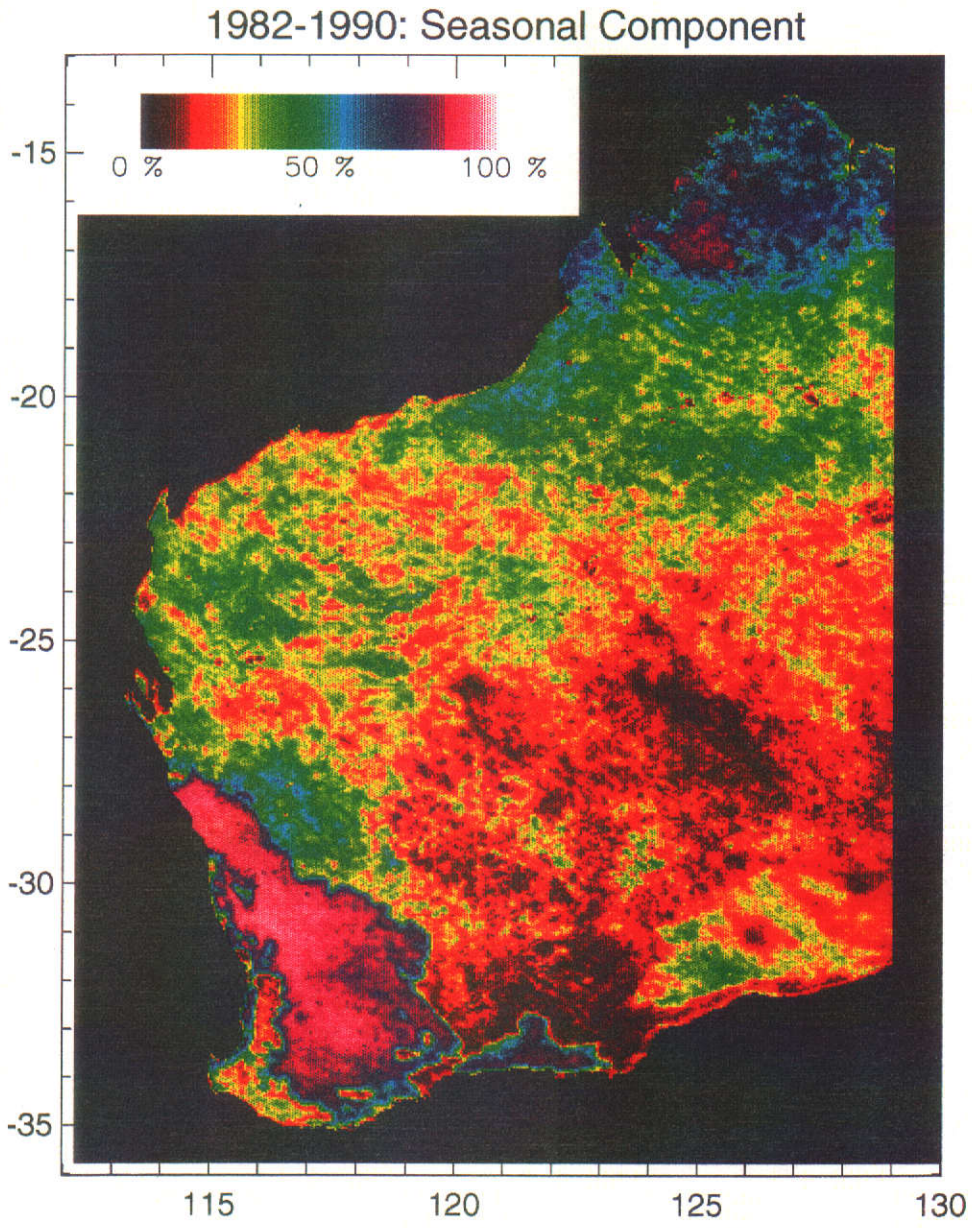

Figure 9.7 Total variance (%) in NDVI time series explained by seasonal component using decomposition

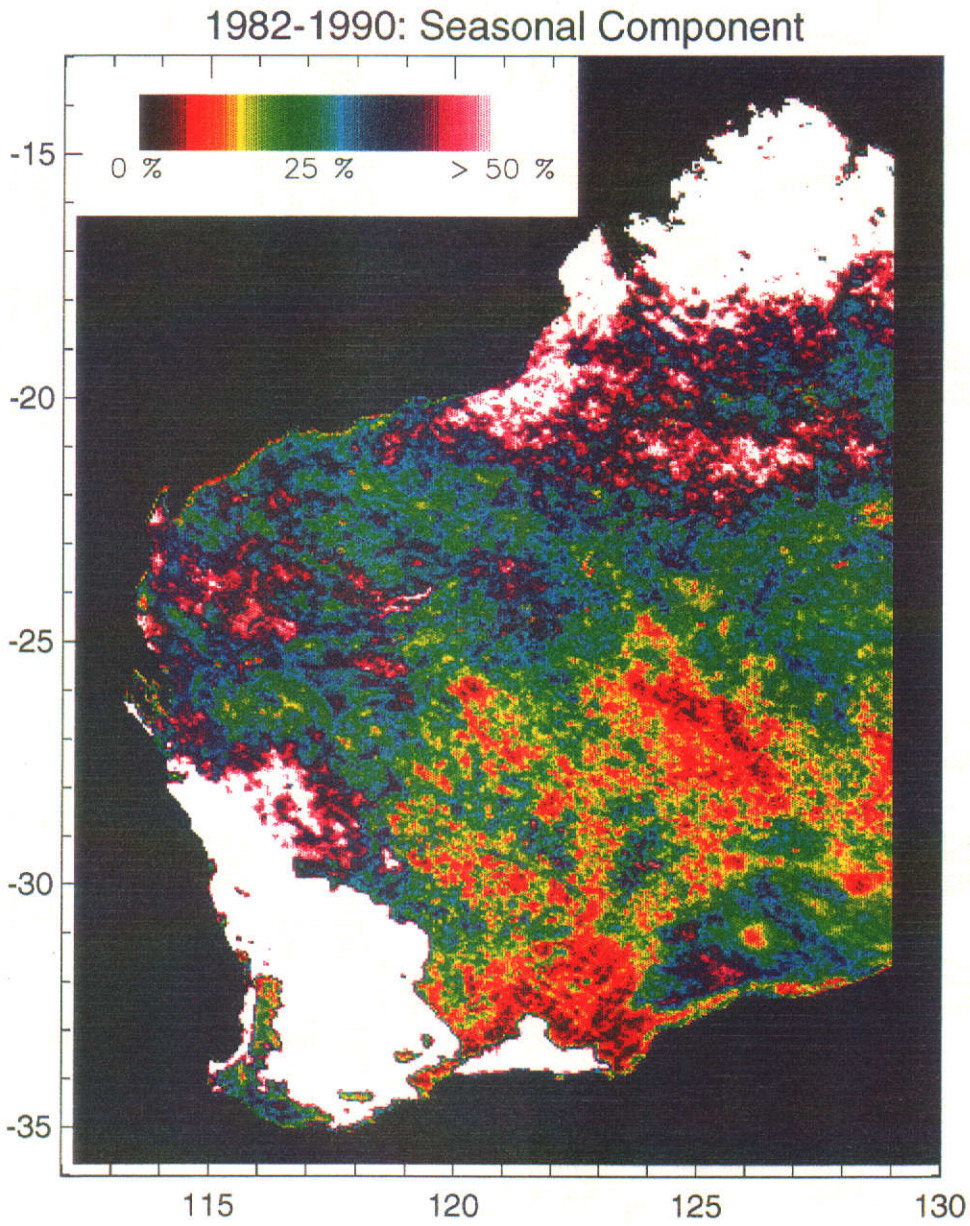

Figure 9.8 Total variance (%) (modified colour scale) in NDVI time series explained by seasonal component using decomposition. (Colour change from Figure 9.7 to highlight arid zones of Western Australia)

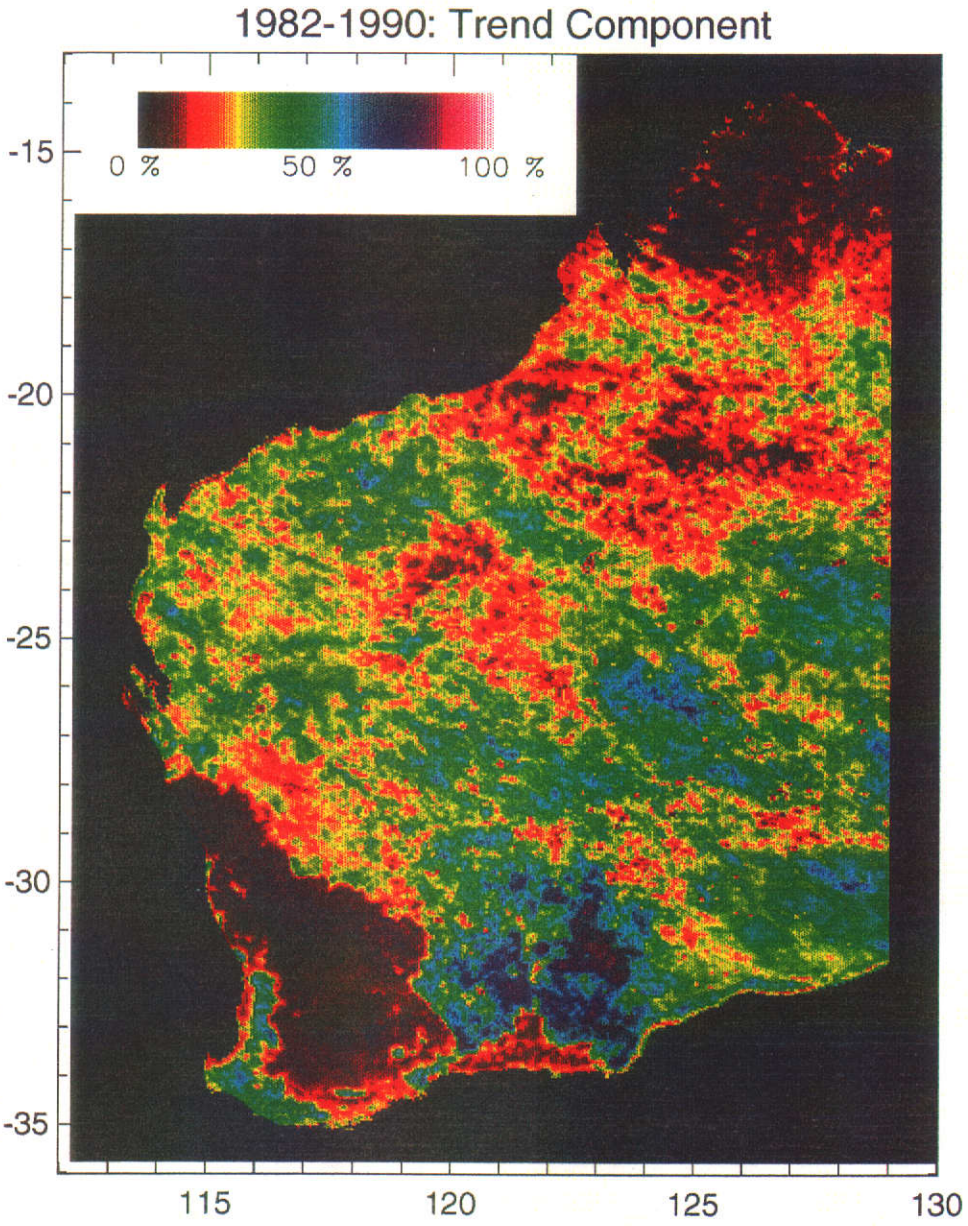

Figure 9.9 Total variance (%) in NDVI time series explained by trend component using decomposition

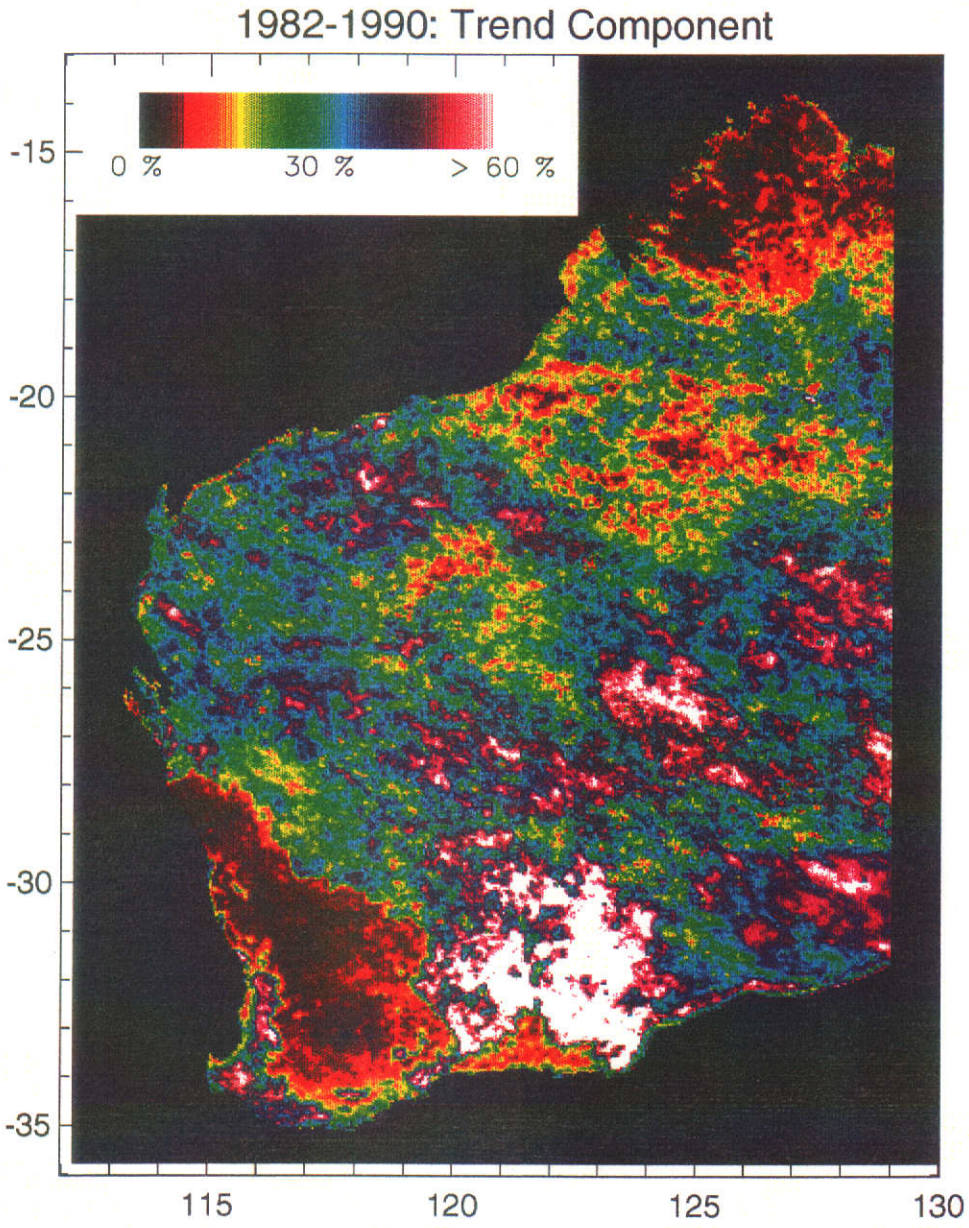

Figure 9.10 Total variance (%) (modified colour scale) in NDVI time series explained by trend component using decomposition. (Colour change from Figure 9.9 to highlight arid zones of Western Australia)

Figure 9.8 highlights details in the arid lands, and indicates that a seasonal component can explain up to 50 percent of the signal in some areas of the Pilbara and Gascoyne regions. A large area indicating a low seasonal component is evident on the Nullarbor Plains (126°E, 31°S). This was investigated and found to be a site that had one extremely good season over the decade. This high growth pulse was in effect all put into the trend and random component for that year, thus lifting their respective contributions to the overall variance.

The trend component (Figure 9.9) indicates that the highly seasonal areas noted above have virtually no variance in the trend component. Conversely, a large area (123°E, 32°S) in the south is shown a being dominated by trend. This area is a eucalypt woodland (Beard, 1981, 1975a) dominated by evergreen plant cover. Station 012065 (Norseman Post Office) is from this area and the time series for this station is shown in Figure 6.2. A close inspection of this time series reveals that the upward trend evident is really a jump which occurred throughout 1984, following good rainfall in December 1983. The NDVI trace climbed about 0.1 units, then levelled off again. It had not yet returned to its original level (NDVI ~ 0.2) at the end of the NDVI time series data in March 1991. This woodland area had a very low seasonal component (Figures 9.7 and 9.8). This may be part of a natural cycle involving regeneration after fire in these communities (Noble and Vines, 1993).

9.5 Discussion

Clearly, the NDVI time series has a distinct structure which varies from region to region. The development of sophisticated data analysis strategies will require a knowledge of the structure of the series. The empirical decomposition model was found to be superior to two other methods in describing that structure in a simple manner. While the autocorrelation function does show greater information about the dynamics of the system, it is more difficult to apply globally applicable interpretations than the decomposition method. The FFT was found not to be suitable due to the difficulty in interpreting the results. Non-sinusoidal signals will be the rule rather than the exception in vegetation studies.

Reporting schemes must be designed given a global understanding of the structure of the data. The method for reporting annual summaries in Chapter 8 is clearly not appropriate for those areas dominated by long term trend. This can be detected by close examination of Figures 8.8, 8.9 and 8.10. For example, Figure 8.8 indicates the region of long term trend (123°E, 32°S) experienced seven seasons out of a possible nine. The mean time of the season (Figure 8.9) was indicated as late summer. However, the confidence interval in that mean time (Figure 8.10) was greater than the pre-defined limit and not calculated. This lack of coherent timing is indicative of a trend in the data.

To use the annual summary technique developed in Chapter 8, those areas which show long term trends should be identified prior to the analysis and removed. Fortunately, the area of land which shows long term trends is limited.

It is difficult to physically interpret the long term trend information. Given the problems in calibration, the trend could simply be an area where the post flight calibration procedure has not worked well. Despite this, there is some evidence to suggest that a large summer rainfall event in December 1983 may have created a flush of perennials (growth and germination), which has persisted throughout the remainder of the decade.

Further studies could be attempted to analyse the nature of the trend and seasonal curves derived using the decomposition technique. In particular, the timing of peak growth could be extracted from the seasonal component. This was not attempted here, as the aim of the study was to investigate structural details of the time series. If such a study were to occur, then extreme caution would need to be exercised. Over the arid lands, the trend generally gets higher after a good season and then slowly declines. Projections based on this trend would be extremely difficult, and possibly misleading.

The demonstration that classical time series methods can be applied to NDVI data opens a whole new world of opportunity for

information extraction from the data. For example, in the highly seasonal areas, a seasonal adjustment could be applied to the data prior to analysis in a similar manner to the adjustments applied to economic time series (e.g. seasonally adjusted unemployment). There is also the possibility of adaptive forecasting techniques being applied. Adaptive techniques provide updated estimates of the time series components through time (Pagan, 1975; Lewandowski, 1982).

9.6 Summary

A method was sought to highlight structural differences in the NDVI time series data. This method was essentially seeking to supplement the extensive data exploration that is common to all time series analysis tasks. However, typical time series data are derived at a point, and the data can be explored by plotting them. In an image data set, there is effectively a time series for every pixel. For the GAC data used in this study there are 166421 potential series to be inspected !

Two principal criteria were set for the selection of a structural analysis technique:

(a) Physical interpretability,

b) Independence (as far as possible) from the input sequence (principally rainfall in this case).

Three techniques were evaluated, the FFT, autocorrelation, and classical decomposition methods. In each case, time series data from a number of stations were used to demonstrate the results of applying each particular technique.

The non-sinusoidal nature of the NDVI signals created a problem when trying to interpret the power spectrum derived from an FFT. This method was subsequently rejected for this reason. The autocorrelation function contains significant information on internal system dynamics and memory of the system. However, the classical decomposition technique was simpler and the underlying structure of the time series could be clearly interpreted.

The aim of describing the series independent of the input sequence was not generally achieved. For areas which experience a relatively regular rainfall, the regularity of the input (i.e. rainfall) creates a corresponding regular signal in the vegetation. However, for most of the arid region, the rainfall is not regular and it is simply not possible to view this system without reference to the system input. Despite this, understanding was gained of broad scale differences in vegetation behaviour between the arid lands used for pastoral purposes, and those which are currently vacant.

Images depicting the relative importance of the trend and seasonal components derived using classical decomposition techniques were written on a pixel by pixel basis. Some areas of

relatively predictable rainfall were found to have a seasonal component, which could explain from 70-90 percent of the variance in the original series. Seasonal adjustments could be applied to these series, which will focus attention on the inter-annual differences in the series.

In contrast, an area of eucalypt woodland in the south was found to be dominated by long term trend. A possible explanation relating to a significant summer rainfall event appeared a likely cause for this behaviour. Such areas should be identified and removed prior to the computation of annual summaries, such as those presented in Chapter 8.

Chapter 10

CONCLUSIONS AND RECOMMENDATIONS

10.1 Conclusions

The NDVI is only one of a number of vegetation indices that have been proposed for the extraction of vegetation signals from multi-spectral observations. Despite proposals to use other indices, the NDVI has remained dominant, possibly due to built-up inertia in the remote sensing community. This study has focussed on the NDVI, as the data were available in that format.

While the original reasons for choosing a particular vegetation index could be described as ad-hoc, more recent work has shown that vegetation indices can be formulated for specific applications. In a continental-scale program, where the monitoring of plant growth is the target, the chosen vegetation index must have two fundamental characteristics:

(a) Be a robust indicator of plant growth across various vegetation types, over differing soil background colours,

(b) Be insensitive to, or able to cope with, changes in sensor calibration and other external influences.

Much of the behaviour of the NDVI noted in the literature can be explained by understanding the fundamental mathematical nature of the NDVI. Vegetation indices have long been viewed as an ad-hoc processing procedure. In future this will not be the case, and

vegetation indices will be formulated to deal with specific tasks in specific applications. The use of ancillary information on vegetation structure will be required.

Significant attention in the literature has focussed on the atmospheric effect on the NDVI. In contrast, little attention has been given to the precision of the NDVI. Conversion of any signal to a digital format involves quantisation. The quantisation interval is commonly known as radiometric precision in remote sensing. Quantisation of the incoming signal imposes a fundamental limit on the precision of both the original observations and on derived quantities, such as vegetation indices.

This study has shown that the precision of the NDVI computed from observations acquired from the AVHRR instrument under typical Australian conditions is about 0.01 NDVI units. However, the precision varies depending on the level of the measured radiance, and is worst for dark targets, such as dense perennial vegetation. The precision of the NDVI also degrades as a function of the cosine of the solar zenith angle. At higher latitudes, the precision is typically worse due to larger solar zenith angles at the time of satellite overpass. This limit is fundamental. Greater precision in the NDVI can be obtained by averaging groups of pixels, but this destroys spatial resolution.

Overall, the mathematical and statistical behaviour of the

NDVI was found to be surprisingly complex. Much of the behaviour of the NDVI can be predicted, given a detailed knowledge of the mathematical nature of the NDVI, and some basic physical principles of remote sensing.

Difficulties with the calibration of the AVHRR instrument became apparent some time after the initial use of the data. One of the great advantages of satellite remote sensing is regular observation. The reliable interpretation of these observations through time requires calibration. Calibration of channels one and two (RED and NIR respectively) on the AVHRR is a linear problem, involving the determination of a gain and an offset.

The offset is routinely observed in space, and is known as the deep space count. Post-flight observations of the deep space counts have shown this quantity to be stable over time, but different from their pre-flight values. Remarkably, no attempt is made by NOAA to use these apparently reliable observations. It is recommended that all users of AVHRR data use the observed deep space counts in preference to pre-flight values.

In contrast, the gain of the AVHRR instrument has been shown in several studies to decline in sensitivity over time. Two distinct types of changes have been recognised:

(a) Large change following launch,

(b) Slow drift over time.

The NDVI is computed using the reflectances from channels one and two of the AVHRR (RED and NIR). Changes in the calibration of each channel, which are not identical, will introduce calibration error into the NDVI.

The results of several post-flight calibration studies reported in the literature are generally inconsistent. Theoretical considerations suggest that the calibration coefficients can be determined to within approximately ± 10 percent of their true values. The results of a simulation study undertaken in this thesis indicate that this is not precise enough for routine computation of the NDVI across several different satellite platforms.

In view of the differences in several post-flight calibration studies, an alternative technique was developed which could provide a relative calibration for multi-temporal NDVI data acquired from several different satellites. This technique was based on the following assumptions:

(a) The error in NDVI due to changes in calibration was approximately additive for each image,

(b) The average NDVI for a large region would remain relatively constant and would only be affected by regular seasonal changes,

(c) Any trend in NDVI over time was a calibration error and should be removed.

This hypothesis was tested and found to give results which agreed remarkably well with those derived theoretically using observations reported in the literature. This agreement provided confidence in the proposed methodology. A moving average, the same length as the seasonal period (12 months in this case), was used to remove seasonal influences from an NDVI time series. This requires at least 12 months of data before the first trend estimate (at six months) can be computed.

For real time users of AVHRR data, the calibration problem still remains. The problem will be particularly acute, when a changeover from one satellite to another occurs. It is likely that the NDVI values computed will change, simply due to the different satellite. To establish relative calibrations between the satellites it may be necessary to continue data acquisition from both satellites for up to one year. This one year period will allow the trend estimate (derived using the moving average method) from both satellites to overlap.

While waiting for the one year overlap period, the only current calibration alternative is to monitor invariant targets for differences in the NDVI. In this study, no truly long term invariant targets could be found. Despite this, the mean value from numerous targets may suffice in the shorter term. Extreme care will be required in this case. These invariant targets should have reflectances in both bands greater than ten percent which will minimise the effect of

quantisation error on the NDVI.

Given the current state of calibration techniques, continual improvements are both anticipated and hoped for in future satellites. Users of AVHRR satellite data need to plan for possible future upgrading of calibration results through time. In particular, a data archival system should be established, which will enable rapid reprocessing of an entire data set as new calibration coefficients come to hand. This data set should at least contain the original observations plus the angles which describe the viewing geometry between the sun and the sensor.

Univariate statistical summaries of the NDVI time series data on a pixel by pixel basis were found to be an effective exploratory analysis technique. While such statistics do ignore the time series nature of the data, they provide useful summaries. In particular, when an image has a land/ocean boundary, the range in NDVI (i.e. maximum - minimum) was an excellent indicator of the worst case positional errors in the data. The standard deviation of the NDVI was a good indicator of the seasonal variability for each pixel over the sampling period. Such simple statistics are not generally suitable for the identification of vegetation boundaries, as the particular pattern of rainfall over the sampling period also affects the result.

The major finding from the statistical analysis was the fundamental importance of the minimum NDVI in any analysis

scheme. Assuming the NDVI is a measure of green vegetation cover, then the minimum NDVI should be an indicator of the minimum green vegetation cover. In arid and semi-arid environments, water deficits and droughts are common, and perennial vegetation will generally be the only remaining green cover under these conditions. In areas of higher rainfall it is reasonable to expect higher perennial biomass, and thus the minimum green cover should be higher. The broad scale agreement was confirmed by a linear regression relating minimum annual rainfall over the decade (1982-1990) to the minimum NDVI value recorded for a number of rainfall stations throughout Western Australia.

Despite the strong global relationship between minimum NDVI and perennial vegetation, local variations in the minimum NDVI can and do exist, which are not related to perennial biomass. Other factors which can cause variations in the minimum NDVI are variations in soil colour and vegetation canopy architecture. These sources of variation have been called landscape factors. Thus, when seeking to compare the NDVI of different sites in the arid and semi-arid zones, the minimum NDVI should be subtracted.

Time series plots indicate qualitatively, the strong relationship that exists between rainfall and NDVI in the arid and semi-arid zones. Rainfall events are typically followed by a pulse in the NDVI some one, two or three months later. This behaviour was expected and is reassuring.

As early as 1973 it was proposed that in arid and semi-arid regions, rainfall created a pulse of growth and that the pulses could be studied and quantified using transfer function techniques in common use in the engineering professions. This hypothesis was tested by establishing linear models between the previous rainfall and the current value of the NDVI for a number of sites. The method adopted differed from previous approaches in that a rigorous method, borrowed from the engineering literature, was used to establish the structure of proposed relationships.

This approach was successful in mid-latitude arid environments in Western Australia. It was possible to predict up to 66 percent of the variance in the NDVI using monthly rainfall alone. However, in the south (30°S), the relationship was not as strong. This was partly attributed to the increased seasonality in evaporation and temperature as a result of higher latitude. In this environment, water balance techniques, which account for varying evaporation, would be preferred over rainfall. In addition, it is also possible that species-specific phenological factors, such as dormancy mechanisms could also impact on the relationship.

In the northern savanna grasslands, the transfer function approach was not adequate. In this environment, the rainfall is highly seasonal, with nearly all rainfall occurring in summer. A sophisticated model would be more appropriate in these environments, where the response to rainfall was also related to the

existing state of the vegetation.

Despite the problems in some areas, the transfer function methodology was not proposed as a globally applicable model. The finding that the NDVI trace could be reproduced as a linear function of the previous monthly rainfall for arid zone sites is encouraging. The species in this region have distinct phenologies. Despite this, the mix of species at the community level is such that a response to rainfall at any time is possible.

The major difference between the transfer function models derived in the arid region, is in the base (or minimum) NDVI used. This may be a function of variation in landscape factors, rather than any real difference in productive capacity. The changes in NDVI, when measured from the base NDVI, are predominantly a linear function of rainfall for those sites where the transfer function approach was successful.

Classical approaches to vegetation monitoring in rangelands using satellite based methods acquire a 'snapshot' of the land surface. Spatial comparison of the measurements derived from this snapshot is often based on the premise that the inputs such as rainfall are the same throughout the image area. However, variations in the amount and timing of rainfall, and associated local runoff invalidate such an assumption. Natural systems are both variable in space, and dynamic in time. Variations detected through

space could be a function of spatially varying inputs through time.

Without the corresponding measurements of the inputs, it is difficult to attribute a cause to the variation observed across the spatial dimension. The difference may just be a function of spatial variation in rainfall. As an example, the minimum NDVI image is a crude method to reconstruct the land surface to a time when all rainfall inputs are similar in the arid and semi-arid zones. Such a technique allows more confident interpretations of the spatial variations observed. This circumstance would be unlikely to occur naturally. Under this scenario, the transfer function should be the target of monitoring, if it is hoped to detect fundamental change in vegetation using AVHRR. Conceptually, by monitoring the coefficients of the transfer function through time, the influence of variable rainfall is removed. This focuses attention on the operation of the system in transforming rainfall, via transpiration, to dry matter production.

Mathematical techniques such as Kalman filters can be used to provide dynamic estimates of the transfer function coefficients through time. Whilst such techniques may possibly be established using the rainfall observed at individual meteorological stations, it would not be of practical use, due to the limited coverage of such stations. Practical application of such a technique would require satellite measurements of rainfall on a spatially comprehensive basis.

In the absence of rainfall information, spatial differences in the NDVI, within a similar vegetation type, must be assumed to be related to differences in rainfall, or water redistribution (i.e. runoff) in a landscape. This approach has also been adopted by other workers.

Annual summaries of plant growth across Western Australia were investigated as a means of summarising the information content of the NDVI time series. Three very simple but essential questions were used to guide the development of the summary technique. These questions were:

(a) Where did the vegetation growth occur ?

(b) When did the major growth period occur ?

(c) How much growth occurred ?

An index, called the API (annual production index) was defined for this purpose. This was defined as the maximum contiguous five monthly integral of the NDVI above the minimum NDVI value. Values for the API have been computed for each calendar year. In addition to this integral, images of the time of the API were also computed. The time that the API occurred each year was the central month of the API integral. All computations were done on a pixel by pixel basis.

The API is based on an assumption that only one major growth period occurs each year. While this was a valid assumption in Western Australia, there will be regions elsewhere where the

assumption is not valid. In these cases appropriate summary techniques will need to be developed.

The annual summary images derived using the above technique clearly demonstrate the enormous spatial and temporal variation that exists in rainfall and plant growth over arid and semi-arid regions of Western Australia. In some years, the overall growth was best described as 'patchy', with areas of potential drought conditions adjacent to others with reasonable conditions. In one year (1988), a broad scale weather pattern was evident.

To look at possible longer term patterns in the data, the nine annual summaries (1982-1990) were then summarised into a decadal summary. The fundamental question to be addressed in this case was how regular was the annual growth in both the amount of growth and the timing of that growth. In some respects, the question is similar to that addressed by bioclimatic classifications.

The mean amount of annual plant growth and an associated standard deviation were computed from the nine annual summary images. The summary of the timing of seasonal growth was a more complicated process. From the individual annual summaries, it was obvious that many arid and semi-arid areas do not receive sufficient rainfall for growth to occur each year. Thus there is no point in computing a mean time for a seasonal growth event that does not occur.

A season/no season threshold in the API was identified by inspection of image histograms and rainfall records. This threshold was used to compute the number of seasons of significant plant growth that had occurred over the nine year period for each pixel. The resulting image indicated that while many parts of the arid zone received at least four growth periods over the nine years, there were also some areas that received only one growth period over that time. Statistical summaries of the timing of seasonal growth were computed only for pixels that had at least four annual growth periods over the nine years.

To deal with the time-based information, circular statistics were introduced. The resulting images indicate that some parts of the arid zone can expect the period of peak growth in July each year, with an uncertainty of approximately one month either way. For many parts of the arid zone, there were insufficient annual growth periods to warrant a summary of the time of that growth.

The threshold in API could be used effectively in continental scale drought monitoring programs. It would be possible to calculate the time since the API was above this threshold for each pixel in a set of time series images, and display the result as an image. A failed season would immediately become obvious, as the time would be greater than 12 months since the API was above the threshold. Areas which experience drought conditions could be identified, and the time since a reasonable season had occurred would be clear. An

information product of this nature has direct relevance in land management agencies throughout Australia and presumably in other regions of the world.

It is tempting to propose a bioclimatic classification on the basis of the results from this work. While regularity is evident in both the agricultural lands of the southwest, and the savanna grasslands in the north, for the arid regions, variability is the normal course of events. In essence the argument is reduced to a debate on the importance of weather versus climate in determining ecosystem behaviour. Weather is the particular pattern of events and is highly variable in both space and time. Climate is a description of typical weather conditions in the longer term. Ecosystems respond to weather, at least in the short term.

Modern theories on vegetation dynamics in arid and semi-arid zones all stress the importance of weather sequences in determining the dynamics of vegetation change. In these theories, the ecosystem is recognised as having both stability and resilience. A change in vegetation, say from grasslands to shrubs, may be brought about by a particular sequence of events. This can occur despite longer term climatic patterns which favour grass species. Once the change occurs, the resilience of the new vegetation may not permit a change back to either the original state, or a new state, until another peculiar (not necessarily similar) sequence of events occurs.

For this reason, it was decided not to attempt a bioclimatic classification based on the results, even though they are an effective description of the effects of weather sequences on plant growth over Western Australia for the period 1982-1990. Further simplification to a bioclimatic classification would purposefully destroy the information on the effects of weather of plant growth.

Throughout this research, many NDVI time series were studied, and it was noted that certain global characteristics of those series were evident. The behaviour of those time series could be essentially categorised as:

(a) Trend related,

(b) Highly seasonal,

(c) Irregular pulses.

The behaviour of time series is an important indicator of the type of analysis procedure that may be suitable for more sophisticated analysis techniques, such as forecasting. This behaviour is readily apparent in time series plots. However, for image based time series is it not possible to individually inspect each time series to check the behaviour and recommend an analysis technique. An attempt was made to use standard diagnostic tools in use in time series analysis to define the character of the image based time series data.

Three principal approaches were investigated. The first of

these was the Fast Fourier Transform (FFT). This is a common technique used in engineering for the analysis of time varying signals. However, it was shown that when the signals are not sinusoidal, it is not possible to interpret the results (i.e. spectrum) consistently. Another technique borrowed from engineering, the auto-correlation function, was also tested. Diagnostic information about the time series could be interpreted from the auto-correlation function by visual inspection. In particular, the 'memory' of the system was indicated in these plots. However, it was difficult to establish a consistent rule to enable essential elements of the auto-correlation to be extracted for summary purposes.

The third technique tested, classical decomposition, proved the most suitable for the purpose. Using this method, the time series is conceptualised as a series composed of trend, season and random components. These components are extracted from the time series. The percentage of the variance explained by each component, and the overall variance of the NDVI time series, were found to be good indicators for spatial comparison of the character of the data.

Using classical decomposition, a seasonal component was found to describe approximately 90 percent of the total variance in the NDVI time series for the agricultural region of the southwest. Similarly, in the savanna grasslands of the north, the seasonal component described some 70 percent of the total variance. Conversely, an area in the south of the State, covered by perennial

Eucalypt woodland, was found to be dominated by trend.

In much of the arid regions, the split was relatively equal between the trend and seasonal components, although this varied spatially. The spatial variations evident in the arid regions are generally not interpretable. The underlying time series model does not provide an effective description of the NDVI time series behaviour, when seasonal growth occurs spasmodically over several years. The spatial variation in seasonal and trend components over these regions could be due to the particular weather sequence during the study period.

The major application of the structural analysis is to segment the study area, into three broad classes of behaviour as follows:

(a) Seasonal dominated,

(b) Trend dominated,

(c) The rest.

For NDVI time series which show strong seasonal behaviour, operational schemes could develop seasonal adjustments of the time series, to focus attention on the year to year variations. In Western Australia, this approach is feasible for both the agricultural region in the southwest, and the savanna grassland of the Kimberley region.

Similarly, regions where the NDVI time series is dominated by trend (such as the Eucalypt woodlands of the Goldfields region),

should be segmented prior to analysis. For regions falling in 'the rest' category (indicated above), the API, or a similar technique which focuses on seasonal production on an annual basis, can be used as a summary technique.

The NOAA satellite provides a unique platform from which to view the dynamic nature of vegetation growth. The broad scale variation in vegetation growth is clearly evident in both the images and time series plots presented in this thesis. Provided due attention is paid to the various steps involved, such as data calibration, then the rewards of being able to monitor vegetation growth over continental sized regions are available. Large centralised computing facilities to process the raw satellite observations will be required both now and in the future. However, the use of processed data, in both research and operational programs, does not necessarily require a huge commitment in computing resources. As an example, all the analysis undertaken in this thesis was performed on a personal computer using commercially available scientific software.

As an increased understanding of the earth is sought, the data acquired by the NOAA satellite will no doubt be superseded by more sophisticated observation platforms. However, it was observations acquired by the NOAA satellite, and subsequent skills developed interpreting those observations, that first genuinely kindled an interest in continental and global scale earth processes, a task for

which satellites are ideally suited.

10.2 Recommendations

Throughout this research program various areas where future research is warranted were identified. These areas are discussed below.

10.2.1 Arid Zone Modelling

The use of simple climatic data in modelling plant growth is commonplace in agricultural regions. For many areas of the rangelands in Australia, over 100 years of rainfall records exist. If such rainfall records can be used to provide reliable estimates of plant growth, then various statistical summaries of seasonal events could be prepared. For example, despite current concerns about drought, there are no long term readily available statistical data for Western Australia which assess the likelihood of drought for various regions. Other more advanced, but equally appropriate statistics, include for example the probability of two (or more) failed seasons in a row. It is often the run of events, rather than any particular event, that is of importance in land management. Existing summaries of rainfall data focus on univariate statistics, without looking at the sequence of events.

Data acquired from the NOAA-AVHRR satellite should be used to validate simple plant growth models across a range of vegetation

types and bioclimatic regimes in the arid and semi-arid zones. Equally as importantly, the data should also be used to generate plausible hypothesises for the construction of suitable models.

Recommendation No. 1

That data acquired from the NOAA-AVHRR satellite be used to validate simple plant growth models which rely on readily available climatic data. These models could then be extended over the length of the rainfall record (i.e. 100 or more years) to provide probabilities of various seasonal events.

10.2.2 Climate Change Research

The prime vehicles for research into global climate change are the so-called GCM's (global circulation models). In such models, the land surface is often considered static. If the behaviour of NDVI is considered indicative of key processes, such as evaporation and transpiration, which are linked to plant growth, then a mean seasonal signal could account for much of the variability in these processes in some regions. Mean seasonal maps of these processes, at say monthly intervals, could be used to infer a dynamic interface between the atmosphere and vegetation in GCM's. Areas where a mean seasonal signal is appropriate could be identified from NOAA-AVHRR data. To test the sensitivity of such models, actual measurements as opposed to seasonal mean values could be used in simulation tests.

Recommendation No. 2

That the classical decomposition technique be used to identify highly seasonal areas from AVHRR NDVI data on a global basis. These regions would then form the basis of a dynamic link between the biosphere and atmosphere in GCM's.

10.2.3 Monitoring of Vegetation Dynamics

The focus in this research has been on seasonal influences on vegetation. Seasonal variability will mask changes in the vegetation type that may be of ecological and economic importance. Monitoring the system transfer function, using both rainfall and NDVI measurements, and a Kalman filter, may be possible in cases where a transfer function can be identified. Dynamic changes in the system transfer function could indicate ecological changes in that system. If such an approach were possible, then practical application of that approach would also require spatially comprehensive estimates of rainfall using satellite systems.

Recommendation No. 3

That the use of Kalman filters be investigated to provide dynamic updates of transfer function models for vegetation monitoring purposes.

10.2.4 Vegetation Indices

In the literature review, it was recognised that vegetation

indices are beginning to be formulated based on explicit physical principles. However, the optimal vegetation index for the extraction of vegetation information (e.g. NPP, LAI, vegetation cover) from spectral observations quite possibly varies according to the plant canopy structure. Existing vegetation mapping contains some information on the canopy structure. These maps could possibly be used to select an optimal vegetation index.

Recommendation No. 4

That research be conducted to investigate the possibility of formulating vegetation indices for different vegetation types based on selected optical properties of the vegetation canopy to optimise the estimation of biophysical parameters (e.g. LAI, height). The selected properties should be readily available from existing (vegetation) structural classification systems.

REFERENCES

Abel, P. (1990) Prelaunch Calibration of the NOAA-11 AVHRR Visible and Near IR Channels, Remote Sensing of Environment, Vol. 31, pp. 237-229.

Abercrombie, M., Hickman, C.J. and Johnson, M.L. (1980) The Penguin Dictionary of Biology, 7th Ed., Penguin Books, Middlesex, England, 323 pp.

Achard, F. and Blasco, F. (1990) Analysis of Vegetation Seasonal Evolution and Mapping of Forest Cover in West Africa with the Use of NOAA AVHRR HRPT Data, Photogrammetric Engineering and Remote Sensing, Vol. 56, No. 10, pp. 1359-1365.

Arbrecht, D. (1994) Personal Communication.

Asrar, G., Fuchs, M., Kanemasu, E.T. and Hatfield, J.L. (1984) Estimating Absorbed Photosynthetic Radiation and Leaf Area Index from Spectral Reflectance in Wheat, Agronomy Journal, Vol. 76, pp. 300-306.

Asrar, G., Myneni, R.B. and Choudhury, B.J. (1992) Spatial Heterogeneity in Vegetation Canopies and Remote Sensing of Absorbed Photosynthetically Active Radiation: A Modelling Study, Remote Sensing of Environment, Vol. 41, pp. 85-103.

Austin, M.P., Williams, O.B. and Belbin, L. (1981) Grassland Dynamics under Sheep Grazing in an Australian Mediterranean Type Climate, Vegetatio, Vol. 47, pp. 201-211.

Azzali, S. (1991) Interpretation of Crop Growth Patterns by Means of NDVI-Time Series in Zambia, Geocarto International, Vol. 3, pp. 15-26.

Baret, F. and Guyot, G. (1991) Potentials and Limits of Vegetation Indices for LAI and APAR Assessment, Remote Sensing of Environment, Vol. 35, pp. 161-173.

Baret, F., Guyot, G. and Major, D.J. (1989) TSAVI: A Vegetation Index Which Minimizes Soil Brightness Effects on LAI and APAR Estimation, in Quantitative Remote Sensing: An Economic Tool for the Nineties. 12th Canadian Symposium on Remote Sensing, Vancouver, BC, July 1989, Vol. 3, pp. 1355-1358.

Baret, F., Vanderbilt, V.C., Rondeaux, G., Pettigrew, R.E., Hancoq, J.F., Biehl, L.L., Sarrouy, C., Daughtry, C.S.T., Steven, M.D., Sarto, A.W., Modro, D.H., Guyot, G., Jacquemoud, S., Horoyan, H., Despontin, C. and Razafindraibe, H. (1992) Directional and Temporal Variability of the APAR/VI Relationships. The Case of a Sunflower Canopy, Proceedings of International Geoscience and Remote Sensing Symposium, Houston, Texas, May 1992, Vol. 2, pp. 1468-1470.

Beard, J.S. (1974-1980) Vegetation Survey of W.A., 1:1000000 Series, University of Western Australia Press, Nedlands, WA.
(1974a) Sheet 2, Great Sandy Desert
(1974b) Sheet 3, Great Victoria Desert
(1975a) Sheet 4, Nullarbor
(1975b) Sheet 5, Pilbara
(1976) Sheet 6, Murchison
(1979) Sheet 1, Kimberley
(1981) Sheet 7, Swan

Beard, J.S. (1990) Plant Life of Western Australia, Kangaroo Press Pty Ltd, Sydney, NSW, 319 pp.

Beard, J.S. and Webb, M.J. (1974) The Vegetation Survey of Western Australia: Its Aims, Objects and Methods, in Sheet 2, Great Sandy Desert, Explanatory Notes to Accompany 1:1000000 Map Sheet No. 2, University of Western Australia Press, Nedlands, WA.

Begue, A. (1993) Leaf Area Index, Intercepted Photosynthetically Active Radiation, and Spectral Vegetation Indices: A Sensitivity Study for Regular-Clumped Canopies, Remote Sensing of Environment, Vol. 46, pp. 45-59.

Belward, A.S. (1992) Spatial Attributes of AVHRR Imagery for Environmental Monitoring, International Journal of Remote Sensing, Vol. 13, No. 2, pp. 193-208.

Bennett, R.J. (1979) Spatial Time Series : Analysis - Forecasting - Control, Pion, London, UK, 674 pp.

Bonifacio, R., Dugdale, G. and Milford, J.R. (1993) Sahelian Rangeland Production in Relation to Rainfall Estimates from Meteosat, International Journal of Remote Sensing, Vol. 14, No. 14, pp. 2695-2711.

Box, E.O., Holben, B.N. and Kalb, V. (1989) Accuracy of the AVHRR Vegetation Index as a Predictor of Biomass, Primary Productivity and Net CO_2 Flux, Vegetatio, Vol. 80, pp. 71-89.

Box, G.E.P. and Jenkins, G.M. (1976) Time Series Analysis, Rev. Ed., Holden-Day, San Francisco, Ca, 575 pp.

Brest, C.L. and Rossow, W.B. (1992) Radiometric Calibration and Monitoring of NOAA AVHRR Data for ISCCP, International Journal of Remote Sensing, Vol. 13, No. 2, pp. 235-273.

Briggs, L.J. and Shantz, H.L. (1913) The Water Requirements of Plants I. Investigations in the Great Plains in 1910 and 1911., U.S. Department Agriculture: Bureau of Plant Industry, Bulletin No. 284.

Brockwell, P.J. and Davis, R.A. (1987) Time Series: Theory and Methods, Springer Verlag, New York, NY, 519 pp.

Brockwell, P.J. and Davis, R.A. (1991) ITSM: An Interactive Time Series Modelling Package for the PC, Springer Verlag, New York, NY, 104 pp.

Brook, K.D., Carter, J.O., Danaher, T.J., McKeon, G.M., Flood, N.R. and Peacock, A. (1992) The Use of Spatial Modelling and Remote Sensing for Monitoring and Forecasting of Drought Related Land Degradation Events in Queensland, Proceedings of 6th Australasian Remote Sensing Conference, Wellington, NZ, November 1992, Vol. 1, pp. 140-149.

Brush, R.J.H. (1988) The Navigation of AVHRR Imagery, International Journal of Remote Sensing, Vol. 9, No. 9, pp. 1491-1502.

Bullock, P.R. (1992) Operational Estimates of Western Canadian Grain Production Using NOAA AVHRR LAC Data, Canadian Journal of Remote Sensing, Vol. 18, No. 1, pp. 23-28.

Bureau of Meteorology (1989) Climate of Australia, Australian Government Publishing Service, Canberra, ACT, 49 pp.

Burroughs, W.J. (1992) Weather Cycles: Real or Imaginary?, Cambridge University Press, Cambridge, UK, 201 pp.

Byrne, G.F. (1973) An Approach to Growth Curve Analysis, Agricultural Meteorology, Vol. 11, pp. 161-168.

Campbell, K.O. (1966) Problems of Adaption of Pastoral Businesses in the Arid Zone, Australian Journal of Agricultural Economics, Vol. 10, pp. 14-26.

Carnahan, J.A. (1981) Mapping at a Continental Level, in Vegetation Classification in Australia, Gillison, A.N. and Anderson, D.J. (eds), ANU Press, Canberra, ACT, pp. 107-113.

Chahine, M.T. (1992) The Hydrological Cycle and its Influence on Climate, Nature, Vol. 359, pp. 373-380.

Charles-Edwards, D.A., Doley, D. and Rimmington, G.M. (1986) Modelling Plant Growth and Development, Academic Press, Sydney, NSW, 227 pp.

Che, N. and Price, J.C. (1992) Survey of Radiometric Calibration Results and Methods for Visible and Near Infrared Channels of NOAA-7, -9 and -11 AVHRRs, Remote Sensing of Environment, Vol. 41, pp. 19-27.

Choudbury, B.J. (1987) Relationships Between Vegetation Indices, Radiation Absorption, and Net Photosynthesis Evaluated by a Sensitivity Analysis, Remote Sensing of Environment, Vol. 22, pp. 209-233.

Christian, C.S. and Stewart, G.A. (1968) Methodology of Integrated Survey, in Aerial Surveys and Integrated Studies, UNESCO, Paris, France, pp. 233-280.

Cihlar, J., D'Iorio, M., Mullins, D. and St-Laurent, L. (1989) Use of Satellite Data and GIS for Environmental Change Studies, Proceedings of National Conference of Canadian Institute of Surveying and Mapping, Ottawa, Canada, Feb - March 1989, pp. 933-943.

Cihlar, J., St-Laurent, L. and Dyer, J.A. (1991) Relation Between the Normalised Difference Vegetation Index and Ecological Variables, Remote Sensing of Environment, Vol. 35, pp. 279-298.

Cooper, G.R. and McGillem, C.D. (1986) Probabilistic Methods of Signal and System Analysis, 2nd Ed., CBS Publishing, New York, NY, 408 pp.

Cridland, S.W., Burnside, D.G. and Smith, R.G.C. (1994) Use by Managers in Rangeland Environments of Near Real Time Satellite Measurements of Seasonal Vegetation Response, Proceedings of 7th Australasian Remote Sensing Conference, March 1994, Melbourne, Australia, Vol. 2, pp. 1134-1141.

Crippen, R.E. (1988) The Dangers of Underestimating the Importance of Data Adjustments in Band Ratioing, International Journal of Remote Sensing, Vol. 9, No. 4, pp. 767-776.

Curran, P.J. (1985) Principles of Remote Sensing, Longman Group, London, UK, 282 pp.

Danaher, T.J., Carter, J.O., Brook, K.D., Peacock, A. and Dudgeon, G.S. (1992) Broad Scale Vegetation Mapping Using NOAA-AVHRR Imagery, Proceedings of 6th Australasian Remote Sensing Conference, Wellington, NZ, November 1992, Vol. 3, pp. 128-137.

Davenport, M.L. and Nicholson, S.E. (1993) On the Relation Between Rainfall and the Normalized Difference Vegetation Index for Diverse Vegetation Types in East Africa, International Journal of Remote Sensing, Vol. 14, No. 12, pp. 2369-2389.

Davis, F.W., Quattrochi, D.A., Ridd, M.K., Lam, N.S., Walsh, S.J., Michaelson, J.C., Franklin, J., Stow, D.A., Johannsen, C.J. and Johnston, C.A. (1991) Environmental Analysis Using Integrated GIS and Remotely Sensed Data: Some Research Priorities, Photogrammetric Engineering and Remote Sensing, Vol. 57, No. 6, pp. 689-697.

Deering, D.W. and Eck, T.F. (1987) Atmospheric Optical Depth Effects on Angular Anisotropy of Plant Canopy Reflectance, International Journal of Remote Sensing, Vol. 8, No. 6, pp. 893-916.

Deering, D.W., Eck, T.F. and Otterman, J. (1990) Bidirectional Reflectances of Selected Desert Surfaces and their Three-Parameter Soil Characterization, Agricultural and Forest Meteorology, Vol. 52, pp. 71-93.

Diallo, O., Diouf, A., Hanan, N.P., Ndiaye, A. and Prevost, Y. (1991) AVHRR Monitoring of Savanna Primary Production in Senegal, West Africa: 1987-1988, International Journal of Remote Sensing, Vol. 12, No. 10, pp. 1259-1279.

D'Iorio, M.A., Cihlar, J. and Morasse, C.R. (1991) Effect of the Calibration of AVHRR Data on the Normalized Difference Vegetation Index and Compositing, Canadian Journal of Remote Sensing, Vol. 17, No. 3, pp. 251-262.

Doorenbos, J. and Kassam, A.H. (1979) Yield Response to Water, FAO Irrigation and Drainage Paper No. 33, Rome, Italy, 193 pp.

Dregne, H.E. and Tucker, C.J. (1988) Green Biomass and Rainfall in Semi-Arid Sub-Saharan Africa, Journal of Arid Environments, Vol. 15, pp. 245-252.

Eastman, J.R. and Fulk, M. (1993) Long Sequence Time Series Evaluation Using Standardized Principal Components, Photogrammetric Engineering and Remote Sensing, Vol. 59, No. 6, pp. 991-996.

Ehrlich, D., Estes, J.E. and Singh, A. (1994) Applications of NOAA-AVHRR 1 km Data for Environmental Monitoring, International Journal of Remote Sensing, Vol. 15, No. 1, pp. 145-161.

Eidenshink, J.C. (1992) The 1990 Conterminous U.S. AVHRR Data Set, Photogrammetric Engineering and Remote Sensing, Vol. 58, No. 6, pp. 809-813.

Elvidge, C.D. and Lyon, R.J.P. (1985) Influence of Rock-Soil Spectral Variation on the Assessment of Green Biomass, Remote Sensing of Environment, Vol. 17, pp. 265-279.

Emery, W.J., Brown, J. and Nowak, P. (1989) AVHRR Image Navigation: Summary and Review, Photogrammetric Engineering and Remote Sensing, Vol. 55, No. 8, pp. 1175-1183.

Emery, W.J. and Ikeda, M. (1984) A Comparison of Geometric Correction Methods of AVHRR Imagery, Canadian Journal of Remote Sensing, Vol. 10, pp. 46-56.

Filet, P., Dudgeon, G., Scanlan, J., Elmes, N., Bushell, J., Quirk, M., Wilson, R. and Kelly, A. (1990) Rangeland Vegetation Monitoring Using NOAA AVHRR Data. 2. Ground Truth, Proceedings of 5th Australasian Remote Sensing Conference, Perth, Western Australia, October 1990, Vol. 1, pp. 218-227.

Fitzpatrick, E.A. and Nix, H.A. (1970) The Climatic Factor in Australian Grassland Ecology, in Australian Grasslands, Moore, R.M. (ed), ANU Press, Canberra, ACT, pp. 3-26.

Fitzpatrick, E.A., Slatyer, R.O. and Krishnan, A.I. (1967) Incidence and Duration of Periods of Plant Growth in Central Australia as Estimated from Climatic Data, Agricultural Meteorology, Vol. 4, pp. 389-404.

Foran, B.D. (1987) Detection of Yearly Cover Change with Landsat MSS on Pastoral Landscapes in Central Australia, Remote Sensing of Environment, Vol. 23, pp. 333-350.

Foran, B.D., Bastin, G., Remenga, E. and Hyde, K.W. (1982) The Response to Season, Exclosure, and Distance from Water of Three Central Australian Pasture Types Grazed by Cattle, Australian Rangeland Journal, Vol. 4, No. 1, pp. 5-15.

Foran, B.D. and Pearce, G. (1990) The Use of NOAA AVHRR and the Green Vegetation Index to Assess the 1988/89 Summer Growing Season in Central Australia, Proceedings of 5th Australasian Remote Sensing Conference, Perth, Western Australia, October 1990, Vol. 1, pp. 198-207.

Fraser, R.S. and Kaufman, Y.J. (1986) Calibration of Satellite Sensors After Launch, Applied Optics, Vol. 25, No. 7, pp. 1177-1185.

Friedel, M.H., Nelson, D.J., Sparrow, A.D., Kinloch, J.E. and the late Maconochie, J.R. (1993) What Induces Central Australian Arid Zone Trees and Shrubs to Flower and Fruit, Australian Journal of Botany, Vol. 41, pp. 307-319.

Frouin, R. and Gautier, C. (1987) Calibration of NOAA-7 AVHRR, GOES-5, and GOES-6 VISSR/VAS Solar Channels, Remote Sensing of Environment, Vol. 22, pp. 73-101.

Gallo, K.P., Daughtry, C.S.T. and Bauer, M.E. (1985) Spectral Estimation of Absorbed Photosynthetically Active Radiation in Corn Canopies, Remote Sensing of Environment, Vol. 17, pp. 221-232.

Gallo, K.P. and Eidenshink, J.C. (1988) Differences in Visible and Near-IR Responses, and Derived Vegetation Indices, for the NOAA-9 and NOAA-10 AVHRRs: A Case Study, Photogrammetric Engineering and Remote Sensing, Vol. 54, No. 4, pp. 485-490.

Gibbs, W.J. (1984) The Great Australian Drought: 1982-1983, Disasters, Vol. 8, pp. 89-104.

Goward, S.N., Markham, B.L., Dye, D.G., Dulaney, W. and Yang, J. (1991) Normalized Difference Vegetation Index Measurements from the Advanced Very High Resolution Radiometer, Remote Sensing of Environment, Vol. 35, pp. 257-277.

Goward, S.N., Tucker, C.J. and Dye, D.G. (1985) North American Vegetation Patterns Observed with the NOAA-t Advanced Very High Resolution Radiometer, Vegetatio, Vol. 64, pp. 3-14.

Graetz, R.D. (1987) Satellite Remote Sensing of Australian Rangelands, Remote Sensing of Environment, Vol. 23, pp. 313-331.

Graetz, R.D. (1990) Remote Sensing of Terrestrial Ecosystem Structure: An Ecologist's Pragmatic View, in Remote Sensing of Biosphere Functioning, Hobbs, R.L. and Mooney, H.A. (eds), Springer Verlag, New York, NY, pp. 5-30.

Graetz, R.D., Fisher, R.P. and Wilson, M.A. (1992) Looking Back: The Changing Face of the Australian Continent, 1972-1992, CSIRO Office of Space Science and Applications, Canberra, ACT, 159 pp.

Graetz, R.D. and Gentle, M.R. (1982) The Relationships Between Reflectance in the Landsat Wavebands and the Composition of an Australian Semi-Arid Shrub Rangeland, Photogrammetric Engineering and Remote Sensing, Vol. 48, pp. 1721-1730.

Graetz, R.D., Pech, R.P. and Davis, A.W. (1988a) The Assessment and Monitoring of Sparsely Vegetated Rangelands Using Calibrated Landsat Data, International Journal of Remote Sensing, Vol. 9, No. 7, pp. 1201-1222.

Graetz, R.D., Walker, B.H. and Walker, P.A. (1988b) The Consequences of Climatic Change for Seventy Percent of Australia, in GREENHOUSE: Planning for Climate Change, Pearman, G.I. (ed), CSIRO Division of Atmospheric Research, Canberra, ACT, pp. 399-420.

Gupta, R.K. (1993) Comparative Study of AVHRR Ratio Vegetation Index and Normalized Difference Index in District Level Monitoring, International Journal of Remote Sensing, Vol. 14, No. 1, pp. 53-73.

Gutman, G.G. (1987) The Derivation of Vegetation Indices from AVHRR Data, International Journal of Remote Sensing, Vol. 8, No. 8, pp. 1235-1243.

Gutman, G.G. (1989) On the Relationship Between Monthly Mean and Maximum-Value Composite Normalized Vegetation Indices, International Journal of Remote Sensing, Vol. 10, No. 8, pp. 1317-1325.

Gutman, G.G. (1990) Towards Monitoring Droughts from Space, Journal of Climate, Vol. 3, pp. 282-295.

Gutman, G.G. (1991) Vegetation Indices from AVHRR: An Update and Future Prospects, Remote Sensing of Environment, Vol. 35, pp. 121-136.

Gutman, G.G. (1992) NOAA Activities in Monitoring Land Climate using the Advanced Very High Resolution Radiometer, Proceedings of 6th Australasian Remote Sensing Conference, Wellington, NZ, November 1992, Vol. 1, pp. 60-69.

Hammer, G.L., Woodruff, D.R. and Robinson, J.B. (1987) Effects of Climatic Variability and Possible Climatic Change on Reliability of Wheat Cropping - A Modelling Approach, Agricultural and Forest Meteorology, Vol. 41, pp. 123-142.

Hamming, R.W. (1989) Digital Filters, 3rd Ed., Prentice-Hall, Englewood Cliffs, New Jersey, USA, 279 pp.

Hatfield, J.L., Kanemasu, E.T., Asrar, G., Jackson, R.D., Pinter Jr., P.J., Reginato, R.J. and Idso, S.B. (1985) Leaf-Area Estimates from Spectral Measurements over Various Planting Dates of Wheat, International Journal of Remote Sensing, Vol. 6, No. 1, pp. 167-175.

Haykin, S. (1989) Modern Filters, Macmillan, New York, NY, 398 pp.

Hellden, U. (1984) Remote Sensing for Drought Impact Assessment - A Study of Land Transformation in Kordofan - Sudan, Advances in Space Research, Vol. 4, No. 11, pp. 165-168.

Henricksen, B.L. (1986) Reflections on Drought: Ethiopia 1983-1984, International Journal of Remote Sensing, Vol. 7, No. 11, pp. 1447-1451.

Henricksen, B.L. and Durkin, J.W. (1986) Growing Period and Drought Early Warning in Africa Using Satellite Data, International Journal of Remote Sensing, Vol. 7, No. 11, pp. 1583-1608.

Hielkema, J.U., Prince, S.D. and Astle, W.L. (1986) Rainfall and Vegetation Monitoring in the Savanna Zone of the Democratic Republic of Sudan Using the NOAA Advanced Very High Resolution Radiometer, International Journal of Remote Sensing, Vol. 7, No. 11, pp. 1499-1513.

Holben, B.N. (1986) Characteristics of Maximum-Value Composite Images from Temporal AVHRR Data, International Journal of Remote Sensing, Vol. 7, No. 11, pp. 1417-1434.

Holben, B.N., Eck, T.F. and Fraser, R.S. (1991) Temporal and Spatial Variability of Aerosol Optical Depth in the Sahel Region in Relation to Vegetation Remote Sensing, International Journal of Remote Sensing, Vol. 12, No. 6, pp. 1147-1163.

Holben, B.N. and Fraser, R.S. (1984) Red and Near-Infrared Sensor Response to Off-Nadir Viewing, International Journal of Remote Sensing, Vol. 5, No. 1, pp. 145-160.

Holben, B.N., Kaufman, Y.J. and Kendall, J.D. (1990) NOAA-11 AVHRR Visible and Near-IR Inflight Calibration, International Journal of Remote Sensing, Vol. 11, No. 8, pp. 1511-1519.

Holben, B.N., Tucker, C.J. and Fan, C. (1980) Spectral Assessment of Soybean Leaf Area and Leaf Biomass, Photogrammetric Engineering and Remote Sensing, Vol. 46, No. 5, pp. 651-656.

Holm, A.McR. (1986) The Assessment of Range Trend in Western Australian Pastoral Shrublands, in Rangelands: A Resource Under Siege - Proceedings of 2nd International Rangelands Congress, Joss, P.J., Lynch, P.W. and Williams, O.B. (eds), Australian Academy of Science, Canberra, ACT, pp. 529.

Holm, A.McR. (1994) Personal Communication.

Honey, F.R. and Tapley, I.J. (1981) A Vegetation Response Model Applied to Range Inventory and Monitoring Using Landsat MSS Data, Proceedings of 15th International Symposium on Remote Sensing of Environment, Ann Arbor, Michigan, May 1981, pp. 823-837.

Huemmrich, K.F. and Goward, S.N. (1992) Spectral Vegetation Indexes and the Remote Sensing of Biophysical Parameters, Proceedings of International Geoscience and Remote Sensing Symposium, Houston, Texas, May 1992, Vol. 2, pp. 1017-1019.

Huete, A.R. (1987) Soil-Dependent Spectral Response in a Developing Plant Canopy, Agronomy Journal, Vol. 79, pp. 61-68.

Huete, A.R. (1988) A Soil-Adjusted Vegetation Index (SAVI), Remote Sensing of Environment, Vol. 25, pp. 295-309.

Huete, A.R. (1989) Soil Influences in Remotely Sensed Vegetation-Canopy Spectra, in Theory and Applications of Optical Remote Sensing, Asrar, G. (ed), John Wiley and Sons, New York, NY, pp. 107-141.

Huete, A.R., Hua, G., Qi, J., Chehbouni, A. and van Leeuwen, W.J.D. (1992) Normalization of Multidirectional Red and NIR Reflectances with the SAVI, Remote Sensing of Environment, Vol. 41, pp. 143-154.

Huete, A.R. and Jackson, R.D. (1987) Suitability of Spectral Indices for Evaluating Vegetation Characteristics on Arid Rangelands, Remote Sensing of Environment, Vol. 23, pp. 213-232.

Huete, A.R., Jackson, R.D. and Post, D.F. (1985) Spectral Response of a Plant Canopy with Different Soil Backgrounds, Remote Sensing of Environment, Vol. 17, pp. 37-53.

Huete, A.R., Post, D.F. and Jackson, R.D. (1984) Soil Spectral Effects on 4-Space Vegetation Discrimination, Remote Sensing of Environment, Vol. 15, pp. 155-165.

Huete, A.R. and Tucker, C.J. (1991) Investigation of Soil Influences in AVHRR Red and Near-Infra-Red Vegetation Index Imagery, International Journal of Remote Sensing, Vol. 12, No. 6, pp. 1223-1242.

Hutchinson, C.F. (1991) Uses of Satellite Data for Famine Early Warning in Sub-Saharan Africa, International Journal of Remote Sensing, Vol. 12, No. 6, pp. 1405-1421.

Jasinski, M.F. (1990) Sensitivity of the Normalized Difference Vegetation Index to Subpixel Canopy Cover, Soil Albedo, and Pixel Scale, Remote Sensing of Environment, Vol. 32, pp. 169-187.

Jensen, J.R. (1986) Introductory Digital Image Processing, Prentice-Hall, Englewood Cliffs, New Jersey, USA, 379 pp.

Jeyaseelan, A.T. and Thiruvengadachari, S. (1993) Suspected Mt. Pinatubo Aerosol Impact on the NOAA AVHRR NDVI over India, International Journal of Remote Sensing, Vol. 14, No. 3, pp. 603-608.

Jupp, D.L.B., Strahler, A.H. and Woodcock, C.E. (1988) Autocorrelation and Regularization in Digital Images. I. Basic Theory, IEEE Transactions Geoscience and Remote Sensing, Vol. 26, No. 4, pp. 463-473.

Jupp, D.L.B., Walker, J. and Penridge, L.K. (1986) Interpretation of Vegetation Structure in Landsat MSS Imagery: A Case Study in Disturbed Semi-Arid Eucalypt Woodlands. Part 2. Model-based Analysis, Journal of Environmental Management, Vol. 23, pp. 35-57.

Jupp, D.L.B. and Woodcock, C.E. (1992) Variance in Directional Radiance of Open Canopies, Proceedings of International Geoscience and Remote Sensing Symposium , Houston, Texas, May 1992, Vol. 2, pp. 1490-1492.

Justice, C.O., Eck, T.F., Tanre, D. and Holben, B.N. (1991) The Effect of Water Vapour on the Normalized Difference Vegetation Index Derived for the Sahelian Region from NOAA AVHRR Data, International Journal of Remote Sensing, Vol. 12, No. 6, pp. 1165-1187.

Justice, C.O., Holben, B.N. and Gwynne, M.D. (1986) Monitoring East African Vegetation Using AVHRR Data, International Journal of Remote Sensing, Vol. 7, No. 11, pp. 1453-1474.

Justice, C.O., Markham, B.L., Townshend, J.R.G. and Kennard, R.L. (1989) Spatial Degradation of Satellite Data, International Journal of Remote Sensing, Vol. 10, No. 9, pp. 1539-1561.

Justice, C.O., Townshend, J.R.G., Holben, B.N. and Tucker, C.J. (1985) Analysis of the Phenology of Global Vegetation Using Meteorological Satellite Data, International Journal of Remote Sensing, Vol. 6, No. 8, pp. 1271-1318.

Kaufman, Y.J. (1989) The Atmospheric Effect on Remote Sensing and its Corrections, in Theory and Applications of Optical Remote Sensing, Asrar, G. (ed), John Wiley and Sons, New York, NY, pp. 336-428.

Kaufman, Y.J. and Holben, B.N. (1993) Calibration of the AVHRR Visible and Near-IR Bands by Atmospheric Scattering, Ocean Glint and Desert Reflection, International Journal of Remote Sensing, Vol. 14, No. 1, pp. 21-52.

Kaufman, Y.J. and Tanre, D. (1992) Atmospherically Resistant Vegetation Index (AVRI) for EOS-MODIS, IEEE Transactions on Geoscience and Remote Sensing, Vol. 30, No. 2, pp. 261-275.

Kauth, R.J. and Thomas, G.S. (1976) The Tasselled Cap - A Graphic Description of the Spectral Development of Agricultural Crops as Seen by Landsat, Proceedings of Symposium on Machine Processing of Remotely Sensed Data, Purdue University, West Lafayette, Indiana, pp. 41-51.

Kennedy, P. (1989) Monitoring the Vegetation of Tunisian Grazing Lands Using the Normalized Difference Vegetation Index, AMBIO, Vol. 18, No. 2, pp. 119-123.

Kerr, Y.H., Imbernon, J., Dedieu, G., Hautecueur, O., Lagouarde, J.P. and Seguin, B. (1989) NOAA AVHRR and its Uses for Rainfall and Evapotranspiration Monitoring, International Journal of Remote Sensing, Vol. 10, No. 4, pp. 847-854.

Kidwell, K. (1991) NOAA Polar Orbiter Data Users Guide. (TIROS-N, NOAA-6, NOAA-7, NOAA-8, NOAA-9, NOAA-10, NOAA-11 and NOAA-12), NOAA, National Environmental Satellite Data and Information Service, Washington, DC.

Kimes, D.S. (1983) Dynamics of Directional Reflectance Factor Distributions for Vegetation Canopies, Applied Optics, Vol. 22, No. 9, pp. 1364-1372.

Kimes, D.S., Harrison, P.R. and Ratcliffe, P.A. (1991) A Knowledge-Based Expert System for Inferring Vegetation Characteristics, International Journal of Remote Sensing, Vol. 12, No. 10, pp. 1987-2020.

Kimes, D.S. and Holben, B.N. (1992) Extracting Spectral Albedo from NOAA-9 AVHRR Multiple View Data Using an Atmospheric Correction Procedure and an Expert System, International Journal of Remote Sensing, Vol. 13, No. 2, pp. 275-289.

Kimes, D.S., Newcomb, W.W., Tucker, C.J., Zonneveld, I.S., Van Wijngaarden, W., De Leeuw, J. and Epema, G.F. (1985) Directional Reflectance Factor Distributions for Cover Types of Northern Africa, Remote Sensing of Environment, Vol. 18, pp. 1-19.

Kirchner, J.A., Kimes, D.S. and McMurtrey III, J.E. (1982) Variation of Directional Reflectance Factors with Structural Changes of a Developing Alfalfa Canopy, Applied Optics, Vol. 21, No. 20, pp. 3766-3774.

Kogan, F.N. (1990) Remote Sensing of Weather Impacts on Vegetation in Non-Homogeneous Areas, International Journal of Remote Sensing, Vol. 11, No. 8, pp. 1405-1419.

Kone, N. (1992) A Geometrical Simulation Algorithm For AVHRR Acquisition, Proceedings of International Geoscience and Remote Sensing Symposium, Houston, Texas, May 1992, Vol. 1, pp. 170-172.

Kriebel, K.T. (1978) Measured Spectral Bidirectional Reflection Properties of Four Vegetated Surfaces, Applied Optics, Vol. 17, No. 2, pp. 253-259.

Kumar, M. and Monteith, J.L. (1982) Remote Sensing of Plant Growth, in Plants and Daylight Spectrum, Smith, H. (ed), Academic Press, London, UK, pp. 133-144.

Lee, T.Y. and Kaufman, Y.J. (1986) Non-Lambertian Effects on Remote Sensing of Surface Reflectance and Vegetation Index, IEEE Transactions on Geoscience and Remote Sensing, Vol. GE-24, No. 1, pp. 699-708.

Le Houerou, H.N. (1984) Rain Use Efficiency: A Unifying Concept in Arid-Land Ecology, Journal of Arid Environments, Vol. 7, pp. 213-247.

Legeckis, R. and Pritchard, K. (1976) Algorithm for Correcting the VHRR Imagery for Geometric Distortions Due to the Earth Curvature, Earth Rotation and Spacecraft Roll Attitude Errors, NOAA Technical Memorandum NESS 77, NOAA, Washington, DC.

Legg, C.A. (1991) A Review of Landsat MSS Image Acquisition Over the United Kingdom, 1976-1988, and the Implications for Operational Remote Sensing, International Journal of Remote Sensing, Vol. 12, No. 1, pp. 93-106.

Lewandowski, R. (1982) Sales Forecasting by FORSYS, Journal of Forecasting, Vol. 1, pp. 205-214.

Li, X. and Strahler, A.H. (1986) Geometric-Optical Bidirectional Reflectance Modeling of a Conifer Forest Canopy, IEEE Transactions on Geoscience and Remote Sensing, Vol. GE-24, No. 6, pp. 906-919.

Lloyd, D. (1989a) A Phenological Description of Iberian Vegetation Using Short Wave Vegetation Index Imagery, International Journal of Remote Sensing, Vol. 10, Nos. 4 and 5, pp. 827-833.

Lloyd, D. (1989b) Mapping Phytophenology Using Shortwave Vegetation Index Imagery, Proceedings of 4th AVHRR Data Users Meeting, Rothenberg, FR Germany, September 1989, pp. 131-136.

Lloyd, D. (1990) A Phenological Classification of Terrestrial Vegetation Cover Using Shortwave Vegetation Index Imagery, International Journal of Remote Sensing, Vol. 11, No. 12, pp. 2269-2279.

Lodwick, G.D. (1978) Measuring Ecological Changes in Multitemporal Landsat Data Using Principal Components Analysis, Proceedings of 12th International Symposium on Remote Sensing of Environment, ERIM, Ann Arbor, Michigan, April, 1978, Vol. 2, pp. 1131-1141.

Lord, D., Desjardins, R.I. and Dube, P.A. (1988) Sun-Angle Effects on the Red and Near Infrared Reflectances of Five Different Crop Canopies, Canadian Journal of Remote Sensing, Vol. 14, No. 1, pp. 46-55.

Los, S. (1993) Calibration Adjustment of the NOAA AVHRR Normalized Difference Vegetation Index without Recourse to Component Channel 1 and 2 Data, International Journal of Remote Sensing, Vol. 14, No. 10, pp. 1907-1917.

Lo Seen Chong, D., Mougin, E. and Gastellu-Etchegorry, J.P. (1993) Relating the Global Vegetation Index to Net Primary Productivity and Actual Evapotranspiration over Africa, International Journal of Remote Sensing, Vol. 14, No. 8, pp. 1517-1546.

Loveland, T.R., Merchant, J.W., Ohlen, D.O. and Brown, J.F. (1991) Development of a Land-Cover Characteristics Database for the Conterminous U.S., Photogrammetric Engineering and Remote Sensing, Vol. 57, No. 11, pp. 1453-1463.

Lynch, M.J. and Marsden, A.J. (1992) Mt Pinatubo Impact on Aerosol Optical Depths in Southern Latitudes, Proceedings of 6th Australasian Remote Sensing Conference, Wellington, NZ, November 1992, Vol. 3, pp. 213-216.

Mabbutt, J.A., Litchfield, W.A., Speck, N.H., Sofoulis, J., Wilcox, D.G., Arnold, J.M. and Wright, R.L. (1963) General Report on Lands of the Wiluna-Meekatharra Area, Land Resources Series No. 7, CSIRO, Melbourne, Victoria, 214 pp.

Macchiato, M., Serio, C., Lapenna, V., and La Rotonda, L. (1993) Parametric Time Series Analysis of Cold and Hot Spells in Daily Temperature: An Application in Southern Italy, Journal of Applied Meteorology, Vol. 32, pp. 1270-1281.

Major, D.J., Baret, F. and Guyot, G. (1990) A Ratio Vegetation Index Adjusted for Soil Brightness, International Journal of Remote Sensing, Vol. 11, No. 5, pp. 727-740.

Makridakis, S. and Wheelwright, S.C. (1989) Forecasting Methods for Management, 5th Ed., John Wiley and Sons, New York, N.Y., 470 pp.

Malingreau, J.P. (1986) Global Vegetation Dynamics: Satellite Observations over Asia, International Journal of Remote Sensing, Vol. 11, pp. 1121-1146.

Malingreau, J.P. and Belward, A.S. (1992) Scale Considerations in Vegetation Monitoring Using AVHRR Data, International Journal of Remote Sensing, Vol. 13, No. 12, pp. 2289-2307.

Marsouin, A. and Brunel, P. (1991) Navigation of AVHRR Images Using ARGOS or TBUS Bulletins, International Journal of Remote Sensing, Vol. 12, No. 7, pp. 1575-1592.

Maselli, F., Conese, C., Petkov, L. and Gilabert, M.A. (1992) Use of NOAA-AVHRR NDVI Data for Environmental Monitoring and Crop Forecasting in the Sahel. Preliminary Results., International Journal of Remote Sensing, Vol. 13, No. 14, pp. 2743-2749.

McAlpine, J.R. (1970) Estimating Pasture Growth Periods and Droughts from Simple Water Balance Models, Proceedings of 11th International Grasslands Congress, Surfers Paradise, Qld, April 1970, pp. 484-487.

McCown, R.L. (1973) An Evaluation of the Influence of Available Soil Water Storage Capacity on Growing Season Length and Yield of Tropical Pastures Using Simple Water Balance Models, Agricultural Meteorology, Vol. 11, pp. 53-63.

McCown, R.L. (1981) The Climatic Potential for Beef Cattle Production in Tropical Australia: Part I - Simulating the Annual Cycle of Liveweight Change, Agricultural Systems, Vol. 6, pp. 303-317.

McKeon, G.M., Rickert, K.G., Ash, A.J., Cooksley, D. and Scattini, W.J. (1982) Pasture Production Model, Proceedings of 14th Biennial Conference of the Australian Society for Animal Production, Brisbane, Queensland, May 1982, pp. 201-204.

Menenti, M., Azzali, S., Verhoef, W. and van Swol, R. (1991) Mapping Agroecological Zones and Time Lag in Vegetation Growth by Means of Fourier Analysis of Time Series of NDVI Images, Report 32, DLO The Winand Staring Centre for Integrated Land, Soil and Water Research, Wageningen, The Netherlands, 46 pp.

Millington, A.C. (1992) Changing Environments: Some Remote Sensing Perspectives on Land Degradation, Proceedings of 6th Australasian Remote Sensing Conference, Wellington, NZ, November 1992, Vol.1, pp.2-10.

Mitchell, A.A. and Wilcox, D.G. (1988) Plants of the Arid Shrublands of Western Australia, University of Western Australia Press and Western Australian Department of Agriculture, Perth, WA, 325 pp.

Mitchell, R.M. and O'Brien, D.M. (1992) Atmospheric Correction of AVHRR Shortwave Imagery, Proceedings of 6th Australasian Remote Sensing Conference, Wellington, NZ, November 1992, Vol. 3, pp. 120-127.

Mitchell, R.M., O'Brien, D.M. and Forgan, B.W. (1992) Calibration of the NOAA AVHRR Shortwave Channels Using Split Pass Imagery: I. Pilot Study, Remote Sensing of Environment, Vol. 40, pp. 57-65.

Monteith, J.L. (1972) Solar Radiation and Productivity in Tropical Ecosystems, Journal of Applied Ecology, Vol. 9, pp. 747-766.

Monteith, J.L. (1977) Climate and Efficiency of Crop Production in Britain, Philosophical Transactions of the Royal Society, Vol. 281, pp. 277-294.

Mott, J.J. (1973) Temporal and Spatial Distribution of an Annual Flora in an Arid Region of Western Australia, Tropical Grasslands, Vol. 7, No. 1, pp. 89-97.

Mott, J.J. (1974) Factors Affecting Seed Germination in Three Annual Species from an Arid region of Western Australia, Journal of Ecology, Vol. 62, pp. 699-709.

Mott, J.J. (1975) The Role of Photoperiod and Temperature in Controlling the Phenology of Three Annual Species from an Arid Region of Western Australia, Journal of Ecology, Vol. 63, pp. 633-641.

Neckel, H. and Labs, D. (1981) Improved Data of Solar Irradiance from 0.33 to 1.25, Solar Physics, Vol. 74, pp. 231-249.

Neckel, H. and Labs, D. (1984) The Solar Radiation Between 3300 and 12500 Å, Solar Physics, Vol. 90, pp. 205-258.

Nix, H.A. (1982) Environmental Determinants of Biogeography and Evolution in Terra Australia, in Evolution of the Flora and Fauna of Arid Australia, Barker, W.R. and Greenslade, P.J.M. (eds), Peacock Publications in Association with Australian Systematic Botany Society and ANZAAS (SA Division), Canberra, ACT, pp. 47-66.

NOAA (1987) Pre-Launch Calibration of Channels 1 and 2 of the Advanced Very High Resolution Radiometer, NOAA Technical Report, NESDIS 36, National Oceanographic and Atmospheric Administration, Washington, DC.

Noble, I.R. (1977) Long-Term Biomass Dynamics in an Arid Chenopod Shrub Community at Koonamore, South Australia, Australian Journal of Botany, Vol. 25, pp. 639-653.

Noble, J.C. and Vines, R.G. (1993) Fire Studies in Mallee (Eucalyptus Spp.) Communities of Western New South Wales: Grass Fuel Dynamics and Associated Weather Patterns, Rangeland Journal, Vol. 15, No. 2, pp. 270-297.

Norwine, J. and Greegor, D.H. (1983) Vegetation Classification Based on Advanced Very High Resolution Radiometer (AVHRR) Satellite Imagery, Remote Sensing of Environment, Vol. 13, pp. 69-87.

Noy-Meir, I. (1973) Desert Ecosystems: Environment and Producers, Annual Review of Ecology and Systematics, Vol. 4, pp. 25-51.

Noy-Meir, I. and Walker, B.H. (1986) Stability and Resilience in Rangelands, in Rangelands: A Resource Under Siege - Proceedings of 2nd International Rangelands Congress, Joss, P.J., Lynch, P.W. and Williams, O.B. (eds), Australian Academy of Science, Canberra, ACT, pp. 21-25.

Odum, H.W. (1963) Ecology, Holt, Rinehart and Winston, Inc. New York, NY, 152 pp.

Ohring, G., Planet, W. and Weinreb, M. (1992) Monitoring Global Change from Operational Satellites: Problems and Prospects, Proceedings of ACSM/ASPRS Annual Convention "Global Change and Education", August 1992, Washington, DC, pp. 140-155.

Pagan, A. (1975) A Note on the Extraction of Components From Time Series, Econometrica, Vol. 43, No. 1, pp. 163-168.

Paltridge, G.W. and Mitchell, R.M. (1990) Atmospheric and Viewing Angle Correction of Vegetation Indices and Grassland Fuel Moisture Content Derived from NOAA/AVHRR, Remote Sensing of Environment, Vol. 31, pp. 121-135.

Payne, A.L., Curry, P.J. and Spencer, G.F. (1987) An Inventory and Condition Survey of Rangelands in the Carnarvon Basin, Western Australia, Western Australian Department of Agriculture Technical Bulletin No.73, Perth, WA, 477 pp.

Pearson, R.L. and Miller, L.D. (1972) Remote Mapping of Standing Crop Biomass for Estimation of the Productivity of the Short Grass Prairie, Pawnee National Grasslands, Proceedings of 8th Symposium on Remote Sensing of Environment, ERIM, Ann Arbor, Michigan, pp. 1357-1381.

Pech, R.P., Graetz, R.D. and Davis, A.W. (1986) Reflectance Modelling and the Derivation of Vegetation Indices for an Australian Semi-Arid Shrubland, International Journal of Remote Sensing, Vol. 7, No. 3, pp. 389-403.

Peters, A.J., Rundquist, D.C. and Wilhite, D.A. (1991) Satellite Detection of the Geographic Core of the 1988 Nebraska Drought, Agricultural and Forest Meteorology, Vol. 57, pp. 35-47.

Peterson, U. (1992) Seasonal Reflectance Factor Dynamics in Boreal Forest Clear-Cut Communities, International Journal of Remote Sensing, Vol. 13, No. 4, pp. 753-772.

Petheram, R.J. and Kok, B. (1986) Plants of the Kimberley Region of Western Australia, Rev. Ed., University of Western Australia Press, Nedlands, Perth, 556 pp.

Philipson, W.R. and Teng, W.L. (1988) Operational Interpretation of AVHRR Vegetation Indices for World Crop Information, Photogrametric Engineering and Remote Sensing, Vol. 54, pp. 54-59.

Pickup, G. (1989) New Land Degradation Survey Techniques for Arid Australia - Problems and Prospects, Australian Rangeland Journal, Vol. 11, No. 2, pp. 74-82.

Pickup, G., Chewings, V.H. and Nelson, D.J. (1993) Estimating Changes in Vegetation Cover over Time in Arid Rangelands Using Landsat MSS Data, Remote Sensing of Environment, Vol. 43, pp. 243-263.

Pittock, A.B. and Nix, H.A. (1986) The Effect of Changing Climate on Australian Biomass Production - A Preliminary Study, Climatic Change, Vol. 8, pp. 243-255.

Pook, E.W. (1984) Canopy Dynamics of Eucalyptus Maculata Hook. I Distribution and Dynamics of Leaf Populations, Australian Journal of Botany, Vol. 32, pp. 387-403.

Price, J.C. (1987a) Radiometric Calibration of Satellite Sensors in the Visible and Near Infrared: History and Outlook, Remote Sensing of Environment, Vol. 22, pp. 3-9.

Price, J.C. (1987b) Calibration of Satellite Radiometers and the Comparison of Vegetation Indices, Remote Sensing of Environment, Vol. 21, pp. 15-27.

Price, J.C. (1988) An Update on Visible and Near Infrared Calibration of Satellite Instruments, Remote Sensing of Environment, Vol. 24, pp. 419-422.

Price, J.C. (1992) Estimating Vegetation Amount from Visible and Near Infrared Reflectances, Remote Sensing of Environment, Vol. 41, pp. 29-34.

Price, J.C. (1993) Estimating Leaf Area Index from Satellite Data, IEEE Transactions on Geoscience and Remote Sensing, Vol. 31, No. 3, pp. 727-734.

Prince, S.D. (1991a) Satellite Remote Sensing of Primary Production: Comparison of Results for Sahelian Grasslands 1981-1988, International Journal of Remote Sensing, Vol. 12, No. 6, pp. 1301-1311.

Prince, S.D. (1991b) A Model of Regional Primary Production for Use with Coarse Resolution Satellite Data, International Journal of Remote Sensing, Vol. 12, No. 6, pp. 1313-1330.

Quarmby, N.A., Milnes, M. and Hindle, T.L. (1993) The Use of Multi-Temporal NDVI Measurements from AVHRR Data for Crop Yield Estimation and Prediction, International Journal of Remote Sensing, Vol. 14, No. 2, pp. 199-210.

Ranson, K.J., Daughtry, C.S.T., Biehl, L.L. and Bauer, M.E. (1985) Sunview Angle Effects on Reflectance Factors of Corn Canopies, Remote Sensing of Environment, Vol. 18, pp. 147-161.

Rao, V.R., Brach, E.J. and Mack, A.R. (1979) Bidirectional Reflectance of Crops and the Soil Contribution, Remote Sensing of Environment, Vol. 8, pp. 115-125.

Research Systems Inc. (1993) IDL : Interactive Data Language - Reference Manual for Version 3.0, Research Systems Inc., Colorado, USA.

Richardson, A.J. and Wiegand, C.L. (1977) Distinguishing Vegetation from Soil Background Information, Photogrammetric Engineering and Remote Sensing, Vol. 43, pp. 1541-1552.

Rickert, K.G. and McKeon, G.M. (1982) Soil Water Balance Model: WATSUP, Proceedings of 14th Biennial Conference of the Australian Society for Animal Production, Brisbane, Queensland, May 1982, pp. 198-200.

Ritchie, J.T. (1972) Model for Predicting Evaporation from a Row Crop with Incomplete Cover, Water Resources Research, Vol. 8, No. 5, pp. 1204-1213.

Robel, J.M. (1991) NOAA's AVHRR Archive, Geocarto International, Vol. 2, pp. 60-64.

Roderick, M.L. (1993) Methods for Calculating Solar Position and Day Length Including Computer Programs and Subroutines, Division of Resource Management Technical Report No. 137, Western Australian Department of Agriculture, Perth, WA, 22 pp.

Roderick, M.L. and Smith, R.G.C. (1992) Use of NOAA Derived Seasonal Vegetation Data within a GIS for Broad Scale Management in Western Australia, Proceedings of 6th Australasian Remote Sensing Conference, Wellington, NZ, November 1992, Vol. 3, pp. 194-198.

Rossow, W.B., Brest, C.L. and Garder, L.C. (1989) Global, Seasonal Surface Variations from Satellite Radiance Measurements, Journal of Climate, Vol. 2, pp. 214-247.

Rouse, J.W., Haas, R.H., Schell, J.A., Deering, D.W. and Harlan, J.C. (1974) Monitoring the Vernal Advancement and Retrogradation (Greenwave Effect) of Natural Vegetation, NASA/GSFC Type III Final Report, Greenbelt, Md, 371 pp.

Russell, J.S. (1981) Geographic Variation in Seasonal Rainfall in Australia - An Analysis of the 80-year Period 1895-1974, Journal of Australian Institute of Agricultural Science, Vol. 47, pp. 59-66.

Seguin, B., Assad, E., Freteaud, J.P., Imbernon, J., Kerr, Y. and Lagouarde, J.P. (1989) Use of Meteorological Satellites for Water Balance Monitoring in Sahelian Regions, International Journal of Remote Sensing, Vol. 10, No. 6, pp. 1101-1117.

Sellers, P.J. (1985) Canopy Reflectance, Photosynthesis and Transpiration, International Journal of Remote Sensing, Vol. 6, No. 8, pp. 1335-1372.

Slater, P.N., Biggar, S.F., Holm, R.G., Jackson, R.D., Mao, Y., Moran, M.S., Palmer, J.M. and Yuan, B. (1987) Reflectance and Radiance-Based Methods for the In-Flight Absolute Calibration of Multispectral Sensors, Remote Sensing of Environment, Vol. 22, pp. 11-37.

Slater, P.N. and Jackson, R.D. (1982) Atmospheric Effects on Radiation Reflected from Soil and Vegetation as Measured by Orbital Sensors Using Various Scanning Directions, Applied Optics, Vol. 21, No. 21, pp. 3923-3931.

Slatyer, R.O. (1957) Significance of the Permanent Wilting Percentage in Studies of Plant and Soil Water Relations, Botanical Review, Vol. 23, pp. 585-636.

Smith, E.L. (1988) Successional Concepts in Relation to Range Condition Assessment, in Vegetation Science Applications for Rangelands Analysis and Management, Tueller, P.T. (ed), Kluwer Academic Publishers, Dordrecht, Netherlands, pp. 113-133.

Smith, G.R., Levin, R.H., Abel, P. and Jacobowitz, H. (1988) Calibration of the Solar Bands of the NOAA-9 AVHRR Using High Altitude Aircraft Measurements, Journal of Atmospheric and Oceanographic Technology, Vol. 5, pp. 631-639.

Smith, R.G.C. (1993) Personal Communication.

Smith, R.G.C. and Choudbury, B.J. (1990) Relationship of Multispectral Satellite Data to Land Surface Evaporation from the Australian Continent, International Journal of Remote Sensing, Vol. 11, No. 11, pp. 2069-2088.

Smith, R.G.C. and Choudhury, B.J. (1991) Analysis of Normalized Difference and Surface Temperature Observations over Southeastern Australia, International Journal of Remote Sensing, Vol. 12, No. 10, pp. 2021-2044.

Smith, R.G.C. and Johns, G.G. (1975) Seasonal Trends and Variability of Soil Moisture Under Temperate Pasture on the Northern Tablelands of New South Wales, Australian Journal of Experimental Agriculture and Animal Husbandry, Vol. 15, pp. 250-255.

Smith, R.G.C., Steiner, J.L., Meyer, W.S. and Erskine, D. (1985) Influence of Season to Season Variability in Weather on Irrigation Scheduling of Wheat: A Simulation Study, Irrigation Science, Vol. 6, pp. 241-251.

Smith, R.G.C. and Stephens, M.J. (1976) Importance of Soil Moisture and Temperature on the Growth of Improved Pasture on the Northern Tablelands of New South Wales, Australian Journal of Agricultural Research, Vol. 27, pp. 63-70.

Smith, R.G.C., Xinmei, H., Lyons, T.J., Hacker, J.H. and Hick, P.T. (1992) Change in Land Surface Albedo and Temperature in Southwestern Australia Following The Replacement of Native Perennial Vegetation By Agriculture: Satellite Observations, IAF Paper No. IAF-92-0117, presented at the 43rd Congress of the International Astronautical Federation, August - September 1992, Washington, DC, International Astronautical Federation, Paris, France.

Snijders, F.L. (1991) Rainfall Monitoring Based on Meteosat Data - A Comparison of Techniques Applied to the Western Sahel, International Journal of Remote Sensing, Vol. 12, No. 6, pp. 1331-1347.

Soufflet, V., Tanre, D., Begue, A., Podaire, A. and Deschamps, P.Y. (1991) Atmospherics Effects on NOAA AVHRR Data over Sahelian Regions, International Journal of Remote Sensing, Vol. 12, No. 6, pp. 1189-1203.

Specht, R.L. (1981) Foilage Projective Cover and Standing Biomass, in Vegetation Classification in Australia, Gillison, A.N. and Anderson, D.J. (eds), ANU Press, Canberra, ACT, pp. 10-21.

Stafford Smith, D.M. (1992) Successors in Succession, Bulletin of the Ecological Society of Australia, Vol. 22, No. 1, pp. 27-30.

Stafford Smith, D.M. and Foran, B. (1992) An Approach to Assessing the Economic Risk of Different Drought Management Tactics on a South Australian Pastoral Sheep Station, Agricultural Systems, Vol. 39, pp. 83-105.

Stafford Smith, D.M. and Morton, S.R. (1990) A Framework for the Ecology of Arid Australia, Journal of Arid Environments, Vol. 18, pp. 255-278.

Stephens, D.J., Walker, G.K. and Lyons, T.J. (1994) Forecasting Australian Wheat Yields with a Weighted Rainfall Index, Agricultural and Forest Meteorology, to be published.

Steven, M.D., Biscoe, P.V. and Jaggard, K.W. (1983) Estimation of Sugar Beet Productivity from Reflection in the Red and Near Infrared Spectral Bands, International Journal of Remote Sensing, Vol. 4, pp. 325-334.

Stuart Crombie, D. (1992) Root Depth, Leaf Area and Daytime Water Relations of Jarrah (Eucalyptus marginata) Forest Overstorey and Understorey During Summer Drought, Australian Journal of Botany, Vol. 40, pp. 113-122.

Tanre, D., Holben, B.N. and Kaufman, Y.J. (1992) Atmospheric Correction Algorithm for NOAA-AVHRR Products: Theory and Application, IEEE Transactions on Geoscience and Remote Sensing, Vol. 30, No. 2, pp. 231-248.

Tarpley, J.D., Schneider, S.R. and Money, R.L. (1984) Global Vegetation Indices from the NOAA-7 Meteorological Satellite, Journal of Climate and Applied Meteorology, Vol. 23, pp. 491-494.

Teillet, P.M. and Holben, B.N. (1992) A Multi-Level Electronic Database for Documentation and Dissemination of Time-Dependent NOAA-AVHRR Calibration Coefficients for the Solar Reflective Channels, Proceedings of 6th Australasian Remote Sensing Conference, Wellington, NZ, November 1992, Vol. 3, pp. 100-109.

Thekaekara, M.P. (1973) Solar Energy Outside the Earth's Atmosphere, Solar Energy, Vol. 14, pp. 109-127.

Toure, A., Condal, A.R. and Brown, R.J. (1991) Analysis of NOAA-9 Vegetation Index and Temperature Time Series of Wheat Fields in Western Canada, Canadian Journal of Remote Sensing, Vol. 17, No. 1, pp. 21-26.

Townshend, J.R.G. (ed) (1992) Improved Global Data for Land Application: A Proposal for a New High Resolution Data Set, Report of the Land Cover Working Group of IGBP-DIS, IGBP Report No. 20, Stockholm, Sweden, 87 pp.

Townshend, J.R.G. and Justice, C.O. (1986) Analysis of the Dynamics of African Vegetation Using the Normalised Difference Vegetation Index, International Journal of Remote Sensing, Vol. 7,No. 11, pp. 1435-1445.

Townshend, J.R.G., Justice, C.O., Gurney, C. and McManus, J. (1992) The Impact of Misregistration on Change Detection, IEEE Transactions on Geoscience and Remote Sensing, Vol. 30, No. 5, pp. 1054-1060.

Tucker, C.J. (1979) Red and Photographic Infrared Linear Combinations for Monitoring Vegetation, Remote Sensing of Environment, Vol. 8, pp. 127-150.

Tucker, C.J. (1980) Radiometric Resolution for Monitoring Vegetation. How Many Bits are Needed?, International Journal of Remote Sensing, Vol. 1, No. 3, pp. 241-254.

Tucker, C.J. and Choudbury, B.J. (1987) Satellite Remote Sensing of Drought Conditions, Remote Sensing of Environment, Vol. 23, pp. 243-251.

Tucker, C.J., Fung, I.Y., Keeling, C.D. and Gammon, R.H. (1986) Relationship Between Atmospheric CO_2 Variations and a Satellite-Derived Vegetation Index, Nature, Vol. 319, pp. 195-199.

Tucker, C.J., Holben, B.N., Elgin, Jr., J.H. and McMurtrey III, J.E. (1980) Relationship of Spectral Data to Grain Yield Variation, Photogrammetric Engineering and Remote Sensing, Vol. 46, No. 5, pp. 657-666.

Tucker, C.J., Holben, B.N., Elgin, Jr., J.H. and McMurtrey III, J.E. (1981) Remote Sensing of Total Dry-Matter Accumulation in Winter Wheat, Remote Sensing of Environment, Vol. 11, pp. 171-189.

Tucker, C.J., Newcomb, W.W., Los, S.O. and Prince, S.D. (1991) Cover: Mean and Inter-Year Variation of Growing Season Normalised Difference Vegetation Index for the Sahel 1981-1989, International Journal of Remote, Vol. 12, No. 6, pp. 1133-1135.

Tucker, C.J. and Sellers, P.J. (1986) Satellite Remote Sensing of Primary Production, International Journal of Remote Sensing, Vol. 7, No. 11, pp. 1395-1416.

Tucker, C.J., Townshend, J.R.G. and Goff, T.E. (1985a) African Land Cover Classification Using Satellite Data, Science, Vol. 227, pp. 369-375.

Tucker, C.J., Vanpraet, C.L., Boerwinkel, E. and Gaston, A. (1983) Satellite Remote Sensing of Total Dry Matter Production in the Senegalese Sahel, Remote Sensing of Environment, Vol. 13, pp. 461-474.

Tucker, C.J., Vanpraet, C.L., Sharman, J. and Van Ittersum, G. (1985b) Satellite Remote Sensing of Total Herbaceous Biomass Production in the Senegalese Sahel: 1980-1984, Remote Sensing of Environment, Vol. 17, pp. 233-249.

van Dijk, A., Callis, S., Sakamoto, C.M. and Decker, W.L. (1987) Smoothing Vegetation Index Profiles: An Alternative Method for Reducing Radiometric Disturbance in NOAA/AVHRR Data, Photogrammetric Engineering and Remote Sensing, Vol. 53, No. 8, pp. 1059-1067.

van Keulen, H. (1975) Simulation of Water Use and Herbage Growth in Arid Regions, Centre for Agricultural Publishing and Documentation, Wageningen, Netherlands, 176 pp.

Viovy, N., Arino, O. and Belward, A.S. (1992) The Best Index Slope Extraction (BISE): A Method for Reducing Noise in NDVI Time-Series, International Journal of Remote Sensing, Vol. 13, No. 8, pp. 1585-1590.

Walter, H. (1984) Vegetation of the Earth and Ecological Systems of the Geo-Biosphere, 3rd Ed., Springer-Verlag, Berlin, Germany, 309 pp.

Waring, E.J. (1969) Some Economic Aspects of the Pastoral Industry in Australia, in Arid Lands of Australia, Slatyer, R.O. and Perry, R.A. (eds), Australian National University Press, Canberra, ACT, pp. 229-257.

Warren Wilson, J. (1981) Analysis of Growth, Photosynthesis and Light Interception for Single Plants and Stands, Annals of Botany, Vol. 48, pp. 507-512.

WASTAC (1991) Western Australian Satellite Technology and Applications Consortium - Annual Report, Perth, Western Australia, 17 pp.

Weidner, R.T. and Sells, R.L. (1973) Elementary Classical Physics (Volume 2), 2nd Ed., Allyn and Bacon, Boston, Mass., 379 pp.

Westoby, M. (1980) Elements of a Theory of Vegetation Dynamics in Arid Rangelands, Israel Journal of Botany, Vol. 28, pp. 169-194.

Westoby, M., Walker, B. and Noy-Meir, I. (1989) Opportunistic Management for Rangelands not at Equilibrium, Journal of Range Management, Vol. 42, No. 4, pp. 266-274.

Wiegand, C.L., Maas, S.J., Aase, J.K., Hatfield, J.L., Pinter Jr., P.J., Jackson, R.D., Kanemasu, E.T. and Lapitan, R.L. (1992) Multisite Analyses of Spectral-Biophysical Data for Wheat, Remote Sensing of Environment, Vol. 42, pp. 1-21.

Wiegand, C.L. and Richardson, A.J. (1984) Leaf Area, Light Interception and Yield Estimates from Spectral Components Analysis, Agronomy Journal, Vol. 76, pp. 543-548.

Wiegand, C.L. and Richardson, A.J. (1990) Use of Spectral Vegetation Indices to Infer Leaf Area, Evapotranspiration and Yield: I. Rationale, Agronomy Journal, Vol. 82, pp. 623-629.

Williamson, H.D. (1989) Reflectance from Shrubs and Under-Shrub Soil in a Semi-Arid Environment, Remote Sensing of Environment, Vol. 29, pp. 263-271.

Zar, J.H. (1984) Biostatistical Analysis, 2nd Ed., Prentice-Hall, Englewood Cliffs, New Jersey, 718 pp.

APPENDIX A - RESULTS OF CALIBRATION SIMULATION

A software package (VICAL) was developed to estimate post flight corrections to the NDVI, given known pre and post flight calibration information for both solar channels on the AVHRR. The output from VICAL is in the form of a report and is self explanatory. The report provides a mean error for the user defined reflectance window (see section 5.5), as well as a polynomial (quadratic) model. The output files for various model runs are shown below.

TABLE OF CONTENTS

vical v1.2 - mlr(c)

SATELLITE: NOAA-7

Input Data File: noaa7.12

Launch Date: 23- 6-1981
Launch Date (Julian Day): 2444778.500000

POST FLIGHT DATA

LINEAR REGRESSION DETAILS - SENSOR GAIN

Dependent Variable: Julian Days since launch
Independent Variable: Sensor Gain

where
SEE is standard error of the estimate
R^2 is coefficient of determination
and
Sensor Gain = Intercept + Slope * JDL
  where JDL = Julian Days since Launch

Channel 1 Data.
Intercept: 0.619678
Slope: 0.000063
SEE: 0.003889
R^2: 0.988690
Num Obs: 4

Channel 2 Data.
Intercept: 0.411255
Slope: 0.000052
SEE: 0.005921
R^2: 0.962610
Num Obs: 4

DEEP SPACE COUNTS - STATISTICS

Channel 1 Data.
Mean: 35.799999
SD: 0.282981
Num Obs: 4

Channel 2 Data.
Mean: 37.575001
SD: 0.349851
Num Obs: 4

CALIBRATION DATA

Output Format:
JD Gain_Ch.1 Gain_Ch.2
UNIVARIATE: Month Year Mean_Err Min_Err Max_Err SD_ERR
POLYNOMIAL: Month Year A0 A1 A2 SEE R^2

where
JD is Julian Day for central day of the month

```
Gain-Ch.1 is gain from linear regression
Gain-Ch.2 is gain from linear regression
Month     is month for the error estimate
Year      is year for the error estimate
Mean_Err  is mean error for entire data set
Min_Err   is max error for entire data set
Max_Err   is min error for entire data set
SD_Err    is std dev of error for entire data set
A0,A1,A2  are polynomial coefficients for a
          quadratic fit
SEE       is standard error of the estimate for
          the polynomial
R^2       is coefficient of determination

and
Calibrated NDVI = Orig NDVI + Error
where
For UNIVARIATE:
Error = Mean_Err
For POLYNOMIAL:
Error = A0 + (A1 * Orig NDVI) + (A2 * Orig NDVI * Orig NDVI)

The error estimate is made for a TRIANGULAR window based on
reflectances of MIN: 3.400000   MAX: 34.599998 in RED and NIR
bands.
Number of points used in estimate: 43071

This is based on a grid resolution of 1 DN


OUTPUT DATA
-------------------------------------------------------------
2444800.500000   0.621063   0.412399
 7 1981    0.020323  -0.007505   0.037964   0.004336
 7 1981    0.014054   0.030480  -0.020760   0.002525   0.660900
-------------------------------------------------------------
2444831.500000   0.623014   0.414011
 8 1981    0.020649  -0.007122   0.038236   0.004292
 8 1981    0.014435   0.030475  -0.021163   0.002525   0.654037
-------------------------------------------------------------
2444862.500000   0.624966   0.415624
 9 1981    0.020972  -0.006743   0.038507   0.004247
 9 1981    0.014818   0.030426  -0.021505   0.002524   0.646948
-------------------------------------------------------------
2444892.500000   0.626855   0.417184
10 1981    0.021283  -0.006378   0.038768   0.004206
10 1981    0.015181   0.030430  -0.021900   0.002523   0.640308
-------------------------------------------------------------
2444923.500000   0.628807   0.418796
11 1981    0.021602  -0.006004   0.039035   0.004163
11 1981    0.015553   0.030430  -0.022302   0.002522   0.633038
-------------------------------------------------------------
2444953.500000   0.630695   0.420357
12 1981    0.021909  -0.005644   0.039293   0.004123
12 1981    0.015916   0.030388  -0.022631   0.002521   0.626152
-------------------------------------------------------------
2444984.500000   0.632647   0.421969
 1 1982    0.022224  -0.005275   0.039558   0.004082
 1 1982    0.016284   0.030380  -0.023018   0.002520   0.618914
-------------------------------------------------------------
2445015.500000   0.634599   0.423581
 2 1982    0.022536  -0.004909   0.039822   0.004043
 2 1982    0.016652   0.030361  -0.023387   0.002520   0.611454
```

```
-------------------------------------------------------------
2445043.500000   0.636362   0.425038
 3 1982    0.022816  -0.004579   0.040058   0.004006
 3 1982    0.016981   0.030346  -0.023720   0.002519   0.604748
-------------------------------------------------------------
2445074.500000   0.638313   0.426650
 4 1982    0.023124  -0.004218   0.040319   0.003968
 4 1982    0.017340   0.030351  -0.024113   0.002518   0.597575
-------------------------------------------------------------
2445104.500000   0.640202   0.428210
 5 1982    0.023420  -0.003870   0.040570   0.003932
 5 1982    0.017690   0.030322  -0.024450   0.002517   0.590000
-------------------------------------------------------------
2445135.500000   0.642154   0.429822
 6 1982    0.023724  -0.003513   0.040828   0.003894
 6 1982    0.018046   0.030306  -0.024812   0.002516   0.582508
-------------------------------------------------------------
2445165.500000   0.644043   0.431383
 7 1982    0.024017  -0.003169   0.041076   0.003859
 7 1982    0.018392   0.030274  -0.025139   0.002516   0.575054
-------------------------------------------------------------
2445196.500000   0.645994   0.432995
 8 1982    0.024316  -0.002817   0.041332   0.003824
 8 1982    0.018745   0.030250  -0.025487   0.002515   0.567227
-------------------------------------------------------------
2445227.500000   0.647946   0.434607
 9 1982    0.024614  -0.002467   0.041585   0.003789
 9 1982    0.019097   0.030214  -0.025815   0.002514   0.559665
-------------------------------------------------------------
2445257.500000   0.649835   0.436168
10 1982    0.024900  -0.002131   0.041829   0.003755
10 1982    0.019433   0.030201  -0.026160   0.002513   0.552123
-------------------------------------------------------------
2445288.500000   0.651787   0.437780
11 1982    0.025194  -0.001785   0.042080   0.003722
11 1982    0.019776   0.030203  -0.026535   0.002512   0.544311
-------------------------------------------------------------
2445318.500000   0.653675   0.439340
12 1982    0.025476  -0.001453   0.042322   0.003691
12 1982    0.020110   0.030167  -0.026846   0.002512   0.536779
-------------------------------------------------------------
2445349.500000   0.655627   0.440953
 1 1983    0.025766  -0.001112   0.042570   0.003659
 1 1983    0.020452   0.030142  -0.027179   0.002511   0.528933
-------------------------------------------------------------
2445380.500000   0.657579   0.442565
 2 1983    0.026054  -0.000774   0.042817   0.003627
 2 1983    0.020790   0.030130  -0.027528   0.002510   0.521296
-------------------------------------------------------------
2445408.500000   0.659342   0.444021
 3 1983    0.026312  -0.000470   0.043039   0.003600
 3 1983    0.021093   0.030116  -0.027837   0.002509   0.514313
-------------------------------------------------------------
2445439.500000   0.661293   0.445634
 4 1983    0.026596  -0.000135   0.043283   0.003572
 4 1983    0.021427   0.030099  -0.028175   0.002509   0.506716
-------------------------------------------------------------
2445469.500000   0.663182   0.447194
 5 1983    0.026869   0.000186   0.043518   0.003544
 5 1983    0.021752   0.030059  -0.028470   0.002508   0.499015
-------------------------------------------------------------
2445500.500000   0.665134   0.448806
 6 1983    0.027150   0.000517   0.043760   0.003516
 6 1983    0.022080   0.030049  -0.028813   0.002507   0.491699
```

```
------------------------------------------------------------
2445530.500000   0.667023   0.450367
 7 1983    0.027419   0.000834   0.043992   0.003490
 7 1983    0.022398   0.030025  -0.029123   0.002507   0.484566
------------------------------------------------------------
2445561.500000   0.668974   0.451979
 8 1983    0.027696   0.001160   0.044232   0.003464
 8 1983    0.022725   0.029999  -0.029439   0.002506   0.476926
------------------------------------------------------------
2445592.500000   0.670926   0.453591
 9 1983    0.027971   0.001484   0.044470   0.003437
 9 1983    0.023048   0.029985  -0.029773   0.002505   0.469196
------------------------------------------------------------
2445622.500000   0.672815   0.455152
10 1983    0.028235   0.001795   0.044699   0.003413
10 1983    0.023359   0.029974  -0.030096   0.002504   0.461814
------------------------------------------------------------
2445653.500000   0.674766   0.456764
11 1983    0.028506   0.002115   0.044933   0.003391
11 1983    0.023680   0.029937  -0.030391   0.002504   0.455060
------------------------------------------------------------
2445683.500000   0.676655   0.458324
12 1983    0.028767   0.002422   0.045160   0.003369
12 1983    0.023987   0.029925  -0.030707   0.002503   0.447851
------------------------------------------------------------
2445714.500000   0.678607   0.459936
 1 1984    0.029035   0.002738   0.045393   0.003347
 1 1984    0.024304   0.029896  -0.031010   0.002502   0.441113
------------------------------------------------------------
2445745.500000   0.680559   0.461549
 2 1984    0.029301   0.003052   0.045625   0.003326
 2 1984    0.024618   0.029869  -0.031313   0.002501   0.434169
------------------------------------------------------------
2445774.500000   0.682384   0.463057
 3 1984    0.029548   0.003344   0.045840   0.003307
 3 1984    0.024909   0.029855  -0.031612   0.002501   0.427743
------------------------------------------------------------
2445805.500000   0.684336   0.464669
 4 1984    0.029811   0.003653   0.046069   0.003286
 4 1984    0.025222   0.029816  -0.031896   0.002500   0.420404
------------------------------------------------------------
2445835.500000   0.686225   0.466230
 5 1984    0.030064   0.003951   0.046289   0.003268
 5 1984    0.025519   0.029801  -0.032198   0.002499   0.414920
------------------------------------------------------------
2445866.500000   0.688177   0.467842
 6 1984    0.030323   0.004258   0.046517   0.003249
 6 1984    0.025824   0.029785  -0.032508   0.002499   0.408771
------------------------------------------------------------
2445896.500000   0.690065   0.469402
 7 1984    0.030572   0.004552   0.046735   0.003231
 7 1984    0.026119   0.029761  -0.032796   0.002498   0.402645
------------------------------------------------------------
2445927.500000   0.692017   0.471015
 8 1984    0.030829   0.004854   0.046959   0.003215
 8 1984    0.026419   0.029754  -0.033114   0.002497   0.397015
------------------------------------------------------------
2445958.500000   0.693969   0.472627
 9 1984    0.031083   0.005155   0.047182   0.003201
 9 1984    0.026722   0.029710  -0.033381   0.002497   0.391460
------------------------------------------------------------
2445988.500000   0.695858   0.474187
10 1984    0.031328   0.005444   0.047396   0.003185
10 1984    0.027011   0.029696  -0.033677   0.002496   0.385449
```

```
-------------------------------------------------------------------
2446019.500000   0.697809   0.475800
11 1984    0.031579   0.005741   0.047618   0.003172
11 1984    0.027309   0.029661  -0.033951   0.002495   0.381055
-------------------------------------------------------------------
2446049.500000   0.699698   0.477360
12 1984    0.031821   0.006026   0.047830   0.003157
12 1984    0.027595   0.029636  -0.034230   0.002495   0.376159
-------------------------------------------------------------------
2446080.500000   0.701650   0.478972
 1 1985    0.032068   0.006319   0.048049   0.003147
 1 1985    0.027889   0.029611  -0.034516   0.002494   0.370783
-------------------------------------------------------------------
2446111.500000   0.703601   0.480585
 2 1985    0.032315   0.006611   0.048266   0.003136
 2 1985    0.028181   0.029582  -0.034792   0.002493   0.367079
```

```
vical v1.2 - mlr(c)
-------------------

SATELLITE: NOAA-9


Input Data File: noaa9.12

Launch Date: 12-12-1984
Launch Date (Julian Day): 2446046.500000


POST FLIGHT DATA

LINEAR REGRESSION DETAILS - SENSOR GAIN
---------------------------------------
Dependent Variable:   Julian Days since launch
Independent Variable: Sensor Gain

where
SEE is standard error of the estimate
R^2 is coefficient of determination
and
Sensor Gain = Intercept + Slope * JDL
  where JDL = Julian Days since Launch

Channel 1 Data.
Intercept: 0.572102
Slope:     0.000101
SEE:       0.003847
R^2:       0.995695
Num Obs:   4

Channel 2 Data.
Intercept: 0.409581
Slope:     0.000038
SEE:       0.003168
R^2:       0.979923
Num Obs:   4


DEEP SPACE COUNTS - STATISTICS
------------------------------
Channel 1 Data.
Mean:      37.875000
SD:        0.095470
Num Obs:   4

Channel 2 Data.
Mean:      39.324997
SD:        0.403436
Num Obs:   4


CALIBRATION DATA
----------------
Output Format:
JD      Gain_Ch.1    Gain_Ch.2
UNIVARIATE: Month  Year  Mean_Err  Min_Err  Max_Err SD_ERR
POLYNOMIAL: Month  Year  A0  A1  A2  SEE  R^2

where
JD        is Julian Day for central day of the month
```

```
Gain-Ch.1 is gain from linear regression
Gain-Ch.2 is gain from linear regression
Month     is month for the error estimate
Year      is year for the error estimate
Mean_Err  is mean error for entire data set
Min_Err   is max error for entire data set
Max_Err   is min error for entire data set
SD_Err    is std dev of error for entire data set
A0,A1,A2  are polynomial coefficients for a
          quadratic fit
SEE       is standard error of the estimate for
          the polynomial
R^2       is coefficient of determination

and
Calibrated NDVI = Orig NDVI + Error
where
For UNIVARIATE:
Error = Mean_Err
For POLYNOMIAL:
Error = A0 + (A1 * Orig NDVI) + (A2 * Orig NDVI * Orig NDVI)

The error estimate is made for a TRIANGULAR window based on
reflectances of MIN: 3.400000   MAX: 34.599998 in RED and NIR
bands.
Number of points used in estimate: 43365

This is based on a grid resolution of 1 DN


OUTPUT DATA
-------------------------------------------------------------
2446139.500000   0.581522   0.413145
 3 1985    0.037244   0.017603   0.041469   0.004235
 3 1985    0.039054   0.012567  -0.041150   0.001542   0.867374
-------------------------------------------------------------
2446170.500000   0.584662   0.414333
 4 1985    0.036187   0.016346   0.040222   0.004045
 4 1985    0.037797   0.012702  -0.039982   0.001543   0.854475
-------------------------------------------------------------
2446200.500000   0.587700   0.415483
 5 1985    0.035171   0.015141   0.039025   0.003867
 5 1985    0.036592   0.012813  -0.038843   0.001544   0.840543
-------------------------------------------------------------
2446231.500000   0.590840   0.416671
 6 1985    0.034128   0.013904   0.037799   0.003683
 6 1985    0.035355   0.012936  -0.037685   0.001545   0.824213
-------------------------------------------------------------
2446261.500000   0.593879   0.417821
 7 1985    0.033127   0.012718   0.036623   0.003514
 7 1985    0.034169   0.013035  -0.036552   0.001545   0.806309
-------------------------------------------------------------
2446292.500000   0.597019   0.419009
 8 1985    0.032100   0.011501   0.035418   0.003340
 8 1985    0.032950   0.013163  -0.035425   0.001546   0.785548
-------------------------------------------------------------
2446323.500000   0.600159   0.420197
 9 1985    0.031080   0.010294   0.034223   0.003172
 9 1985    0.031742   0.013268  -0.034282   0.001547   0.762326
-------------------------------------------------------------
2446353.500000   0.603198   0.421346
10 1985    0.030101   0.009136   0.033325   0.003015
10 1985    0.030583   0.013367  -0.033184   0.001548   0.736256
```

2446384.500000	0.606337	0.422534			
11 1985	0.029096	0.007948	0.032416	0.002860	
11 1985	0.029393	0.013474	-0.032065	0.001548	0.706469
2446414.500000	0.609376	0.423684			
12 1985	0.028130	0.006807	0.031548	0.002714	
12 1985	0.028250	0.013584	-0.031001	0.001549	0.673645
2446445.500000	0.612516	0.424872			
1 1986	0.027140	0.005638	0.030662	0.002568	
1 1986	0.027078	0.013682	-0.029892	0.001550	0.636648
2446476.500000	0.615656	0.426060			
2 1986	0.026156	0.004477	0.029788	0.002436	
2 1986	0.025919	0.013754	-0.028763	0.001551	0.594012
2446504.500000	0.618492	0.427133			
3 1986	0.025274	0.003437	0.029009	0.002319	
3 1986	0.024880	0.013809	-0.027737	0.001551	0.553262
2446535.500000	0.621632	0.428321			
4 1986	0.024303	0.002294	0.028157	0.002207	
4 1986	0.023737	0.013887	-0.026635	0.001552	0.504364
2446565.500000	0.624671	0.429471			
5 1986	0.023371	0.001196	0.027345	0.002102	
5 1986	0.022637	0.013964	-0.025581	0.001553	0.454528
2446596.500000	0.627811	0.430659			
6 1986	0.022415	0.000070	0.026516	0.002008	
6 1986	0.021509	0.014045	-0.024503	0.001553	0.402160
2446626.500000	0.630849	0.431808			
7 1986	0.021496	-0.001011	0.025725	0.001931	
7 1986	0.020430	0.014092	-0.023429	0.001554	0.352524
2446657.500000	0.633989	0.432996			
8 1986	0.020553	-0.002120	0.024920	0.001865	
8 1986	0.019317	0.014180	-0.022383	0.001555	0.307685
2446688.500000	0.637129	0.434184			
9 1986	0.019616	-0.003220	0.024126	0.001817	
9 1986	0.018217	0.014227	-0.021292	0.001555	0.268868
2446718.500000	0.640168	0.435334			
10 1986	0.018715	-0.004277	0.023369	0.001789	
10 1986	0.017161	0.014277	-0.020252	0.001556	0.241011
2446749.500000	0.643308	0.436522			
11 1986	0.017792	-0.005360	0.022598	0.001772	
11 1986	0.016076	0.014327	-0.019186	0.001556	0.228772
2446779.500000	0.646347	0.437672			
12 1986	0.016904	-0.006401	0.021863	0.001770	
12 1986	0.015034	0.014377	-0.018164	0.001557	0.230395
2446810.500000	0.649487	0.438860			
1 1987	0.015993	-0.007469	0.021115	0.001795	
1 1987	0.013966	0.014421	-0.017109	0.001558	0.245562
2446841.500000	0.652627	0.440048			
2 1987	0.015088	-0.008529	0.020378	0.001827	
2 1987	0.012906	0.014461	-0.016058	0.001558	0.273796

2446869.500000	0.655463	0.441121			
3 1987	0.014276	-0.009479	0.019723	0.001872	
3 1987	0.011956	0.014487	-0.015104	0.001559	0.306770
2446900.500000	0.658603	0.442309			
4 1987	0.013383	-0.010524	0.019008	0.001934	
4 1987	0.010909	0.014534	-0.014080	0.001559	0.349979
2446930.500000	0.661641	0.443459			
5 1987	0.012525	-0.011528	0.018328	0.002004	
5 1987	0.009906	0.014557	-0.013069	0.001560	0.394528
2446961.500000	0.664781	0.444647			
6 1987	0.011644	-0.012557	0.017637	0.002088	
6 1987	0.008874	0.014604	-0.012063	0.001561	0.441368
2446991.500000	0.667820	0.445796			
7 1987	0.010797	-0.013546	0.016979	0.002177	
7 1987	0.007886	0.014613	-0.011052	0.001561	0.485541
2447022.500000	0.670960	0.446984			
8 1987	0.009928	-0.014561	0.016310	0.002275	
8 1987	0.006870	0.014644	-0.010043	0.001562	0.528940
2447053.500000	0.674100	0.448172			
9 1987	0.009064	-0.015568	0.015653	0.002381	
9 1987	0.005862	0.014668	-0.009034	0.001562	0.569371
2447083.500000	0.677139	0.449322			
10 1987	0.008234	-0.016536	0.015029	0.002487	
10 1987	0.004894	0.014680	-0.008051	0.001563	0.605213
2447114.500000	0.680279	0.450510			
11 1987	0.007382	-0.017529	0.014395	0.002602	
11 1987	0.003901	0.014694	-0.007046	0.001563	0.639002
2447144.500000	0.683317	0.451660			
12 1987	0.006563	-0.018483	0.013793	0.002716	
12 1987	0.002946	0.014712	-0.006088	0.001564	0.668461
2447175.500000	0.686457	0.452848			
1 1988	0.005722	-0.019461	0.013183	0.002837	
1 1988	0.001968	0.014710	-0.005078	0.001564	0.695897
2447206.500000	0.689597	0.454036			
2 1988	0.004887	-0.020433	0.012585	0.002960	
2 1988	0.000995	0.014729	-0.004105	0.001565	0.720489
2447235.500000	0.692535	0.455147			
3 1988	0.004111	-0.021336	0.012036	0.003077	
3 1988	0.000092	0.014728	-0.003177	0.001565	0.741160
2447266.500000	0.695675	0.456335			
4 1988	0.003286	-0.022294	0.011461	0.003203	
4 1988	-0.000867	0.014732	-0.002201	0.001566	0.761035
2447296.500000	0.698713	0.457485			
5 1988	0.002493	-0.023215	0.010916	0.003326	
5 1988	-0.001788	0.014731	-0.001256	0.001566	0.778307
2447327.500000	0.701853	0.458673			
6 1988	0.001679	-0.024160	0.010366	0.003455	
6 1988	-0.002732	0.014720	-0.000274	0.001567	0.794354

```
-------------------------------------------------------------------
2447357.500000    0.704892    0.459823
 7 1988     0.000897  -0.025068    0.009844    0.003580
 7 1988    -0.003641   0.014719    0.000654    0.001567    0.808346
-------------------------------------------------------------------
2447388.500000    0.708032    0.461011
 8 1988     0.000093  -0.026000    0.009317    0.003709
 8 1988    -0.004574   0.014713    0.001614    0.001568    0.821394
-------------------------------------------------------------------
2447419.500000    0.711172    0.462199
 9 1988    -0.000705  -0.026925    0.008803    0.003839
 9 1988    -0.005499   0.014703    0.002570    0.001568    0.833175
-------------------------------------------------------------------
2447449.500000    0.714211    0.463348
10 1988    -0.001473  -0.027814    0.008318    0.003965
10 1988    -0.006389   0.014692    0.003490    0.001569    0.843502
-------------------------------------------------------------------
2447480.500000    0.717350    0.464536
11 1988    -0.002261  -0.028727    0.007829    0.004095
11 1988    -0.007302   0.014679    0.004434    0.001569    0.853196
```

```
vical v1.2 - mlr(c)
-------------------

SATELLITE: NOAA-11


Input Data File: noaa11.12

Launch Date: 24- 9-1988
Launch Date (Julian Day): 2447428.500000


POST FLIGHT DATA

LINEAR REGRESSION DETAILS - SENSOR GAIN
---------------------------------------
Dependent Variable:   Julian Days since launch
Independent Variable: Sensor Gain

where
SEE is standard error of the estimate
R^2 is coefficient of determination
and
Sensor Gain = Intercept + Slope * JDL
  where JDL = Julian Days since Launch

Channel 1 Data.
Intercept: 0.602594
Slope:     -0.000014
SEE:       0.004083
R^2:       0.749890
Num Obs:   3

Channel 2 Data.
Intercept: 0.410000
Slope:     0.000000
SEE:       0.000000
R^2:       -inf
Num Obs:   3


DEEP SPACE COUNTS - STATISTICS
------------------------------
Channel 1 Data.
Mean:      40.000000
SD:        0.000000
Num Obs:   3

Channel 2 Data.
Mean:      40.000000
SD:        0.000000
Num Obs:   3


CALIBRATION DATA
----------------
Output Format:
JD      Gain_Ch.1    Gain_Ch.2
UNIVARIATE: Month  Year  Mean_Err  Min_Err  Max_Err SD_ERR
POLYNOMIAL: Month  Year  A0  A1  A2  SEE  R^2

where
JD        is Julian Day for central day of the month
```

```
Gain-Ch.1 is gain from linear regression
Gain-Ch.2 is gain from linear regression
Month     is month for the error estimate
Year      is year for the error estimate
Mean_Err  is mean error for entire data set
Min_Err   is max error for entire data set
Max_Err   is min error for entire data set
SD_Err    is std dev of error for entire data set
A0,A1,A2  are polynomial coefficients for a
          quadratic fit
SEE       is standard error of the estimate for
          the polynomial
R^2       is coefficient of determination

and
Calibrated NDVI = Orig NDVI + Error
where
For UNIVARIATE:
Error = Mean_Err
For POLYNOMIAL:
Error = A0 + (A1 * Orig NDVI) + (A2 * Orig NDVI * Orig NDVI)

The error estimate is made for a TRIANGULAR window based on
reflectances of MIN: 3.400000   MAX: 34.599998 in RED and NIR
bands.
Number of points used in estimate: 60031

This is based on a grid resolution of 1 DN


OUTPUT DATA
-------------------------------------------------------------
2447510.500000   0.601470   0.410000
12 1988    0.060873   0.019148   0.072500   0.012558
12 1988    0.072016  -0.013971  -0.065204   0.001005   0.993597
-------------------------------------------------------------
2447541.500000   0.601046   0.410000
 1 1989    0.061174   0.019259   0.072853   0.012617
 1 1989    0.072366  -0.014025  -0.065507   0.001005   0.993660
-------------------------------------------------------------
2447572.500000   0.600621   0.410000
 2 1989    0.061476   0.019370   0.073206   0.012674
 2 1989    0.072718  -0.014092  -0.065793   0.001004   0.993718
-------------------------------------------------------------
2447600.500000   0.600237   0.410000
 3 1989    0.061749   0.019471   0.073526   0.012721
 3 1989    0.073039  -0.014167  -0.066035   0.001004   0.993768
-------------------------------------------------------------
2447631.500000   0.599813   0.410000
 4 1989    0.062050   0.019582   0.073879   0.012783
 4 1989    0.073384  -0.014177  -0.066399   0.001004   0.993831
-------------------------------------------------------------
2447661.500000   0.599402   0.410000
 5 1989    0.062344   0.019689   0.074222   0.012834
 5 1989    0.073730  -0.014266  -0.066649   0.001004   0.993881
-------------------------------------------------------------
2447692.500000   0.598977   0.410000
 6 1989    0.062646   0.019800   0.074576   0.012892
 6 1989    0.074080  -0.014310  -0.066966   0.001004   0.993941
-------------------------------------------------------------
2447722.500000   0.598566   0.410000
 7 1989    0.062939   0.019907   0.074918   0.012944
 7 1989    0.074423  -0.014386  -0.067231   0.001003   0.993992
```

2447753.500000	0.598142	0.410000			
8 1989	0.063242	0.020019	0.075273	0.013001	
8 1989	0.074777	-0.014453	-0.067523	0.001003	0.994046
2447784.500000	0.597717	0.410000			
9 1989	0.063544	0.020130	0.075628	0.013060	
9 1989	0.075127	-0.014487	-0.067859	0.001003	0.994101
2447814.500000	0.597306	0.410000			
10 1989	0.063838	0.020237	0.075971	0.013111	
10 1989	0.075475	-0.014595	-0.068082	0.001003	0.994150
2447845.500000	0.596881	0.410000			
11 1989	0.064140	0.020348	0.076327	0.013174	
11 1989	0.075821	-0.014594	-0.068461	0.001003	0.994209
2447875.500000	0.596470	0.410000			
12 1989	0.064435	0.020456	0.076671	0.013219	
12 1989	0.076169	-0.014699	-0.068693	0.001002	0.994252
2447906.500000	0.596046	0.410000			
1 1990	0.064738	0.020567	0.077026	0.013281	
1 1990	0.076519	-0.014729	-0.069031	0.001002	0.994308
2447937.500000	0.595621	0.410000			
2 1990	0.065042	0.020678	0.077382	0.013341	
2 1990	0.076879	-0.014839	-0.069266	0.001002	0.994357
2447965.500000	0.595237	0.410000			
3 1990	0.065317	0.020778	0.077704	0.013387	
3 1990	0.077197	-0.014876	-0.069563	0.001002	0.994404
2447996.500000	0.594813	0.410000			
4 1990	0.065620	0.020890	0.078061	0.013445	
4 1990	0.077552	-0.014957	-0.069831	0.001001	0.994453
2448026.500000	0.594402	0.410000			
5 1990	0.065915	0.020997	0.078406	0.013501	
5 1990	0.077896	-0.015006	-0.070144	0.001001	0.994498
2448057.500000	0.593977	0.410000			
6 1990	0.066218	0.021108	0.078763	0.013561	
6 1990	0.078247	-0.015043	-0.070475	0.001001	0.994552
2448087.500000	0.593566	0.410000			
7 1990	0.066514	0.021216	0.079108	0.013612	
7 1990	0.078594	-0.015108	-0.070767	0.001001	0.994596
2448118.500000	0.593142	0.410000			
8 1990	0.066818	0.021327	0.079466	0.013675	
8 1990	0.078947	-0.015173	-0.071056	0.001001	0.994646
2448149.500000	0.592717	0.410000			
9 1990	0.067123	0.021438	0.079823	0.013724	
9 1990	0.079307	-0.015259	-0.071329	0.001000	0.994688
2448179.500000	0.592306	0.410000			
10 1990	0.067418	0.021546	0.080170	0.013782	
10 1990	0.079651	-0.015321	-0.071615	0.001000	0.994734
2448210.500000	0.591881	0.410000			
11 1990	0.067723	0.021657	0.080528	0.013843	
11 1990	0.080009	-0.015410	-0.071876	0.001000	0.994780

```
-------------------------------------------------------------------
2448240.500000   0.591470   0.410000
12 1990    0.068019   0.021765   0.080875   0.013895
12 1990    0.080357  -0.015498  -0.072133   0.001000   0.994824
-------------------------------------------------------------------
2448271.500000   0.591046   0.410000
 1 1991    0.068323   0.021876   0.081234   0.013958
 1 1991    0.080709  -0.015525  -0.072482   0.001000   0.994873
-------------------------------------------------------------------
2448302.500000   0.590621   0.410000
 2 1991    0.068630   0.021987   0.081592   0.014012
 2 1991    0.081071  -0.015621  -0.072745   0.000999   0.994913
-------------------------------------------------------------------
2448330.500000   0.590237   0.410000
 3 1991    0.068907   0.022088   0.081917   0.014056
 3 1991    0.081396  -0.015706  -0.072977   0.000999   0.994950
```

```
vical v1.3 - mlr(c)
-------------------
SATELLITE: NOAA-7
Input Data File: noaa7.13
DEEP SPACE COUNTS - STATISTICS
------------------------------
Channel 1 Data.
Mean:       35.799999
SD:         0.282981
Num Obs:    4

Channel 2 Data.
Mean:       37.575001
SD:         0.349851
Num Obs:    4


CALIBRATION DATA
----------------
Output Format:
JD   MONTHS    Gain_Ch.1    Gain_Ch.2
UNIVARIATE: Month  Year  Mean_Err  Min_Err  Max_Err SD_ERR
POLYNOMIAL: Month  Year  A0  A1  A2  SEE  R^2

where
JD         is Julian Day for central day of the month
MONTHS     is months elapsed since launch
Gain-Ch.1  is gain from linear regression for this month
Gain-Ch.2  is gain from linear regression for this month
Month      is month for the error estimate
Year       is year for the error estimate
Mean_Err   is mean error for entire data set
Min_Err    is max error for entire data set
Max_Err    is min error for entire data set
SD_Err     is std dev of error for entire data set
A0,A1,A2   are polynomial coefficients for a
           quadratic fit
SEE        is standard error of the estimate for
           the polynomial
R^2        is coefficient of determination

and
Calibrated NDVI = Orig NDVI + Error
where
For UNIVARIATE:
Error = Mean_Err
For POLYNOMIAL:
Error = A0 + (A1 * Orig NDVI) + (A2 * Orig NDVI * Orig NDVI)

The error estimate is made for a TRIANGULAR window based on
reflectances of MIN: 3.400000   MAX: 34.599998 in RED and NIR
bands.
Number of points used in estimate: 43071

This is based on a grid resolution of 1 DN


OUTPUT DATA
-----------------------------------------------------------------
2444770.500000   0.000000   0.591000   0.420000
 6 1981    0.048992   0.026432   0.063418   0.004010
 6 1981    0.048012   0.027415  -0.053659   0.002447   0.627256
```

```
-------------------------------------------------------------
2444800.500000   1.000000   0.593230   0.422330
 7 1981    0.049730   0.027314   0.064108   0.004107
 7 1981    0.048893   0.027316  -0.054509   0.002445   0.645163
-------------------------------------------------------------
2444831.500000   2.000000   0.595460   0.424660
 8 1981    0.050462   0.028189   0.064794   0.004208
 8 1981    0.049765   0.027211  -0.055338   0.002443   0.663815
-------------------------------------------------------------
2444862.500000   3.000000   0.597690   0.426990
 9 1981    0.051185   0.029055   0.065472   0.004311
 9 1981    0.050637   0.027056  -0.056098   0.002441   0.678031
-------------------------------------------------------------
2444892.500000   4.000000   0.599920   0.429320
10 1981    0.051902   0.029914   0.066147   0.004427
10 1981    0.051485   0.027005  -0.056974   0.002439   0.697117
-------------------------------------------------------------
2444923.500000   5.000000   0.602150   0.431650
11 1981    0.052613   0.030764   0.066816   0.004523
11 1981    0.052342   0.026838  -0.057701   0.002437   0.710119
-------------------------------------------------------------
2444953.500000   6.000000   0.604380   0.433980
12 1981    0.053316   0.031607   0.067480   0.004630
12 1981    0.053190   0.026685  -0.058442   0.002435   0.722622
-------------------------------------------------------------
2444984.500000   7.000000   0.606610   0.436310
 1 1982    0.054012   0.032443   0.068139   0.004747
 1 1982    0.054013   0.026630  -0.059288   0.002433   0.738409
-------------------------------------------------------------
2445015.500000   8.000000   0.608840   0.438640
 2 1982    0.054703   0.033269   0.068794   0.004848
 2 1982    0.054843   0.026495  -0.060033   0.002431   0.749886
-------------------------------------------------------------
2445043.500000   9.000000   0.611070   0.440970
 3 1982    0.055386   0.033491   0.069442   0.004965
 3 1982    0.055673   0.026306  -0.060705   0.002429   0.759711
-------------------------------------------------------------
2445074.500000  10.000000   0.613300   0.443300
 4 1982    0.056062   0.033711   0.070086   0.005086
 4 1982    0.056481   0.026211  -0.061481   0.002427   0.770998
-------------------------------------------------------------
2445104.500000  11.000000   0.615530   0.445630
 5 1982    0.056732   0.033928   0.070726   0.005200
 5 1982    0.057287   0.026082  -0.062208   0.002425   0.781382
-------------------------------------------------------------
2445135.500000  12.000000   0.617760   0.447960
 6 1982    0.057397   0.034143   0.071360   0.005308
 6 1982    0.058086   0.025952  -0.062930   0.002423   0.790762
-------------------------------------------------------------
2445165.500000  13.000000   0.619990   0.450290
 7 1982    0.058056   0.034356   0.071988   0.005420
 7 1982    0.058880   0.025803  -0.063618   0.002421   0.799701
-------------------------------------------------------------
2445196.500000  14.000000   0.622220   0.452620
 8 1982    0.058708   0.034567   0.072614   0.005529
 8 1982    0.059665   0.025677  -0.064328   0.002420   0.808099
-------------------------------------------------------------
2445227.500000  15.000000   0.624450   0.454950
 9 1982    0.059354   0.034776   0.073235   0.005642
 9 1982    0.060437   0.025584  -0.065074   0.002418   0.816151
-------------------------------------------------------------
2445257.500000  16.000000   0.626680   0.457280
10 1982    0.059994   0.034982   0.073850   0.005763
10 1982    0.061205   0.025469  -0.065781   0.002416   0.824031
```

```
-------------------------------------------------------------
2445288.500000  17.000000   0.628910   0.459610
11 1982    0.060628   0.035187   0.074460   0.005878
11 1982    0.061971   0.025323  -0.066442   0.002414   0.831091
-------------------------------------------------------------
2445318.500000  18.000000   0.631140   0.461940
12 1982    0.061257   0.035389   0.075067   0.005993
12 1982    0.062727   0.025208  -0.067140   0.002412   0.837377
-------------------------------------------------------------
2445349.500000  19.000000   0.633370   0.464270
 1 1983    0.061880   0.035590   0.075669   0.006105
 1 1983    0.063481   0.025060  -0.067788   0.002410   0.843532
-------------------------------------------------------------
2445380.500000  20.000000   0.635600   0.466600
 2 1983    0.062499   0.035788   0.076266   0.006201
 2 1983    0.064223   0.024949  -0.068480   0.002409   0.849112
-------------------------------------------------------------
2445408.500000  21.000000   0.637830   0.468930
 3 1983    0.063113   0.035985   0.076857   0.006293
 3 1983    0.064962   0.024810  -0.069124   0.002407   0.854808
-------------------------------------------------------------
2445439.500000  22.000000   0.640060   0.471260
 4 1983    0.063717   0.036180   0.077447   0.006430
 4 1983    0.065693   0.024689  -0.069787   0.002405   0.859973
-------------------------------------------------------------
2445469.500000  23.000000   0.642290   0.473590
 5 1983    0.064318   0.036373   0.078032   0.006543
 5 1983    0.066424   0.024521  -0.070383   0.002403   0.864686
-------------------------------------------------------------
2445500.500000  24.000000   0.644520   0.475920
 6 1983    0.064914   0.036564   0.078611   0.006652
 6 1983    0.067142   0.024392  -0.071021   0.002402   0.869525
-------------------------------------------------------------
2445530.500000  25.000000   0.646750   0.478250
 7 1983    0.065507   0.036753   0.079185   0.006736
 7 1983    0.067858   0.024248  -0.071637   0.002400   0.873680
-------------------------------------------------------------
2445561.500000  26.000000   0.648980   0.480580
 8 1983    0.066091   0.036940   0.079757   0.006865
 8 1983    0.068567   0.024107  -0.072249   0.002398   0.877919
-------------------------------------------------------------
2445592.500000  27.000000   0.651210   0.482910
 9 1983    0.066671   0.037126   0.080325   0.006978
 9 1983    0.069271   0.023964  -0.072854   0.002397   0.881736
-------------------------------------------------------------
2445622.500000  28.000000   0.653440   0.485240
10 1983    0.067247   0.037310   0.080888   0.007083
10 1983    0.069961   0.023866  -0.073503   0.002395   0.885914
-------------------------------------------------------------
2445653.500000  29.000000   0.655670   0.487570
11 1983    0.067817   0.037492   0.081446   0.007198
11 1983    0.070652   0.023727  -0.074099   0.002393   0.889423
-------------------------------------------------------------
2445683.500000  30.000000   0.657900   0.489900
12 1983    0.068382   0.037673   0.081999   0.007307
12 1983    0.071338   0.023592  -0.074698   0.002392   0.892631
-------------------------------------------------------------
2445714.500000  31.000000   0.660130   0.492230
 1 1984    0.068946   0.037852   0.082551   0.007382
 1 1984    0.072019   0.023439  -0.075262   0.002390   0.895913
-------------------------------------------------------------
2445745.500000  32.000000   0.662360   0.494560
 2 1984    0.069498   0.038029   0.083098   0.007530
 2 1984    0.072686   0.023355  -0.075911   0.002388   0.899159
```

```
-------------------------------------------------------------
2445774.500000  33.000000   0.664590   0.496890
 3 1984    0.070051   0.038204   0.083641   0.007623
 3 1984    0.073354   0.023222  -0.076491   0.002387   0.902012
-------------------------------------------------------------
2445805.500000  34.000000   0.666820   0.499220
 4 1984    0.070596   0.038378   0.084179   0.007739
 4 1984    0.074019   0.023070  -0.077043   0.002385   0.904757
-------------------------------------------------------------
2445835.500000  35.000000   0.669050   0.501550
 5 1984    0.071139   0.038550   0.084712   0.007833
 5 1984    0.074676   0.022939  -0.077616   0.002384   0.907435
-------------------------------------------------------------
2445866.500000  36.000000   0.671280   0.503880
 6 1984    0.071675   0.038721   0.085244   0.007951
 6 1984    0.075326   0.022810  -0.078177   0.002382   0.910135
-------------------------------------------------------------
2445896.500000  37.000000   0.673510   0.506210
 7 1984    0.072211   0.038890   0.085772   0.008035
 7 1984    0.075983   0.022599  -0.078638   0.002380   0.912421
-------------------------------------------------------------
2445927.500000  38.000000   0.675740   0.508540
 8 1984    0.072737   0.039058   0.086296   0.008159
 8 1984    0.076621   0.022489  -0.079213   0.002379   0.914878
-------------------------------------------------------------
2445958.500000  39.000000   0.677970   0.510870
 9 1984    0.073263   0.039224   0.086815   0.008248
 9 1984    0.077255   0.022388  -0.079809   0.002377   0.916980
-------------------------------------------------------------
2445988.500000  40.000000   0.680200   0.513200
10 1984    0.073781   0.039389   0.087330   0.008365
10 1984    0.077887   0.022238  -0.080326   0.002376   0.919197
-------------------------------------------------------------
2446019.500000  41.000000   0.682430   0.515530
11 1984    0.074297   0.039552   0.087841   0.008461
11 1984    0.078510   0.022137  -0.080906   0.002374   0.921215
-------------------------------------------------------------
2446049.500000  42.000000   0.684660   0.517860
12 1984    0.074809   0.039714   0.088351   0.008556
12 1984    0.079132   0.021999  -0.081428   0.002373   0.923216
-------------------------------------------------------------
2446080.500000  43.000000   0.686890   0.520190
 1 1985    0.075316   0.039875   0.088857   0.008662
 1 1985    0.079748   0.021870  -0.081960   0.002371   0.925102
-------------------------------------------------------------
2446111.500000  44.000000   0.689120   0.522520
 2 1985    0.075819   0.040034   0.089359   0.008763
 2 1985    0.080360   0.021746  -0.082495   0.002370   0.926855
```

```
vical v1.3 - mlr(c)
-------------------
SATELLITE: NOAA-9
Input Data File: noaa9.13
DEEP SPACE COUNTS - STATISTICS
------------------------------
Channel 1 Data.
Mean:       37.875000
SD:         0.095470
Num Obs:    4

Channel 2 Data.
Mean:       39.324997
SD:         0.403436
Num Obs:    4


CALIBRATION DATA
----------------
Output Format:
JD   MONTHS    Gain_Ch.1    Gain_Ch.2
UNIVARIATE: Month  Year  Mean_Err  Min_Err  Max_Err SD_ERR
POLYNOMIAL: Month  Year  A0  A1  A2  SEE  R^2

where
JD         is Julian Day for central day of the month
MONTHS     is months elapsed since launch
Gain-Ch.1  is gain from linear regression for this month
Gain-Ch.2  is gain from linear regression for this month
Month      is month for the error estimate
Year       is year for the error estimate
Mean_Err   is mean error for entire data set
Min_Err    is max error for entire data set
Max_Err    is min error for entire data set
SD_Err     is std dev of error for entire data set
A0,A1,A2   are polynomial coefficients for a
           quadratic fit
SEE        is standard error of the estimate for
           the polynomial
R^2        is coefficient of determination

and
Calibrated NDVI = Orig NDVI + Error
where
For UNIVARIATE:
Error = Mean_Err
For POLYNOMIAL:
Error = A0 + (A1 * Orig NDVI) + (A2 * Orig NDVI * Orig NDVI)

The error estimate is made for a TRIANGULAR window based on
reflectances of MIN: 3.400000   MAX: 34.599998 in RED and NIR
bands.
Number of points used in estimate: 43365

This is based on a grid resolution of 1 DN


OUTPUT DATA
-----------------------------------------------------------------
2446139.500000   3.000000   0.582690   0.426990
 3 1985    0.050204   0.024523   0.056846   0.006685
 3 1985    0.054530   0.010585  -0.055213   0.001532   0.947473
```

```
-------------------------------------------------------------
2446170.500000   4.000000   0.584920   0.429320
 4 1985    0.050880   0.024751   0.057652   0.006815
 4 1985    0.055341   0.010465  -0.055937   0.001531   0.949505
-------------------------------------------------------------
2446200.500000   5.000000   0.587150   0.431650
 5 1985    0.051549   0.024976   0.058452   0.006950
 5 1985    0.056138   0.010393  -0.056714   0.001530   0.951469
-------------------------------------------------------------
2446231.500000   6.000000   0.589380   0.433980
 6 1985    0.052211   0.025200   0.059243   0.007079
 6 1985    0.056933   0.010273  -0.057423   0.001530   0.953269
-------------------------------------------------------------
2446261.500000   7.000000   0.591610   0.436310
 7 1985    0.052868   0.025420   0.060028   0.007208
 7 1985    0.057723   0.010139  -0.058104   0.001529   0.954952
-------------------------------------------------------------
2446292.500000   8.000000   0.593840   0.438640
 8 1985    0.053518   0.025639   0.060806   0.007333
 8 1985    0.058504   0.010022  -0.058803   0.001529   0.956556
-------------------------------------------------------------
2446323.500000   9.000000   0.596070   0.440970
 9 1985    0.054163   0.025855   0.061576   0.007457
 9 1985    0.059284   0.009851  -0.059421   0.001528   0.958051
-------------------------------------------------------------
2446353.500000  10.000000   0.598300   0.443300
10 1985    0.054800   0.026069   0.062340   0.007587
10 1985    0.060045   0.009772  -0.060153   0.001528   0.959486
-------------------------------------------------------------
2446384.500000  11.000000   0.600530   0.445630
11 1985    0.055431   0.026281   0.063097   0.007719
11 1985    0.060811   0.009600  -0.060756   0.001527   0.960836
-------------------------------------------------------------
2446414.500000  12.000000   0.602760   0.447960
12 1985    0.056057   0.026491   0.063847   0.007844
12 1985    0.061557   0.009529  -0.061484   0.001527   0.962113
-------------------------------------------------------------
2446445.500000  13.000000   0.604990   0.450290
 1 1986    0.056678   0.026698   0.064591   0.007963
 1 1986    0.062308   0.009377  -0.062101   0.001526   0.963295
-------------------------------------------------------------
2446476.500000  14.000000   0.607220   0.452620
 2 1986    0.057292   0.026904   0.065328   0.008086
 2 1986    0.063052   0.009223  -0.062710   0.001525   0.964412
-------------------------------------------------------------
2446504.500000  15.000000   0.609450   0.454950
 3 1986    0.057900   0.027107   0.066059   0.008211
 3 1986    0.063774   0.009187  -0.063463   0.001525   0.965505
-------------------------------------------------------------
2446535.500000  16.000000   0.611680   0.457280
 4 1986    0.058503   0.027309   0.066783   0.008331
 4 1986    0.064502   0.009051  -0.064078   0.001524   0.966521
-------------------------------------------------------------
2446565.500000  17.000000   0.613910   0.459610
 5 1986    0.059101   0.027508   0.067501   0.008452
 5 1986    0.065224   0.008917  -0.064694   0.001524   0.967496
-------------------------------------------------------------
2446596.500000  18.000000   0.616140   0.461940
 6 1986    0.059693   0.027705   0.068212   0.008572
 6 1986    0.065937   0.008796  -0.065317   0.001523   0.968398
-------------------------------------------------------------
2446626.500000  19.000000   0.618370   0.464270
 7 1986    0.060280   0.027901   0.068918   0.008685
 7 1986    0.066645   0.008670  -0.065929   0.001523   0.969285
```

```
-------------------------------------------------------------
2446657.500000  20.000000   0.620600   0.466600
 8 1986    0.060861   0.028094   0.069617   0.008807
 8 1986    0.067348   0.008539  -0.066527   0.001522   0.970103
-------------------------------------------------------------
2446688.500000  21.000000   0.622830   0.468930
 9 1986    0.061438   0.028286   0.070310   0.008918
 9 1986    0.068047   0.008386  -0.067094   0.001522   0.970912
-------------------------------------------------------------
2446718.500000  22.000000   0.625060   0.471260
10 1986    0.062008   0.028476   0.070997   0.009041
10 1986    0.068732   0.008299  -0.067735   0.001521   0.971676
-------------------------------------------------------------
2446749.500000  23.000000   0.627290   0.473590
11 1986    0.062574   0.028664   0.071679   0.009151
11 1986    0.069414   0.008184  -0.068335   0.001521   0.972413
-------------------------------------------------------------
2446779.500000  24.000000   0.629520   0.475920
12 1986    0.063135   0.028850   0.072354   0.009269
12 1986    0.070100   0.008000  -0.068843   0.001520   0.973091
-------------------------------------------------------------
2446810.500000  25.000000   0.631750   0.478250
 1 1987    0.063691   0.029034   0.073024   0.009380
 1 1987    0.070773   0.007867  -0.069409   0.001520   0.973753
-------------------------------------------------------------
2446841.500000  26.000000   0.633980   0.480580
 2 1987    0.064242   0.029217   0.073688   0.009494
 2 1987    0.071437   0.007763  -0.070006   0.001519   0.974395
-------------------------------------------------------------
2446869.500000  27.000000   0.636210   0.482910
 3 1987    0.064788   0.029398   0.074347   0.009606
 3 1987    0.072101   0.007610  -0.070532   0.001519   0.975008
-------------------------------------------------------------
2446900.500000  28.000000   0.638440   0.485240
 4 1987    0.065330   0.029577   0.075000   0.009712
 4 1987    0.072758   0.007480  -0.071087   0.001518   0.975578
-------------------------------------------------------------
2446930.500000  29.000000   0.640670   0.487570
 5 1987    0.065866   0.029755   0.075647   0.009828
 5 1987    0.073407   0.007361  -0.071647   0.001518   0.976147
-------------------------------------------------------------
2446961.500000  30.000000   0.642900   0.489900
 6 1987    0.066398   0.029931   0.076289   0.009937
 6 1987    0.074054   0.007212  -0.072162   0.001517   0.976686
-------------------------------------------------------------
2446991.500000  31.000000   0.645130   0.492230
 7 1987    0.066926   0.030105   0.076926   0.010043
 7 1987    0.074694   0.007086  -0.072705   0.001517   0.977193
-------------------------------------------------------------
2447022.500000  32.000000   0.647360   0.494560
 8 1987    0.067449   0.030278   0.077558   0.010151
 8 1987    0.075319   0.007031  -0.073332   0.001516   0.977695
-------------------------------------------------------------
2447053.500000  33.000000   0.649590   0.496890
 9 1987    0.067967   0.030449   0.078184   0.010259
 9 1987    0.075945   0.006923  -0.073886   0.001516   0.978165
-------------------------------------------------------------
2447083.500000  34.000000   0.651820   0.499220
10 1987    0.068481   0.030618   0.078805   0.010366
10 1987    0.076570   0.006790  -0.074402   0.001515   0.978622
-------------------------------------------------------------
2447114.500000  35.000000   0.654050   0.501550
11 1987    0.068991   0.030786   0.079421   0.010471
11 1987    0.077189   0.006660  -0.074918   0.001515   0.979066
```

```
-------------------------------------------------------------
2447144.500000  36.000000   0.656280   0.503880
12 1987    0.069497   0.030953   0.080032   0.010572
12 1987    0.077800   0.006559  -0.075464   0.001514   0.979491
-------------------------------------------------------------
2447175.500000  37.000000   0.658510   0.506210
 1 1988    0.069998   0.031118   0.080639   0.010676
 1 1988    0.078415   0.006382  -0.075904   0.001514   0.979899
-------------------------------------------------------------
2447206.500000  38.000000   0.660740   0.508540
 2 1988    0.070495   0.031281   0.081240   0.010782
 2 1988    0.079014   0.006289  -0.076453   0.001514   0.980299
-------------------------------------------------------------
2447235.500000  39.000000   0.662970   0.510870
 3 1988    0.070988   0.031443   0.081836   0.010884
 3 1988    0.079616   0.006149  -0.076936   0.001513   0.980675
-------------------------------------------------------------
2447266.500000  40.000000   0.665200   0.513200
 4 1988    0.071476   0.031604   0.082428   0.010988
 4 1988    0.080207   0.006045  -0.077459   0.001513   0.981046
-------------------------------------------------------------
2447296.500000  41.000000   0.667430   0.515530
 5 1988    0.071961   0.031763   0.083015   0.011087
 5 1988    0.080802   0.005875  -0.077890   0.001512   0.981395
-------------------------------------------------------------
2447327.500000  42.000000   0.669660   0.517860
 6 1988    0.072442   0.031920   0.083597   0.011187
 6 1988    0.081386   0.005752  -0.078380   0.001512   0.981737
-------------------------------------------------------------
2447357.500000  43.000000   0.671890   0.520190
 7 1988    0.072919   0.032077   0.084175   0.011288
 7 1988    0.081969   0.005605  -0.078830   0.001511   0.982076
-------------------------------------------------------------
2447388.500000  44.000000   0.674120   0.522520
 8 1988    0.073392   0.032232   0.084748   0.011385
 8 1988    0.082545   0.005482  -0.079311   0.001511   0.982387
-------------------------------------------------------------
2447419.500000  45.000000   0.676350   0.524850
 9 1988    0.073861   0.032385   0.085317   0.011484
 9 1988    0.083114   0.005378  -0.079810   0.001510   0.982698
-------------------------------------------------------------
2447449.500000  46.000000   0.678580   0.527180
10 1988    0.074326   0.032538   0.085881   0.011579
10 1988    0.083686   0.005205  -0.080214   0.001510   0.982997
-------------------------------------------------------------
2447480.500000  47.000000   0.680810   0.529510
11 1988    0.074788   0.032689   0.086441   0.011679
11 1988    0.084245   0.005111  -0.080716   0.001510   0.983290
```

```
vical v1.3 - mlr(c)
-------------------
SATELLITE: NOAA-11
Input Data File: noaa11.13
DEEP SPACE COUNTS - STATISTICS
------------------------------
Channel 1 Data.
Mean:       40.000000
SD:         0.000000
Num Obs:    3

Channel 2 Data.
Mean:       40.000000
SD:         0.000000
Num Obs:    3


CALIBRATION DATA
----------------
Output Format:
JD   MONTHS    Gain_Ch.1    Gain_Ch.2
UNIVARIATE: Month  Year  Mean_Err  Min_Err  Max_Err SD_ERR
POLYNOMIAL: Month  Year  A0  A1  A2  SEE  R^2

where
JD         is Julian Day for central day of the month
MONTHS     is months elapsed since launch
Gain-Ch.1  is gain from linear regression for this month
Gain-Ch.2  is gain from linear regression for this month
Month      is month for the error estimate
Year       is year for the error estimate
Mean_Err   is mean error for entire data set
Min_Err    is max error for entire data set
Max_Err    is min error for entire data set
SD_Err     is std dev of error for entire data set
A0,A1,A2   are polynomial coefficients for a
           quadratic fit
SEE        is standard error of the estimate for
           the polynomial
R^2        is coefficient of determination

and
Calibrated NDVI = Orig NDVI + Error
where
For UNIVARIATE:
Error = Mean_Err
For POLYNOMIAL:
Error = A0 + (A1 * Orig NDVI) + (A2 * Orig NDVI * Orig NDVI)

The error estimate is made for a TRIANGULAR window based on
reflectances of MIN: 3.400000   MAX: 34.599998 in RED and NIR
bands.
Number of points used in estimate: 60031

This is based on a grid resolution of 1 DN


OUTPUT DATA
-----------------------------------------------------------------
2447510.500000   3.000000   0.540690   0.372600
12 1988    0.065514   0.020850   0.077935   0.013423
12 1988    0.077427  -0.014913  -0.069763   0.001002   0.994435
```

```
-------------------------------------------------------------
2447541.500000    4.000000    0.542920    0.373800
 1 1989     0.065130    0.020710    0.077485    0.013352
 1 1989     0.076977   -0.014819   -0.069406    0.001002    0.994373
-------------------------------------------------------------
2447572.500000    5.000000    0.545150    0.375000
 2 1989     0.064748    0.020571    0.077039    0.013283
 2 1989     0.076529   -0.014715   -0.069064    0.001002    0.994310
-------------------------------------------------------------
2447600.500000    6.000000    0.547380    0.376200
 3 1989     0.064370    0.020432    0.076596    0.013214
 3 1989     0.076092   -0.014672   -0.068645    0.001002    0.994246
-------------------------------------------------------------
2447631.500000    7.000000    0.549610    0.377400
 4 1989     0.063995    0.020295    0.076156    0.013141
 4 1989     0.075658   -0.014629   -0.068230    0.001003    0.994179
-------------------------------------------------------------
2447661.500000    8.000000    0.551840    0.378600
 5 1989     0.063622    0.020158    0.075719    0.013071
 5 1989     0.075223   -0.014552   -0.067866    0.001003    0.994112
-------------------------------------------------------------
2447692.500000    9.000000    0.554070    0.379800
 6 1989     0.063252    0.020022    0.075285    0.013003
 6 1989     0.074787   -0.014434   -0.067560    0.001003    0.994048
-------------------------------------------------------------
2447722.500000   10.000000    0.556300    0.381000
 7 1989     0.062883    0.019887    0.074854    0.012941
 7 1989     0.074355   -0.014348   -0.067211    0.001003    0.993987
-------------------------------------------------------------
2447753.500000   11.000000    0.558530    0.382200
 8 1989     0.062519    0.019753    0.074427    0.012867
 8 1989     0.073934   -0.014303   -0.066818    0.001004    0.993915
-------------------------------------------------------------
2447784.500000   12.000000    0.560760    0.383400
 9 1989     0.062156    0.019620    0.074002    0.012796
 9 1989     0.073512   -0.014236   -0.066454    0.001004    0.993845
-------------------------------------------------------------
2447814.500000   13.000000    0.562990    0.384600
10 1989     0.061795    0.019488    0.073580    0.012733
10 1989     0.073090   -0.014149   -0.066117    0.001004    0.993780
-------------------------------------------------------------
2447845.500000   14.000000    0.565220    0.385800
11 1989     0.061437    0.019356    0.073162    0.012668
11 1989     0.072674   -0.014095   -0.065739    0.001005    0.993713
-------------------------------------------------------------
2447875.500000   15.000000    0.567450    0.387000
12 1989     0.061083    0.019226    0.072746    0.012598
12 1989     0.072258   -0.013995   -0.065434    0.001005    0.993639
-------------------------------------------------------------
2447906.500000   16.000000    0.569680    0.388200
 1 1990     0.060730    0.019096    0.072333    0.012534
 1 1990     0.071848   -0.013933   -0.065074    0.001005    0.993570
-------------------------------------------------------------
2447937.500000   17.000000    0.571910    0.389400
 2 1990     0.060378    0.018967    0.071923    0.012473
 2 1990     0.071438   -0.013861   -0.064730    0.001005    0.993505
-------------------------------------------------------------
2447965.500000   18.000000    0.574140    0.390600
 3 1990     0.060031    0.018839    0.071516    0.012405
 3 1990     0.071036   -0.013812   -0.064365    0.001006    0.993428
-------------------------------------------------------------
2447996.500000   19.000000    0.576370    0.391800
 4 1990     0.059685    0.018711    0.071112    0.012339
 4 1990     0.070629   -0.013708   -0.064076    0.001006    0.993357
```

```
-------------------------------------------------------------------
2448026.500000  20.000000   0.578600   0.393000
 5 1990    0.059340   0.018585   0.070710   0.012280
 5 1990    0.070228  -0.013643  -0.063728   0.001006   0.993289
-------------------------------------------------------------------
2448057.500000  21.000000   0.580830   0.394200
 6 1990    0.059000   0.018459   0.070312   0.012212
 6 1990    0.069837  -0.013618  -0.063341   0.001006   0.993210
-------------------------------------------------------------------
2448087.500000  22.000000   0.583060   0.395400
 7 1990    0.058661   0.018334   0.069916   0.012151
 7 1990    0.069440  -0.013531  -0.063035   0.001007   0.993139
-------------------------------------------------------------------
2448118.500000  23.000000   0.585290   0.396600
 8 1990    0.058323   0.018210   0.069522   0.012090
 8 1990    0.069045  -0.013445  -0.062732   0.001007   0.993065
-------------------------------------------------------------------
2448149.500000  24.000000   0.587520   0.397800
 9 1990    0.057989   0.018086   0.069132   0.012027
 9 1990    0.068661  -0.013419  -0.062352   0.001007   0.992988
-------------------------------------------------------------------
2448179.500000  25.000000   0.589750   0.399000
10 1990    0.057656   0.017963   0.068744   0.011970
10 1990    0.068268  -0.013313  -0.062076   0.001007   0.992919
-------------------------------------------------------------------
2448210.500000  26.000000   0.591980   0.400200
11 1990    0.057327   0.017841   0.068358   0.011904
11 1990    0.067888  -0.013273  -0.061725   0.001008   0.992835
-------------------------------------------------------------------
2448240.500000  27.000000   0.594210   0.401400
12 1990    0.056998   0.017720   0.067976   0.011847
12 1990    0.067505  -0.013204  -0.061408   0.001008   0.992764
-------------------------------------------------------------------
2448271.500000  28.000000   0.596440   0.402600
 1 1991    0.056673   0.017600   0.067595   0.011784
 1 1991    0.067129  -0.013177  -0.061037   0.001008   0.992683
-------------------------------------------------------------------
2448302.500000  29.000000   0.598670   0.403800
 2 1991    0.056349   0.017480   0.067218   0.011726
 2 1991    0.066752  -0.013102  -0.060737   0.001008   0.992606
-------------------------------------------------------------------
2448330.500000  30.000000   0.600900   0.405000
 3 1991    0.056027   0.017361   0.066843   0.011668
 3 1991    0.066379  -0.013059  -0.060395   0.001009   0.992528
```

APPENDIX B: FINAL CALIBRATION CORRECTIONS APPLIED TO GAC (NDVI) DATA SET

The corrections listed below were applied (added) to the original NDVI monthly images to create a consistent time series data set. See chapter 5 for a full discussion.

Satellite	NDVI Error Estimate
NOAA 7	Error = 0.0323
NOAA 9	Error = 0.1046 - 0.00148 x M where M = months (July 1981=0)
NOAA 11	Error = 0.0713

Table B1. Method of computation of the NDVI error estimates. (Note: Error = $NDVI_{post}$ - $NDVI_{pre}$)

File name	Error	File name	Error
jul81.grd	0.032	apr85.grd	0.038
aug81.grd	0.032	may85.grd	0.036
sep81.grd	0.032	jun85.grd	0.035
oct81.grd	0.032	jul85.grd	0.033
nov81.grd	0.032	aug85.grd	0.032
dec81.grd	0.032	sep85.grd	0.030
jan82.grd	0.032	oct85.grd	0.029
feb82.grd	0.032	nov85.grd	0.027
mar82.grd	0.032	dec85.grd	0.026
apr82.grd	0.032	jan86.grd	0.024
may82.grd	0.032	feb86.grd	0.023
jun82.grd	0.032	mar86.grd	0.021
jul82.grd	0.032	apr86.grd	0.020
aug82.grd	0.032	may86.grd	0.018
sep82.grd	0.032	jun86.grd	0.017
oct82.grd	0.032	jul86.grd	0.015
nov82.grd	0.032	aug86.grd	0.014
dec82.grd	0.032	sep86.grd	0.012
jan83.grd	0.032	oct86.grd	0.011
feb83.grd	0.032	nov86.grd	0.0098
mar83.grd	0.032	dec86.grd	0.0084
apr83.grd	0.032	jan87.grd	0.0069
may83.grd	0.032	feb87.grd	0.0054
jun83.grd	0.032	mar87.grd	0.0039
jul83.grd	0.032	apr87.grd	0.0024
aug83.grd	0.032	may87.grd	0.0010
sep83.grd	0.032	jun87.grd	-0.00047
oct83.grd	0.032	jul87.grd	-0.0019
nov83.grd	0.032	aug87.grd	-0.0034
dec83.grd	0.032	sep87.grd	-0.0049
jan84.grd	0.032	oct87.grd	-0.0063
feb84.grd	0.032	nov87.grd	-0.0078
mar84.grd	0.032	dec87.grd	-0.0093
apr84.grd	0.032	jan88.grd	-0.010
may84.grd	0.032	feb88.grd	-0.012
jun84.grd	0.032	mar88.grd	-0.013
jul84.grd	0.032	apr88.grd	-0.015
aug84.grd	0.032	may88.grd	-0.016
sep84.grd	0.032	jun88.grd	-0.018
oct84.grd	0.032	jul88.grd	-0.019
nov84.grd	0.032	aug88.grd	-0.021
dec84.grd	0.032	sep88.grd	-0.022
jan85.grd	0.032	oct88.grd	-0.024
feb85.grd	0.032	nov88.grd	-0.025
mar85.grd	0.039	dec88.grd	0.071

File name	Error
jan89.grd	0.071
feb89.grd	0.071
mar89.grd	0.071
apr89.grd	0.071
may89.grd	0.071
jun89.grd	0.071
jul89.grd	0.071
aug89.grd	0.071
sep89.grd	0.071
oct89.grd	0.071
nov89.grd	0.071
dec89.grd	0.071
jan90.grd	0.071
feb90.grd	0.071
mar90.grd	0.071
apr90.grd	0.071
may90.grd	0.071
jun90.grd	0.071
jul90.grd	0.071
aug90.grd	0.071
sep90.grd	0.071
oct90.grd	0.071
nov90.grd	0.071
dec90.grd	0.071
jan91.grd	0.071
feb91.grd	0.071
mar91.grd	0.071